TECHNICAL UNIVERSITY OF GDAŃSK
MARINE CIVIL ENGINEERING DEPARTMENT

WAVE-INDUCED PORE PRESSURE OSCILLATIONS IN SANDY SEABED SEDIMENTS

Waldemar Magda

Gdańsk, 1998

WAVE-INDUCED PORE PRESSURE OSCILLATIONS IN SANDY SEABED SEDIMENTS

Waldemar Magda

Marine Civil Engineering Department
Technical University of Gdańsk

Published by:

Marine Civil Engineering Department
Technical University of Gdańsk
G. Narutowicza 11/12
80-952 Gdańsk, Poland

Tel. (+48) 58 347-2611
Fax (+48) 58 347-1436
E-mail wmag@sunrise.pg.gda.pl

Printed by:

GRAFIX
Piastowska 70
80-363 Gdańsk, Poland

ISBN 83-905144-5-1

To my mother and father

There must be something worth living for
There must be something worth trying for
Even something worth dying for!
And if one man can stand tall
There must be some hope for us all
Somewhere, somewhere in the spirit of man.

from Jeff Wayne's musical version of
"The War Of The Worlds" by Georg H. Wells

Contents

Acknowledgements

This book is a corrected copy of the author's Ph.D. Thesis, defended at the Technical University of Gdańsk, Poland, on the 7^{th} of July 1992, containing the most important results of the study carried out in the Soil Mechanics and Foundation Engineering Institute, University of Hannover, Germany, during the years 1989-1991.

I would like to express my deepest gratitude to Professor Bolesław Mazurkiewicz, Ph.D., D.Sc., D.h.c., Civ. Eng., the Head of the Marine Civil Engineering Department, Faculty of Environmental Engineering, Technical University of Gdańsk, the supervisor of the Ph.D. Thesis, for his kind and encouraging support, his interest and guidance during all the phases of the study. Professor Mazurkiewicz's experience and extensive knowledge have been of great value to overcome the difficulties I have met. The continuous collaboration with Professor Mazurkiewicz has given me an opportunity to have a better insight not only into different scientific problems but also brought me onto a higher level of understanding of all difficult questions which are continuously faced to a human being.

I am greatly indebted to Professor Werner Richwien, Ph.D., D.Sc., Civ. Eng., Soil Mechanics and Foundation Engineering Institute, University of Hannover, for providing the excellent facilities necessary to carry out the study. He introduced me to the complex area of soil mechanics and, by his enthusiasm combined with his extensive knowledge of both theoretical and practical aspects of this science, impressed me during the years and made this work possible. I appreciate Professor Richwien for his invaluable advice and assistance.

I wish to thank Professor Zygmunt Meyer, Ph.D., D.Sc., Civ. Eng., Professor Michał Topolnicki, Ph.D., D.Sc., Civ. Eng., and Professor Werner Richwien, Ph.D., D.Sc., Civ. Eng., the official referees of the thesis, for their constructive critisism of the manuscript and offering many useful comments and suggestions on various sections of the work.

My special thanks also go to my close co-workers and colleagues from the Marine Civil Engineering Department, Faculty of Environmental Engineering, Technical University of Gdańsk, who were so kind and helpful in fulfilling all my routine duties during my leave in Hannover. Their round-the-clock friendship and personal support during last years have formed a basis for eager working.

With pleasure, I express my thanks to my collaborator Herbert Seehausen for introducing me to the tricky skills of the laboratory tests. His excellent technical assistance, even during the darkest hours of the night has been necessary for the successfull outcome of my work. Thanks Herbert!

Finally, my warmest thanks belong to my parents. To my mother and farther I owe speciall thanks for both tolerating my moody personality and providing much moral support and stoically withstood my many expressions of frustration and anxiety during all the years. I wish to thank them very cordially for their confidence in me, patience and love in the whole my life and especially during the period of this study when I was absent in Gdańsk for most of the time of my leave in Hannover.

This study has been financially supported by grants from the German Research Foundation (DFG) directed to the Special Collaborative Programme – 205 "Coastal Engineering" (Sonderforschungsbereich – 205 "Küsteningenieurwesen").

Summary

The Thesis deals with the very important engineering problem of the behaviour of sandy seabed sediments due to wave-induced cyclic loading. The main focus of the work is an analysis of the pore pressure distribution with depth, the knowledge of which is necessary for a proper and realistic description of transient and cyclic changes in the stress-state existing within the soil.

The contents of the Thesis are divided into six Chapters.

In Chapter 1, a proposition of the Thesis is submitted, and the general assumptions, under which the Thesis is to be proved, are given. The main goal of the work was to study the influence of different soil saturation conditions on the process of cyclic oscillations in the pore pressure induced by a continuous passage of surface water waves.

From many existing theories which have been developed for the case of a stiff or elastc two-phase medium, a theory proposed by Madsen (1978) was chosen. This theory, which is relatively sophisticated regarding the number of soil-water parameters, is not so taxing for the engineer to manipulate and to transform into a mathematical simulation of the instantaneous wave-induced pore pressure oscillations in seabed sediments. The theory allows, among other things, an investigation of the effect of partly saturated soil conditions by permitting optional compressibility of the pore fluid.

The main assumptions used to examine the Thesis can be summarised as follows:

- the soil skeleton and the pore fluid are compressible,
- the behaviour of the soil skeleton is ruled by the linear theory of elasticity,
- the flow of the pore fluid through a porous medium is laminar and governed by Darcy's law,
- the dissipation capabilities of the seabed sediments are large enough to prevent a development of the pore pressure accumulation (which is sometimes called the residual pore pressure, excess pore pressure, permanent pore pressure, or pore pressure build-up) from one loading cycle to the next,
- the waves are regular, as defined by the linear theory for small-amplitude surface waves,
- the seabed consists of homogeneous and isotropic sandy sediments,
- the soil skeleton can be treated as either fully saturated or partly saturated,
- the seabed layer has a finite thickness, limited by the existence of an impermeable and stiff base.

Chapter 2 contains a review and comparison of different published theories of the wave-induced pore pressure cyclic oscillations in the seabed. Firstly, a theory by Putnam (1949) is cited. Its general assumptions (incompressibility of both the soil skeleton and the pore fluid), afford the simplest known solution for the wave-induced pore pressure; it takes the form of the Laplace equation (potential theory solution), and therefore it is

independent of any parameters characterizing the two-phase soil/pore-fluid medium. A further theoretical development has led to another solution presented by Moshagen & Tørum (1975). This differs from earlier one in that it assumes a compressibility (related, however, only to the soil skeleton). As a consequence, the partial differential equation describing the wave-induced pore pressure fluctuations within the seabed sediments takes the form of the diffusion equation (also known as the consolidation equation or the heat conduction equation).

The analysis and discussion of the wave-induced pore pressure theories clearly showes that all simplified theories (*i.e.*, those which assume incompressibility of the soil skeleton or pore fluid, or both) are special cases of more advanced theories, which assume realistic properties of the soil/pore-fluid mixture as much as possible; the most important assumption seems to be the compressibility of both components of the two-phase medium. Therefore, greater emphasis has been given to this fact in the next part of the review. Thus, three theories were considered, *i.e.* those by Madsen (1978), Yamamoto *et al.* (1978), and Okusa (1985[a]). All of them fulfil the aforementioned requirements concerning compressibility of the two phases. Additionally, they permit the study of anisotropy in soil permeability. These theories, which are founded on the same assumptions, use the same governing equation which resembles in its form an extended diffusion equation, and known in the literature as the storage equation. In fact, it is a combination of the Laplace equation and the diffusion equation. The only difference between these theories is the manner in which they obtain a general solution to the main partial differential equation.

The conclusion of the literature review is that any suitable theory should contain the compressibility of both the soil skeleton and the pore fluid. This is a necessary condition for a realistic approach. This means that all simplified theoretical considerations and equations have to be rejected because they are not able to reproduce the soil/pore-fluid interaction adequately. This statement implies that the governing equations, required for the subsequent analysis, are necessarily complicated, and that analytical solutions can only be expected in the case of simple boundary conditions.

Presented also in Chapter 2 is a review of results from various laboratory tests on the phenomenon of wave-induced pore pressure cyclic oscillations in sandy seabed sediments. The review concludes that until present there has been a dearth of detailed investigations, in which the modelling and controlling of some of the very important, indeed decisive soil/pore-fluid parameters, such as the degree of saturation or the soil permeability, has been possible. For this reason, the theoretical considerations disclosed in the following Chapters were verified later by means of specially prepared model tests and laboratory investigations.

Chapter 3 treats the subject of the properties of the soil skeleton and the pore fluid by characterization of their basic physical parameters. In reality, seabed sediments are three-phase media where the soil skeleton, water, and air contained in soil pores are the components. However, solutions for the wave-induced pore pressure cyclic oscillations in a three-phase medium are very complicated and therefore not practically widely applicable. In order to deal with this problem it was necessary to make a simplification by assuming the medium under consideration is represented by only two phases, *i.e.* soil skeleton and pore fluid, where the pore fluid consists of a mixture of water and air occupying the soil pores. After the discussion of the main soil parameters (shear modulus, Poisson's ratio, permeability, porosity), the next part of Chapter 3 relates to a search for a practical formula capable of defining the elastic properties of the pore fluid. It was proved that the compressibility of water containing small air particles is most dependant on the amount of the air present, *i.e.* the degree of saturation. Using

a few computational examples, it was shown what dramatic changes in compressibility can occur when the degree of saturation deviates by only few percent, or even a fraction of percent, from fully saturated conditions.

Many formulas for the pore fluid compressibility have been proposed to give a mathematical relation which is practically applicable. In most cases, however, they require a knowledge of parameters which are extremely difficult or even impossible to measure to satisfactory accuracy (*e.g.*, the diameter of air bubbles existing in the water, or the surface tension between water-phase and air-phase). The meaning of air solubility in water and its influence on pore fluid compressibility was also taken into account and discussed. Finally, as a result of a wide comparison of many approaches available in literature, the equation proposed by Verruijt (1969) was accepted for further study. The choice of such simple formula permits the computation of the pore fluid compressibility from knowledge of only basic parameters (*i.e.*, the compressibility of a pure water, the degree of saturation, and the absolute hydrostatic pressure exisiting in a certain depth of the seabed). Although the formula is very simple, it reflects the physical phenomena perfectly, giving a quantity with a practically acceptable accuracy.

The range of validity of the chosen formula covers the degree of saturation between $S = 1$ (*i.e.*, fully saturated soil) and $S \cong 0.85$ (*i.e.*, partly saturated soil). In order to investigate and quantify partly saturated conditions in natural seabed sediments, a series of *in-situ* sampling was carried out along the shoreline of a tidal area. Computed values and their statistical analysis confirmed the existence of partly saturated soil conditions.

Chapter 4 opens with a brief description of Madsen's (1978) pore pressure theory, adopted for further analysis. A detailed analysis of the mathematical operations, required to obtain a particular solution analytically, indicated that Madsen's theory was the most convenient as regards the implementation of boundary conditions. The basic two-dimensional partial differential equations result from the equilibrium conditions in horizontal and vertical directions and from the requirement of mass conservation. The basic physical assumptions are that the soil skeleton obeys Hook's law and the pore fluid flow obeys Darcy's law. A presentation of the governing partial differential equation of the 6^{th} order is followed by a discussion of the boundary conditions necessary to derive a particular solution, assuming a finite thickness of the permeable seabed layer sited on a stiff and impermeable base. A development of an extention to the existing particular solution for a layered system with finite thickness was motivated by a future requirement to verify results from model tests, in which only a relatively small thickness of the permeable layer can be physically modelled. It must be emphased, however, that the aforementioned sophisticated pore pressure theories have been published together with particular solutions only for the case of infinite thickness of the seabed sediments. An analytical solution of the governing equation with the 'finite-thickness layer' boundary conditions is much more complicated in comparison with the case of infinite-thickness layer but, on the other hand, it was essential to be able to verify the theory on the basis of model test results. A finite thickness of seabed sediments can also exist in the natural environment.

Using the general solution for the pore pressure, published by Madsen (1978), a particular solution for a permeable layer of finite thickness was derived analytically. The solution, presented in terms of the amplitude and the phase lag of the pore pressure oscillations within the seabed sediments, was tested and discussed considering, among other parameters: the influence of the layer thickness, the degree of saturation, the type of stiff and impermeable base (*i.e.*, rough or smooth), the soil skeleton compressibility, and the soil permeability. The results, gained from the parameter study, showed the predominant influence of the degree of saturation, the soil permeability, and the thick-

ness of the seabed layer, on the distribution of the wave-induced pore pressure cyclic oscillations with depth. It appeared also that the character of the impermeable base seems to be of little practical consequence and the soil skeleton compressibility becomes important only when the soil sediments are in a loose state.

The derived analytical solution is two-dimensional and, therefore, this solution can be a very useful tool in the verification of results from large-scale model tests. However, the intended implementation of small-scale laboratory tests prompted also an elaboration of a one-dimensional mathematical model for the wave-induced pore pressure oscillations. Such a solution was derived in Chapter 4 and studied for even wider range of soil/pore-fluid parameters than it was possible for the large-scale modelling. The solution to the ordinary one-dimensional partial differential equation was obtained using the Crank-Nicolson numerical method.

Chapter 5 contains a description of model tests intended to illustrate the pore pressure response and verify the theoretical considerations by modelling various soil skeleton and pore fluid parameters. Large-scale model tests performed in a large wave-flume made it possible to study the pore pressure phenomenon under quasi-natural conditions. A soil layer, 0.5 m thick, formed by a medium sand, was cyclically loaded by surface water waves. The regular waves applied in the tests were characterized by a wave period $T = 3 - 10$ s and a wave height $H = 0.25 - 1.0$ m. All the tests were performed at a constant water depth $h = 4.5$ m. The sand layer was instrumented with 10 pore pressure transducers installed in two vertical profiles. Measurements of the hydrodynamic bottom pressure proved to be in a very good agreement with values predicted theoretically from the linear theory for waves of a small amplitude (Airy's theory). The large-scale model tests confirmed qualitatively the pore pressure amplitude attenuation with depth, together with a simultaneously associated increase of the phase lag in pore pressure oscillations. However, the difference between measured and calculated values becomes significant when the soil parameters (*i.e.*, the coefficient of permeability and the degree of saturation) are taken as determined in standard soil mechanics testing procedure. This result indicates distinctly an important and general dilemma of the problem:

- Simple theories go along with parameters from standard tests, which can be obtained easily, but these theories are not good enough to describe the governing problem in a sufficient and proper way.
- Taking more sophisticated theories, they may be well-prepared to describe the governing phenomena accurately but they need parameters determined very precisely because the influence of varying parameters is decisive. However, the parameters obtained from standard tests (based on soil mechanics field and laboratory testing practice) proof to be not sufficient concerning their accuracy; sometimes it is even not possible to obtain parameters with the necessary degree of accuracy.

To get a quantitative insight into the problem, small-scale laboratory tests were carried out. The seabed layer was modelled in a homogeneous sand column, 0.2 m in diameter and 0.9 m high. The main series of tests was preceded by an initial series where a possible range of densities of the sand model was established. A very precise control of density in the model under preparation was achieved by applying a special technique of sand pouring, where the height of pouring and the pouring intensity control were responsible for an exact degree of density. The small-scale model permitted also very accurate measurements of the degree of saturation. In addition to gravitational saturation, in which the water flows through the soil skeleton from the bottom of the model upwards, some trials were done in order to model the possible extreme values of

the degree of saturation. Thus, pouring the sand through the water with simultaneous vibration of the model resulted in almost fully saturated conditions. Alternatively, by applying a total dewatering of the model followed by re-saturation, relatively low values of the degree of saturation were obtained. Few types of sand, characterized by d_{50} ranging from 0.23 to 1.0 mm, were used in tests, allowing the permeability capabilities of the sand model to be influenced. The surface of the sand column was loaded hydrodynamically by cyclic changes of the water pressure head; the applied period of water-table oscillations $T = 1 - 2$ s and the amplitude up to $A = 0.4$ m.

Comparison of distributions of pore pressure amplitudes and phase lags with depth, obtained from the small-scale model tests and calculated theoretically, showed a good quantitative agreement. Only in the case of sand with relatively large soil particles ($d_{50} = 1.0$ mm), and in tests where the extremely low value of the degree of saturation ($S = 0.83$) was modelled, did significant differences appear. In the former case, this could have been caused by specific water flow conditions in the soil where the application of Darcy's law is suspect. In the latter case, the extremely low values of the degree of saturation obtained were almost equal to the lower limit ($S \cong 0.85$) of the practical applicability of the formula defining the pore fluid compressibility. However, despite these two exceptions, the results from all other tests proved the applicability of Madsen's theory in describing the wave-induced pore pressure cyclic oscillations within the seabed sediments.

Chapter 6 contains a discussion of one of possible practical engineering applications of the analytically derived and experimentally verified solution for the pore pressure response in the sandy seabed layer of finite thickness. The considered problem relates to the question of vertical stability of a submarine pipeline buried in seabed sediments. Using the 'finite-thickness layer' solution, derived from the storage model of the pore pressure response to water waves propagating above the seabed, the hydrodynamic uplift force, acting on the pipeline, was derived. Until now, all known solutions, resulting from the potential theory (Laplace's equation), have the drawbacks because the contribution of some of important soil/pore-fluid parameters are omitted in the solution. The proposed solution for the hydrodynamic uplift force, which takes these parameters into account, is discussed with reference to the soil saturation conditions and the thickness of the permeable soil layer. Computational examples show evidently that the hydrodynamic uplift force can reach its maximum, for a given depth of burial and wave loading conditions, when the degree of saturation approaches a particular value. Since this value always lies within the range of realistic soil saturation conditions, the design of submarine buried pipelines has to be made for the case of maximum hydrodynamic uplift force, regardless what the actual degree of saturation is.

The example of a submarine pipeline buried in seabed sediments is a good representation of important problems that can face both coastal and offshore engineers, showing clearly the potential and the necessity of the application of the storage model of the wave-induved pore pressure response in permeable seabed sediments, that allows to take into account the relative compressibility of the two-phase medium.

Summary (in Polish)

Rozprawa doktorska pt. „Rozkład ciśnienia porowego w gruncie dna morskiego pozostającego pod wpływem falowania powierzchniowego" poświęcona jest bardzo ważnemu z punktu widzenia inżynierskiego zagadnieniu zachowania się piaszczystego podłoża dna morskiego w wyniku ciągłego oddziaływania cyklicznego obciążenia pochodzącego od falowania powierzchniowego. W pracy skoncentrowano się głównie na problemie analizy rozkładu okresowo zmiennego ciśnienia porowego na głębokości w dnie morskim, znajomość którego jest niezbędna dla poprawnego opisu aktualnego stanu naprężenia panującego w gruncie.

Materiał zawarty w niniejszej pracy ujęty jest w sześciu Rozdziałach.

Rozdział 1 prezentuje tezę rozprawy wraz z podstawowymi założeniami przyjętymi dla przeprowadzenia jej dowodu. I tak, tezą pracy jest stwierdzenie o dominującym wpływie stopnia nawodnienia (saturacji) gruntu na generację cyklicznych oscylacji ciśnienia porowego w gruncie dna morskiego pod wpływem falowania powierzchniowego. Uzupełnieniem powyższej tezy jest również stwierdzenie poprawności teorii Madsena (1978) odnoszącej się do ciśnień porowych, ze szczególnym uwzględnieniem jej rozwiązania dla warstwy gruntu o ograniczonej miąższości, oraz jej przydatności w zastosowaniu do niektórych problemów inżynierii morskiej i brzegowej.

Dowód dla tak postawionej tezy przeprowadzono przy następujących założeniach:

- zarówno szkielet gruntowy, jak i ciecz porową cechuje ściśliwość,
- odkształcenia w rozpatrywanym ośrodku wodno-gruntowym podlegają prawom i związkom liniowej teorii sprężystości,
- przepływ cieczy porowej w gruncie ma charakter laminarny i podlega prawu Darcy,
- dysypacja ciśnienia porowego wygenerowanego w ciągu jednego cyklu obciążenia dna morskiego falowaniem powierzchniowym jest wystarczająca by nie dopuścić do stopniowej akumulacji tego ciśnienia (ang. *residual pore pressure, excess pore pressure, permanent pore pressure,* lub *pore pressure build-up*) wraz z kolejnymi cyklami obciążenia,
- falowanie powierzchniowe opisane jest prostą funkcją harmoniczną wynikającą z liniowej teorii fal o małej amplitudzie,
- materiał dna morskiego utworzony jest z jednorodnego oraz izotropowego gruntu piaszczystego,
- ośrodek gruntowo-wodny traktowany jest jako nawodniony całkowicie lub częściowo,
- warstwa gruntu dna morskiego jest o skończonej miąższości i zalega nad sztywnym i nieprzepuszczalnym podłożem.

W Rozdziale 2 dokonano przeglądu i porównania opublikowanych w literaturze światowej teorii generacji cyklicznych zmian ciśnienia porowego w piaszczystym gruncie dna morskiego pod wpływem falowania powierzchniowego. Jako pierwszą, wy-

mieniono teorię zaproponowaną przez Putnama (1949). Podstawowe założenia tej teorii (dotyczące nieściśliwości tak samego szkieletu gruntowego, jak i cieczy porowej) powodują, iż jej rozwiązanie dla ciśnienia porowego, będące najprostszym ze znanych, opisane jest równaniem Laplace'a. Cechą charakterystyczną takiego właśnie rozwiązania teorii potencjalnej jest jego niezależność od jakichkolwiek parametrów fizycznych opisujących ośrodek wodno-gruntowy i wyłączne uzależnienie od geometrii rozpatrywanego układu.

Dalszy rozwój teorii ciśnienia porowego doprowadził do opracowania kolejnego rozwiązania, przykładem którego może być np. teoria przedstawiona przez Moshagena i Tøruma (1975). Podstawową różnicą jaka cechuje to rozwiązanie od poprzednio wspomnianego jest przyjęcie założenia ściśliwości ale tylko względem szkieletu gruntowego. Skutkiem tego, równanie opisujące cykliczne zmiany ciśnienia porowego w gruncie przyjęło formę równania dyfuzji, znanego również pod nazwą równania konsolidacji, czy też równania przewodnictwa cieplnego.

Biorąc pod uwagę, że zarówno szkielet gruntowy, jak i ciecz porową cechuje zawsze pewna ściśliwość, w dalszym etapie pracy skoncentrowano się na analizie teorii uwzględniających ten właśnie fakt. Należy tu przede wszystkim wymienić teorie opracowane przez Madsena (1978), Yamamoto i in. (1978) oraz Okusę ($1985^{(a)}$). Ich uniwersalność polega również na przyjęciu założenia dotyczącego anizotropii ośrodka gruntowego względem jego przepuszczalności. Wymienione trzy teorie opierają się na identycznych podstawach i opisane są tymi samymi wyjściowymi równaniami różniczkowymi cząstkowymi: obok dwóch równań równowagii w płaskim układzie odniesienia występuje równanie trzecie, które jest rozbudowaną formą równania dyfuzji i znane jest pod nazwą równania pojemnościowego (ang. *storage equation*). Jedynym elementem różniącym wspomniane teorie jest sposób otrzymania rozwiązania ogólnego dla podstawowego równania różniczkowego cząstkowego. Szczegółowa analiza poszczególnych operacji matematycznych niezbędnych dla uzyskania ostatecznego rozwiązania szczególnego pokazała, że teoria Madsena (1978) jest najbardziej dogodną dla dokonywania wszelkich przekształceń związanych z problemem uwzględnienia niezbędnych warunków brzegowych.

Przeprowadzona analiza istniejących teorii ciśnienia porowego wykazała, że teorie uproszczone, zakładające nieściśliwość szkieletu gruntowego lub cieczy porowej lub obu ich jednocześnie, stanowią przypadki szczególne teorii bardziej zaawansowanych przyjmujących w swych założeniach realistyczne wartości parametrów wodno-gruntowych; chodzi tu głównie o jednoczesne przyjęcie ściśliwości tak dla samego szkieletu gruntowego, jak i dla cieczy porowej. Rozwiązania płynące m.in. z teorii Putnama (1949) oraz Moshagena i Tøruma (1975) wyznaczają granice zakresu możliwych rozwiązań płynących z teorii Madsena (1978), Yamamoto i in. (1978) oraz Okusy ($1985^{(a)}$).

W Rozdziale 2 znaleźć można również charakterystykę niektórych, bardziej znamiennych badań laboratoryjnych zjawiska cyklicznych oscylacji ciśnienia porowego w gruncie piaszczystym, opublikowanych dotychczas w literaturze światowej. Podstawowym wnioskiem z dokonanego przeglądu jest przekonanie o braku jak dotąd szczegółowych badań, które zapewniałyby możliwość modelowania i kontroli niektórych parametrów wodno-gruntowych, np. stopnia nawodnienia gruntu oraz współczynnika filtracji, mających decydujące znaczenie dla przebiegu zjawiska cyklicznych oscylacji ciśnienia porowego w gruncie dna morskiego wywołanych falowaniem powierzchniowym. Z tego głównie względu, rozważania teoretyczne zawarte w dalszej części pracy poparte są wynikami specjalnie dla tego celu przygotowanych badań laboratoryjnych, tak w dużej, jak i małej skali, co pozwoliło na dokładną weryfikację zaproponowanego rozwiązania dla ciśnienia porowego w przepuszczalnej warstwie gruntu dna morskiego o ograniczonej miąższości.

W Rozdziale 3 omówiono właściwości rozpatrywanego ośrodka wodno-gruntowego oraz scharakteryzowano go biorąc pod uwagę jego podstawowe parametry fizyczne. W warunkach rzeczywistych, dno morskie jest ośrodkiem trójfazowym, w którym wyszczególnić można szkielet gruntowy oraz wodę i gaz (w gruntach piaszczystych jest to najczęściej powietrze) zawarte w porach gruntu, jako jego elementy składowe. Jednakże, rozwiązanie dla ciśnienia porowego w ośrodku trójfazowym jest sprawą niezmiernie skomplikowaną, a jego praktyczne zastosowanie z punktu widzenia czysto inżynierskiego jest mało przydatne. Dlatego też, koniecznym okazało się dokonanie pewnego uproszczenia, polegającego na umownym przyjęciu materiału dna morskiego jako ośrodka dwufazowego utworzonego z szkieletu gruntowego i cieczy porowej, przy czym ciecz porowa reprezentuje tu mieszaninę wody i powietrza wypełniających pory gruntu. Po omówieniu ważniejszych parametrów fizycznych cechujących szkielet gruntowy (np.: moduł sprężystości, współczynnik Poissona, współczynnik filtracji, porowatość), przystąpiono w dalszej części Rozdziału 3 do szukania praktycznej formuły opisującej sprężyste własności cieczy porowej. W trakcie przeprowadzonej analizy wykazano, że ściśliwość mieszaniny wody i zawartych w niej drobnych cząstek powietrza zależna jest przede wszystkim od ilości tegoż powietrza, czyli od tzw. stopnia nawodnienia gruntu. Posługując się kilkoma przykładami pokazano w jak dramatyczny sposób potrafi zmienić się ściśliwość cieczy porowej, gdy stopień nawodnienia maleje tylko o kilka procent, a nawet o ułamek procenta, przyjmując – jako wyjściowe – warunki gruntu nawodnionego. Poszukiwania związków o praktycznej przydatności, określających ściśliwość cieczy porowej, wykazały istnienie wielu rozwiązań, posługiwanie się większością których wymaga jednak znajomości trudnych do zmierzenia parametrów, takich jak np.: średnica zawartych w wodzie porowej cząstek powietrza, czy też wartość napięcia powierzchniowego panującego na granicy woda-powietrze. Przedyskutowane zostało również znaczenie zjawiska rozpuszczalności cząstek powietrza w wodzie porowej i jego wpływ na wartość ściśliwości cieczy porowej.

Wynikiem dokonanego porównania, przeprowadzonego dla kilku podstawowych zależności, był ostateczny wybór związku zaproponowanego przez Verruijta (1969), umożliwiającego obliczenie ściśliwości cieczy porowej przy znajomości tylko takich podstawowych parametrów, jak: ściśliwość wody (bez domieszek powietrza), stopień nawodnienia gruntu oraz absolutne ciśnienie statyczne panujące na rozpatrywanej głębokości w dnie morskim. Pomimo tego, że zakres stosowalności powyższego związku określony jest dla stopnia nawodnienia zawartego w przedziale od $S = 1$ do $S \cong 0.85$, to jednak w celu potwierdzenia istnienia w rzeczywistości warunków nie w pełni nawodnionego gruntu dna morskiego, jak również określenia z pewnym przybliżeniem rzeczywistej jego wartości, wykonano szereg badań *in-situ* w strefie linii brzegowej obszaru pływowego. Zarówno otrzymane bezpośrednio z pomiarów wartości stopnia nawodnienia, jak i dalsza ich statystyczna analiza potwierdziły możliwość istnienia nie w pełni nawodnionego gruntu dna morskiego.

Rozdział 4 poświęcono krótkiemu opisowi przyjętej do dalszej analizy teorii ciśnienia porowego, podanej przez Madsena (1978). Po zaprezentowaniu postaci ogólnej rozwiązania głównego równania różniczkowego cząstkowego, omówiono warunki brzegowe, przyjęcie których umożliwia znalezienie rozwiązania szczególnego dla przepuszczalnej warstwy gruntu dna morskiego o ograniczonej miąższości i zalegającego nad sztywnym i nieprzepuszczalnym podłożem. Konieczność znalezienia takiego właśnie rozwiązania podyktowana była głównie zamiarem dokonania weryfikacji wyników własnych badań laboratoryjnych, w których możliwe jest wyłącznie modelowanie przepuszczalnej warstwy gruntu dna morskiego o stosunkowo niewielkiej, skończonej miąższości. Warto w tym momencie podkreślić, że wraz z opublikowanymi teoriami, Madsen (1978), Ya-

mamoto i in. (1978) oraz Okusa (1985[a]) przedstawili również rozwiązania szczególne dla ciśnienia porowego, jednakże tylko przy założeniu nieskończenie dużej miąższości dla przepuszczalnej warstwy gruntu dna morskiego. Rozwiązanie zagadnienia, które uwzględniałoby warunki brzegowe sformułowane dla warstwy gruntu o skończonej miąższości, jest już sprawą dużo bardziej skomplikowaną.

Opierając się na rozwiązaniu ogólnym dla ciśnienia porowego, przedstawionym przez Madsena (1978), wyprowadzono i zaproponowano rozwiązanie dla cyklicznych oscylacji ciśnienia porowego w przepuszczalnej warstwie gruntu o ograniczonej miąższości. Jak już wspomniano, takie potraktowanie problemu podyktowane było przede wszystkim potrzebą przygotowania narzędzia obliczeniowego do analizy wyników z badań laboratoryjnych. Trzeba tu jednak również zaznaczyć, że sytuacja przepuszczalnej (np. piaszczystej) warstwy gruntu o ograniczonej miąższości, zalegającej ponad warstwą nieprzepuszczalną, może także pojawić się w warunkach rzeczywistego środowiska morskiego.

Otrzymane rozwiązanie analityczne, przedstawione w formie amplitudy i przesunięcia fazowego cyklicznych oscylacji ciśnienia porowego na głębokości w dnie morskim, poddano dyskusji badając m.in. wpływ miąższości warstwy gruntowej, ściśliwości cieczy porowej (modelowanej stopniem nawodnienia gruntu), modułu sprężystości szkieletu gruntowego oraz rodzaju sztywnego i nieprzepuszczalnego podłoża (np. podłoże porowate lub gładkie) zalegającego pod przepuszczalną warstwą gruntową. Przeprowadzona analiza wykazała dominujące znaczenie zarówno warunków nawodnienia gruntu, jak i przepuszczalności gruntu oraz miąższości warstwy gruntowej na rozkład ciśnienia porowego na głębokości w dnie. Wpływ charakteru nieprzepuszczalnego podłoża okazał się praktycznie rzecz biorąc znikomy, a sprężystość szkieletu gruntowego zaczyna odgrywać istotną rolę tylko w przypadku gruntu będącego w stanie luźnym.

Analityczne rozwiązania pochodzące z teorii Madsena (1978) opisane są w przestrzeni dwuwymiarowej, a tym samym mogą one z powodzeniem służyć weryfikacji wyników podstawowych badań laboratoryjnych przeprowadzanych w dużej skali. Jednakże zamiar wykonania badań laboratoryjnych również w małej skali pociągnął za sobą konieczność opracowania dodatkowego modelu jednowymiarowego dla ciśnienia porowego. Tak więc, w Rozdziale 4 sformułowano takie właśnie zagadnienie i dokonano ilustracji jego rozwiązania dla parametrów wodno-gruntowych charakteryzujących warunki przeprowadzania badań modelowych w małej skali. Rozwiązanie jednowymiarowego równania różniczkowego cząstkowego otrzymano na drodze numerycznej, stosując metodę Crank-Nicolsona.

Rozdział 5 zawiera opis szeregu badań laboratoryjnych zaplanowanych z myślą szczegółowego zbadania rzeczywistego zachowania się ciśnienia porowego w gruncie piaszczystym, poddanym działaniu falowania powierzchniowego, modelując różne wartości głównych parametrów wodno-gruntowych.

Jako pierwsze, przeprowadzono badania w dużym kanale falowym, którego rozmiary pozwoliły na symulację warunków falowych i gruntowych zbliżonych do występujących w warunkach naturalnych. Warstwę gruntu o miąższości $0,5\,\mathrm{m}$, utworzoną z piasku średnioziarnistego, poddano cyklicznemu działaniu progresywnego falowania powierzchniowego. Zastosowane w badaniach parametry fali regularnej zawierały się w następujących granicach: okres fali $T = 3 - 10\,\mathrm{s}$ oraz wysokość fali $H = 0,25 - 1,0\,\mathrm{m}$, przy głębokości wody wynoszącej $h = 4,5\,\mathrm{m}$. W warstwie gruntowej zainstalowano 10 czujników (po 5 w każdym z dwóch profili pionowych) do pomiaru ciśnienia porowego.

Na podstawie dokonanych pomiarów ciśnienia hydrodynamicznego w poziomie dna morskiego stwierdzono jego zadawalającą zgodność z wartościami obliczonymi na podstawie liniowej teorii Airy'ego dla fal o małej amplitudzie, a zaistniałe różnice nie przekraczały kilku procent wartości teoretycznych. Przede wszystkim jednak, badania laboratoryjne przeprowadzone w dużej skali potwierdziły w sposób jakościowy zjawiska zanikania (tłumienia) amplitudy oraz wzrostu przesunięcia fazowego cyklicznych oscylacji ciśnienia porowego na głębokości w piaszczystym gruncie modelowanego dna morskiego.

Celem dokonania ilościowej oceny obu wyżej wspomnianych zjawisk wykonano cykl badań laboratoryjnych w małej skali, gdzie jednorodna warstwa gruntowa modelowana była w cylindrycznej kolumnie o średnicy $0,2\,\mathrm{m}$ i wysokości $0,9\,\mathrm{m}$. Główną serię badań poprzedziły wstępne badania mające na celu określenie zakresu możliwych do otrzymania stopni zagęszczenia ośrodka gruntowego. Pomocną w tym zakresie okazała się specjalnie opracowana technika sypania piasku, w której to stała kontrola wysokości sypania piasku pozwalała uzyskiwać zamierzone, ale przede wszystkim jednorodne zagęszczenie modelu gruntowego. Mała skala modelu umożliwiała również dokonanie dokładnego pomiaru stopnia nawodnienia gruntu. Poza nawadnianiem modelu wymuszonym przepływem grawitacyjnym wody przez pory gruntu, wykonano kilka prób wytworzenia ekstremalnych warunków nawodnienia gruntu. I tak, stosując sypanie piasku bezpośrednio do wody, połączone z jednoczesną wibracją całego modelu, uzyskiwano stosunkowo wysoki stopień nawodnienia gruntu; stosując natomiast chwilowe odwodnienie całego modelu, a następnie jego natychmiastowe powtórne nawodnienie, otrzymywano niskie wartości stopnia nawodnienia. W badaniach użyto kilka rodzajów piasku, którego średnice miarodajne zawierały się w przedziale $d_{50} = 0,23 - 1,0\,\mathrm{mm}$. Specjalnie skonstruowany system tłokowy, umieszczony w głowicy kolumny modelu, pozwolił na symulację obciążenia warstwy gruntu ciśnieniem hydrodynamicznym o okresie oscylacji $T = 1 - 2\,\mathrm{s}$ i amplitudzie do $A = 0,4\,\mathrm{m}$ słupa wody.

Porównanie teoretycznie obliczonych wartości amplitud i przesunięć fazowych cyklicznych oscylacji ciśnienia porowego na głębokości w gruncie piaszczystym z wynikami pomiarów przeprowadzonych na modelu wykonanym w małej skali wykazało ich zadowalającą zgodność. Jedynie w przypadku modelu zbudowanego z piasku o stosunkowo dużej średnicy miarodajnej ($d_{50} = 1,0\,\mathrm{mm}$) oraz w przypadku stosunkowo niskiego stopnia nawodnienia gruntu ($S = 0.83$) pojawiły się dość znaczne różnice. Tłumaczyć to należy prawdopodobnie tym, że po pierwsze – przepływ wody porowej w gruncie o dość znacznych średnicach ziaren nie jest już w zadawalający sposób opisany prawem Darcy, a po drugie – znajdując się w dolnej strefie ($S \cong 0.85$) obszaru stosowalności związku pozwalającego wyznaczyć ściśliwość cieczy porowej, obliczona wartość ściśliwości obarczona jest już znaczącym błędem. Jednakże poza tymi dwoma wyjątkowymi sytuacjami, wszystkie pozostałe badane przypadki wykazały dobrą zgodność wyników badań laboratoryjnych z wartościami obliczonymi teoretycznie (analitycznie lub numerycznie), potwierdzając jednoznacznie poprawność przyjętej do analizy teorii opisującej cykliczne oscylacje ciśnienia porowego wywołane progresywnym falowaniem powierzchniowym nad dnem piaszczystym.

Rozdział 6 stanowi ilustrację jednego z możliwych, praktycznych zastosowań teoretycznego rozwiązania teorii Madsena (1978) cyklicznych oscylacji ciśnień porowych, otrzymanego w niniejszej pracy dla przypadku przepuszczalnej warstwy gruntu dna morskiego o ograniczonej miąższości. Omówiony przykład dotyczy problemu stateczności rurociągu podmorskiego zagłębionego w dnie. Posługując się szczególnym rozwiązaniem teorii Madsena (1978), uzyskano rozwiązanie pozwalające na określenie rozkładu ciśnienia porowego na obwodzie rurociągu. Rozwiązanie to daje m.in. możliwość wyz-

naczenia wartości siły wyporu hydrodynamicznego, działającej na rurociąg podmorski zagłębiony w dnie i wywołanej progresywnym falowaniem powierzchniowym. Znane dotychczas rozwiązania tego zagadnienia opierały się wyłącznie na rozwiązaniu równania Laplace'a, co było ich dużą wadą, gdyż nie zawierały żadnych możliwości uwzględnienia znaczenia nawet tylko niektórych, istotnych parametrów wodno-gruntowych. Zaproponowane rozwiązanie dla siły wyporu hydrodynamicznego przedyskutowano z punktu widzenia wpływu stopnia nawodnienia gruntu oraz miąższości przepuszczalnej warstwy gruntu dna morskiego.

Przykład rurociągu podmorskiego zagłębionego w dnie reprezentuje sobą istotne problemy, z jakimi można się spotkać w inżynierii morskiej i brzegowej, wykazując jednoznacznie możliwość i zarazem potrzebę praktycznego zastosowania teorii cyklicznych oscylacji ciśnienia porowego wywołanego progresywnym falowaniem powierzchniowym, opracowanej przy założeniu istnienia ściśliwości tak samej cieczy porowej, jak i szkieletu gruntowego.

Chapter 1

Main thesis and main assumptions

Over the last 40 years there has been a lot of work performed on the prediction of wave-induced pore pressures, stresses and displacements in the seabed sediments. These predictions are based upon the assumptions that the wave loading acting upon the seabed is sinusoidal in form and the seabed has homogeneous and elastic properties. Under these conditions, various analytical solutions have been developed. However, such solutions are limited because partly saturated soil conditions, that introduce a certain but meaningful compressibility to the pore fluid, and a finite thickness of the permeable seabed layer, make the analytical solutions rather complex to be derived.

Here arises the main aim of the present work which is, namely, a study of wave-induced cyclic oscillations of the pore pressure within a sandy seabed for a particular case of partly saturated seabed sediments and a limited thickness of the seabed layer. An intention of the author was also to present a verification of the derived finite-thickness solution by means of laboratory modelling (small- and large-scale model tests) as well as to illustrate the application of the theoretical solution in some practical problems from the coastal and offshore engineering.

The following thesis is submitted:

> *Soil saturation conditions play a predominant role in generation of instantaneous pore pressure cyclic oscillations induced in seabed sediments by surface waves loading.*
>
> *The wave-induced pore pressure theory by Madsen (1978), represented here by the 'finite-thickness layer' particular solution, obtained by the author in terms of the analytical functions and verified experimentally, gives a realistic picture of the soil-water system interaction under natural environmental conditions (i.e., partly saturated seabed sediments), contributing thereby to more precise design procedures in foundation engineering.*

This proposition will be tried to be proved under the following main assumptions:

- the soil skeleton and the pore fluid are compressible media,
- deformations of the soil skeleton are governed by the linear theory of elasticity,
- a flow of the pore fluid is laminar and governed by Darcy's law,

- a rate of the pore pressure dissipation within one period of wave loading is high enough to prevent a long-term accumulation of the pore pressure, also known as the pore pressure build-up, residual pore pressure, permanent pore pressure or excess pore pressure (Fig. 1.1),
- progressive surface waves are defined according to Airy's linear theory for waves of small amplitude,
- a seabed material consists of an uniform and anisotropic (with respect to soil permeability) sandy sediments,
- seabed sediments are treated as fully saturated or partly saturated,
- a permeable sandy seabed layer has a finite thickness and is underlaid by a stiff and impermeable base.

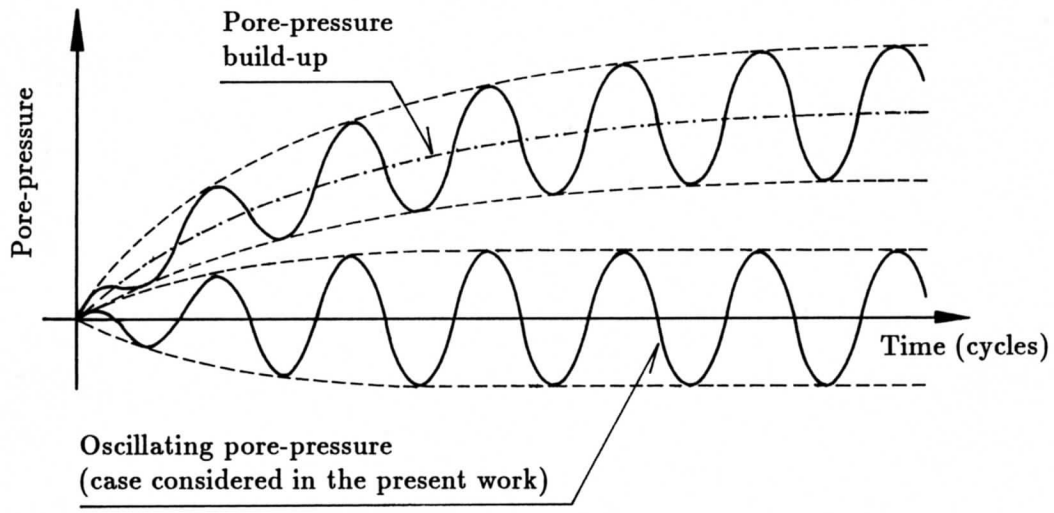

Figure 1.1 Distinguishing between instantaneous pore pressure (cyclic oscillations) and pore pressure build-up (continuous increase)

A short review of existing pore pressure theories is presented in Chapter 2. Different theories are compared and analysed from their assumptions point of view.

Complex properties of the three-phase medium like the soil-water-gas mixture are discussed in Chapter 3 where the problem of pore fluid compressibility, which mainly influences the character (*i.e.*, magnitude and phase lag) of wave-induced pore pressure oscillations, and particularly the relation between the degree of saturation of the seabed sediments and the pore fluid compressibility are specially emphased and widely analysed.

Practical situations show very often that a layered permeable seabed of a finite thickness is found instead of a homogeneous half-space. The different properties of soil skeleton and pore fluid in a layered seabed and, especially, the impermeable boundary condition at the bottom of the seabed layer, may have a strong influence on the wave-induced pore pressure cyclic oscillations. In order to study this effect, the instantaneous pore pressure response in the homogeneous permeable seabed layer of finite thickness, overlaying a stiff and impermeable base, is analysed in Chapter 4. Such a simple seabed stratification can be also considered as a component case of a more advanced multi-layered seabed system.

Chapter 5 brings a detailed description of the large- and small-scale model tests performed to obtained necessary data that could be used in verification of the formerly derived analytical solution.

Finally, Chapter 6 illustrates one of possible engineering applications of the 'finite-thickness layer' solution for the wave-induced pore pressure oscillations in seabed sediments. And thus, a vertical stability of a submarine pipeline buried in seabed sediments is considered and investigated, assuming different relative compressibilities of seabed sediments, and different thicknesses of the permeable seabed layer.

Chapter 2

Review of existing theories

2.1 Theoretical approaches

The wave-induced pore pressure and seepage forces in the seabed as well as the damping of water waves have been the subject of several investigations and theoretical considerations over the last 40 years (*e.g.*: Biot, 1941; Putnam, 1949; Reid & Kajiura, 1957; Hunt, 1959; Murray, 1965; Sleath, 1970; Liu, 1973; Moshagen & Tørum, 1975; Prevost *et al.*, 1975; Massel, 1976; Yamamoto, 1977, 1978, 1981, 1983; Madsen, 1978; Yamamoto *et al.*, 1978; Phillips *et al.*, 1979; Mei & Foda, 1981; Nago, 1981; Finn *et al.*, 1983; Tsui & Helfrich, 1983; McDougal & Sollitt, 1984; Nago & Maeno, 1984, 1986, 1987; Kraft *et al.*, 1985; Okusa, 1985$^{(a)}$, 1985$^{(b)}$; Chari *et al*, 1987; Spierenburg, 1987; Muthukrishnaiah, 1989; Gatmiri, 1990).

Putnam (1949) assumed that the pressure variation at the sea bottom due to wave motion induces currents in the permeable layer, and that these currents in turn dissipate some of the mechanical energy of the waves. The analysis, required to estimate the energy loss due to flow of water into and out of the permeable seabed as the pressure varies about the mean hydrostatic pressure, was based upon the following assumptions:

- the sea bottom is horizontal and the permeable material has uniform permeability,
- the permeable material does not move,
- the water motion is two-dimensional,
- viscous flow prevails in the permeable material (Darcy's law is applicable),
- the pore fluid is incompressible,
- the problem is a potential flow problem.

The above assumptions imply that Putnam (1949) investigated transient Darcy's law for flow in a homogeneous, inelastic (rigid) and isotropic soil due to monochromatic wave-induced pressure fluctuations travelling along the sea bottom. The assumptions of incompressible water and a non-deformable grain skeleton in the seabed was also the basis of investigations made by Reid & Kajiura (1957), and Liu (1973). Under this assumption, the application of Darcy's law leads to the potential equation, described by the Laplace equation, for variations of the pore water pressure in the seabed:

$$\Delta p \doteq \nabla^2 p \doteq \frac{\partial^2 p}{\partial x^2} + \frac{\partial^2 p}{\partial z^2} = 0 \tag{2.1}$$

where: Δp - laplacian of p-function,
∇ - Hamilton's operator (also called the nabla),
p - wave-induced pore (water) pressure [kPa],
x, z - horizontal and vertical coordinates of the Cartesian coordinates system, respectively, [m].

Sleath (1970) and Moshagen & Tørum (1975) presented the solution of the above problem in a seabed of finite depth when linear and unidirectional waves pass over it, in the absence of any sea structure.

The problem of damping of small amplitude gravity waves propagating over a permeable seabed was also the subject of investigations made by Hunt (1959) in terms of the viscous-flow theory. Murray (1965), using the same theory but for different boundary conditions at the seabed surface, obtained a complete solution with accordingly different results when compared with Hunt (1959).

The preceeding analyses were all based on the assumption of incompressible pore water and soil skeleton and with the flow in the porous seabed governed by Darcy's law. In this case, if the seabed is isotropic in permeability, the pore pressure is governed by the Laplace equation and independent of the permeability of the seabed. The solution developed by Moshagen & Tørum (1975) was based upon the potential theory whilst the main assumption for the theoretical model of the seabed response was that the pore water is compressible (compressibility of pore water is mainly due to inclusion of small amount of air into the water; the pore water is then practically two-phase medium and, in order to make a distinction with respect to the pure water, is called the pore fluid), and that the seabed material is anisotropic (with respect to soil permeability) with a completely rigid grain skeleton. The flow in the seabed was considered to be two-dimensional and in Darcy's law range, while the soil was assumed to be fully or partly saturated. Under these assumptions, the governing equation for the pore pressure in seabed sediments becomes the diffusion equation (also known as the consolidation equation or the heat conduction equation) which for the case of isotropic permeability conditions can be written as:

$$\frac{\partial^2 p}{\partial x^2} + \frac{\partial^2 p}{\partial z^2} = \frac{1}{c_d} \frac{\partial p}{\partial t} \tag{2.2}$$

where, additionally:
p - wave-induced pore (fluid) pressure [kPa],
c_d - coefficient of diffusion [m^2/s],
t - time [s].

The coefficient of diffusion depends on the porosity and permeability of soil as well as the unit weight and the compressibility (inverse of the bulk modulus) of pore fluid according to the following formula:

$$c_d = \frac{kn\beta'}{\gamma} \tag{2.3}$$

where: c_d - coefficient of diffusion [m^2/s],
k - coefficient of permeability for isotropic soil [m/s],

n - porosity of soil [-],
β' - compressibility of pore fluid ($\beta' = 1/K'$) [m^2/kN],
K' - bulk modulus of pore fluid [kPa],
γ - unit weight of pore fluid ($\gamma = \rho g$) [kN/m^3],
ρ - density of pore fluid [Mg/m^3],
g - acceleration due to gravity [m/s^2].

Moshagen & Tørum (1975) found that the inclusion of pore fluid compressibility in the analysis of wave-induced pore pressures in a porous soil altered significantly the vertical seepage forces acting on the soil.

A similar conclusion can be drawn from the proposition made by Prevost *et al.* (1975). They pointed out that the assumption made by Moshagen & Tørum (1975), regarding the relative compressibilities of the pore fluid and the soil skeleton, appears somewhat unrealistic and therefore they suggested to treat the soil as compressible and the pore fluid as incompressible. For a soil of low permeability, they presented a simple solution for the pore pressure distribution which was showed to be identical with the solution obtained from the analysis based on incompressible pore fluid and soil skeleton. This can only certify a minor sensitivity of the solution for pore pressure on the compressibility of soil skeleton, especially when a dense and very dense state of soil is assumed. An incompressible pore fluid (*i.e.*, pore water), however, forms the assumption which is hardly to believe and far away from reality.

Nakamura *et al.* (1973), similar to Moshagen & Tørum (1975), treated again the seabed as a rigid permeable porous medium whilst the water was assumed to be compressible. These assumptions lead again to an equation for the pore pressure in the same form as that of the diffusion equation.

Massel (1976) considered analytically the case of propagation of gravity waves over a permeable bottom, assuming laminar transition of turbulent flow, pore fluid compressibility and soil skeleton consolidation. Taking into account the non-linear damping and the inertia term in the momentum equation in place of Darcy's law for a rigid porous bed, it was concluded that the influence of the permeability on the pressure distribution in both sea and seabed is negligibly small and that the result is essentially the same as that from the Laplace equation.

For many purposes in soil mechanics, it is permissible to uncouple the soil solid part (*i.e.*, soil skeleton) and the fluid part of any analysis in order to treat them separately. However, it may also be desirable on occasion to analyse the true coupled performance of a composite continuum, in which the two phases interact. Examples of practical importance would involve external loads which vary in time, and structure-foundation interaction analyses where the generation of foundation pore pressure is completely dependent upon the relative stiffness of the components of the system. That is, a stiff or inhomogeneous structure causes different pore pressures from a flexible or homogeneous one.

In many practical problems appeared in the coastal engineering, there are many subsoil stratifications and hydrotechnical structures that can be treated as vertically two-dimensional. Assuming also that the seabed is loaded by harmonic waves characterized by long crests parallel to each other, then as a result the seabed is deformed under plain strain conditions. Under these conditions, the following two equations, describing elastic deformations of the soil skeleton, together with the so-called storage equation constitute the coupled problem and can be written as:

$$G\left(\frac{\partial^2 u_x}{\partial x^2}+\frac{\partial^2 u_x}{\partial z^2}\right)+\frac{G}{1-2\nu}\frac{\partial}{\partial x}\left(\frac{\partial u_x}{\partial x}+\frac{\partial u_z}{\partial z}\right)=\frac{\partial p}{\partial x} \tag{2.4a}$$

$$G\left(\frac{\partial^2 u_z}{\partial x^2}+\frac{\partial^2 u_z}{\partial z^2}\right)+\frac{G}{1-2\nu}\frac{\partial}{\partial z}\left(\frac{\partial u_x}{\partial x}+\frac{\partial u_z}{\partial z}\right)=\frac{\partial p}{\partial z} \tag{2.4b}$$

$$\frac{k_x}{k_z}\frac{\partial^2 p}{\partial x^2}+\frac{\partial^2 p}{\partial z^2}-\frac{\gamma n\beta'}{k_z}\frac{\partial p}{\partial t}=\frac{\gamma}{k_z}\left(\frac{\partial u_x}{\partial x}+\frac{\partial u_z}{\partial z}\right) \tag{2.4c}$$

where: p - wave-induced pore pressure [kPa],
u_x, u_z - soil displacements in x- and z-direction, respectively, [m],
G - shear modulus for isotropic soil [kPa],
ν - Poisson's ratio for isotropic soil [-],
k_x, k_z - coefficients of soil permeability in x- and z-direction, respec., [m/s],
γ - unit weight of pore fluid [kN/m^3],
β' - compressibility of pore fluid [m^2/kN],
n - porosity of soil [-],
t - time [s],
x, z - horizontal and vertical coordinates of the Cartesian coordinates system, respectively, [m].

The first Eq. (2.4a) is formed from the equilibrium condition in the x-direction, the second Eq. (2.4b) is formed from the equilibrium condition in the z-direction, and the third Eq. (2.4c) comes from the continuity principles incorporating Darcy's law of fluid flow through a porous medium. The last equation assumes anisotropic conditions as far as the soil permeability is concerned. Assuming an isotropic permeability, however, Eq. (2.4c) can be written in the following simplified form:

$$\beta' n\frac{\partial p}{\partial t}+\frac{\partial}{\partial t}\left(\frac{\partial u_x}{\partial x}+\frac{\partial u_z}{\partial z}\right)=\frac{k}{\gamma}\left(\frac{\partial^2 p}{\partial x^2}+\frac{\partial^2 p}{\partial z^2}\right) \tag{2.4d}$$

where, additionally:
k - coefficient of permeability for isotropic soil [m/s].

The problem of response of the seabed to water waves was the subject of a number of papers published by Yamamoto (1977, 1981, 1983) and Yamamoto *et al.* (1978). The solution presented concerns a poro-elastic seabed whilst the proposed model is based on the three-dimensional consolidation theory developed by Biot (1941). The soil skeleton obeys Hook's law, *i.e.* the soil has linear, reversible, isotropic, and non-retarded mechanical properties. The movement of the pore fluid is assumed to obey Darcy's law.

A solution based on similar assumptions to those introduced by Yamamoto (1977) was presented by Madsen (1978) who also adopted the governing equation, for flow of a compressible fluid in a homogeneous compressible porous medium, in the form of the consolidation equation of Biot (1941) or storage equation given by Verruijt (1969). The pore pressure and effective stresses are assumed to be induced by a plane progressive wave described by the linear wave theory, although it is stated that the general solution for a progressive wave may be readily extended to non-linear progressive plane waves or to random ocean waves by employing the principle of superposition, thanks to the assumption of the linear elastic behaviour of the seabed sediment. The flow in the porous bed is assumed to be governed by Darcy's law for an anisotropic property of permeability of the medium.

Yamamoto *et al.* (1978) indicated theoretically that the seabed response to waves is strongly dependent on the permeability, the stiffness of the porous medium, and the compressibility of the pore fluid. The earlier solutions for the pore pressure response by various authors are given as the limiting cases of the solution presented by Yamamoto *et al.* (1978). The theoretical values calculated from their theory lie between the solutions of the Laplace equation by Putnam (1949) and the diffusion equation by Nakamura *et al.* (1973) and Moshagen & Tørum (1975).

Madsen (1978) and Yamamoto *et al.* (1978) employed Biot's consolidation equations for the pore pressure and effective stresses in a plane poro-elastic seabed and obtained analytical solutions. Since their final governing equation was a linear partial differential equation of the 6^{th} order, it was rather complex to visualize the physical meaning of the solutions, which were represented in terms of the pore pressure and the displacement components. Okusa ($1985^{(a)}$) solved the problem of the wave-induced pore pressure and effective stresses in a poro-elastic sediment, using the compatibility equation under elastic conditions. All assumptions are the same as in Madsen's (1978) theory. The only difference is that the governing equation has been reduced to a linear partial differential equation of the 4^{th} order which helped more clear understanding the physical meaning of the solution. In deriving the governing equations for partly saturated sediments the conventional assumptions employed in Biot's theory have been used with the following additions:

- the water and gas phases within the sediment can be considered as a single compressible fluid,
- the effects of gas diffusing through water and the movement of water vapour are ignored,
- the effective stress principle is unchanged from the normal definition for fully saturated soils.

Okusa ($1985^{(a)}$) discussed also a problem of the phase lag (also called the time shift) phenomenon existing in a gas-laden sediment for the wave-induced pore pressure and stresses.

Mei & Foda (1980) showed that the boundary layer approximation, well-known in fluid mechanics, greatly facilitates the solution of Biots's equation for a variety of boundary conditions. For sufficiently high frequencies, typical for ocean and seismic waves, a boundary layer of Stokes' type was shown to exist near the free surface of the solid. Outside the boundary layer, fluid and the solid skeleton move together according to the laws of classical elasticity for a single phase. In the vicinity of the seabed surface, however, the pore fluid has more freedom in flowing into and out of the soil skeleton and, thereby, the difference in movement velocities of the two phases exists. This division simplifies the analysis of the equations governing the two phases.

In order to estimate the influence of certain parameters on the pore pressure solution, a simple analytical approximation has been obtained by Verruijt (1980). The solutions presented for wave-induced pressures in the seabed are based on either one of the following three assumptions for soils:

- the seabed soils are rigid and non-deformable,
- the seabed soils are an elastic continuum and no water is present within the soils,
- the seabed soils are poro-elastic (governed by Biot's three-dimensional consolidation theory which takes into account soil deformations, volume change, and pore fluid flow).

Similarly, for the kinematics of the sea, different wave theories were chosen (*e.g.*, Airy's wave linear theory, Stokes' wave theory, cnoidal wave theory, and solitary wave theory). Considering that the seabed soils are subjected to complex three-dimensional stress-strain histories involving cycles of loading, unloading and subsequent reloading, Verruijt (1969) concluded that the above mentioned three soil models may not, due to their basic assumptions, be adequate to cope with such complex cyclic histories. This may indicate that for this case, a poro elastic-plastic model could be introduced which would allow a proper description of the stress-strain properties of saturated soils subjected to cyclic loading paths.

Spierenburg (1987) modelled the effect of a layered soil system, in which a permeable soil layer of a finite thickness overlaying a stiff impermeable base was considered as the extreme of a layered seabed. He presented two methods of solution for the response of a finite layer to water waves. In the first method the problem is treated analytically by solving the partial differential equations to derive a general solution. The second method is based on a variational principle, in which the problem is formulated by an integral that replaces the set of basic differential equations. It was shown by Spierenburg (1987) that this approximation technique is only appropriate for relatively thin layers when the ratio of the permeable layer thickness to the wavelength, d/L, is less than $1/(2\pi)$.

Nago & Maeno (1987) investigated the behaviour of pore pressure and effective stress in a near-saturated sand bed under variations in the water pressure on its surface. The vertical one-dimensional analytical model, suitable to handle the important question of the finite thickness of permeable sand layer, was verified by experiments. Nago & Maeno (1987) pointed out that the most important factor in the whole investigated phenomenon seems to be a small amount of air present in the sand bed.

The wave-induced pore pressure and effective stresses in partly saturated submarine sediments were treated not only analytically but also by means of the finite element method (FEM). By using the general theory of behaviour of the saturated poro-elastic media (Biot, 1941), and its simplified formulation, the well-known equations of consolidation were obtained by Gatmiri (1990) who made a comparative study with the infinite depth solution given by Yamamoto *et al.* (1978) and Madsen (1978), investigating the effects of seabed thickness, permeability and soil stiffness on the wave-induced pore pressures, effective normal stresses, shear stresses, horizontal and vertical displacement at the mud line and with depth in the seabed.

A similar approach was presented by Nago & Maeno (1984), who developed the theoretical method to analyse the pore pressures in the sandy seabed under the oscillating surface water pressure. The derived fundamental equations for the general three-dimensional model of sand layer under the oscillating water pressure were treated numerically (FEM) and verified by experiments for the two-dimensional problems. In their theoretical treatment, Nago & Maeno (1984) assumed that:

- the sandy seabed is composed of three phases, *i.e.*: sand grains, water and air; the porosity of water-air system is the sum of two parts made up of water and air,
- the sandy seabed is near-saturated, *i.e.* the amount of air present is considered to be very small in comparison to the total volume of the porous part,
- the sandy seabed skeleton is deformed in accordance with Hooke's law, but the deformation of sand grains themselves is negligible,
- the density of water changes with the compressibility of water,
- the volume of air changes in accordance with Boyle's law,
- the pore water moves in accordance with Darcy's law.

A comparison of important assumptions, related to the soil and pore fluid parameters, obtained from some of the main pore pressure theories reviewed above, is presented in a tabular form (Tab. 2.1).

Table 2.1
Comparison of main assumptions in different theories describing wave-induced pore pressure oscillations in seabed sediments

Assumptions / Author(s)	Soil skeleton				Pore fluid	
	Incompressible	Compressible	Permeability		Incompressible	Compressible
			Isotropic	Anisotropic		
Putnam (1949)	•		•		•	
Reid & Kajiura (1957)	•		•		•	
Sleath (1970)	•			•	•	
Liu (1973)	•		•		•	
Moshagen & Tørum (1975)	•			•		•
Madsen (1978)		•		•		•
Yamamoto *et al.* (1978)		•	•			•
Nago & Maeno (1984)		•	•			•
Okusa (1985)		•	•			•

2.1.1 Character of the wave-induced pore pressure solution

The problem considered in the present work is two-dimensional. A homogeneous and isotropic sediment layer of a constant thickness, d, underlaid by a rigid and impermeable base, is assumed. The x-axis is taken on the horizontal seabed surface and the positive direction of the z-axis is taken vertically downwards from the seabed surface. Regular long-crested progressive waves are propagating from left to right on a constant water depth h (Fig. 2.1).

At the top of the seabed, the pressure fluctuations follow the movement of surface waves. Therefore, the pressure at the seabed surface (so-called the hydrodynamic bottom pressure) is assumed to be periodic. Its value may be measured (*in-situ* or in a laboratory experiment), or determined by a higher-order wave theories. In any event, the periodic signal can be expanded in a Fourier series and it is, therefore, sufficient to study a singular sinusoidal fluctuation. Assuming the soil skeleton response to be governed by the linear theory of elasticity, the final result, related to the wave-induced soil displacements, soil stresses, and pore pressure, can be always easily achieved by a simple superposition of the results obtained for a series of singular sinusoidal oscillations of the surface wave loading.

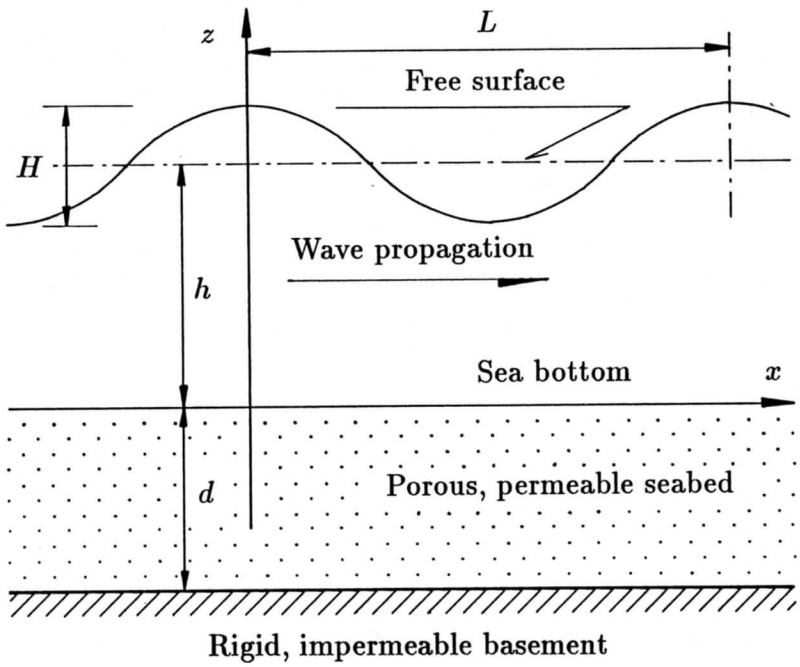

Figure 2.1 Definition sketch for the wave-induced pore pressure analysis

Above the surface of the seabed, it is assumed that the wave loading (forcing or inducing function) is travelling in the form of a two-dimensional harmonic wave (*e.g.*, propagating sinusoidal surface wave):

$$z = -(h + \eta_w) = -\left[h + \frac{H}{2}\cos(ax - \omega t)\right] \tag{2.5}$$

where: η_w - water surface elevation, with respect to the still water level, [m],
h - water depth [m],
H - wave height [m],
a - wave number ($a = 2\pi/L$) [m^{-1}],
L - wavelength [m],
ω - wave angular frequency ($\omega = 2\pi/T$) [s^{-1}],
T - wave period [s],
t - time [s],
x, z - horizontal and vertical coordinates of the Cartesian coordinates system [m].

Resulting from the surface wave oscillation, the hydrodynamic bottom pressure oscillation, derived from Airy's linear wave theory, is given as:

$$p_b = P_0 \cos(ax - \omega t) \tag{2.6}$$

with

$$P_0 = \frac{H}{2}\gamma_w \frac{1}{\cosh(ah)} \tag{2.7}$$

where, additionally:
p_b - hydrodynamic bottom pressure [kPa],

P_0 - amplitude of the hydrodynamic bottom pressure [kPa],
γ_w - unit weight of water [kN/m^3].

Since all the above mentioned investigators assumed that the loading boundary condition is periodic in both time and horizontal space, it is reasonable to assume that the solution sought is a steady state (periodic) solution, and the dependent variables (*i.e.*, both the soil displacements and the pore pressure) can be expressed in terms of periodic functions in time, with the same frequency ω, and in space, with the same wave number a.

For the convenience, especially in mathematical descriptions of the problems where a relative compressibility of the two-phase seabed medium is assumed, the use of complex variables was introduced. It is understood that only the real part of the complex solution has a physical meaning, and is to be considered the solution to the problem at hand. In the following it is implicitly assumed that only the real part of any complex solution constitutes a solution to a given problem. Additionally, if there is a complex variable appearing in any equation given in the following, the unit given after the explanation of this complex variable in the equation legend will always pertain to the real part and the imaginary part of the complex variable, and must not be related with the complex variable as a whole.

Taking the above into account, the surface wave motion equation [see Eq. (2.5)], and the wave-induced boundary condition imposed at the surface of the porous seabed [Eq. (2.6)], can be respectively presented in terms of complex variables as:

$$\eta_w = \frac{H}{2}\Re\{\exp[i(ax - \omega t)]\} \tag{2.8}$$

and

$$p_b = P_0\Re\{\exp[i(ax - \omega t)]\} \tag{2.9}$$

where, additionally:
$\Re\{\ \}$ - denotes a real part of $\{\ \}$,
i - imaginary unit ($i = \sqrt{-1}$).

If it is assumed that the harmonic wave loading is the dominant loading flow, then under poro-elastic conditions, it can also be assumed that any particular variable ϕ (representing either the hydrodynamic bottom pressure, or wave-induced soil displacement, or wave-induced pore pressure), which is dependent on x, z and t, can be given in the complex-valued trigonometric form as:

$$\phi(x,z,t) = \tilde{\phi}(z)[\cos(ax - \omega t) + i\sin(ax - \omega t)] \tag{2.10}$$

which can be also written, for convenience, in the exponential form as:

$$\phi(x,z,t) = \tilde{\phi}(z)\exp[i(ax - \omega t)] \tag{2.11}$$

where, additionally:
ϕ - arbitrary harmonic function (complex-valued), dependent on x, z and t,
$\tilde{\phi}$ - arbitrary function (complex-valued), related to ϕ-function and dependent on z only.

The introduction of complex variables was allowed because of the linearity of the governing equations used by the authors of the pore pressure theories. This suggested

also that all variables will depend on x and t in the form given by the forcing function, *i.e.*, $\exp[i(ax - \omega t)]$. This greatly facilitated the subsequent analysis since the differentiation of any variable with respect to x or t reduced to the variable itself multiplied by (ia) or $(-\omega t)$, respectively.

Consequently, the wave-induced soil displacements and pore pressure may be written in the form:

$$u_x(x,z,t) = \tilde{u}_x(z)\exp[i(ax - \omega t)] \tag{2.12a}$$

$$u_z(x,z,t) = \tilde{u}_z(z)\exp[i(ax - \omega t)] \tag{2.12b}$$

$$p(x,z,t) = \tilde{p}(z)\exp[i(ax - \omega t)] \tag{2.12c}$$

where: u_x - horizontal (*i.e.*, in x-direction) displacement of soil (complex-valued), dependent on x, z and t, [m],
$\tilde{u}_x$ - horizontal displacement of soil (complex-valued), dependent on z only, [m],
u_z - vertical (*i.e.*, in z-direction) displacement of soil (complex-valued), dependent on x, z and t, [m],
$\tilde{u}_z$ - vertical displacement of soil (complex-valued), dependent on z only, [m],
p - wave-induced pore pressure (complex-valued), dependent on x, z and t, [kPa],
$\tilde{p}$ - wave-induced pore pressure (complex-valued), dependent on z, [kPa],
a - wave number [m^{-1}],
ω - wave angular frequency [s^{-1}],
t - time [s],
x, z - horizontal and vertical coordinates of the Cartesian coordinates system, respectively, [m],
i - imaginary unit.

Equations (2.12a) to (2.12c) give the complex-valued solutions. A momentary (*i.e.*, for an arbitraty time-point denoted by t) value of the wave-induced pore pressure, for example, in the permeable seabed layer (for any arbitrary point in space, denoted by x and z), can be easily obtained by extracting a real part from the complex-valued pore pressure solution:

$$p' = \Re\{p\} \tag{2.13}$$

where: p' - wave-induced pore pressure (real-valued) [kPa],
p - wave-induced pore pressure (complex-valued) [kPa],
$\Re\{\ \}$ - denotes a real part of $\{\ \}$.

Taking the properties of complex variables into account (Fig. 2.2), there is also another method of presentation of the wave-induced pore pressure solution, namely in terms of two characteristic parameters, *i.e.*: the amplitude and the phase lag (also called the time shift) of pore pressure oscillations:

$$P = |p| = \sqrt{(\Re\{p\})^2 + (\Im\{p\})^2} \tag{2.14a}$$

$$\delta = \arctan\left(\frac{\Im\{p\}}{\Re\{p\}}\right) \tag{2.14b}$$

where: P - amplitude of the wave-induced pore pressure [kPa],
$|p|$ - modulus of the complex-valued wave-induced pore pressure [kPa],
δ - phase lag of the wave-induced pore pressure oscillations [rad],
p - wave-induced pore pressure (complex-valued) [kPa],
$\Re\{\ \}$ - denotes a real part of $\{\ \}$,
$\Im\{\ \}$ - denotes an imaginary part of $\{\ \}$.

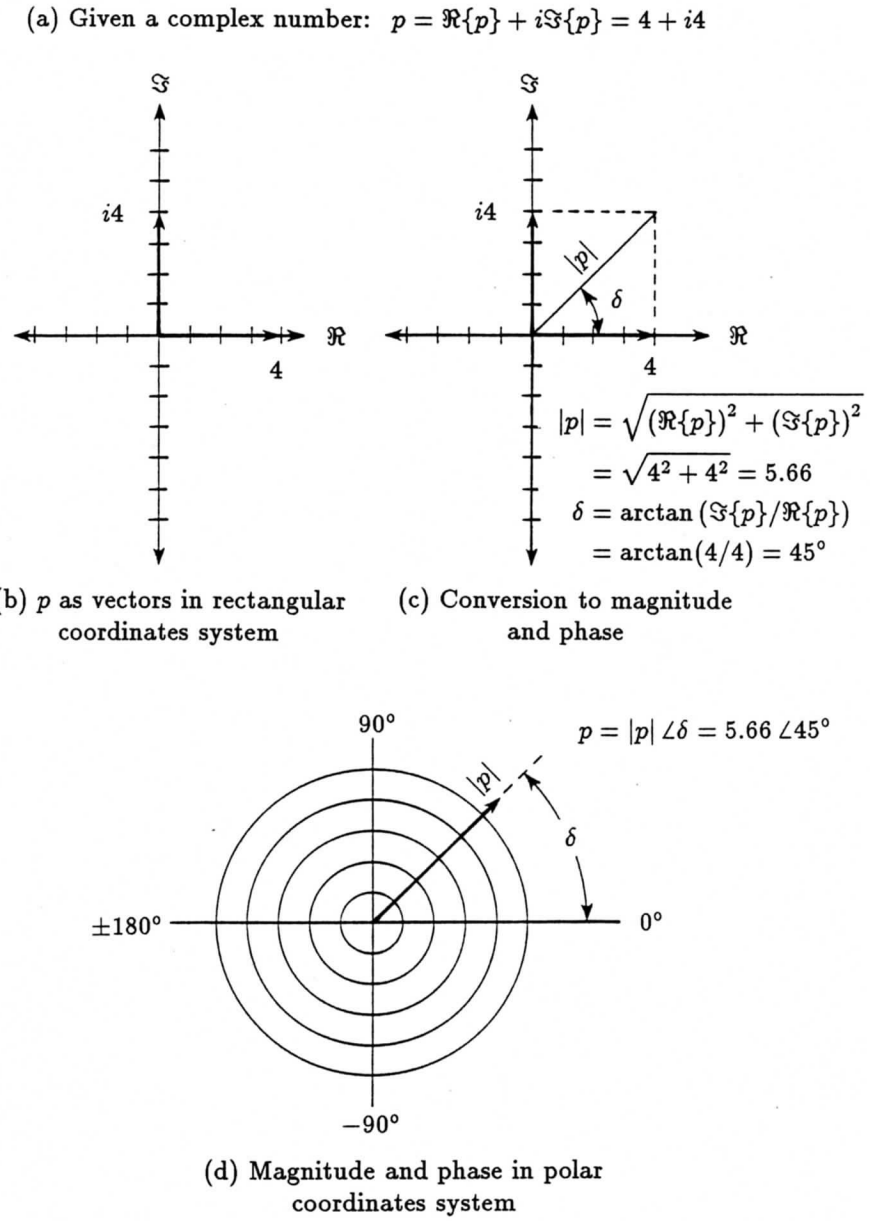

Figure 2.2 Complex number expressed in rectangular and polar form [Ramirez, 1985]

The amplitude, P, and the phase lag, δ, of the wave-induced pore pressure oscillations constitute entirely the wave-induced pore pressure solution. The both of these parameters are independent of x and t, being funcions of z only. A proper combination of these two parameters allows to present a momentary value of the wave-induced pore pressure in the permeable seabed layer, using – this time – a real-valued variables only. And thus:

$$p' = P\cos(ax - \omega t + \delta) \tag{2.15}$$

where: p' - wave-induced pore pressure (real-valued) [kPa],
P - amplitude of the wave-induced pore pressure [kPa],
δ - phase lag of the wave-induced pore pressure oscillations [rad],
a - wave number [m^{-1}],
ω - wave angular frequency [s^{-1}],
t - time [s],
x - horizontal coordinate of the Cartesian coordinates system [m].

For simplicity and convenience of presentation of pore pressure results, the momentary value, p', and the amplitude, P, of the wave-induced pore pressure oscillations, are very often given in relative and dimensionless forms obtained by dividing them by the amplitude of the hydrodynamic bottom pressure, P_0. Denoting the new relative and dimensionless parameters by a super-imposed 'bar', one obtains:

$$\bar{p} = \frac{p'}{P_0} \tag{2.16a}$$

$$\bar{P} = \frac{P}{P_0} \tag{2.16b}$$

where: $\bar{p}$ - relative (and dimensionless) wave-induced pore pressure [-],
$\bar{P}$ - relative (and dimensionless) amplitude of the wave-induced pore pressure [-],
p' - wave-induced pore pressure (real-valued) [kPa],
P - amplitude of the wave-induced pore pressure [kPa],
P_0 - amplitude of the hydrodynamic bottom pressure [kPa].

Yamamoto *et al.* (1978) presented general solutions for vertical and horizontal displacements of the soil skeleton and pore pressure in a semi-infinite (half-space) domain. It is interesting to note that the solution for the response in a fully saturated seabed under undrained conditions is the same as that obtained by Putnam (1949) who assumed that soil is rigid and the water is incompressible. The solutions for the pore pressure, soil displacements, and soil stress components in a fully saturated and semi-infinite seabed (*i.e.*, of infinite thickness) can be written as (Yamamoto *et al.*, 1978):

$$p = P_0 \exp(-az)\exp[i(ax - \omega t)] \tag{2.17a}$$

$$u_x = -iaz\exp(-az)\frac{P_0}{2aG}\exp[i(ax - \omega t)] \tag{2.17b}$$

$$u_z = (1 + az)\exp(-az)\frac{P_0}{2aG}\exp[i(ax - \omega t)] \tag{2.17c}$$

$$\sigma'_x = -\sigma'_z = P_0 az\exp(-az)\exp[i(ax - \omega t)] \tag{2.17d}$$

$$\tau' = -\frac{1}{i}P_0 az\exp(-az)\exp[i(ax - \omega t)] \tag{2.17e}$$

where: p - wave-induced pore pressure (complex-valued) [kPa],
u_x - horizontal displacement of soil (complex-valued) [m],
u_z - vertical displacement of soil (complex-valued) [m],
σ'_x - horizontal effective normal stresses (complex-valued) [kPa],
σ'_z - vertical effective normal stresses (complex-valued) [kPa],
τ' - effective shear stress (complex-valued) [kPa],
G - shear modulus for isotropic soil [kPa].

2.2 Experimental verifications

Besides the numerous theoretical solutions (from quite simplified to more advanced) for the wave-induced pore pressure prediction, the published laboratory and field data are very scare, while all experimental investigations can be divided into two groups, namely: site investigations and laboratory tests.

Cross *et al.* (1979) investigated wave-induced pore pressures in the near-shore fine sand seabed by means of a vertical piezometer. The theoretical relationship developed by Putnam (1949) is reported to predict adequately the magnitude of wave-induced pore pressure and their attenuation with depth below the seafloor. An agreement was also found by Sleath (1970) who introduced different permeabilities in the vertical and horizontal directions.

In a laboratory study on the stability of buried pipelines, Phillips *et al.* (1979) concluded that the potential theory did not generally give an accurate representation of the transmission of wave-induced pressures through the sand when compared to their test results. Their tests indicated also that the theoretical prediction made by Moshagen & Tørum (1975) overestimates the magnitude of the pore pressure response, and underestimates the actual phase lag in pressure transmission through the soil as a function of depth. This discrepancy between theoretical and measured values indicates above all that the assumption concerning rigidity of the soil structure was inaccurate.

Dunlap *et al.* (1978), Bennett & Faris (1979), and Cross *et al.* (1979) have presented the results of experiments on the pore pressure generation in the sediments of Mississippi and coastal zone of Pacific. However, they are mainly related to the long-term changes. The relation of the observed pressure to the surface oscillations was not considered.

Massel & Kaczmarek (1988) reported a study of pore pressure behaviour in a natural sandy seabed in the coastal zone of the Baltic Sea. The pore pressure attenuation was measured at several levels in the porous medium under the wind waves action. The collected data were used to analyse the problem from the statistical and spectral point of view. The comparison of experimental data with various theoretical solutions demonstrated that the boundary layer approximation by Mei & Foda (1980) and the solution by Yamamoto *et al.* (1978) properly reflect the observed physical mechanism.

In 1988 and 1989 the Soil Mechanics Group at the University in Oxford made many visits to five UK coastline locations in order to carry out measurements of wave- and tide-induced pore pressures (Thomas, 1991). The results of measurements showed that there is a higher degree of wave amplitude reduction with depth for the short-period waves than for those of long-period waves. The observed pore pressure response was also quantified. During this research, in order to analyse the arbitrary pressure waves, the Discrete Fourier Transform analysis was applied to each wave in turn. This procedure separated out each wave into a spectum of sinusoidal waves over a range of wave periods. Using both the analytical solution of Yamamoto *et al.* (1978) and their own mathematical model, an excellent comparison between theory and practice in Geotechnical Engineering was pointed out.

Okusa (1985[b]) carried out wave-induced pore pressure measurements at four sites around Shimizu Harbour, Central Japan. According to his observations the measured pore pressures in seabed sediments decrease faster than the predicted ones for fully saturated sediments. The existence of pore gas in the sediment or other damping mechanisms are mentioned to be required to explain the observed phenomenon.

Yamamoto *et al.* (1978) compared the theoretical results with wave tank experimental data on pore pressure in coarse and fine sand beds which were described to contain a small amount of air. An agreement between the theory and the experiment was estimated as a good one which indicated that, according to the theoretical assumptions, the seabed response to waves is strongly influenced by the permeability and the stiffness of the soil. The data for coarse sand showed practically no phase lag and were in a very good accordance with the theoretical values determined by the solution of the Laplace equation for finite thickness given by Putnam (1949). The comparison of measured data with the previously proposed theories is concluded that none of these theories are adequate for predicting the wave-induced pore pressure cyclic oscillations in the fine sand. The potential solution by Putnam (1949) predicts a much more smaller pressure attenuation with depth in the seabed, comparing to the solution of the diffusion equation given by Moshagen & Tørum (1975) and Nakamura *et al.* (1973). A direct determination of the soil-water-air mixture parameters (*e.g.*, soil permeability, degree of saturation) was not made in tests performed by Yamamoto *et al.* (1978), so that direct comparisons between their theory and the experiments could not be done.

Tsui & Helfrich (1983) presented results of measured wave-induced pore pressures in a model sand layer. Their report is probably one of the best from all the published information because the test preparation and execution procedure are documented very clearly and in detail. It is stated that the measured pressures varied with the wave height and period, sand layer thickness, and sand density. For short-period waves, measured pressures compare well with theoretical (Stokes' 2^{nd} order wave theory) pressures on the surface of the sand layer. Measured pressures were greater than theoretical when the model wave period was greater than 1.7 s. Pressures within a sand layer were observed to decrease more rapidly with depth than predicted by many of the published pore pressure theories. The existence of the pore pressure phase lag was also found, however, this phenomenon was reported to be not well-understood.

A similar study was made by McDougal & Sollitt (1984) where large-scale laboratory experiments were conducted to validate Biot's consolidation model for cyclic loading of layered seabeds. A horizontal layered soil system was modelled with an impermeable bottom, fine sand lower layer, geotextile between layers and gravel surface layer. Vertical pressure profile measurements demonstrated a hyperbolic decay of pressure amplitude with depth in accordance with Biot's theory. Results were shown to be linearly proportional to wave amplitude. Increased pressure attenuation with depth was observed with increasing wave frequency.

Demars & Vanover (1985) examined experimentally the effects of water wave loading on the pressure and stress distributions within a sandy seabed model in a laboratory wave tank. They proved that the potential theory acurately predicted wave-induced pore pressures in a stiff, fully saturated and permeable sandbed.

Chari *et al.* (1987) reported results of experiments in a soil wave tank in which the pore pressure variation profile inside a porous seabed of sand was measured for different wave types. His tests showed that for porous seabed sediments the pore pressure developed below the mudline is the major factor causing the instability. Using storm wave conditions, shallow slope failures of 2 to 3 m depth were indicated to be likely to happen on underwater seabed slopes with an inclination of 10 %.

Muthukrishnaiah (1989) confirmed the observation of Tsui & Helfrich (1983) that the density, porosity, and permeability of the soil have a very significant influence on the wave-induced pore pressure which Putnam's (1949) theory completely ignores.

2.3 Conclusions

Many theories, describing the wave-induced pore pressure cyclic oscillations in sandy seabed sediments have been derived and published. Among them, there are theories which are simple from the mathematical point of view [*e.g.*, the potential theory by Putnam (1949)], being based on the assumptions of incompressible pore fluid and soil skeleton. These rigorous assumptions are far away from the realistic conditions of the soil and pore fluid two-phase medium. The above presented review showed that all simplified theories are mostly extreme cases of more advanced theories and have to be treated only as approximating methods. Others, more advanced theories (*e.g.*: Yamamoto *et al.*, 1978; Madsen, 1978; Okusa, 1985[a]) seem to be enough developed in order, at least, to describe the governing problem by introducing additional but meaningful parameters, thereby giving a possibility of wide analyses of real soil-water conditions.

There is an evident lack of information on physical sea bottom parameters when site investigations are performed. Only a wave climate is well-recognized and defined in these cases. In some of the available reports, the results are presented where the first measuring point in a vertical profile is located few meters below the seabed surface, omitting thereby the upper part of sediments, from where the information on pore pressure amplitude and phase lag could be of a great interest for many engineering problems.

A short review of some representative laboratory investigations indicates the following remarks:

- in majority, results obtained from tests are reported to be observed and not measured which is a certification for only a qualitative character of conduced tests,
- in few cases a good agreement between measured pore pressures values and those obtained from the potential theory (Putnam, 1949) is proved, but the sand used for experiments was always reported to be stiff and fully saturated,
- authors, mentioning the potential theory (Putnam, 1949) as a good tool for describing the pore pressure distribution with depth, say nothing about the way of the phase lag interpretation (using this theory it is impossible to incorporate the phase lag effect into a mathematical model and to predict its value),
- not all of the soil-water-air mixture (*i.e.*, pore fluid) parameters are given when presenting results of pore pressure measurements; very seldom information on saturation conditions exists – if any, they are described as fully saturated or partly saturated, but not quantified by concise values.

Taking the above into account, the following conclusions can be drawn concerning the aim of further studies:

- a wide range of theoretical descriptions of the governing problem exists; only these theories should be considered which contain soil and pore fluid parameters, importance of which is reported in both theoretical parameter studies and observations from laboratory and site investigations,
- a best-fitting theory must also be adapted to solve problems with boundary conditions typical for laboratory investigations – this requirement is necessary for any comparison between theory and experiment,
- as far as an experiment is concerned, measurements must supply a quantitative picture of the pore pressure oscillations due to wave action to give a precise answer on a possible application of a certain pore pressure theory into many different practical engineering problems.

Chapter 3

Properties of the soil-water-air three-phase medium

3.1 Soil skeleton

3.1.1 Saturated and partly saturated soil

Soil is composed of solid particles with intervening spaces. As shown in Fig. 3.1, using the nomenclature wide-accepted in soil mechanics, the solid particles of the system are referred to the soil skeleton, and the spaces in the system to the pore spaces, pores, or voids. The pore spaces are usually filled with water and air. A soil in which the pore spaces are completely filled with water is called fully saturated, or simply – saturated. If any gas (*e.g.*, air) is present in the pore spaces, the soil is used to be called partly saturated, or simply – near-saturated. For convenience, and in order to distinguish between a pure water and a water-gas mixture, the mixture of water and gas is called the pore fluid.

A real soil is a complex multi-phase system. Its properties depend on the size and shape characteristics of the constituent parts, or phases, on their relative volumes and weights, and finally on the interactions between them. A soil medium can be composed of either two or three different phases. In a completely dry soil there are two phases, namely the solid particles and the pore air. A fully saturated soil is also a two-phase medium, being composed of the solid soil particles and the pore water, whereas a partly saturated soil is represented by a three-phase system where the third component is formed by the pore air. All the components of a soil are shown in Fig. 3.2.

3.1.2 Porosity

Porosity and void ratio are used to describe numerically the same quantity, namely, the relative volume of the voids in the soil. The porosity is the ratio of the volume of voids to the total volume of soil (see Fig. 3.2), *i.e.*:

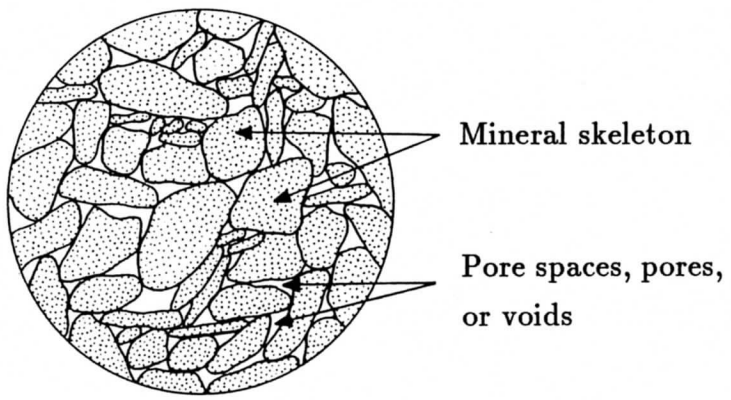

Figure 3.1 Constituents of soil [Dunnicliff, 1988]

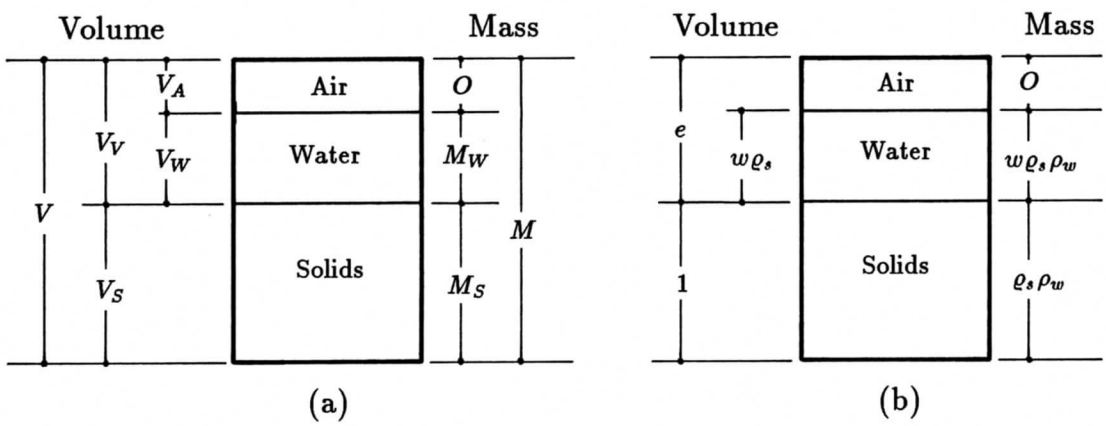

Figure 3.2 Phase diagrams [Craig, 1983]

$$n = \frac{V_v}{V_t} \tag{3.1}$$

where: n - porosity [-],
V_v - volume of voids in soil skeleton [m^3],
V_t - total volume of soil [m^3].

The void ratio is the ratio of the volume of voids to the volume of solids (see Fig. 3.2), *i.e.*:

$$e = \frac{V_v}{V_s} \tag{3.2}$$

where: e - void ratio [-],
V_v - volume of voids in soil skeleton [m^3],
V_s - volume of solids in soil (volume of soil skeleton) [m^3].

The void ratio and the porosity, respectively, are inter-related as follows:

$$e = \frac{n}{1-n} \tag{3.3}$$

$$n = \frac{e}{1+e} \tag{3.4}$$

where: e - void ratio [-],
n - porosity [-].

The only granular system for which porosity can be determined by relatively simple mathematical methods is a package of uniform spheres. In the loosest stable arrangement of equal-sized spheres, when sphere centres from a rectangular space lattice (cubic package) and each sphere is in contact with six neighbourning spheres, the maximum porosity is $n = 0.476$; in the densest state of package, when sphere centres from a rhombohedral array and each sphere is in contact with 12 neighbourning spheres, porosity is $n = 0.259$.

In the case of coarse and medium sand the porosity can vary from 0.4 to 0.45 and from 0.25 to 0.32 for loose and dense state, respectively. Porosities of a uniform fine sand range from 0.45 to 0.48 and from 0.33 to 0.36 for loose and dense state, respectivelly (Kézdi, 1974).

Information on values of porosity for sandy seabed sediments, citied and used by the authors of the formerly mentioned pore pressure theories, is rather coherent. And thus: $n = 0.3$ (Moshagen & Tørum, 1975), $n = 0.4$ (Madsen, 1978; dense sand), $n = 0.3$ (Yamamoto, 1981; North Sea geotechnical design condition), $n = 0.4$ (Nago & Maeno, 1986).

This range of possible values of the soil porosity was confirmed by *in-situ* measurements performed on German coastline of the North Sea (Magda & Davidov, 1990) where the mean from more than 200 sand samples was found to be $n = 0.36$.

3.1.3 Degree of saturation

Soil saturation is quantitatively characterized by the degree of saturation, given in percentage or as a fraction, which is the ratio of the volume of water in the soil to the total volume of void spaces (see Fig. 3.2):

$$S = \frac{V_w}{V_v} \tag{3.5}$$

where: S - degree of saturation [-],
V_w - volume of water in soil pores [m^3],
V_v - volume of voids in soil skeleton [m^3].

The degree of saturation can range between the limits $S = 0$, for a completely dry soil, and $S = 1$, for a fully saturated soil. It is also convenient to introduce additionally the water content definition (also called the moisture content) which is the ratio of the mass of water to the mass of solids in the soil:

$$w = \frac{m_w}{m_s} \tag{3.6}$$

where: w - water content [-],
m_w - mass of water in soil pores [kg],
m_s - mass of solids in soil (mass of soil skeleton) [kg].

The degree of saturation can be now expressed as:

$$S = \frac{w\varrho_s}{e} \tag{3.7}$$

where: S - degree of saturation [-],
w - water content [-],
ϱ_s - specific gravity of solid soil particles [-],
e - void ratio [-].

In order to calculate the degree of saturation, the water content and the void ratio need to be determined by laboratory measurements. Regarding the specific gravity of the solids, the use of the tabulated average values will normally be accurate enough.

Figure 3.3 shows a linear relationship between the degree of saturation, S, and the water content, w, where the range of the degree of saturation for partly saturated soils is divided into four subintervals.

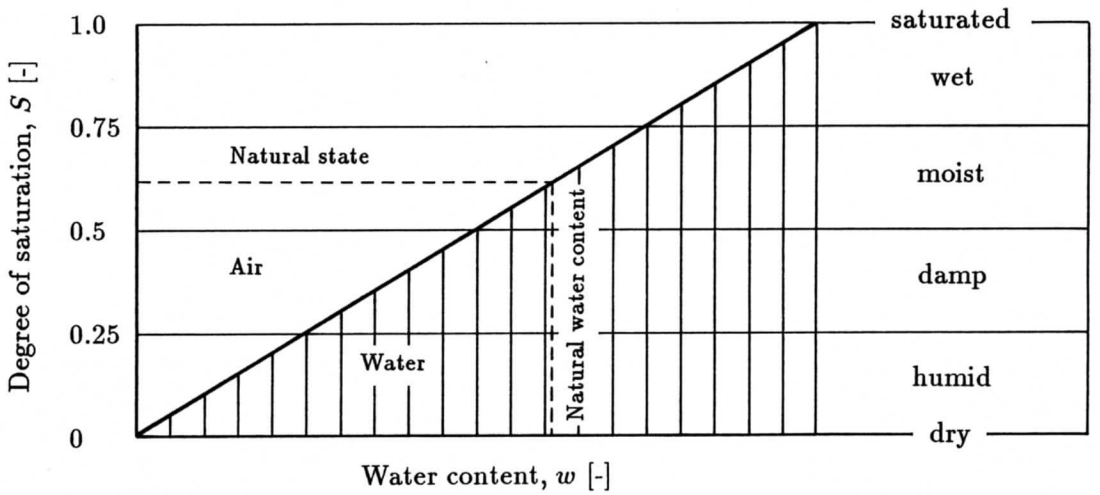

Figure 3.3 Degree of saturation versus water content [Kézdi, 1974]

Saturation conditions are very often desribed by the air content:

$$n_a = n(1 - S) \tag{3.8}$$

where: n_a - porosity of soil occupied by air content [-],
n - porosity of soil [-],
S - degree of saturation [-].

Generally, the determination of the content of air, which is present in the form of small entrapped bubbles dispersed throughout the soil, is very problematic and difficult to perform with a satisfactory accuracy.

As it will be shown in the following, the degree of saturation has a direct influence on the compressibility of pore fluid and, therefore, plays a very important role in the process of the wave-induced pore pressure cyclic oscillations within the sandy seabed. It has a great bearing on many applications in both onshore and offshore engineering.

3.1.3.1 *In-situ* measurements and their statistical analysis

A better knowledge of a real value or possible range of values of the degree of saturation typical for the natural environmental conditions is very needed as an important input parameter for many different mathematical modellings and numerical computations. A well-known characteristic of soil saturation conditions can be also very helpful when performing laboratory investigations and making a comparative analysis of a certain phenomenon observed under both laboratory and natural conditions.

In order to get a better insight into the problem, the measuring campaign was conducted on the sea-side of Norderney Island, located very close to the German coastline of the North Sea (Magda & Davidov, 1990). The main task of the expedition was to perform sampling of the seabed sediment and to gather as much sandy bottom samples as possible for determining the degree of saturation typical for natural environmental conditions. During the expedition, 186 samples of sandy seabed sediments were taken underwater in different phases of the tidal motion (*i.e.*, low tide and high tide). The degree of saturation was calculated using the following practical expresion:

$$S = \frac{\frac{m_{ws}}{V_t} w \varrho_s}{(1+w)\varrho_s \rho_w - \frac{m_{ws}}{V_t}} \tag{3.9}$$

where: S - degree of saturation [-],
m_{ws} - mass of wet soil sample [kg],
V_t - total volume of soil sample [m],
w - water content [-],
ϱ_s - specific gravity of solid soil particles (with respect to the density of pure water) [-],
ρ_w - density of water [kg/m^3].

On the basis of the values measured on Norderney Island, a further data analysis was made using a statistical approach in three common statistical terms, namely: the mean, the standard deviation, and the coefficient of variation.

A representative value for the specific gravity of solid soil particles was found as the mean from 8 samples randomly selected from the whole group of 186 samples, and was equal $\bar{\varrho}_s = 2.66$. Using this value together with other measured values (m_{ws} and w), assuming $\rho_w = 1,020\,\mathrm{kg/m^3}$ for sea water, and applying Eq. (3.9), the mean value of the degree of saturation, for the total group of 186 samples, was found to be $\bar{S} = 0.967$, whereas the standard deviation $\sigma_S = 0.037$.

The coefficient of variation is given as:

$$V_{var} = \frac{\sigma_v}{\bar{v}} \tag{3.10}$$

where: V_{var} - coefficient of variation of random variable **v**, [-],
σ_v - standard deviation of random variable **v**, [the same unit as for **v**],
$\bar{v}$ - mean of random variable **v**, [the same unit as for **v**],

Therefore, the coefficient of variation of the degree of saturation, computed directly on the basis of the measured soil parameters (w and m_{ws}), equals $V_{var}(S) = 0.038$.

The quality of the performed measurements of the wet sample mass, m_{ws}, the water content, w, the specific gravity of solid soil particles, ϱ_s, and the computation of the degree of saturation, S, can be estimated when comparing the coefficient of variation, calculated in the present analysis with values published in the literature.

When rewieving the calculated values of the degree of saturation, it was noticed that some of them (23 from 186 tests, which is 12.37 %) have values higher than 1. From a physical point of view it is impossible to have a degree of saturation $S > 1$, however, from an engineering point of view this result is not so much surprising because of the nature of the testing procedure used and a certain testing variability. Furthermore, rejection of tests that plot above the ZAVL (Zero-Air-Voids-Line; $S = 1$) distorts any statistical findings from the field sampling and may have important engineering and economic consequences (Schmertmann, 1989). On the other hand, values of the degree of saturation $S > 1$ cannot be directly used for the evaluation of the mean of the degree of saturation to characterize average, real soil saturation conditions.

In order to overcome this problem, a statistical analysis of the measured soil parameters can be very useful. By adopting one of the statistical distributions analytically formulated, it becomes possible to calculate the expected percentage of tests which are characterized by computed values of $S > 1$. It appears that the normal (Gaussian) distribution gives the most convinient shape in terms of mathematics. Schmertmann (1989) confirmed also that on the basis of general impressions from his experience and from the literature, as well as from specific comparisons using normal distributions to describe the variability in some soil parameters in tests, acceptable approximations are achieved. The calculations of the normal distribution, performed in the present work, were based on the formulas for:

- the normal probability density function, $f_n(v)$,
- the normal probability distribution function, $P_n(v)$.

A random variable **v** follows the normal distribution if its probability density function is given by (Bendat & Piersol, 1971):

$$f_n(v) = \frac{1}{\sigma_v \sqrt{2\pi}} \exp\left[-\frac{(v-\bar{v})^2}{2\sigma_v^2}\right] \tag{3.11}$$

where: $f_n(v)$ - normal probability density function of random variable **v**, [-],
v - value of random variable **v**, [the same unit as for **v**],
σ_v - standard deviation of random variable **v**, [the same unit as for **v**],
$\bar{v}$ - mean of random variable **v**, [the same unit as for **v**].

A more convenient form of the normal distribution, however, can be obtained by using a standarized random variable $\mathbf{v}'$, the value of which is given by:

$$v' = \frac{v - \bar{v}}{\sigma_v} \tag{3.12}$$

Thus, the normal probability density function can be expressed by:

$$f_n(v') = \frac{1}{\sqrt{2\pi}} \exp\left[-\frac{(v')^2}{2}\right] \tag{3.13}$$

and the normal probability distribution function is:

$$P_n(v') \doteq P_n(\mathbf{v}' \leq v') = \frac{1}{\sqrt{2\pi}} \int_{-\infty}^{v'} \exp\left(-\frac{\xi^2}{2}\right) d\xi \tag{3.14}$$

The normal probability distribution function, $P_n(v')$, informs about the expected percentage of random events characterized by values lower or equal to a value of v'. If one has to compute $P_n(\mathbf{v} > v')$ [*e.g.*, $P_n(S > 1)$], Eq. (3.14) must be changed into the following form:

$$P_n(\mathbf{v}' > v') = \frac{1}{\sqrt{2\pi}} \int_{v'}^{\infty} \exp\left(-\frac{\xi^2}{2}\right) d\xi \tag{3.15}$$

The field and laboratory tests for the mass of wet sand sample, water content, and specific gravity of soil have very little, if any, interdependence. Calculations showed that the results from repeated tests varied approximately symetrically around their means in a normally distributed, random manner. After assuming independence and randomness of the variables in Eq. (3.9), one can use the first two terms of the Taylor series to obtain a first-order approximation of the variability in the degree of saturation. The following gives the differential equation for the first-order approximation:

$$\sigma_S \cong \sqrt{\left(\frac{\partial S}{\partial m_{ws}}\sigma_m\right)^2 + \left(\frac{\partial S}{\partial w}\sigma_w\right)^2 + \left(\frac{\partial S}{\partial \varrho_s}\sigma_\varrho\right)^2} \tag{3.16}$$

where: σ_S - standard deviation of degree of saturation [-],
S - degree of saturation [-],
m_{ws} - mass of wet sample [kg],
σ_m - standard deviation of mass of wet sample [kg],
w - water content [-],
σ_w - standard deviation of water content [-],
ϱ_s - specific gravity of solid soil particles (with respect to the density of pore fluid) [-],
σ_ϱ - standard deviation of specific gravity of solid soil particles [-].

Using Eq. (3.9), one can derive individual parts of Eq. (3.16). And thus,

$$\frac{\partial S}{\partial m_{ws}} = \frac{\frac{1}{V_t} w \frac{\varrho_s^2}{\rho_w}(1+w)}{\left[(1+w)\varrho_s - \frac{m_{ws}}{V_t}\right]^2} \tag{3.17a}$$

$$\frac{\partial S}{\partial w} = \frac{\frac{m_{ws}}{V_t}\frac{\varrho_s}{\rho_w}\left(\varrho_s - \frac{m_{ws}}{V_t}\right)}{\left[(1+w)\varrho_s - \frac{m_{ws}}{V_t}\right]^2} \tag{3.17b}$$

$$\frac{\partial S}{\partial \varrho_s} = \frac{-\frac{m_{ws}{}^2}{V_t}\, w \frac{1}{\rho_w}}{\left[(1+w)\varrho_s - \frac{m_{ws}}{V_t}\right]^2} \tag{3.17c}$$

where, additionally:

V_t - total volume of soil sample [m^3].

Table 3.1 gives a comparison of the coefficients of variations published by Schmertmann (1989), with those obtained in the present analysis. The values of the coefficient of variation obtained from Norderney Island data are rather close to the values, described by Schmertmann (1989) as $V_{var}^{(low)}$. Low values of the coefficient of variation can certify and prove a good quality of the applied sampling procedure.

Table 3.1
Comparison of coefficients of variation

Soil parameter	After Schmertmann (1989)			'Norderney'
	$V_{var}^{(low)}$ [%]	$V_{var}^{(avg)}$ [%]	$V_{var}^{(high)}$ [%]	V_{var} [%]
m_{ws}	1.5	3	6	1.2
w	7.5	15	30	5.1
ϱ_s	1.0	2	4	—
S (analytical)	7.0	14	28	4.3

In the above described procedure it is assumed that the volume of the sample, V_t, as well as the density of water, ρ_w, have constant values for all the samples. This assumption seems to be correct because, if any, the variations of these parameters compared with the variation of the mass of wet sand sample and the water content is supposed to be very small. The variability values for the mass of wet sand and the water content found from the samples taken on Norderney Island are in a very good accordance with those presented by Schmertmann (1989) and denoted by $V_{var}^{(low)}$. Because of that fact, the variability of the third parameter, *i.e.* the specific gravity of soil, which is needed for the calculation of the standard deviation of the degree of saturation [Eq. (3.16)], was taken directly from Schmertmann's (1989) publication where $V_{var}^{(low)}(\rho_s) = 1.0$.

The standard deviation of the degree of saturation computed analytically $\sigma_S^{(a)} = 0.041$, using the statistical approach described above [see Eq. (3.16)], is only slightly larger than the value calculated directly from the measured soil parameters ($\sigma_S = 0.037$). The same is with the coefficient of variation of the degree of saturation; the analytically

comupted value, $V_{var}^{(a)}(S) = 0.043$ (see Tab. 3.1), exceeds slightly the value computed directly from the measured soil parameters [$V_{var}(S) = 0.038$].

Assuming that the deviation in the degree of saturation is in accordance with the normal distribution, Fig. 3.4 presents the distribution of the degree of saturation from the field sampling and shows that the equivalent normal distribution gives a reasonable approximation thereof.

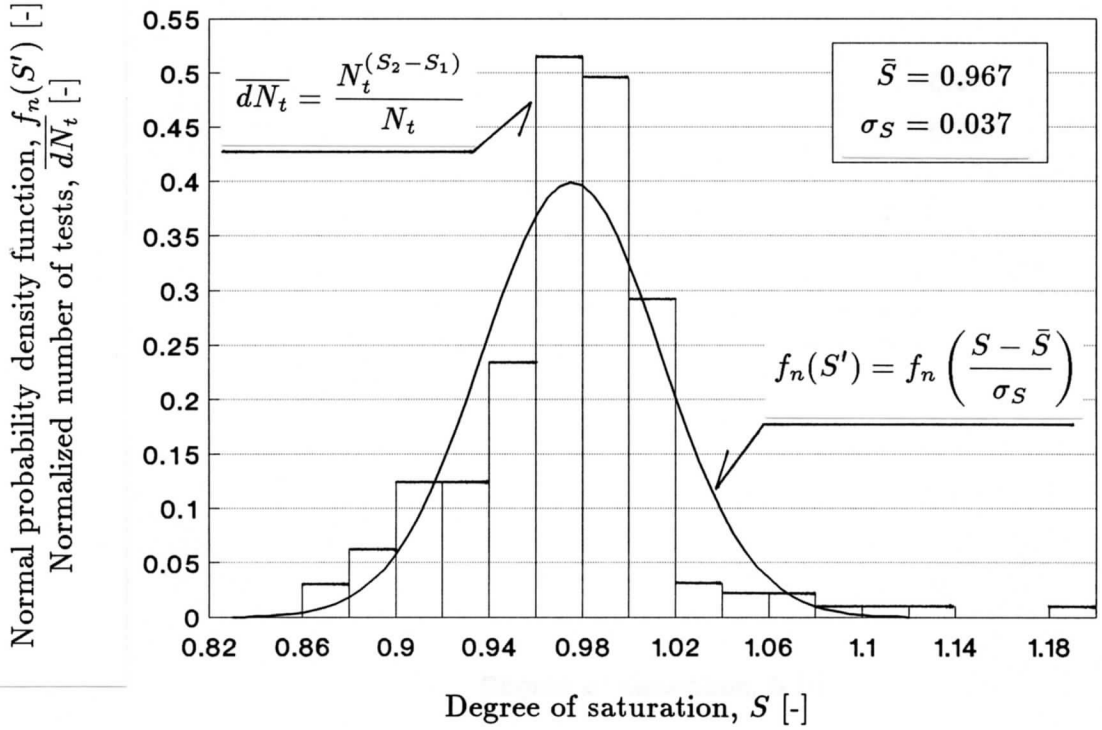

Figure 3.4 Field data showing approximate normal distribution for calculated values of degree of saturation (based on seabed sampling from Norderney Island) [Magda & Davidov, 1990]

If the normal distribution approximation is accepted, the next step that can be done is to calculate the standard deviation, using Eq. (3.16), for different, hypothetically assumed, mean values of the degree of saturation. Then, using the formula for the normal probability distribution function, Eq. (3.15), or entering appropriate tables of normal distribution values, one can finally obtain the expected percentage of tests that will compute with $S > 1$. In the present work, this calculation was performed numerically where the procedure of numerical integration, using the extended midpoint rule, had to be implemented because of the integral to be calculated is an improper integral, the upper limit of which approaches infinity [see Eq. (3.15)].

A graphical presentation of the calculated values of the probability $P(S > 1)$ is illustrated in Fig. 3.5. By entering the probability curve (obtained for the coefficients of variation of 'Norderney Sand' parameters) for $P(S > 1) = 12.37\,\%$, one can easily read out (see Point P_S) that the mean value of the degree of saturation equals $\bar{S}^{(a)} \cong 0.95$.

Comparing the analytical result $\bar{S}^{(a)} \cong 0.95$, obtained taking the variability of the degree of saturation into account, with the mean value $\bar{S} = 0.967$, evaluated directly from the field sampling and laboratory test measurements, a very good agreement was found that can only confirm a proper assumption of the normal distribution for the

statistical analysis of the degree of saturation from *in-situ* measurements. Additionally, the analytically obtained result, slightly smaller than the directly computed value of the degree of saturation, is more realistic because the meaning of tests with $S > 1$ is taken into account throught the statistical approach that assumes the possibility of man-made errors in soil testing procedures.

The finally obtained result for the mean degree of saturation confirms undoubtedly the existence of partly saturated seabed sediments in the natural environment. This has obviously important consequences for the coastal engineering practice. This problem will be dealed with in the following.

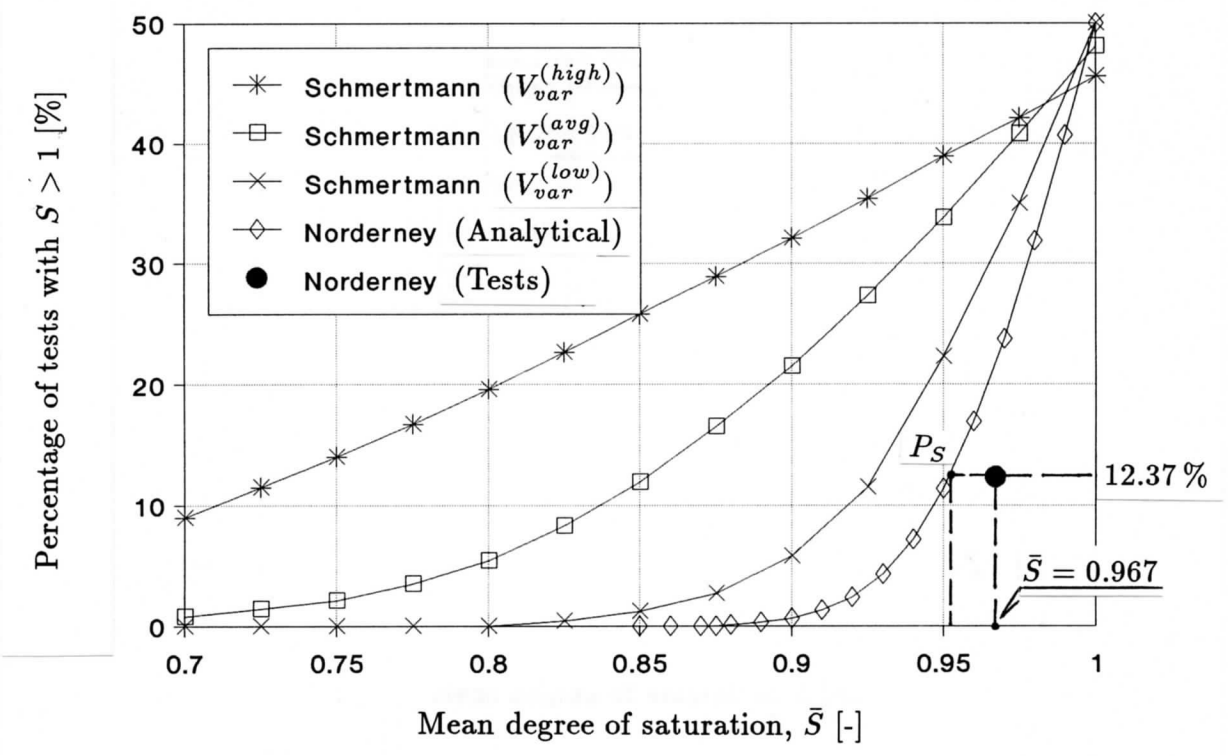

Figure 3.5 Analytical values of percentage of field tests expected to plot above ZAVL ($S > 1$), computed for 'Norderney Sand' variabilities from Tab. 3.1, and assuming $\bar{\varrho}_s = 2.66$

3.1.4 Elastic parameters

Displacement solutions from the theory of elasticity can be used at relatively low stress levels, so as for seabed sediments loaded by surface water waves is believed to be. These solutions require a knowlegde of the values of Young's modulus, E, and Poisson's ratio, ν, for the soil, either for undrained conditions or in terms of effective stress. Poisson's ratio is required for certain stress solutions. It should be noted that the shear modulus:

$$G = \frac{E}{2(1+\nu)} \tag{3.18}$$

where: G - shear modulus for isotropic soil [kPa],
E - Young's modulus of elasticity for isotropic soil [kPa],
ν - Poison's ratio for isotropic soil [-],

is independent of the drainage conditions, assuming that the soil is isotropic.

In the following, the above mentioned constants will be used in sense of linear elasticity, *i.e.* describing a material having a linear, reversible stress-strain relationship. Additionally, since the considered seabed material is assumed to be anisotropic only with respect to soil permeability, the term 'isotropic' used in the description of the shear modulus and Young's modulus of the soil will be omitted in the following.

The volumetric strain of an element of linearly elastic material under three principal stresses is given by:

$$\frac{\Delta V_t}{V_{ti}} = \frac{1-2\nu}{E}(\sigma_1 + \sigma_2 + \sigma_3) \tag{3.19}$$

where: ΔV_t - increment of total volume of soil [m^3],
V_{ti} - initial total volume of soil [m^3],
E - Young's modulus of elasticity [kPa],
ν - Poison's ratio of soil [-],
$\sigma_1, \sigma_2, \sigma_3$ - total principal stresses in x-, y- and z-direction, respectively, [kPa].

If the above expression is assumed to be applied to soil-like media, then for undrained conditions $\Delta V_t/V_{ti} = 0$, hence $\nu = 0.5$. If consolidation takes place, then $\Delta V_t/V_{ti} > 0$ and $\nu < 0.5$ for drained or partially drained conditions.

The value of Young's modulus, E, can be estimated from the curve relating principal stress difference and axial strain in an appropriate triaxial test. The value is usually determined as the secant modulus between the origin and one-third of the peak stress, or over the actual stress range in the particular problem. However, because of the effects of sampling disturbance, it is preferable to determine E, or G, from the results of *in-situ* tests. One such method is to apply load increments to a test plate, either in a shallow pit or at the bottom of a large-diameter borehole, and to measure the resulting vertical displacements. The value of E is then calculated using the relevant displacement solution, with an appropriate value of Poisson's ratio, ν, being assumed. The shear modulus, G, can be determined *in-situ* by means of the pressuremeter.

Poisson's ratio may be evaluated from the ratio of lateral strain to axial strain during a triaxial compression test with axial loading. During the early range of strains, for which the concepts from theory of elasticity are of use, Poisson's ratio is varying with strain. Poisson's ratio for sand becomes constant only for large strains which imply failure, and then has a value greater than 0.5. Poisson's ratio is less than 0.5 only during the early stages of such a test where the specimen decreases in volume.

Because of this behaviour, it is very difficult to make an exact evaluation of the value of ν. Fortunately, the value of ν usually has a relatively small effect upon engineering predictions of a certain phenomena. For the early stages of a first loading of sand, when particle rearrangements are important, ν typically has values of about 0.1 to 0.2. During cyclic loading ν becomes more of a constant, with values from 0.3 to 0.4.

Values of the shear modulus and Poisson's ratio used by different authors of the pore pressure theories are shortly reviewed and compared here. And thus, Yamamoto *et al.* (1978) stated that the value of shear modulus for soils varies from about $G = 4.8 \times 10^5$ kPa for very dense sand to $G = 4.8 \times 10^2$ kPa for silt and clay, and Poisson's

ratio was assumed to be $\nu = 0.33$. Madsen's (1978) values of the shear modulus and Poisson's ratio are $G = 10^5$ kPa and $\nu = 0.3$, respectively. Okusa (1985[a]) presented elastic properties of the soil in terms of soil compressibility which was assumed to be $\alpha = 9.18 \times 10^{-5}$ m^2/kN, for loose sand, and $\alpha = 1.84 \times 10^{-5}$ m^2/kN, for dense sand. A recalculation of these values, using the following equation:

$$G = \frac{3(1-2\nu)}{2(1+\nu)\alpha} \tag{3.20}$$

where: G - shear modulus of soil [kPa],
ν - Poison's ratio of soil [-],
α - compressibility of soil [m^2/kN],

results in $G = 5 \times 10^3$ kPa and $G = 2 \times 10^4$ kPa, respectively, assuming Poisson's ratio $\nu = 0.3$, for loose sand, and $\nu = 0.33$, for North Sea sand. Nago & Maeno (1986) reported the soil shear modulus $G = 3.42 \times 10^5$ kPa and Poisson's ratio $\nu = 0.48$, whereas the EAU German Recommendations (1986) give the limits for loose and dense sand from $G = 6 \times 10^3$ kPa to $G = 7 \times 10^4$ kPa, respectively, assuming $\nu = 0.3$.

In general, it can be noted that the mean value of the shear modulus, used by some researchers in their example calculations, oscillates about $G \cong 10^5 - 10^6$ kPa, for dense sand, and $G \cong 10^3 - 10^4$ kPa, for loose sand, whereas the values of Poisson's ratio given by the same authors are coherent, $\nu = 0.3 - 0.33$, showing only one exception, in which the value assumed by Nago & Maeno (1986) seems to be higher.

3.1.5 Permeability

Water flows through a saturated soil in accordance with Darcy's empirical law:

$$v_q = \frac{q}{A} = k i_h \tag{3.21}$$

where: v_q - discharge velocity [m/s],
q - volumetric discharge of water [m^3/s],
A - cross-sectional area of soil, corresponding to the volumetric discharge, q, [m^2],
k - coefficient of soil permeability [m/s],
i_h - hydraulic gradient [-].

The coefficient of soil permeability depends primarily on the average size of the pores, which in turn is related to the distribution of particle sizes, particle shape and soil structure. In general, smaller soil particles imply smaller average sizes of pores and lower coefficients of permeability.

The coefficient of permeability varies also with temperature, upon which the viscosity of the water depends. If the value of k measured at 20° is taken as 100 %, then the values at 10° and 0° are 77 % and 56 %, respectively (Craig, 1983).

The coefficient of permeability can also be represented by the equation:

$$k = \frac{\gamma_w}{\eta_v} k_\eta \tag{3.22}$$

where: k - coefficient of soil permeability [m/s],
γ_w - unit weight of water [kN/m^3],
η_v - dynamic viscosity of water [kPa · s],
k_η - absolute coefficient of permeability, depending only on soil skeleton characteristics, [m^2].

For sands, Hazen's formula gives an approximate value of k in the following form (Craig, 1983):

$$k = 10^{-2} d_{10}^2 \tag{3.23}$$

where: k - coefficient of soil permeability [m/s],
d_{10} - effective (characteristic) size, corresponding to 10 %-ordinate on grain-size distribution curve [mm].

Formula (3.23) applies to clean filter sands that occur in loose packing. It does not take into account the effect of density. Also the use of the effective size is entirely arbitrary.

Typical values of k for different types of soil are shown in Tab. 3.2.

Table 3.2
Coefficient of permeability (m/s) [Craig, 1983]

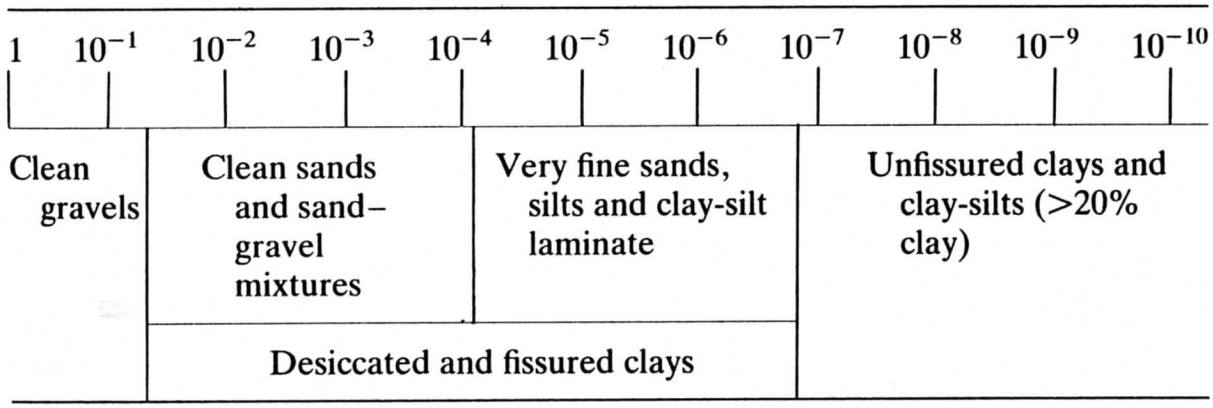

Numerous other relationships have been developed by various investigators. Among them is the formula, proposed by Casagrande, which reflects the effect of void ratio on the coefficient of permeability:

$$k = 1.4 k_{0.85} e^2 \tag{3.24}$$

where: k - coefficient of soil permeability [m/s],
$k_{0.85}$ - coefficient of soil permeability at a void ratio of 0.85 [m/s],
e - void ratio [-].

The influence of void ratio on the coefficient of permeability is shown in Chardabellas' formula [Keźdi, 1974]:

$$k = a_1 e^{a_2} \tag{3.25}$$

where: k - coefficient of soil permeability [m/s],
e - void ratio [-],
a_1 - constant, representing the coefficient of soil permeability at a void ratio of 1.0 and showing the order of magnitude of k, [-],
a_2 - constant (values ranging from 2 to 5), indicating the rate of change of k with the change of e, [-].

The above empirical relationships do not supply solutions for the coefficient of permeability with a high accuracy, and therefore they have to be treated only as a first approximation. In most cases the coefficient of permeability should be determined by means of direct measurements, especially when the investigated phenomenon, like wave-induced pore pressure oscillations in sandy seabed sediments, is strongly dependent and very sensitive on the soil permeability. A detailed measurement is also of a special importance as far as partly saturated soils are concerned.

Permeability in the sense used in the preceding discussion cannot be spoken of in three-phase soils. The three phases may be arranged into various structural patterns and may move separately and at different velocities in relation to each other. Combined tests on the permeability of soil to air and to water can lead to an understanding of this problem. The concept of relative permeability must be introduced (Keźdi, 1974). This term means the ratio of the coefficient of permeability measured in a three-phase state of the soil to that measured in the fully saturated state of the soil. This ratio is a function of the degree of saturation. Test results typical for the behaviour of sands are presented in Fig. 3.6, where relative permeabilities are plotted against the degree of saturation.

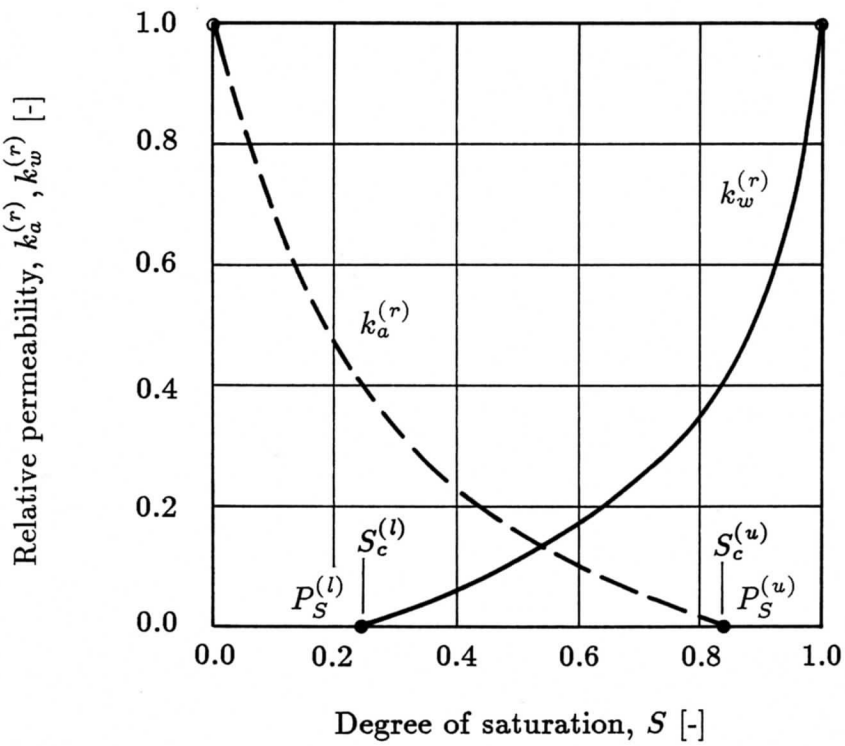

Figure 3.6 Relative permeability to air and water of three-phase sand versus degree of saturation [Keźdi, 1974]

From Fig. 3.6 it can be seen that below the lower critical value of the degree of saturation ($S_c^{(l)} \cong 0.2$) the relative permeability of soil to water, $k_w^{(r)}$, is zero. In other words, water cannot penetrate through the soil unless the degree of saturation is increased above this critical value. A similar curve can be obtained for the relative permeability of soil to air, $k_a^{(r)}$. If an assemblage of grains is sufficiently dry, the pore spaces filled with air form continuous passages permitting an almost unhindered flow of air and a high relative air permeability results. With increasing degree of saturation, the relative permeability to air reduces rapidly and may, at the upper critical value of the degree of saturation ($S_c^{(l)} \cong 0.8$), diminish to zero. Beyond that point the pore air can exist only in the form of entrapped bubbles and is thus forced to move along with the pore water. In this state, a separate movement of the gaseous phase in relation to the liquid phase is possible only if the gas presses water out of the pores, but then the degree of saturation must also change. The lower and upper critical states, represented in Fig. 3.6 by points $P_S^{(l)}$ and $P_S^{(u)}$, respectively, are of great importance from a practical point of view. If $S < S_c^{(l)} \cong 0.2$ (Point $P_S^{(l)}$), the soil only sucks water in but does not let it through. In this state the apparent cohesion of sands is the greatest. Beyond the upper critical state (Point $P_S^{(u)}$; $S > S_c^{(u)} \cong 0.8$), the soil behaves as if it were fully saturated.

Values of the coefficient of permeability for seabed sediments can be found in some of the publications on the pore pressure theories. And thus, Moshagen & Tørum (1975) characterized coarse sand by $k = 10^{-2}$ m/s, and fine sand by $k = 10^{-4}$ m/s. Madsen (1978) used in his calculation examples two values of the coefficient of permeability: $k = 10^{-2}$ m/s, for 1.0 mm sand, and $k = 3 \times 10^{-4}$ m/s, for 0.2 mm sand. Yamamoto (1981) gave $k = 10^{-4}$ m/s as a design value for the North Sea geotechnical conditions. Okusa (1985[a]) distinguished also two values, namely: $k = 10^{-4}$ m/s, for loose sand, and $k = 10^{-5}$ m/s, for dense sand. Nago & Maeno (1986) indicated $k = 1.5 \times 10^{-4}$ m/s as input data for their calculations.

In general, the value of coefficient of permeability $k = 10^{-4}$ m/s seems to be the most representative for fine-medium sand in a loose state. For the same type of sand, but in a dense state, an increase in the coefficient of soil permeability is logically expected. However, the increase will not exceed a value which is one order higher (*i.e.*, $k = 10^{-3}$ m/s) than the value typical for a loose state of the sand.

3.2 Pore fluid compressibility

Air is a mixture of several gases plus varying amounts of water vapour. It behaves essentially in accordance with the ideal gas law. Therefore, assuming an isothermal process (*i.e.*, with a constant temperature), Boyle-Mariotte's law can be applied (Skorko, 1971):

$$P_g V_g = const \tag{3.26}$$

where: P_g - absolute pressure of gas [kPa],
V_g - volume of gas [kmol].

Considering a certain amount of gas, the above equation of state takes the form of Clapeyron's equation (Skorko, 1971):

$$P_g V_g = W_g R T_a \tag{3.27}$$

where: P_g - absolute pressure of gas [kPa],
V_g - volume of gas [m^3],
W_g- amount of gas [kmol],
R - universal molar gas constant [8.314 kJ/(kmol · K)],
T_a - absolute temperature [K].

The ideal gas law is often written in terms of the specific volume:

$$P_g v_g = R T_a \tag{3.28}$$

in which:

$$v_g = \frac{1}{\rho_g} = \frac{V_g}{W_g} \tag{3.29}$$

where, additionally:
v_g - specific volume of gas [m^3/kmol],
ρ_g - density of gas [kmol/m^3].

Isothermal (*i.e.*, for $T = const$) compressibility of any fluid (*i.e.*, liquid or gas) is defined as:

$$\beta_f = -\frac{1}{v_f}\frac{dv}{dP_f} \tag{3.30}$$

where: β_f - isotermal compressibility of fluid [m^2/kN],
v_f - specific volume of fluid at a certain temperature (gas: [m^3/kmol]; liquid: [m^3/kg]),
P_f - absolute fluid pressure [kPa].

The specific volume of air can be easily derived from the ideal gas law [Eq. 3.28]:

$$v_a = \frac{R T_a}{P_a} \tag{3.31}$$

where: v_a - specific volume of air [m^3/kmol],
R - universal molar gas constant [kJ/(kmol · K)],
T_a - absolute temperature [K],
P_a - absolute air pressure [kPa].

The specific volume can be differentiated with respect to pressure. Substitution into the compressibility Eq. (3.30) shows that the compressibility of air is inversely proportional to the absolute air pressure:

$$\beta_a = \frac{1}{P_a} \tag{3.32}$$

where: β_a - compressibility of air [m^2/kN],
P_a - absolute air pressure [kPa].

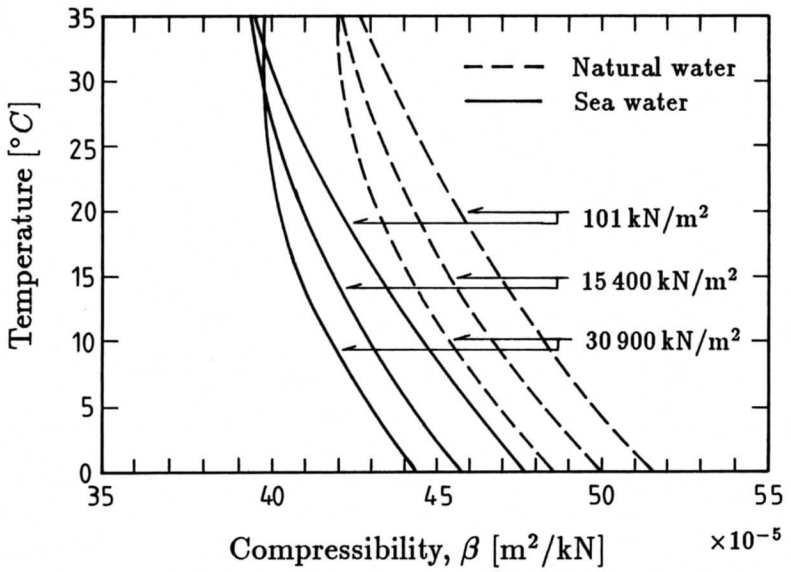

Figure 3.7 Isothermal compressibility for fresch and salt water [Dorsey, 1940]

The compressibility of water can be obtained from the density results. It also has been directly measured (Dorsey, 1940; see Fig. 3.7). The compressibility of water-air mixtures is derived using a direct proportioning of the air and water, and in accordance with the compressibility definition.

The total volume of the water-air mixture is composed of water and free air (note that the volume of dissolved air is within the volume of water). For the compressibility of the water-air mixture, Eq. 3.30 becomes (Fredlund, 1976):

$$\beta' = -\frac{1}{V_w + V_a}\left(\frac{dV_w}{dP_r} + \frac{dV_a}{dP_r}\right) \tag{3.33}$$

where: β' - compressibility of water-air mixture [m^2/kN],
V_w - volume of water in water-air mixture [m^3],
V_a - volume of free air in water-air mixture [m^3],
P_r - absolute reference pressure [kPa].

Applying the chain rule of differentiation, Eq. 3.33 changes into:

$$\beta' = -\frac{1}{V_w + V_a}\left(\frac{dV_w}{dP_w}\frac{dP_w}{dP_r} + \frac{dV_a}{dP_a}\frac{dP_a}{dP_r}\right) \tag{3.34}$$

Either the air pressure or the water pressure can be used as a reference pressure. If the water pressure is used as a reference, the following pore pressure parameter can be defined:

$$B_{aw} = \frac{dP_a}{dP_w} \tag{3.35}$$

where: B_{aw} - pore pressure parameter [-],
P_a - absolute pressure in air part of water-air mixture [kPa],
P_w - absolute pressure in water part of water-air mixture [kPa].

When the water-air mixture is in the absence of a solid, the pore pressure parameter, B_{aw}, will equal 1. On the other hand, in the presence of a solid, the surface tension effects will result in differing rates of pore air and pore water pressure change. The pore pressure parameter, B_{aw}, should always be less than 1 for undrained loading, becoming equal to 1 at a fully saturated state of the soil.

At this point, Kelvin's equation could be incoroporated:

$$P_a = P_w + \frac{2\sigma_t}{r_b} \tag{3.36}$$

where: P_a - absolute pressure in air part of water-air mixture [kPa],
P_w - absolute pressure in water part of water-air mixture [kPa],
σ_t - water-air surface tension of free air bubbles [kN/m],
r_b - free air-bubble radius (radius of curvature of water-air meniscus) [m].

However, it will not assist in solving for the new pore pressure parameter. Differentiation of Kelvin's equation gives:

$$\frac{dP_a}{dP_w} = 2\sigma_t \frac{d(r_b^{-1})}{dP_w} + 1 \tag{3.37}$$

This excercise merely incorporates another unknown variable which is the radius of curvature of the water-air meniscus. Attempts have been made to use this equation in the compressibility relationships for water-air mixtures (Schuurman, 1966). However, this equation does not assist in solving practical problems since it incorporates a new unmeasurable quantity.

Using the water pressure as a reference pressure, Eq. (3.34) becomes:

$$\beta' = -\frac{1}{V_w + V_a}\left(\frac{dV_w}{dP_w} + \frac{dV_a}{dP_a} B_{aw}\right) \tag{3.38}$$

where: β' - compressibility of pore fluid [m^2/kN],
V_w - volume of water in water-air mixture [m^3],
V_a - volume of free air in water-air mixture [m^3],
P_w - absolute pressure in water part [kPa],
P_a - absolute pressure in air part [kPa],
B_{aw} - pore pressure parameter [-].

The compressibility of the free air can be envisaged in terms of appling Boyle's law to the free air and Henry's law to a portion of air going into solution:

$$\frac{dV_a}{dP_a} = \frac{(V_{ab} + V_{ad})}{P_a} \tag{3.39}$$

where, additionally:
V_{ab} - volume of free air bubbles in water-air mixture [m^3],
V_{ad} - volume of air dissolved in water-air mixture [m^3].

Substituting Eq. (3.39) into the compressibility equation [Eq. (3.38)], and writing the volumes of air and water in terms of initial degree of saturation, one obtains:

$$\beta' = S\beta_w + B_{aw}\frac{(1-S)}{P_a} + B_{aw}\frac{Sh_{sl}}{P_a} \tag{3.40}$$

where: β' - compressibility of pore fluid [m^2/kN],
S - degree of saturation [-],
β_w - compressibility of pure water [m^2/kN],
B_{aw} - pore pressure parameter [-],
P_a - absolute pressure in air part [kPa],
h_{sl} - coefficient of volumetric solubility of air in water [-].

The first term in the above equation accounts for the compressibility of the pure water, the second term accounts for Boyle's law being applied to the free air and the third term accounts for the air driven into solution in accordance with Henry's law.

The disadvantage of Eq. (3.40) is that the parameter B_{aw} is not known and must be measured. In general, the actual air pressure varies and is difficult to be determined in the case of non-coherent air bubbles (Barends, 1980).

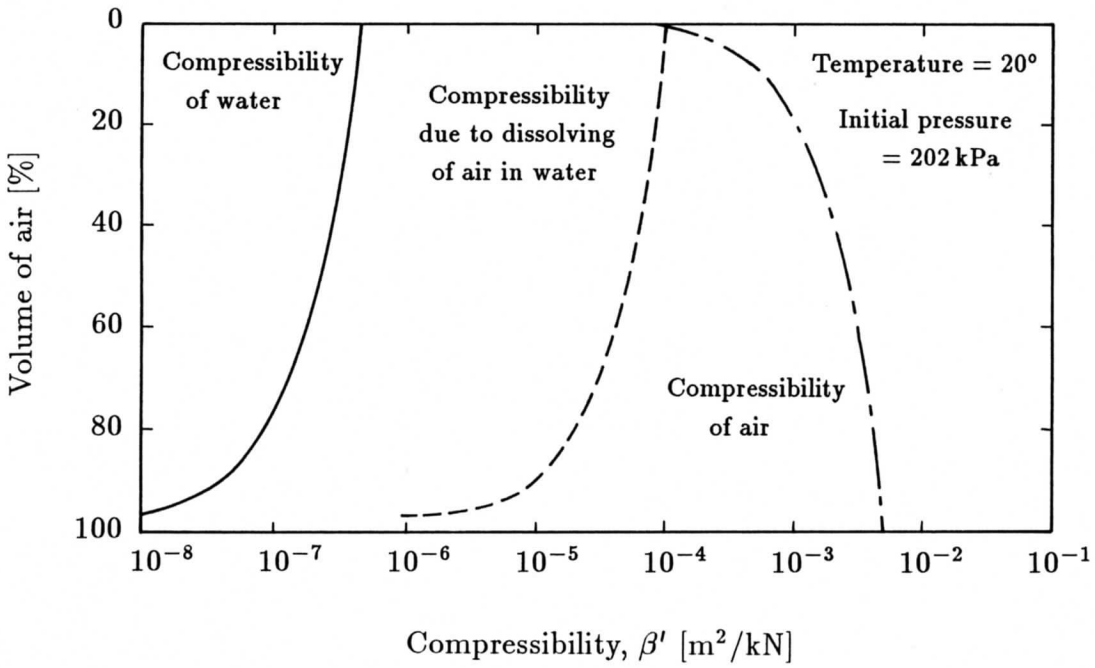

Figure 3.8 Components of compressibility of miscible and immescible water-air mixtures [Fredlund, 1976]

Figure 3.8 shows the significance of the variables contributing to the compressibility, for the case of $B_{aw} = 1$ and the initial absolute air pressure $P_a = 202$ kPa. The compressibility due to the solution of air in water is approximately two orders of magnitude greater than the compressibility due to the pure water. The plot also shows that the compressibility of the pure water is of significance only for the case of a fully saturated soil and that the effect of air dissolving in water becomes significant for air volumes less than approximately 20 % of the total void volume.

Figure 3.9 shows the amplification effect of air solubility in water on the compressibility of water-air mixture, for several values of the initial air pressure. The effect of the solution of air seems to be the same (on a logarythmic scale) regardless of the air pressure.

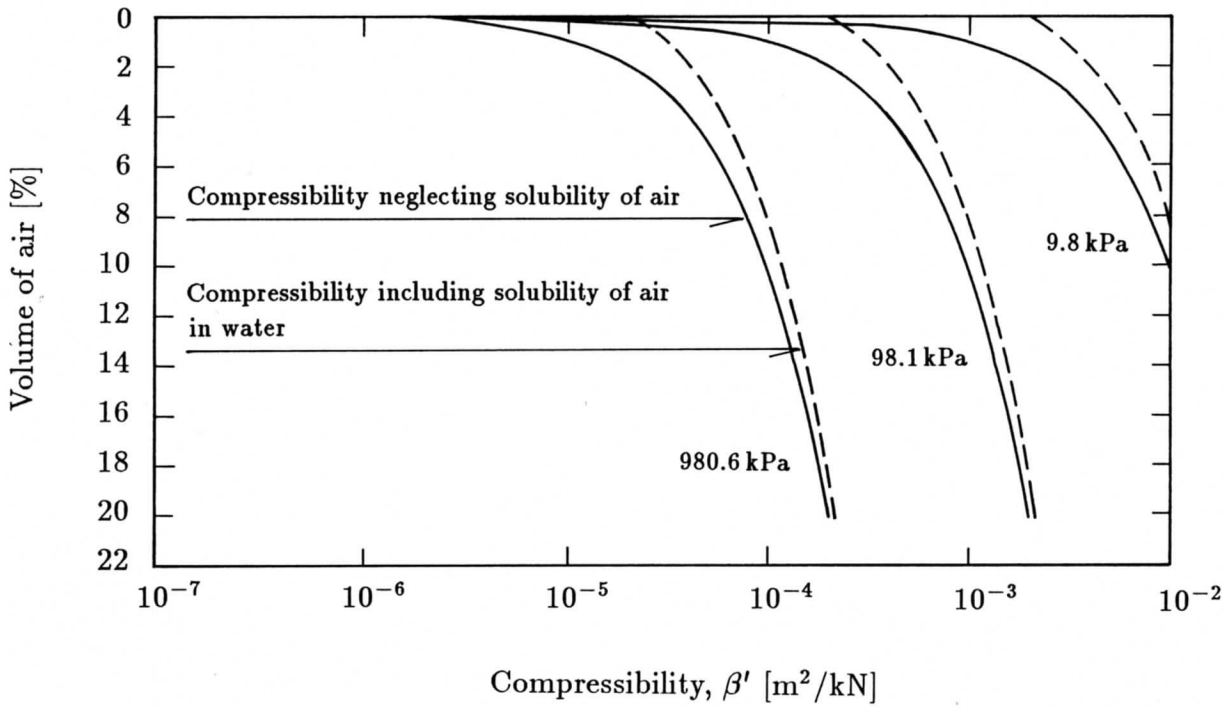

Figure 3.9 Effect of solubility of air in water on compressibility of water-air mixture [Fredlund, 1976]

The experimental data on the density of water indicate that air dissolves in water by fitting within the water structure, causing essentially no disruption. To understand this mechanism further, Fredlund (1976) considered a piston and cylinder arrangement with a porous stone, having a porosity of approximately 2 %, at the base of the cylinder (Fig. 3.10). The porous stone is to simulate the behaviour of the water. An imaginary valve was placed at the contact between the free air and the porous stone. In this way, the movement of air into the stone can be controlled. The air in the porous stone simulates the air dissolved in water. It should be noted that the above analogy lacks in that the air pressure cannot differ from the water pressure.

Initially, the cylinder contains a volume that is porous stone and a volume that is air, subjected to equal pressures. Initially, the imaginary valve is closed and the load on the piston is increased. The air above the porous stone compresses (Boyle's law simulation). When the imaginary valve is opened, some additional air passes into the porous stone (Henry's law simulation). As the piston load is increased, this process continues until all the free air has gone into the porous stone. At this point, there is a discontinuity since all the applied load is taken by the porous stone.

The above analogy assists in vizualizing the density and compressibility of the water-air mixture subjected to various pressures. The density of the mixture can be derived based on the conservation of masses. This law is also the fundamental basis for the compressibility relationship since compressibility is, by definition, the inverse of the

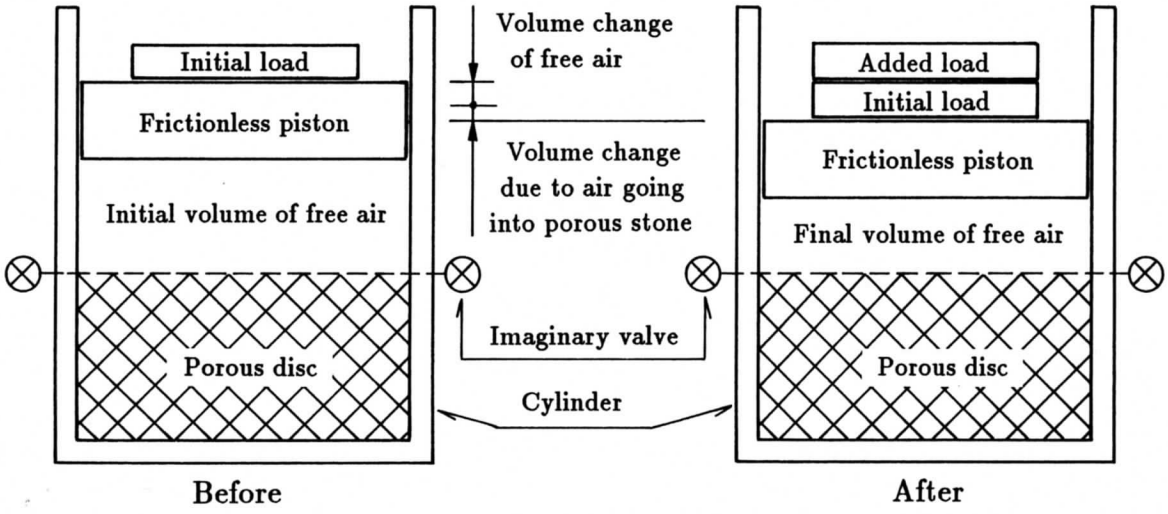

Figure 3.10 Piston and porous stone analogy [Fredlund, 1976]

change in density with respect to the change in pressure. The amount of air going into or coming out of solution is time-dependent and is either ignored or taken into account, depending upon the engineering problem being considered.

Air is dissolved in water in accordance with Henry's law which states that the weight of gas dissolved in a fixed quantity of liquid, at constant temperature, is directly proportional to the pressure of the gas above the solution. The starting point for applying Henry's law is given by the coefficient of solubility of each gas in water (Tab. 3.3). This coefficient of gas solubility in water, H_{sl}, is the total weight of each gas that can be dissolved in water (under 100 kPa pressure). If the weights of dissolved air were extracted from the water and compressed at the same pressure as acting on the free air above the water, the volume occupied is described by the volumetric coefficient of solubility, h_{sl}.

Table 3.3
Solubility of air in water [Dorsey, 1940]

Temperature [°C]	Weight of air per weight of water, H_{sl} [-]			Vol. of air per vol. of water h_{sl} [-]
	Oxygen	Nitrogen, etc.	Air	
0	14.56×10^{-6}	23.87×10^{-6}	38.43×10^{-6}	0.02918
4	13.06×10^{-6}	21.59×10^{-6}	34.65×10^{-6}	0.02632
10	11.25×10^{-6}	18.82×10^{-6}	30.07×10^{-6}	0.02284
15	10.07×10^{-6}	17.00×10^{-6}	27.07×10^{-6}	0.02055
20	9.11×10^{-6}	15.51×10^{-6}	24.62×10^{-6}	0.01868
25	8.28×10^{-6}	14.24×10^{-6}	22.52×10^{-6}	0.01708
30	7.55×10^{-6}	13.10×10^{-6}	20.65×10^{-6}	0.01564

3.2.1 Comparison of existing formulas

The problem of pore water compressibility in connection with saturation of soils was treated by many scientists. Some of them (*e.g.*: Madsen, 1978; Yamamoto *et al.*, 1978; Nago & Maeno, 1984; Okusa, 1985[(a)]) used in their works already existing formulas, in most cases considerably simplified, containing the relationship between the degree of saturation and the compressibility of pore fluid (*i.e.*, water-air mixture). A certain assumption concerning this relationship was necessary to perform an analysis on the pore pressure oscillations in partly saturated soils under sea-waves loading. Other group of authors (*e.g.*: Skempton & Bishop, 1954; Koning, 1963; Schuurman, 1966; Verruijt, 1969; Fredlund, 1976; Barends, 1980) put more attention to the theoretical background of the relationship concerned, deriving gradually more general, but also more sophisticated formulas, reviewed and discussed by Magda (1990[(b)]).

Of primary interest from an engineering standpoint is the mathematical formulation of the compressibility relationship for the fluid phase of a partly saturated soil. An understanding of compressibility is of importance with respect to the pore air and pore water pressures developed under undrained loading of partly saturated soil (Fredlund, 1976).

The dramatic increase in compressibility due to the presence of a small amount of air is of significance in studying the pore pressure reactions of soils. The pore pressure parameter, B, depends on the compressibility of the pore fluid (Skempton, 1954):

$$B = \frac{1}{1 + \dfrac{n\beta'}{\alpha}} \tag{3.41}$$

where: B - Skempton's pore pressure parameter [-],
n - porosity of soil [-],
β' - compressibility of pore fluid [m^2/kN],
α - compressibility of soil skeleton [m^2/kN].

Gas in marine sediments has been found in various parts of the world but with a special concentration in areas of high biogenic activity such as the mouth of rivers or deltas. A prime example is the Mississippi Delta where the occurrence of gas in the sediment has been reported by several investigators (*e.g.*, Esrig & Kirby, 1977).

Degrees of saturation *in-situ* of partly saturated marine sediments normally lie in the range of 0.85 to 1.0 (Esrig & Kirby, 1977). Under these conditions, the gas exists in discrete occluded bubbles with no connections between them. This was also observed in the laboratory by Nageswaran (1983) who performed tests on soils containing discrete occluded gas bubbles with saturation ranging between 0.85 and 1.0.

The structure of partly saturated marine soils can vary significantly depending on the relative sizes of the gas bubbles and the soil grains. Wheeler *et al.* (1991) presented two extreme cases of the possible structure of a gassy soil. Figure 3.11(a) shows the case, in which the pore gas exists in numerous small bubbles within the pores of the soil matrix, whereas Fig. 3.11(b) presents an alternative soil structure, in which the fewer gas bubbles are much larger than the soil grains. Terzaghi (1943) termed the gas in the second of these options 'gas voids', as opposed to 'gas bubbles' for the first case.

The majority of investigators in the field of partly saturated marine soils, including Ghaboussi & Wilson (1973), Yamamoto *et al.* (1978), Madsen (1978), Okusa (1985[(a)]),

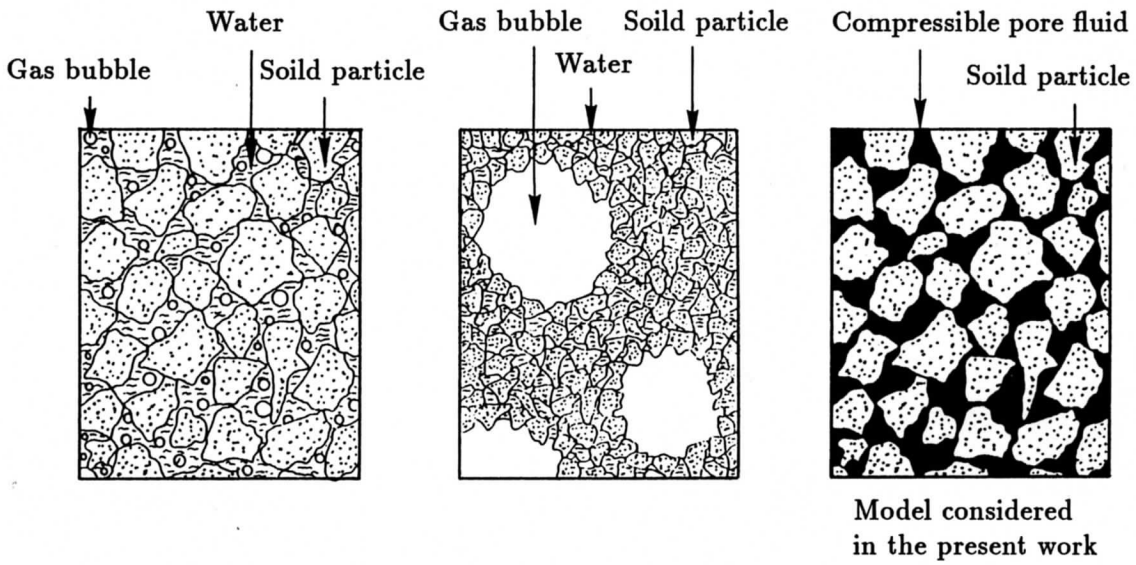

Figure 3.11 Schematic representation of partly saturated soil [Wheeler *et al.*, 1991]: (a) containing small gas bubbles in soil matrix, (b) containing large gas voids in soil matrix, (c) idealized as saturated with compressible pore fluid

and Spierenburg (1987), have assumed that for a soil saturated above the critical saturation, that is when the gas is in occluded form, the structure of the soil becomes as illustrated in Fig. 3.11(a). Under this assumption, it has been assumed that the two fluid phases of gas and water have equal pore pressure and can be represented by a single compressible pore fluid, as illustrated in Fig. 3.11(c). This is the model which was assumed in the present work for further consideration. This results in the pore fluid compressibility given by the following expression:

$$\beta' = (1 - H_{sl})\, S\beta + (1 - S + H_{sl}S)\, \beta_a \tag{3.42}$$

where: β' - compressibility of pore fluid [m^2/kN],
H_{sl} - Henry's coefficient of air solubility in water [-],
S - degree of saturation [-],
β - compressibility of pure water [m^2/kN],
β_a - compressibility of air [m^2/kN].

It must be noted that Henry's coefficient of solubility, H_{sl}, must be set to zero for a fully saturated soil. The term $(1 - H_{sl})$ arises due to the fact that when the water compresses, the reduced volume of the water is unable to hold the same amount of dissolved gas.

The following brings a brief review of the compressibility-saturation relationships together with specific values of the compressibility of water-air mixture used in considerations and calculations presented by the authors of the above mentioned pore pressure theories.

For partly saturated soils, the effective compressibility of the pore fluid may exceed the compressibility of pure water by a considerable number (Madsen, 1978). Thus, a

simple analysis by Verruijt (1969) indicates an upper bound for the compressibility of the pore fluid (*i.e*, water-air mixture) to be:

$$\beta' = \beta_w + \frac{1 - S}{P_h} \qquad \text{for} \qquad 1 - S \ll 1 \tag{3.43}$$

where: β' - compressibility of pore fluid [m^2/kN],
β_w - compressibility of pure water [m^2/kN],
S - degree of saturation [-],
P_h - absolute hydrostatic pressure ($P_h = p_{at} + p_h$, where: $p_{at} = 101.325\,kPa$ is the atmospheric pressure, and p_h is the hydrostatic pressure) [kPa].

Table 3.4 shows how strong the dependence of the pore fluid compressibility, calculated from Eq. (3.43), on saturation soil conditions is. The pore fluid compressibility was computed for two different cases of water depth *i.e*: $h = 4.5\,m$ (*e.g.*, laboratory conditions in a wave flume) and $h = 20.0\,m$ (*e.g.*, natural conditions in a coastal region), assuming the compressibility of pure water to be $\beta_w = 4.2 \times 10^{-7}\,m^2/kN$.

It can be clearly seen that the reduction of the degree of saturation from 1.0 to 0.99 (*i.e.*, only 1%) causes a dramatic increase of the pore fluid compressibility where the order of difference is about 10^2.

TABLE 3.4

Dependence of the pore fluid compressibility on the degree of saturation [(a) $P_h = 145.5\,kPa$ (for $h = 4.5\,m$), (b) $P_h = 297.5\,kPa$ (for $h = 20.0\,m$)]

Degree of saturation S [-]	Compressibility of pore fluid β' [m^2/kN]	
	(*a*) $h = 4.5\,m$	(*b*) $h = 20.0\,m$
1.00	4.20×10^{-7}	4.20×10^{-7}
0.999	7.29×10^{-6}	3.78×10^{-6}
0.99	6.91×10^{-5}	3.40×10^{-5}
0.97	2.07×10^{-4}	1.01×10^{-4}
0.95	3.44×10^{-4}	1.69×10^{-4}
0.90	6.88×10^{-4}	3.37×10^{-4}

Madsen (1978) gave some data concerning the pore fluid compressibility for different saturation conditions and water depth above the seabed. The data is illustrated by the term ($\gamma_w \beta'$), where: γ_w is the unit weight of water, and β' is the pore fluid compressibility. And thus, assuming the pore fluid to be water, $\gamma\beta' = \gamma\beta_w = 4 \times 10^{-6}\,m^{-1}$ for a fully saturated soil. For the degree of saturation $S = 0.99$ and water depth of 10 m, the effective compressibility of the pore fluid is reported to be as high as $\gamma_w\beta' = 10^{-3}\,m^{-1}$, whereas the pore fluid compressibility equals $\gamma_w\beta' = 10^{-2}m^{-1}$, for saturation conditions of $S = 0.965$ and water depth 7 m. Assuming the pore fluid to be water ($\gamma_w \cong 10\,kN/m^3$), the pore fluid compressibility can be easily found:

- for a fully saturated soil ($S = 1.0$) and water as a pore fluid

$$\beta' = \beta_w = 4 \times 10^{-7}\,m^2/kN$$

- for saturation $S = 0.99$

$$\beta' = 10^{-4}\,\mathrm{m^2/kN}$$

- for saturation $S = 0.965$

$$\beta' = 10^{-3}\,\mathrm{m^2/kN}$$

In fact, the values presented by Madsen (1978) for partly saturated sediments differ from these calculated directly from Eq. (3.43). Assuming correct values of the absolute hydrostatic pressure, the respective values of pore fluid compressibility, calculated according to Eq. (3.43) are equal to:

- for saturation $S = 0.99$ and water depth $h = 10\,\mathrm{m}$

$$\beta' = 5 \times 10^{-5}\,\mathrm{m^2/kN}$$

- for saturation $S = 0.965$ and water depth $h = 7\,\mathrm{m}$

$$\beta' = 2 \times 10^{-4}\,\mathrm{m^2/kN}$$

However, these diferences are smaller than one order of magnitude and can be used in the first approximation. In water depths greater than *ca* 25 m, most gases will go into solution and the compressibility of the pore fluid would approach that of pure water (Madsen, 1978). In large scale laboratory experiments where a sand bed is artificially constructed, it is extremely difficult to achieve fully saturated conditions. The pore pressure results presented by Madsen (1978) for partly saturated soils ($S = 0.965$) demonstrate therefore that one should excercise extreme caution when interpreting model results in which the compressibility of the pore fluid may be a factor.

A similar approach was done by Okusa ($1985^{(a)}$). He considered a submarine sediment containing gas, the pressure of which is assumed to be equal to the pore pressure. Using Henry's law and Boyle's law under a constant temperature, the relation for the pore fluid compressibility has the following form (Okusa, $1985^{(a)}$):

$$\beta' = S\beta_w + (1 - S)\beta_a \tag{3.44}$$

where: β' - compressibility of pore fluid [$\mathrm{m^2/kN}$],
S - degree of saturation [-],
β_w - compressibility of pure water [$\mathrm{m^2/kN}$],
β_a - compressibility of air [$\mathrm{m^2/kN}$].

This equation is based on the assumption that the gas and water pressures are equal (*i.e.*, the effect of surface tension is ignored). Equation (3.44) also ignores the movement of gas into the solution. This second assumption is completely justifiable, because the wave period is likely to be much shorter than the time required for the solution process.

Yamamoto *et al.* (1978) presented quite the same formula as Madsen (1978) did. The only difference is that instead of the compressibility parameter they used a parameter describing the bulk modulus of elasticity of pore fluid. If the pore water is absolutely air-free, the bulk modulus of pore fluid, K', is equal to the bulk modulus of elasticity of pure water, K_w. However, if the pore water contains even a very small amount of air, the bulk modulus of elasticity of pore fluid decreases drastically and K' is related to K_w by (Yamamoto *et al.*, 1978; Verruijt, 1969):

$$\frac{1}{K'} = \frac{1}{K_w} + \frac{1-S}{P_h} \tag{3.45}$$

where: K' - bulk modulus of elasticity of pore fluid [kPa],
K_w - bulk modulus of elasticity of pure water [kPa],

S - degree of saturation [-],
P_h - absolute hydrostatic pressure [kPa].

If the soil is saturated with water, and if the pore water does not contain gases ($S = 1.0$), then the apparent modulus of elasticity, K', is equal to the modulus of elasticity of pure water, $K_w = 1.9 \times 10^6$ kPa. If the sand is saturated in 95 % ($S = 0.95$) with water at atmospheric pressure, the modulus of elasticity of pore fluid is, from Eq. (3.45), $K' = 9.5 \times 10^2$ kPa. Inverting the values of bulk modulus, one can easily obtain the values of compressibility:

- fully saturated soil ($S = 1.0$) and pure water as a pore fluid

$$\beta' = \beta_w = 5.3 \times 10^{-7}\ \mathrm{m^2/kN}$$

- partly saturated soil ($S = 0.95$)

$$\beta' = 1.1 \times 10^{-3}\ \mathrm{m^2/kN}$$

The first value, which is independent on the water depth, stays in a good accordance with the value presentes by Madsen (1978). The accuracy of the second compressibility value is impossible to be judged because no information on water depth conditions are supplied by Yamamoto *et al.* (1978).

In the publication by Nago & Maeno (1984) one can find only a value of the compressibility of pure water which is shown to be $\beta_w = 4.46 \times 10^{-7}\ \mathrm{m^2/kN}$, and which corresponds very well to adequate values indicated by Madsen (1978) and Yamamoto *et al.* (1978). Moshagen & Tørum (1975) assumed the bulk modulus of water to be $K_w = 2.3 \times 10^6$ kPa which in terms of the water compressibility is $4.35 \times 10^{-7}\ \mathrm{m^2/kN}$. The values of the compressibility of pure water, given by Moshagen & Tørum (1975), Madsen (1978), Yamamoto *et al.* (1978) and Nago & Maeno (1984) are practically the same.

Bishop & Eldin (1950) and Skempton & Bishop (1954) based their approximate calculation of the compressibility of water-air mixture on Boyle's law and also incorporated Henry's law to describe the effects of the solubility of air in water. The surface tension was disregarded by them. Water vapour, bonded bubbles and pore water compressibility were also not taken into account. They proposed the following formula:

$$\beta' = (1 - S_i + h_{sl} S_i)\, P_i / P_h^2 \tag{3.46}$$

where: β' - compressibility of pore fluid [$\mathrm{m^2/kN}$],
S_i - degree of saturation at initial state [-],
h_{sl} - coefficient of volumetric solubility of air in water [-],
P_i - absolute pore pressure at initial state [kPa],
P_h - absolute hydrostatic pressure [kPa].

Koning (1963) and Verruijt (1969) included fluid compressibility and treated a water-air mixture as an immiscible fluid and computed compressibility using Boyle's

law, but disregarded solubility, water vapour pressure and bonded bubbles. They only partly accounted for the influence of the surface tension between air and water, and for practical purposes, where small pressure changes occur, their formula is sufficient and is expressed as:

$$\beta' = S\beta_w + \frac{1-S}{P_h} \tag{3.47}$$

where: β' - compressibility of pore fluid [m^2/kN],
S - degree of saturation [-],
β_w - compressibility of pure water [m^2/kN],
P_h - absolute hydrostatic pressure [kPa].

The first attempt to take into account the influence of all possible factors on the compressibility of the water-air mixture was made by Schuurman (1966) who tried to account for the surface tension effects by directly applying Kelvin's cappilary model equation. The given theory is only right in relation to the degree of saturation in excess of 85 % where the free air is assumed to be present in the form of bubbles. The bubbles are either the same size as the pores or smaller. In deriving the compressibility equation, it was neccesary to assume the number and size of air bubbles. Therefore, the final equation becomes unusable from the engineering point of view.

Fredlund (1976) suggested that it is not neccesary to include Kelvin's equation, since it results in a useless formula for the compressibility of pore fluid. Furthermore, he introduced instead of Kelvin's equation, which embeds the surface tension, another pore pressure parameter, B_{aw} (see Eq. 3.35), which incorporates in fact the surface tension influence. The parameter seems to be nearly equal to unity in many practical cases.

3.2.2 Simplifications and choice for the present work

With the aid of previously mentioned laws and simplifications, Barends (1980) found a convenient expression for the resultant compressibility of a water-air mixture in a porous medium. The following assumptions are made in his analysis:

- the water-air mixture comprises water, dissolved air, isometric free bubbles surrounded by water, and bonded bubbles partly adhered to solid surfaces,
- the degree of saturation is 85 % or more ($S \geq 0.85$),
- the bubbles contain free air and water vapour,
- conforming the Boyle-Mariotte law, the air density is proportional to the air pressure,
- the water-air surface tension of free bubbles, the representative bonded bubble radius, the water vapour pressure and the air solubility coefficient are considered as constants,
- diffusion of air in water is disregarded and successive states of equilibrium are considered.

The fluid pressure can be expressed as a function of the initial state and the degree of saturation (Barends, 1980):

$$\beta' = \beta_w + \frac{[1-(1-h_{sl})\,S]^2}{S\,(1-h_{sl})\,[1-(1-h_{sl})\,S_i]\left(P_i - w + \dfrac{2\sigma_t}{r_{bi}}\right) - \dfrac{2\sigma_t}{3r_{bi}}\,[1-(1-h_{sl})\,S]^2\,\sqrt[3]{\dfrac{(1-S_i-v_b)}{(1-S-v_b)^4}}} \tag{3.48}$$

where: β' - compressibility of pore fluid [m^2/kN],
β_w - compressibility of pure water [m^2/kN],
S - degree of saturation [-],
h_{sl} - coefficient of volumetric solubility of air in water [-],
S_i - initial degree of saturation [-],
P_i - initial absolute pore fluid pressure [kPa],
w - water-vapour pressure [kPa],
σ_t - water-air surface tension of free air bubbles [kN/m],
r_{bi} - initial free air bubble radius [m],
v_b - relative volume of bonded air bubbles [-].

The existence of bonded bubbles plays a minor role concerning the value of the pore fluid compressibility when the pore fluid pressure is less than the critical pressure (this is very often a practical case). If, additionally, the water vapour pressure and the surface tension are disregarded, Eq. (3.48) becomes:

$$\beta' = \beta_w + \frac{[1-(1-h_{sl})\,S]^2}{S\,(1-h_{sl})\,[1-(1-h_{sl})\,S_i]\,P_i} \tag{3.49}$$

Barends (1980) mentioned a value of the compressibility of pure water as equal to $5 \times 10^{-7}\,m^2/kN$ which stays in a very good accordance with the values presented by Fredlund (1976), Madsen (1978), Yamamoto *et al.* (1978), Nago & Maeno (1984).

Applying Eq. (3.49) for the degree of saturation $S = 0.99$ at the atmospheric pressure $p_{at} = 101.3\,kPa$, and assuming the coefficient of volumetric solubility of air in water $h_{sl} = 0.02$, the compressibility of water-air mixture is $\beta' = 3.0 \times 10^{-4}\,m^2/kN$, which shows to be the same with that obtained by Fredlund (1976).

It is important to note that when introducing the coefficient of volumetric solubility of air in water $h_{sl} = 0$ into Eq. (3.49), and assuming independence of the degree of saturation from the pore fluid pressure, one obtains exactly Eq. (3.43) or Eq. (3.45), proposed by Koning (1963) and Verruijt (1969), and used by many researchers, among others: Madsen (1978), Yamamoto *et al.* (1978), and Okusa (1985[a]). For a high degree of saturation, Eq. (3.47) seems to describe properly the relation between the degree of saturation and the pore fluid compressibility.

Equation (3.49) does not work properly for a very high degree of saturation together with a simultaneous assumption that the coefficient of volumetric solubility of air in water is a constant. Following Eq. (3.49) for fully saturated soil conditions ($S = 1.0$), and assuming $h_{sl} = 0.02$ and $P_h = 200\,kPa$, the compressibility is equal to $\beta' \cong 10^{-4}\,m^2/kN$, which is about 10^3 times higher than the compressibility of pure water. It is surely because the coefficient of volumetric solubility of air in water is assumed to be constant. At a certain critical soil saturation condition, S_{cr}, the amount of air existing in water in terms of free bubbles is equal to the amount of air, described by the coefficient of volumetric solubility, which is supposed to go into solution. Therefore, it is proposed in

the present work to assume that the degree of saturation higher than the critical value $S_{cr} = 1 - h_{sl}$ implies values of the coefficient of volumetric solubility of air in water smaller than for $S \leq S_{cr}$, where h_{sl} is assumed to be maximum and constant. And thus, the modified Eq. (3.49) can be written as:

$$\beta' = \beta_w + \frac{(1 - h'_{sl}S)^2}{Sh'_{sl}(1 - h'_{sl}S_i)\,P_i} \tag{3.50}$$

where the new incorporated parameter h'_{sl} is conditionally equal to:

$$h'_{sl} = S_{cr} = 1 - h_{sl} \qquad \text{for} \qquad S \leq S_{cr} = 1 - h_{sl} \tag{3.51a}$$

$$h'_{sl} = S \qquad \text{for} \qquad S > S_{cr} = 1 - h_{sl} \tag{3.51b}$$

The dependence of the new defined parameter h'_{sl} on the degree of saturation is grafically presented in Fig. 3.12.

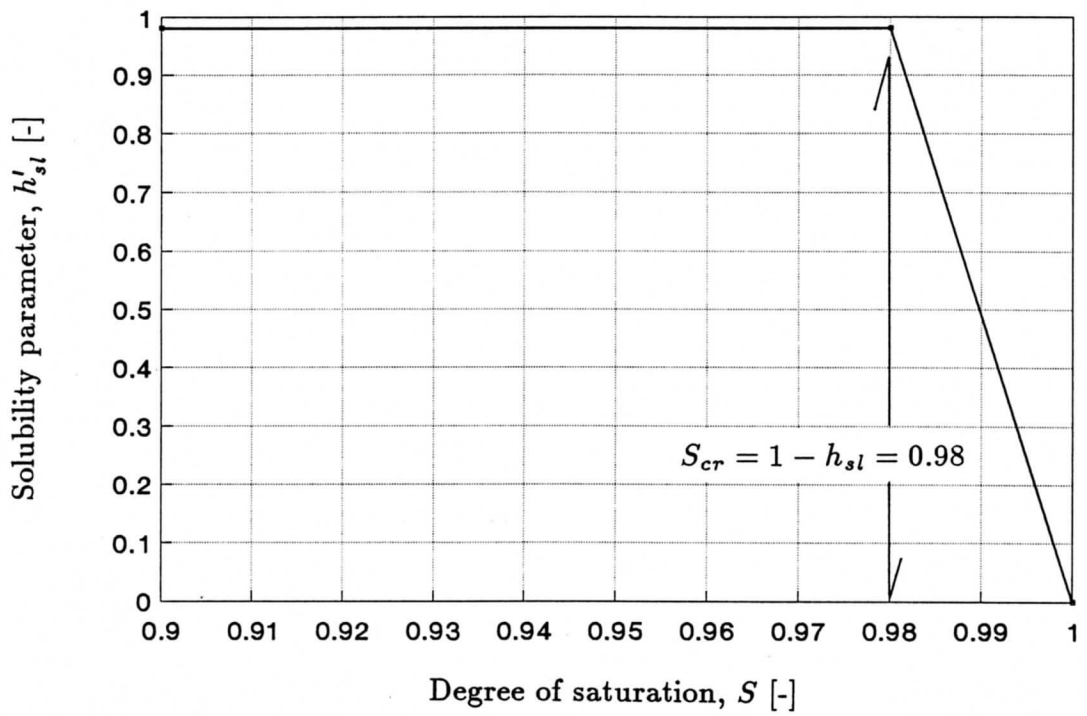

Figure 3.12 Modified solubility parameter h'_{sl} [Eq. (3.50) with Eqs. (3.51a,b); $h_{sl} = 0.02$ and $P_h = 200\,\text{kPa}$ are assumed]

Figure 3.13 presents a comparison of compressibility values of the pore fluid compressibility, using Eq. (3.43) [or Eq. (3.45)], Eq. (3.40) for $B_{aw} = 1$ [or Eq. (3.47)], Eq. (3.49), and Eq. (4.50) together with Eqs. (3.51a) and (3.51b), assuming $h_{sl} = 0.02$ and $P_h = 200\,\text{kPa}$.

The results coming from Eq. (3.49) must be disqualified due to relatively different and wrong behaviour, compared with the other equations, for the degree of saturation approaching unity. Taking into account that saturation conditions of sandy seabed sediments are normally characterized by the degree of saturation relatively close to unity, it is proposed to use Eq. (3.43) in computations of the compressibility of pore

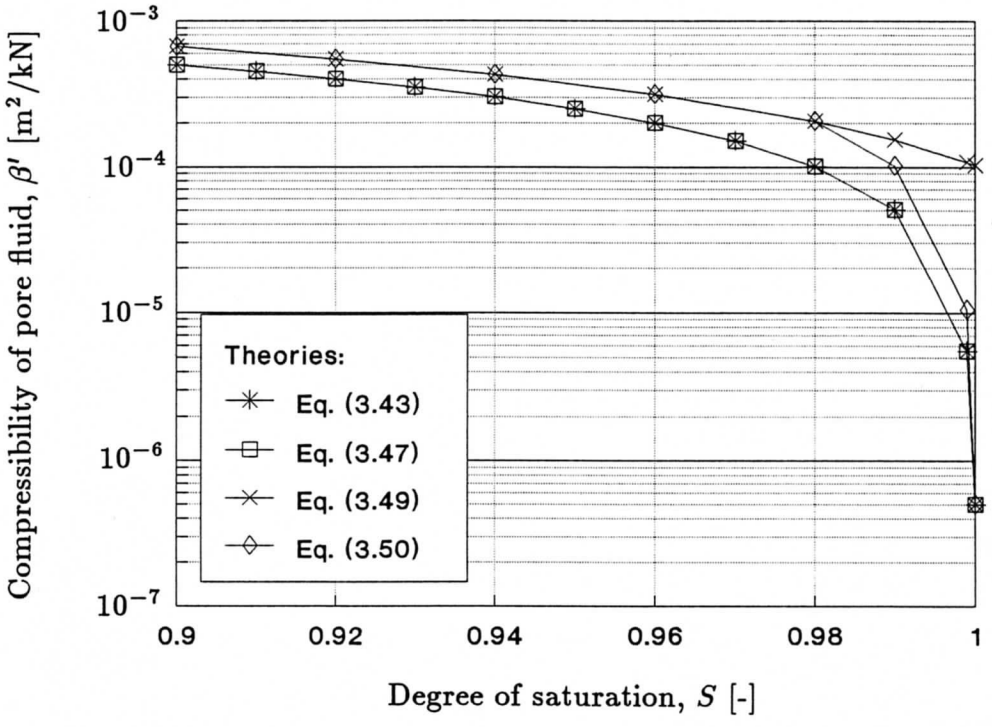

Figure 3.13 Comparison of different formulas for compressibility of pore fluid

fluid in the following analysis of the wave-induced pore pressure cyclic oscillations in sandy soils. Other formulas could be also used but:

- they are too complicated from the practical point of view, and some parameters are hardly measureable,
- the results are similar to these obtained from Eq. (3.43).

3.3 Conclusions

The compressibility of the pore fluid constitutes one of the most important parameter involved in a mathematical description of the wave-induced pore pressure oscillations in the seabed. A high sensitivity of the solution to the pore pressure on the pore fluid compressibility, especially when the soil is partly saturated, requires that the value of compressibility used in calculation procedures must be defined with a high accuracy.

It was shown that Eq. (3.43) proposed by Verruijt (1969) and correlating directly the compressibility with the degree of saturation, brings satisfactory accuracy when comparing with other existing formulas. Moreover, the above mentioned relationship has a strong practical importance because Eq. (3.43) does not contain parameters (*e.g.*, diameter of air bubbles) describing a micro-structure of the three-phase medium. In Eq. (3.43) the number of different factors is reduced to only one very meaningful parameter, namely, the degree of saturation.

As a link between theoretical considerations and practical implications, the *in-situ* measurements of the degree of saturation were performed on the beach of Norderney

Island, subjected to continuous tidal movements. During the measuring campaigne, numerous samples were taken from sandy seabed sediments being under the water level at the moment of sampling. Series of laboratory measurements and statistical analysis were performed to supply information about a real, mean value of the degree of saturation typical for sandy seabed sediments under the natural environmental conditions. It was found that the soil material of that area was partly saturated and the mean value of the degree of saturation was equal $\bar{S} = 0.95$.

Partly saturated seabed sediments, found under the natural environmental conditions, confirmed the need of taking into account the pore fluid compressibility into the theoretical formulation of the considered problem of the wave-induced pore pressure in seabed sediments. The results of the measurements showed also that partly saturated soil conditions have to be taken into account at least in these situations where the coastline zone is concerned. Partly saturation of seabed sediments can be explained by either a turbulent water motion, due to a continuous wave breaking action typical for transitional and shallow water conditions, or alternative saturations and dewaterings of seabed sediments, due to tidal water movements.

The variability (defined by the coefficient of variation) in measured soil parameters, compared with these published in the literature, confirms a very good quality of the whole procedure applied for the sand sampling. The statistical analysis confirmed also the assumption of a well-fitted normal distribution approximation to the distribution of the degree of saturation from *in-situ* sampling.

In most practical cases, where the upper layer of seabed sediments is concerned, the hydrostatic pressure, p_h, is computed with respect to the point laying on the seabed surface, and set to a constant in computations of the pore pressure distribution induced in seabed sediments by a surface water wave motion. However, if a computational depth in the seabed is relatively large (*i.e.*, comparable with the head of atmospheric pressure, p_{at}) the assumption of a constant value of the absolute hydrostatic pressure, P_h, can lead to meaningful errors. This has, however, no important meaning for the coastal engineering practice because most of the problems concerns only with an upper (*i.e.*, up to few metres) part of seabed sediments.

Chapter 4

Pore pressure distribution in a sea-bed layer of finite thickness

4.1 Pore pressure and effective stress principle

When the pore spaces are filled with pure water (*i.e.*, fully saturated soil), the pressure in the water is called the pore water pressure. If the pore spaces are filled with a pore fluid (*i.e.*, a mixture of water and gas; partly saturated soil), the pressure in the pore fluid is called the pore fluid pressure, or simply – pore pressure. The last term, as more general, can be sucsessfully used in both two main cases of soil saturation conditions. The pore pressure acts in all directions with equal intensity.

A pore pressure can be positive, the so-called overpressure, when the pore pressure is greater than the initial hydrostatic pressure. A pore pressure can also be negative, the so-called underpressure, defined as the pore pressure that is less than the initial hydrostatic pressure. A pore pressure can be increased or decreased by applying or removing, respectively, a compressive force to the soil. A pore pressure can also increase or decrease when a shear force is applied to a soil, in which the mineral soil skeleton is in a loosely or densely, respectively, packed state. The present study considers changes in the pore pressure, with respect to the initial hydrostatic state defined by the still water level, due to cyclic oscillations of the hydrodynamic pressure at the sea bottom as a result of water waves action. Therefore, this type of pore pressure is very often called the wave-induced pore pressure or the hydrodynamic pore pressure (Fig. 4.1).

The importance of the forces transmitted through the soil skeleton from particle to particle was recognized in 1923 when Terzaghi presented the principle of effective stress, an intuitive relationship based on experimental data. The principle applies only to fully saturated soils and relates the following three stresses (Craig, 1992):

- the total normal stress on a plane within the soil mass is the force per unit area transmitted in a normal direction across the plane, imagining the soil to be a solid (single-phase) material,
- the pore pressure is the pressure of the water filling the void space between the solid particles,

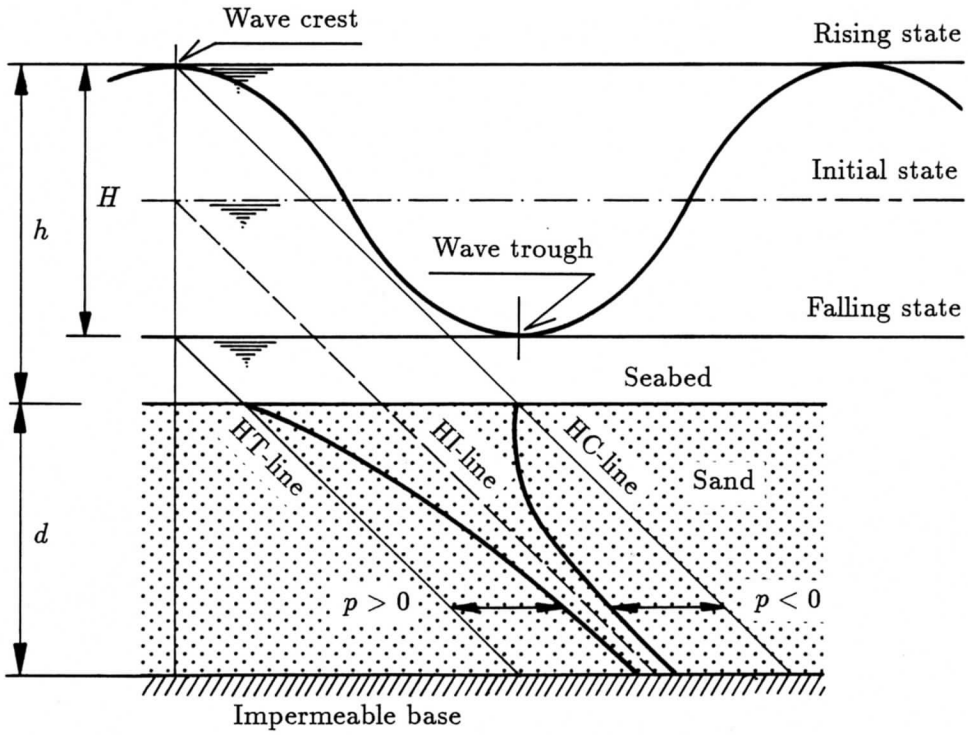

Figure 4.1 Qualitative range of cyclic oscillations of the wave-induced pore pressure, p, in permeable seabed sediments, due to water wave loading

- the effective normal stress on the plane represents the stress transmitted through the soil skeleton only.

The effective stress principle can be given by the following relationship:

$$\sigma = \sigma' + p_t \tag{4.1}$$

where: σ - total normal stress [kPa],
σ' - effective normal stress [kPa],
p_t - pore pressure [kPa].

A soil mass, having a horizontal surface and with the water table at a surface level, is considered. The total vertical stress (*i.e.*, the total normal stress on a horizontal plane) at depth z is equal to the weight of all material (soil-water mixture) per unit area above that depth, *i.e.*:

$$\sigma_z = \gamma_{sat} z \tag{4.2}$$

where: σ_z - total vertical stress [kPa],
γ_{sat} - unit weight of saturated soil [kN/m^3],
z - depth in seabed [m].

A more proper name for the pore pressure, p_t, would be the total pore pressure. This is due to the fact that this pore pressure could be a sum of a hydrostatic pressure (with a still water surface in or above soil sediments), since the void space between the

solid particles is continuous, and a wave-induced instantaneous pore pressure. Therefore, at depth z:

$$p_t = p_h + p(z) = \gamma_w z + p(z) \tag{4.3}$$

where: p_t - total pore pressure [kPa],
p_h - hydrostatic pore pressure [kPa],
p - wave-induced pore pressure [kPa],
γ_w - unit weight of water [kN/m^3],
z - depth in seabed [m].

Comparing Eqs. (4.1) to (4.3), the effective vertical stress at depth z can be given as:

$$\begin{aligned} \sigma' &= \sigma_z - p_t = \\ &= (\gamma_{sat} - \gamma_w)\, z - p(z) = \gamma' z - p(z) \end{aligned} \tag{4.4}$$

where: σ' - effective normal stress [kPa],
σ_z - total vertical stress [kPa],
p_t - total pore pressure [kPa],
p - wave-induced pore pressure [kPa],
γ_{sat} - unit weight of saturated soil [kN/m^3],
γ_w - unit weight of water [kN/m^3],
γ' - buoyant unit weight of soil [kN/m^3],
z - depth in seabed [m].

In the case of partly saturated soils, one part of the void space is occupied by water and another part by air. Due to the surface tension, the total pore pressure, p_t, must always be less than the pore air pressure. Unless the degree of saturation is close to unity, the pore air will form continuous channels through the soil, and the pore water will be concentrated in regions around the interparticle contacts. The boundaries between pore water and pore air will be in the form of menisci which radii will depend on the size of the pore spaces within the soil. Part of any wavy plane through the soil will therefore pass through water and part through air.

Bishop (1960) proposed the following effective stress equation for partly saturated soils:

$$\sigma = \sigma' + p_a - \lambda (p_a - p_t) \tag{4.5}$$

where: σ - total normal stress [kPa],
σ' - effective normal stress [kPa],
p_a - pore air pressure [kPa],
λ - parameter, determined experimentally, related primarily to soil saturation conditions, [-],
p_t - total pore pressure [kPa].

The term $(p_a - p_t)$ is a measure of a suction in the soil. For a fully saturated soil ($S = 1$), $\lambda = 1$, and for a completely dry soil ($S = 0$), $\lambda = 0$. Equation (4.5) thus degenerates to Eq. (4.1) when $S = 1$. The value of λ is also influenced, to some extent, by the soil structure and the way the particular degree of saturation was brought about.

Equation (4.5) is not convenient for use in practice because of the presence of parameter λ which is difficult to define.

If the degree of saturation is close to unity it is likely that the pore air will exist in the form of bubbles within the pore water, and it is possible to draw a wavy plane through the pore water only. The soil can then be considered as a saturated soil but with the pore fluid having higher compressibility than pure water due to the presence of the air bubbles. Equation (4.1) may then represent the effective stress with a sufficient accuracy for most practical purposes (Craig, 1983).

Many advanced solutions for the prediction of the pore pressure cyclic oscillations are, among others, strongly dependent on the compressibility of the pore fluid (*i.e.*, water-air mixture) where air is partly dissolved in water and partly entrapped as air-bubbles in pores of the soil. The formerly discussed relationship, between the amount of air existing in the pore fluid and the compressibility of the pore fluid, can be defined using a very common and surprisingly simple formula proposed by Verruijt (1969) [see Eq. (3.43) and Tab. 3.4].

An example of a direct influence of the degree of saturation on the wave-induced pore pressure that can be produced by surface wave loading is shown in Fig. 4.2, using the analytical solution derived by Madsen (1978) for the case of infinite thickness of the permeable seabed layer.

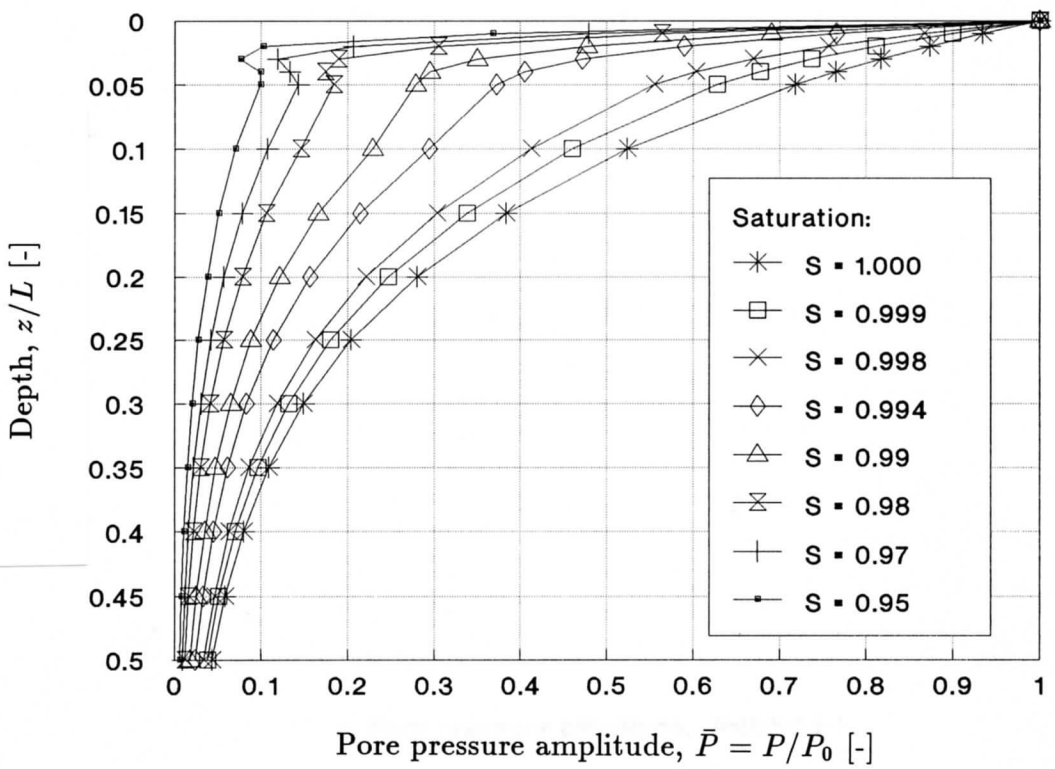

Figure 4.2 Example of wave-induced pore pressure amplitude attenuation with depth in seabed sediments, for different values of degree of saturation ['infinite-thickness layer' solution of Madsen (1978); computed for: $E = 10^5$ kPa, $k = 10^{-4}$ m/s, $n = 0.4$, $\nu = 0.3$, $h = 20$ m, $T = 6$ s, and $\beta = 4.2 \times 10^{-7}$ m^2/kN]

It is very easy to recognize that changes in the degree of saturation even by a relatively small increment, in the range which is supposed to be found under natural

environmental conditions, cause significant changes in the pore pressure distribution in seabed sediments. This certifies how meaningful this parameter is. Therefore, it can also emphase the necessity of checking and proving values of the degree of saturation under natural conditions by means of *in-situ* measurements.

Firstly, in order to enable a comparison with the final solution searched for in this work, two different cases of the wave-induced pore pressure solution, assuming: (1) both the soil skeleton and the pore fluid incompressible (*i.e.*, potential problem), and (2) the soil skeleton incompressible whereas the pore fluid compressible (*i.e.*, diffusion problem) will be briefly described in the following.

4.2 Potential problem

Assuming that the seabed consists of sand or dense silt, the pore fluid flow and soil displacement can be decoupled because these geological materials are relatively stiff. For this case, named as the potential model, the pore fluid flow may be modeled by Darcy's equation while the soil skeleton is considered inelastic. Considering uniform permeability of the soil, and invoking conservation of mass for an incompressible fluid, this yields to a geometrical problem only, defined by the Laplace equation [see Eq. (2.1)] for the dynamic pore pressure response of the seabed.

The wave-induced pore pressure distribution in a permeable seabed can be found by solving Laplace's equation together with appropriate boundary conditions. On the top of the seabed, a pressure wave (hydrodynamic bottom pressure) is moving in phase with the surface water wave. The hydrodynamic bottom pressure oscillations, and the amplitude thereof, can be well-approximated using Airy's linear theory of small-amplitude waves [see Eqs. (2.6) and (2.7)].

If the permeable seabed layer is infinitely deep, the wave-induced pore pressure must vanish asymptotically with depth in seabed sediments. Taking the above into account, the geometrical problem to be solved can be given as a system of three coupled equations:

$$\nabla^2 p = 0 \tag{4.6a}$$

$$p_b = P_0 \cos[i(ax - \omega t)] \qquad \text{for} \quad z = 0 \tag{4.6b}$$

$$p \to 0 \qquad \text{as} \quad z \to \infty \tag{4.6c}$$

where: p - wave-induced pore pressure (complex-valued) [kPa],
p_b - hydrodynamic bottom pressure oscillations (complex-valued) [kPa],
P_0 - amplitude of the hydrodynamic bottom pressure [kPa],
a - wave number [m^{-1}],
ω - wave angular frequency [s^{-1}],
t - time [s],
x, z - horizontal and vertical coordinates of the Cartesian coordinates system, respectively, [m],
i - imaginary unit ($i = \sqrt{-1}$).

If, on the other hand, the permeable seabed layer has a limited thickness (see Fig. 2.1), the boundary condition of no flow of the pore fluid perpendicular to the

impermeable and rigid base has to be assumed. This implies that Eq. (4.6c) must be replaced by an alternative boundary condition in the following form:

$$\frac{\partial p}{\partial z} = 0 \qquad \text{for} \qquad z = d \tag{4.6d}$$

The pore-pressure at any point within the seabed can be determined from a solution of the boundary value problem, consisting of the main Laplace equation [Eq. (4.6a)] and the boundary conditions [Eqs. (4.6b), and (4.6c) or Eq. (4.6d)].

Assuming the permeable seabed layer to be of infinite thickness, the wave-induced pore pressure solution, being the solution to the Laplace equation, is rather simple and can be written as:

$$p = P_0 \exp(-az) \cos[i(ax - \omega t)] \tag{4.7}$$

where, additionally:

p - wave-induced pore pressure (complex-valued) [kPa].

This potential solution was first developed by Putnam (1949) and later veryfied by Ried & Kajiura (1957) who showed that the inertial effects can be neglected, justifying thereby the use of Darcy's law.

Introducing another boundary condition [see Eq. (4.6d)] in the form of impermeable base located under the permeable seabed layer, the wave-induced pore pressure in the seabed is also obtained from the solution of the Laplace equation, and can be presented as:

$$p = P_0 \frac{\cosh[a(d-z)]}{\cosh(ad)} \cos[i(ax - \omega t)] \tag{4.8}$$

where, additionally:

d - thickness of the permeable seabed layer [m].

For simplicity and convenience of presentation of pore pressure results, the wave-induced pore pressure, p, can be given in its relative and dimensionless form, as it was shown in Section 2.2.1, by dividing the momentary pore pressure, $\Re\{p\} = p'$, by the amplitude of the hydrodynamic bottom pressure, P_0. And thus, Eqs. (4.7) and (4.8) can be respectively replaced by:

$$\bar{p} = \exp(-az) \cos(ax - \omega t) \tag{4.9}$$

$$\bar{p} = \frac{\cosh[a(d-z)]}{\cosh(ad)} \cos(ax - \omega t) \tag{4.10}$$

where, additionally:

$\bar{p}$ - relative (and dimensionless) wave-induced pore pressure [-].

As an example, Fig. 4.3 presents the pore pressure distribution with depth in the seabed of infinite thickness, computed for five different characteristic phases of the first half of the wave loading cycle; the picture from the second half can be easily achieved by a mirror-mapping of the picture from the first one.

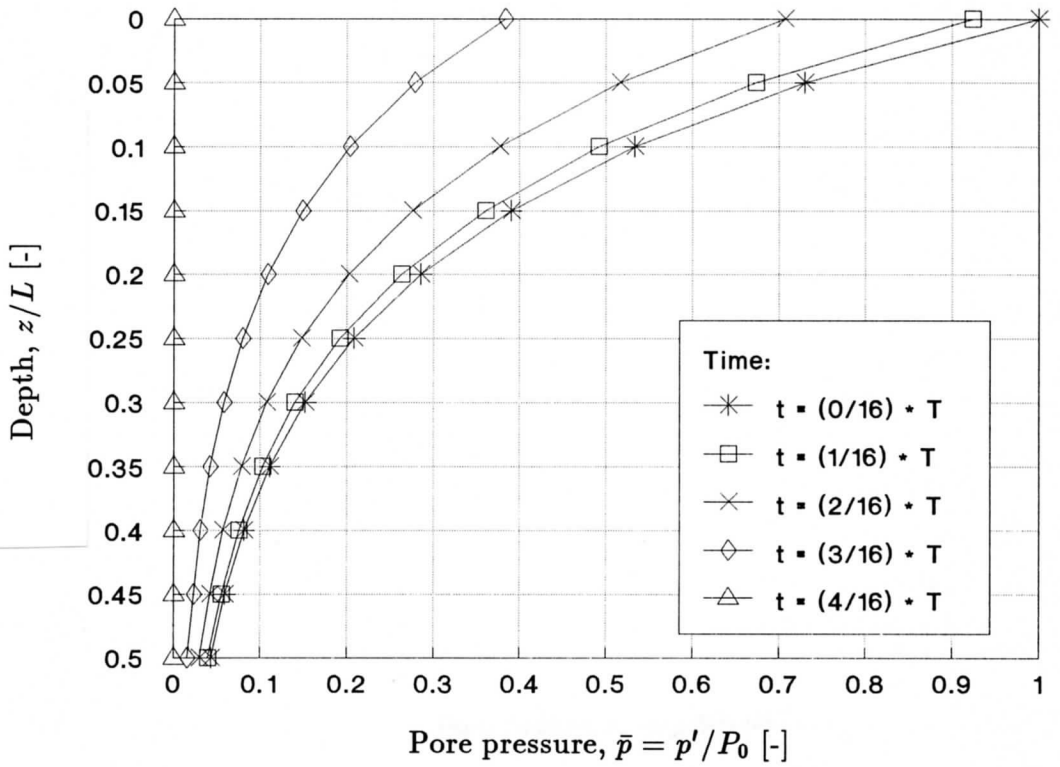

Figure 4.3 Wave-induced pore pressure distribution with depth in permeable seabed layer of infinite thickness, computed for different phases of wave loading cycle (potential problem)

Figure 4.4 compares the 'infinite-' and the 'finite-thickness layer' solution to the amplitude of wave-induced pore pressure cyclic oscillations, computed for different thicknesses of the permeable seabed layer (the seabed thickness is given in a relative and dimensionless form, *i.e.* d/L, where d is the thickness of the permeable seabed layer, and L is the wavelength). It can be indicated how the impermeable boundary condition, imposed at the base of the permeable seabed layer, increases the pore pressure amplitude when approaching the lower boundary. Figure 4.5 illustrates the difference between the 'infinite-' and the 'finite-thickness layer' solutions to the pore pressure amplitude at the lower impermeable boundary, using the following two additional parameters, *i.e*:

$$P_1^{(i-f)} = \bar{P}^{(i)} - \bar{P}^{(f)} \tag{4.11}$$

$$P_2^{(i-f)} = \frac{\bar{P}^{(i)} - \bar{P}^{(f)}}{\bar{P}^{(i)}} \tag{4.12}$$

where: $P_1^{(i-f)}$ - absolute difference (between 'infinite-' and 'finite-thickness layer' solutions) in the pore pressure amplitude at impermeable base [-],

$P_2^{(i-f)}$ - relative difference (between 'infinite-' and 'finite-thickness layer' solutions) in the pore pressure amplitude at impermeable base [-],

$\bar{P}^{(i)}$ - relative pore pressure amplitude at impermeable base, obtained from the 'infinite-thickness layer' solution, [-],

$\bar{P}^{(f)}$ - relative pore pressure amplitude at impermeable base, obtained from the 'finite-thickness layer', solution [-].

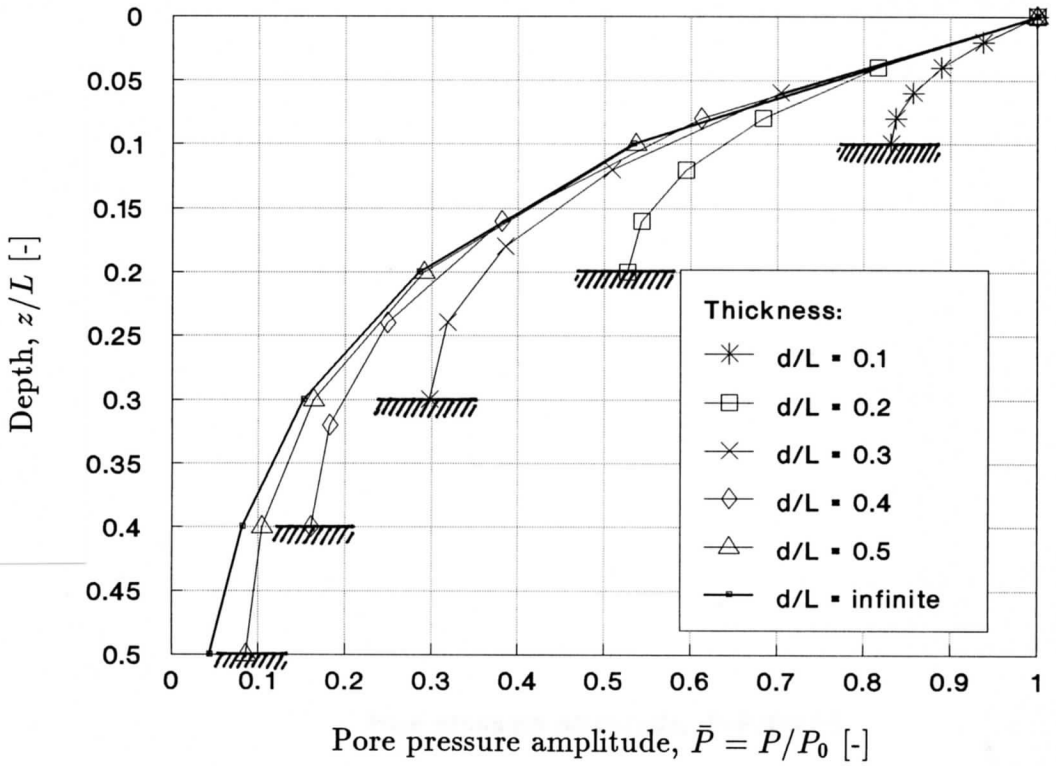

Figure 4.4 Wave-induced pore pressure amplitude distribution with depth in permeable seabed layer of different thicknesses (potential problem)

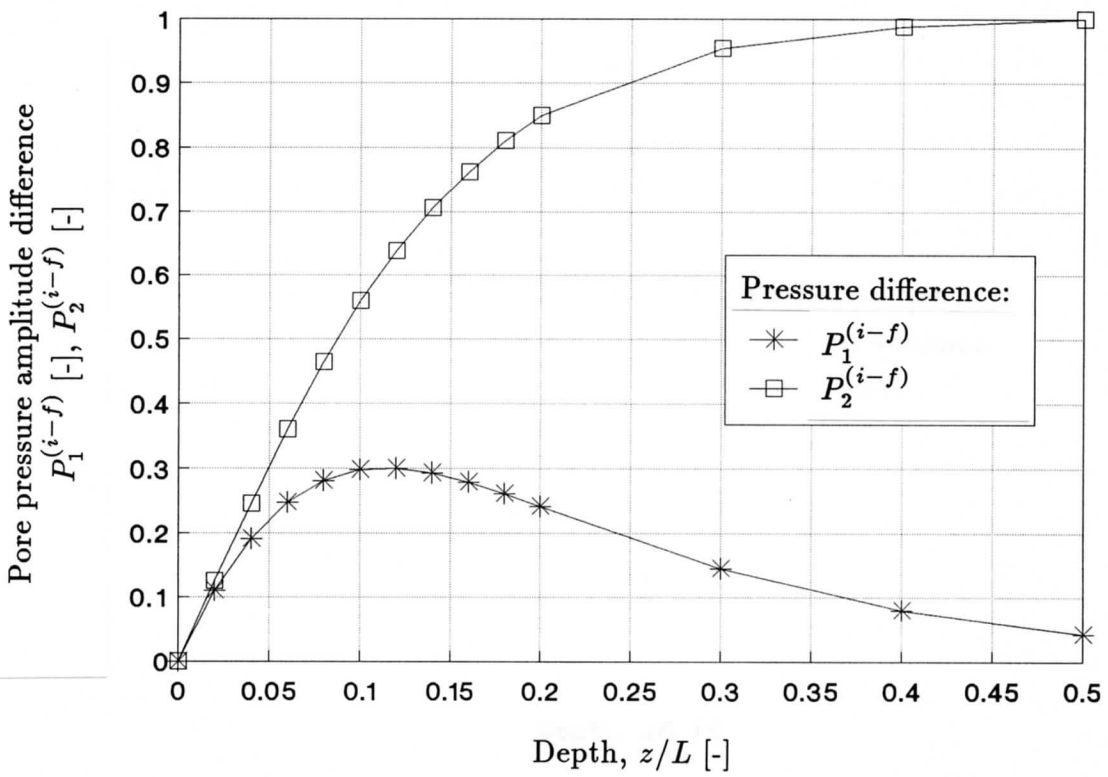

Figure 4.5 Wave-induced pore pressure amplitude difference, between 'infinite-' and 'finite-thickness layer' solutions, at bottom of permeable seabed layer (potential problem)

Although the relative difference $P_2^{(i-f)}$ can approach a value of 1 for greater thicknesses, the absolute difference $P_1^{(i-f)}$ reaches its maximum for $d/L \cong 0.1$, becoming smaller for all other values of the relative thickness, d/L.

4.3 Diffusion problem

Under realistic conditions, the pore fluid is represented by a two-phase medium where the water and air components can be distinguished. However, in order to simplify the calculation procedure, the compressibility of this two-phase medium can be defined by a very convenient, from the engineering practice point of view, formula proposed by Verruijt (1969) [see Eq. (3.43) in Chapter 3], and applicated by many researchers (*e.g.*: Madsen, 1978; Yamamoto *et al.*, 1978; Okusa, 1985[a]) into their wave-induced pore pressure theories. The formula, describing the pore fluid compressibility in terms of soil saturation conditions, represented by the degree of saturation, has already been given in Eq. (3.43).

An analytical solution to the diffusion problem [see Eq. (2.2)], describing the wave-induced pore pressure response in seabed sediments under the assumption of compressibility for the pore fluid, was initially presented by Moshagen & Tørum (1975). Assuming the same boundary conditions as for the potential problem [see Eq. (4.6b) to Eq. (4.6d)], their solution, more complicated than the solution to the potential problem, can be presented as follows:

- for infinite thickness of the permeable seabed layer

$$\bar{p} = \Re\left\{\exp\left[-\mu\left(\frac{k_x}{k_z}\right)^{1/2} z\right]\exp[i(ax-\omega t)]\right\} \tag{4.13}$$

- for finite thickness of the permeable seabed layer

$$\bar{p} = \Re\left\{\frac{\cosh\left[\mu\left(\frac{k_x}{k_z}\right)^{1/2}(d-z)\right]}{\cosh\left[\mu\left(\frac{k_x}{k_z}\right)^{1/2} d\right]}\exp[i(ax-\omega t)]\right\} \tag{4.14}$$

in which μ is a complex-valued parameter, as defined by the following relations:

$$\mu = |\mu|\exp[iArg(\mu)] \tag{4.15a}$$

$$|\mu| = \left[a^4 + \left(\frac{\omega n\gamma}{k_x K'}\right)^2\right]^{1/4} \tag{4.15b}$$

$$Arg(\mu) = \frac{1}{2}\arctan\left(\frac{n\gamma L^2}{2\pi k_x K' T}\right) \tag{4.15c}$$

where: $\bar{p}$ - relative wave-induced pore pressure [-],
k_x, k_z - coefficients of soil permeability in x- and z-direction, respect., [m/s],
K' - apparent bulk modulus of pore fluid ($K' = 1/\beta'$) [kPa],

β' - compressibility of pore fluid [m^2/kN],
n - porosity of soil [-],
γ - unit weight of pore fluid [kN/m^3],
a - wave number [m^{-1}],
L - wavelength [m],
d - thickness of the permeable seabed layer [m],
ω - wave angular frequency [s^{-1}],
T - wave period [s],
t - time [s],
x, z - horizontal and vertical coordinates of the Cartesian coordinates system, respectively, [m],
μ - parameter (complex-valued) [m^{-1}],
$|\mu|$ - modulus of complex-valued parameter μ [m^{-1}],
$Arg(\mu)$ - argument of complex-valued parameter μ [rad],
$\Re\{\ \}$ - real part of $\{\ \}$,
i - imaginary unit ($i = \sqrt{-1}$).

Equation (4.13), or Eq. (4.14), gives the wave-induced pore pressure solution based on the diffusion model of the two-phase seabed medium. The solution is given in the form presented by Eq. 2.13. As it was already mentioned in Section 2.2.1, it is also possible to present the pore pressure solution in the form given in Eq. (2.15), in terms of the amplitude (modulus of the complex-valued wave-induced pore pressure, p) [see Eq. (2.14a)] and the phase lag (argument of the complex-valued wave-induced pore pressure, p) [see Eq. (2.14b)] of wave-induced pore pressure oscillations in the seabed.

4.3.1 Results of example calculations

In order to perform illustrative calculations of the wave-induced pore pressure oscillations in seabed sediments, governed by the diffusion problem, the following input data were used:

- porosity of soil $n = 0.4$
- coefficient of permeability $k = 10^{-2}, 10^{-4}\,m/s$ $(k = k_x = k_z)$
- degree of saturation $S = 0.95 - 1.0$ (from partly to fully saturated soil)
- permeable seabed layer of finite thickness ($d = 0.5\,m$)
  - wave period $T = 6\,s$
  - water depth $h = 4.5\,m$
- permeable seabed layer of infinite thickness (half-space; $d = \infty$)
  - wave period $T = 8\,s$
  - water depth $h = 20\,m$

Results of computations performed for the case of infinite thickness of the permeable seabed layer are presented in Figs. 4.6 to 4.10 (the layer only up to a depth of $z = L/2$ is illustrated), whereas the case of finite thickness is shown in Figs. 4.11 to 4.14.

In the first step, high permeable ($k = 10^{-2}\,m/s$) sandy sediments were assumed for computations. Figures 4.6 and 4.7 show, respectively, the wave-induced pore pressure amplitude and the phase lag distribution with depth in the permeable seabed layer. In the case of fully saturated soil conditions ($S = 1$), the pore pressure amplitude and

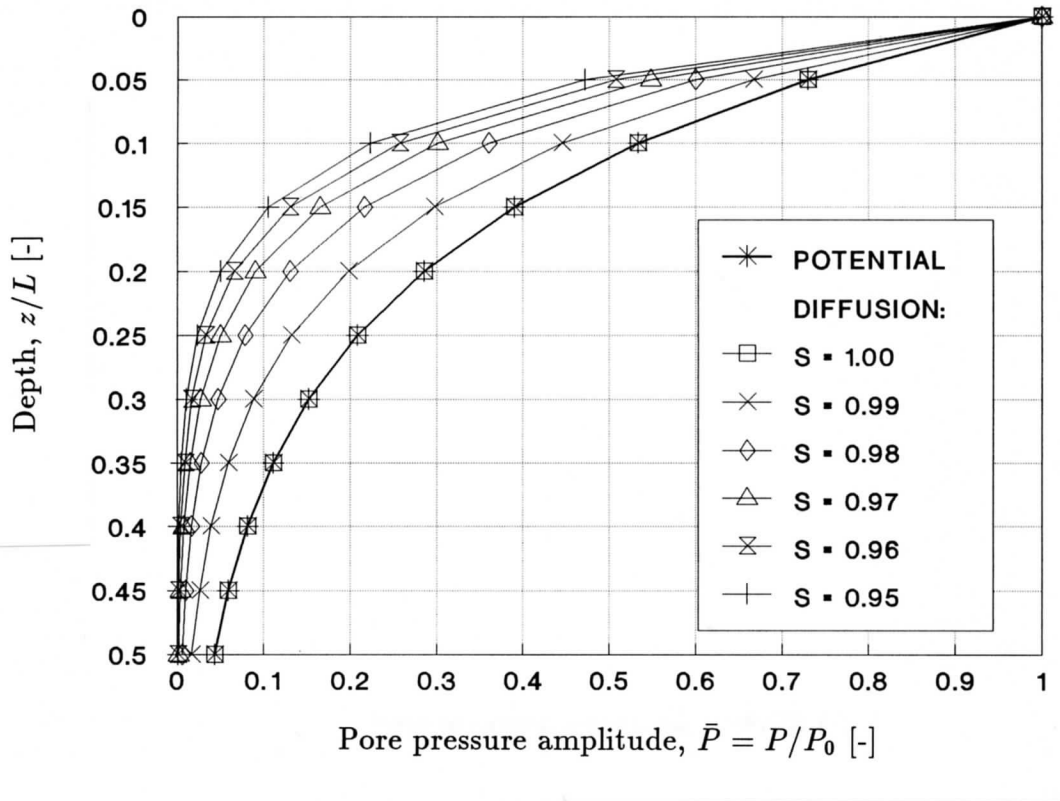

Figure 4.6 Wave-induced pore pressure amplitude distribution with depth in permeable seabed layer of infinite thickness, and for different soil saturation conditions (diffusion problem; $k = 10^{-2}$ m/s)

the phase lag do not differ from the potential solution. However, introducing partly saturated soil conditions, the pore pressure attenuation, accompanied by the increase in phase lag, is indicated. The phase lag is linearly dependent on the depth in seabed sediments. It is interesting to note that at a depth of one half of the wavelength, soil saturation conditions $S = 0.95 - 0.96$ induce the pore pressure oscillations shifted approximately 360° (*i.e.*, one period of wave loading) with respect to oscillations of the hydrodynamic bottom pressure. Figure 4.8 shows the pore pressure distribution in the vertical profile just under the wave crest ($kx - \omega t = 0$) or, treating it as a mirror image, under the wave trough ($kx - \omega t = \pi$).

Analogous to Figs. 4.6 and 4.7, Figs. 4.9 and 4.10 present the results of computations with a less permeable ($k = 10^{-4}$ m/s) sandy seabed layer of infinite thickness. A much stronger pore pressure attenuation can be easily recognized. Practically, already for $S = 0.99$, the pore pressure oscillations vanish when the depth approaches $z = 0.1L$. Simultaneously, a very strong increase in the phase lag is observed where, at a depth of $z = L/2$, the phase lag is approximately fivefold of the period of water loading oscillations.

If relatively high soil permeability and small ($d = 0.5$ m) limited thickness of the permeable seabed layer are assumed, the pore pressure is only very slightly attenuated (Fig. 4.11), and the influence of different soil saturation conditions can be only indicated from the phase lag distribution with depth (Fig. 4.12), although the phase lag is very small and can be neglected from the practical point of view. The seabed layer reacts almost immediately to the wave-induced pressure oscillations at the seabed surface, and therefore there is almost no pore pressure demping effects in seabed sediments.

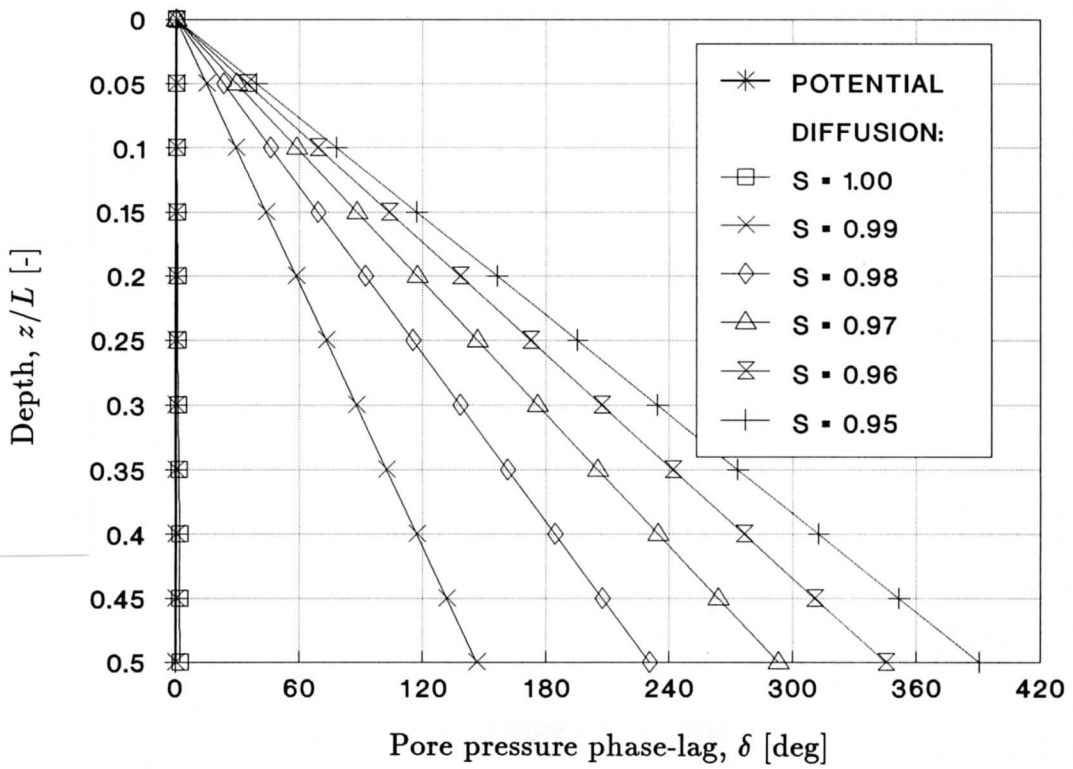

Figure 4.7 Wave-induced pore pressure phase-lag distribution with depth in permeable seabed layer of infinite thickness, and for different soil saturation conditions (diffusion problem; $k = 10^{-2}$ m/s)

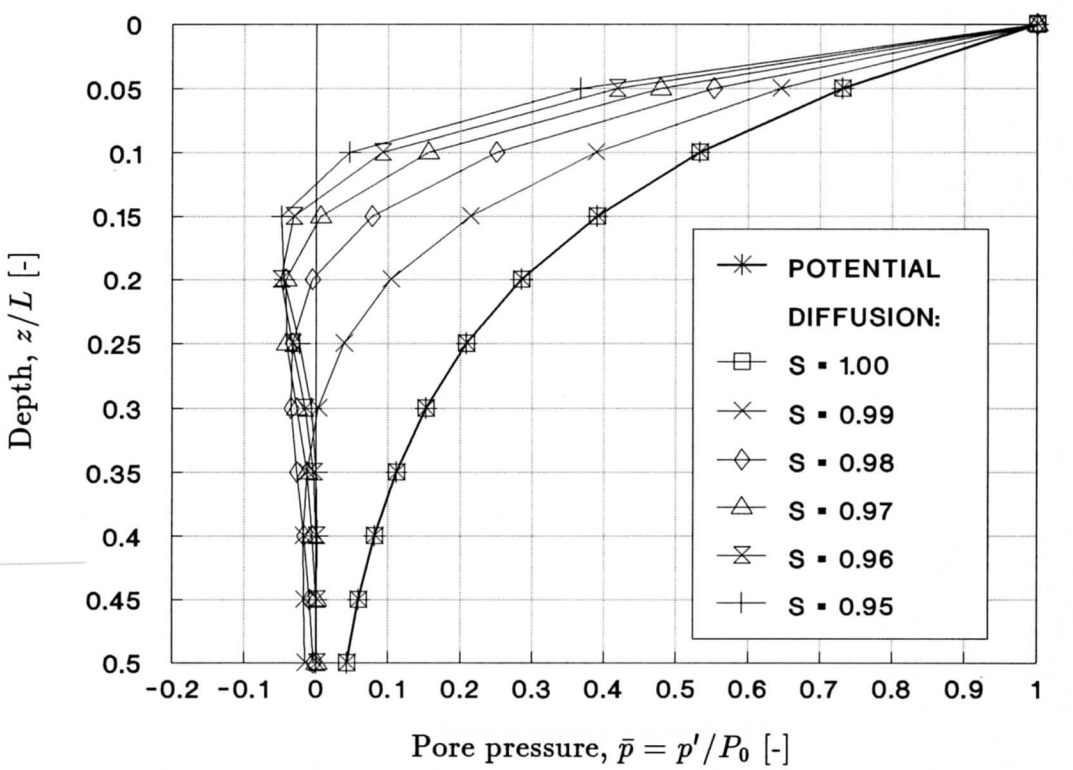

Figure 4.8 Wave-induced pore pressure distribution with depth in permeable seabed layer of infinite thickness, under wave crest or wave trough, and for different soil saturation conditions, (diffusion problem; $k = 10^{-2}$ m/s)

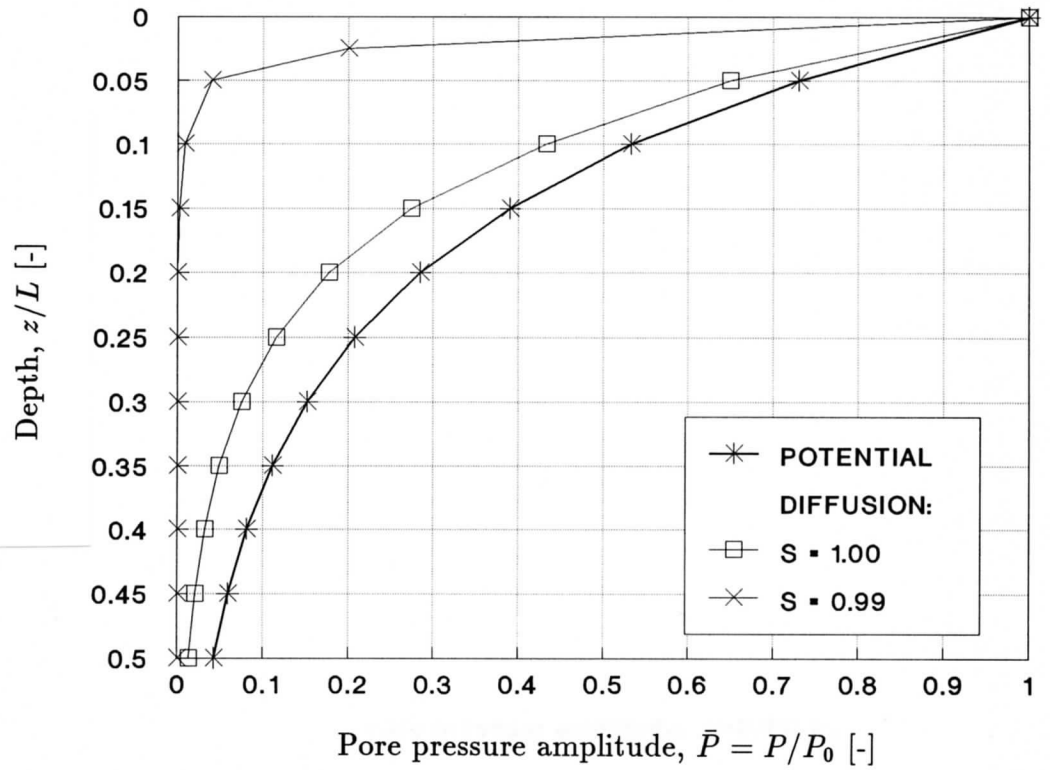

Figure 4.9 Wave-induced pore pressure amplitude distribution with depth in permeable seabed layer of infinite thickness, and for different soil saturation conditions (diffusion problem; $k = 10^{-4}$ m/s)

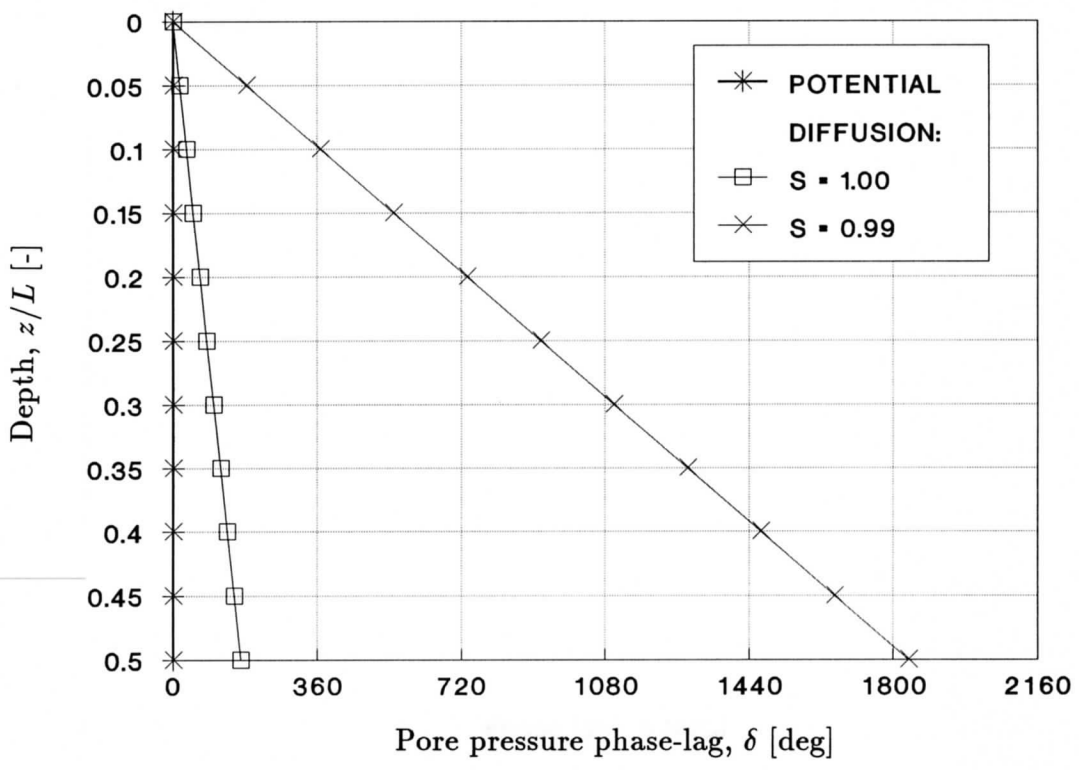

Figure 4.10 Wave-induced pore pressure phase-lag distribution with depth in permeable seabed layer of infinite thickness, and for different soil saturation conditions (diffusion problem; $k = 10^{-4}$ m/s)

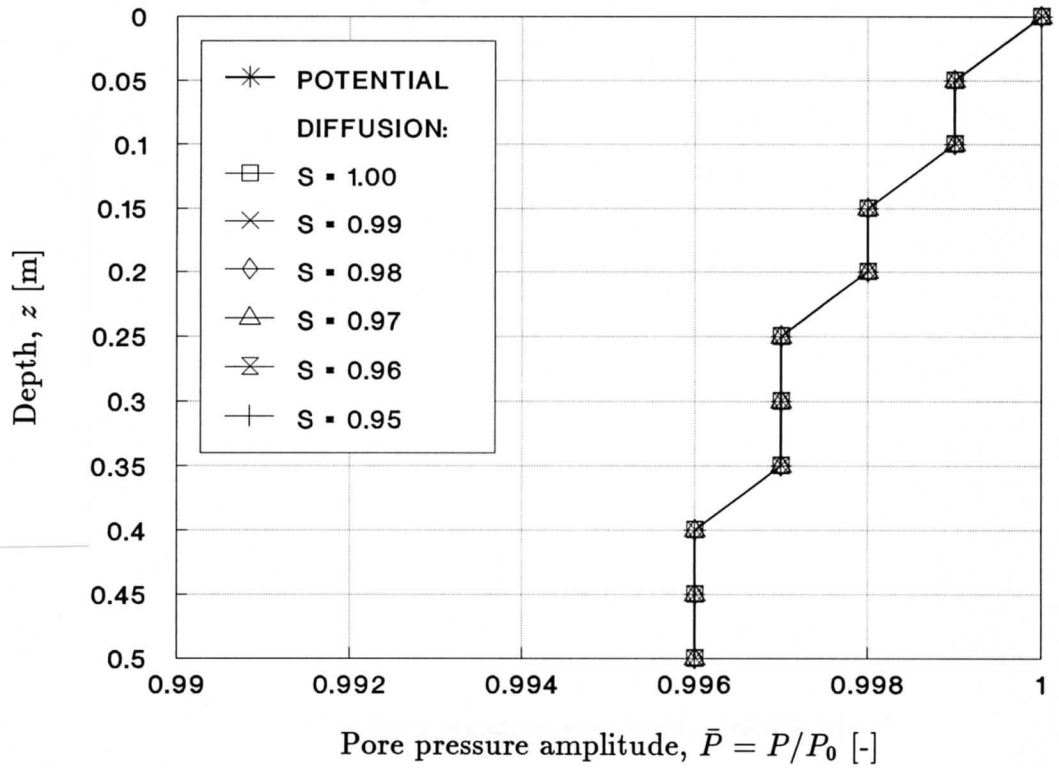

Figure 4.11 Wave-induced pore pressure amplitude distribution with depth in permeable seabed layer of finite thickness, and for different soil saturation conditions (diffusion problem; $k = 10^{-2}$ m/s)

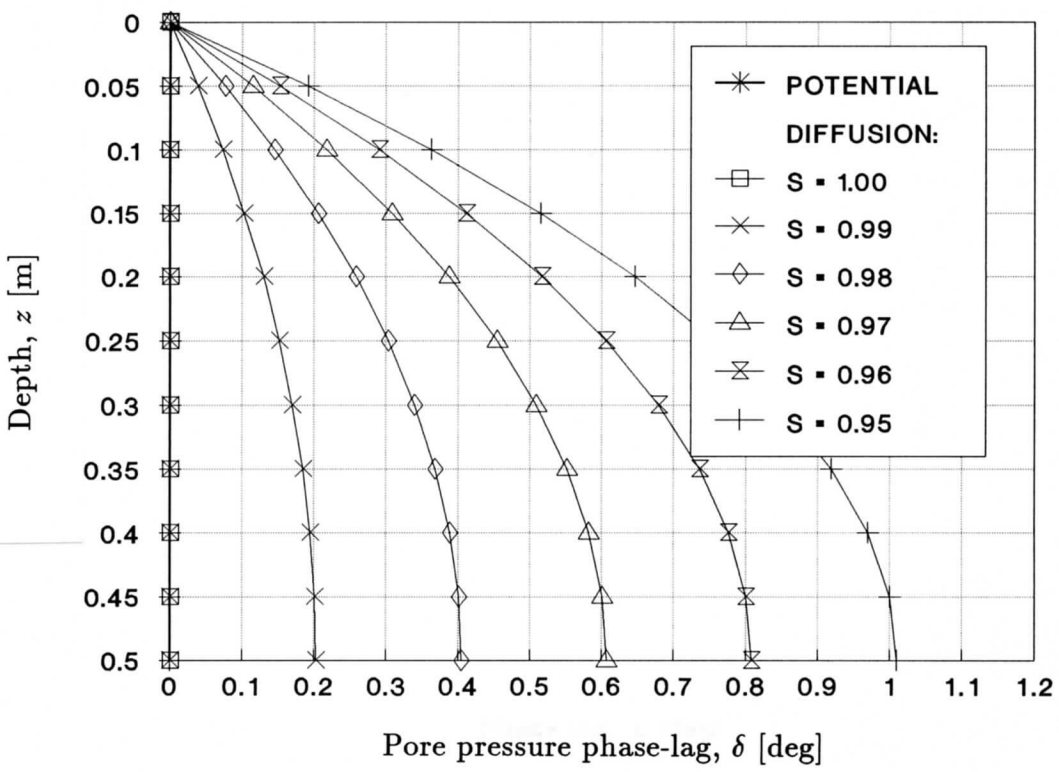

Figure 4.12 Wave-induced pore pressure phase-lag distribution with depth in permeable seabed layer of finite thickness, and for different soil saturation conditions (diffusion problem; $k = 10^{-2}$ m/s)

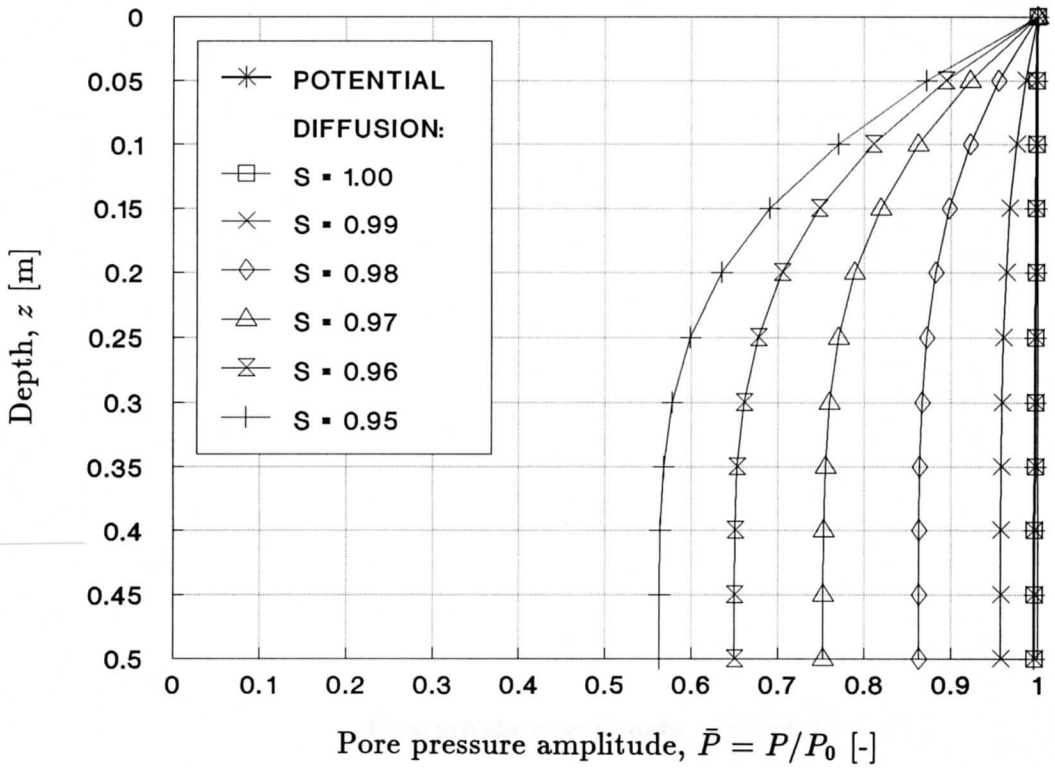

Figure 4.13 Wave-induced pore pressure amplitude distribution with depth in permeable seabed layer of finite thickness, and for different soil saturation conditions (diffusion problem; $k = 10^{-4}$ m/s)

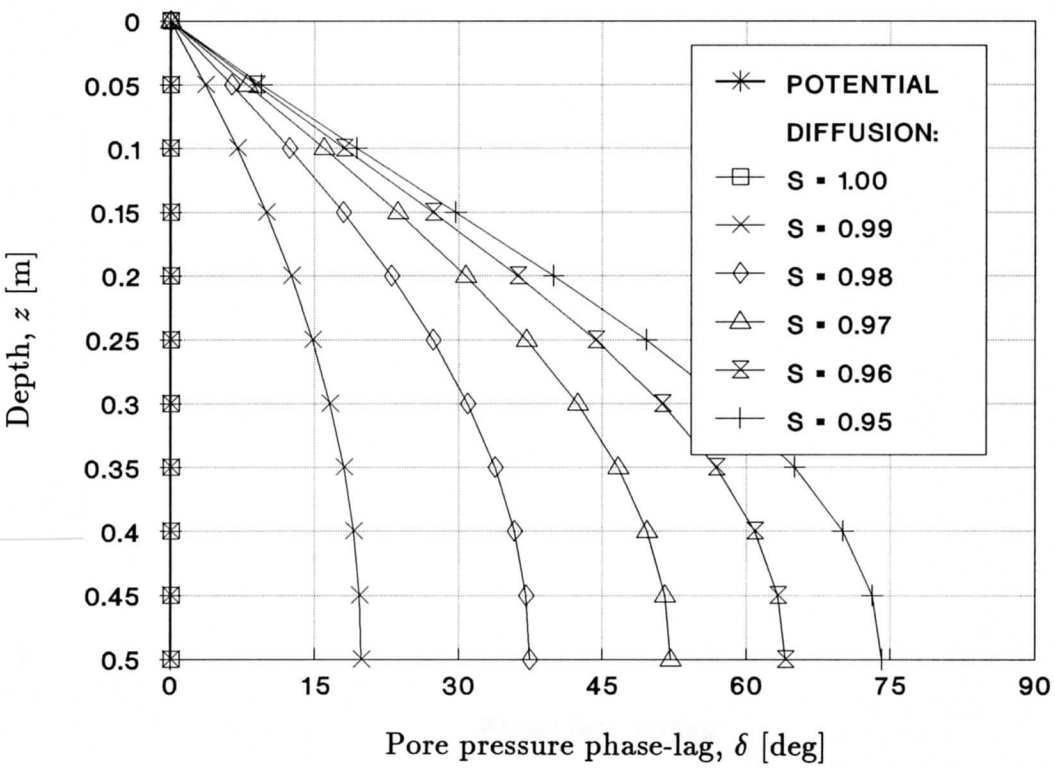

Figure 4.14 Wave-induced pore pressure phase-lag distribution with depth in permeable seabed layer of finite thickness, and for different soil saturation conditions (diffusion problem; $k = 10^{-4}$ m/s)

However, assuming lower permeability conditions (*e.g.*, $k = 10^{-4}$ m/s), the pore pressure attenuation (Fig. 4.13) and the phase lag (Fig. 4.14) become meaningful, depending strongly on the pore fluid compressibility which, in turn, is a direct function of soil saturation conditions represented by the degree of saturation, S.

4.4 Storage problem – two-dimensional analytical solution

Distinguishing between the two compressibility models of the two-phase system, *i.e.*: (1) potential model, where the soil skeleton and pore fluid are treated as incompressible, and (2) diffusion model, where only the pore fluid is assumed to be compressible, the available solutions for the wave-induced pore pressure were presented in former Sections 4.2 and 4.3 of the present work.

For many purposes in soil mechanics, it is permissible to uncouple the solid and fluid parts of the two-phase medium in order to treat two simpler analyses separately. This can be done only when at least one of the two-phase components (*i.e.*, soil skeleton or pore fluid) is considered to be incompressible. However, it may be also desirable on occasion to analyse the true coupled performance of a composite continuum, in which the two phases interact. Examples of practical importance would involve external loads which vary in time, and structure-foundation interaction analyses where the pore pressure response in the foundation is completely dependent upon the relative stiffness of the components of the two-phase system. That is, a stiff or inhomogeneous structure causes different pore pressures from a flexible or homogeneous one.

Appropriate analytical solutions to this problem were presented, among others, by Madsen (1978), Yamamoto *et al.* (1978), Yamamoto (1981), and Okusa (1985[a]). The following description of the two-dimensional analytical solution is based on the theory proposed by Madsen (1978). It is a general theory for the pore pressure and effective stresses induced in a porous seabed by ocean waves. Both the pore fluid and the soil skeleton are considered compressible, and the flow in the porous seabed is assumed to be governed by Darcy's law for an anisotropic medium. The main goal of this part of the work is to derive an explicit solution for the wave-induced pore pressure under the assumption of a finite thickness of the permeable seabed layer. The 'finite-thickness layer' solution has a very important bearing on further analysis of laboratory test results but would also have a wide application to several engineering problems considered to happen under natural environmental conditions.

The 'finite-thickness layer' solution will be derived for the instantaneous pore pressure induced in the seabed by surface water wave propagation. The effect of a layered soil profile on the pressure distribution is emphasized here, considering a limited thickness of a single permeable seabed layer resting on a stiff and impermeable base. It is supposed that the stress level remains within the elastic range. The fundamental description of the deformation of a saturated porous medium has been accomplished by Biot (1941) and is known as Biot's theory of consolidation. The problem is treated analytically in the classic way; using the general solution to the governing partial differential equation, given by Madsen (1978), and applaying proper boundary conditions, an explicite solution will be derived.

4.4.1 Basic equations

In many practical problems appeared in the coastal engineering, there are many subsoil stratifications and hydrotechnical structures that can be treated as vertically two-dimensional. Assuming also that the seabed is loaded by simple two-dimensional harmonic surface water waves characterized by long crests parallel to each other, then as a result, the seabed is deformed under plain strain conditions (see Fig. 2.1).

Another basic assumption is that the soil skeleton obeys Hook's law (*i.e.*, the soil has linear, reversible, isotropic, nonretarded, and mechanical properties). Since the relatively small oscillatory deformations with respect to the hydrostatic equilibrium state are of interest, such idealized assumption may be reasonable. Following the concept of linear consolidation or poro-elasticity, three basic equations exist. From Terzaghi's principle of effective stress together with Hooke's law, defined by the shear modulus, G, and Poisson's ratio, ν, of the soil skeleton, the two equations describing equilibrium in x- and z-directions are as follows [Yamamoto *et al.*, 1978; Mazurkiewicz, 1985]:

$$G\nabla^2 u_x + \left(\frac{G}{1-2\nu}\right)\frac{\partial \epsilon}{\partial x} = \frac{\partial p}{\partial x} \tag{4.16a}$$

$$G\nabla^2 u_z + \left(\frac{G}{1-2\nu}\right)\frac{\partial \epsilon}{\partial z} = \frac{\partial p}{\partial z} \tag{4.16b}$$

where: G - shear modulus of soil [kPa],
∇ - nabla ($\nabla = \partial/\partial x + \partial/\partial z$),
u_x, u_z - wave-induced displacements of soil skeleton in x- and z-direction, respectively, [m],
ν - Poisson's ratio [-],
ϵ - volumetric strain of soil skeleton (defined to be positive for elongation) [-],
p - wave-induced pore pressure [kPa],
x, z - horizontal and vertical coordinates of the Cartesian coordinates system [m].

The inertia term associated with the movement of sediment particles can be neglected, and this was justified by Massel (1976). The last two equations, describing the elastic equilibrium of a medium, can be also written in the following general form, in which the wave-induced total stress is resolved into the wave-induced effective stress and the wave-induced pore pressure (Haar, 1966):

$$\frac{\partial \sigma_x'}{\partial x} + \frac{\partial \tau'}{\partial z} = -\frac{\partial p}{\partial x} \tag{4.17a}$$

$$\frac{\partial \tau'}{\partial x} + \frac{\partial \sigma_z'}{\partial z} = -\frac{\partial p}{\partial z} \tag{4.17b}$$

where: σ_x', σ_z' - wave-induced effective stresses in x- and z-direction, respect., [kPa],
τ' - wave-induced effective shear stress [kPa],
p - wave-induced pore pressure [kPa],
x, z - horizontal and vertical coordinates of the Cartesian coordinates system, respectively, [m].

The volumetric strain of the soil skeleton is defined as:

$$\epsilon = \epsilon_x + \epsilon_z = \frac{\partial u_x}{\partial x} + \frac{\partial u_z}{\partial z} \tag{4.18}$$

where: ϵ - volumetric strain of soil (defined to be positive for elongation) [-],
ϵ_x, ϵ_z - normal strains of soil in x- and z-direction, respectively, [-].

The third equation, constituing the required system of three coupled partial differential equations, is the storage equation describing continuity for the pore fluid [Madsen, 1978; Yamamoto *et al.*, 1978]:

$$\frac{k}{\gamma}\nabla^2 p = n\beta' \frac{\partial p}{\partial t} + \frac{\partial \epsilon}{\partial t} \tag{4.19}$$

where: k - coefficient of permeability for isotropic soil [m/s],
γ - unit weight of pore fluid [kN/m^3],
∇ - nabla ($\nabla = \partial/\partial x + \partial/\partial z$),
p - wave-induced pore pressure [kPa],
n - porosity of soil [-],
β' - compressibility of pore fluid [m^2/kN],
ϵ - volumetric strain of soil [-],
t - time [s].

Equation (4.19) is derived from conservation of mass of the pore fluid [Okusa, 1985]:

$$\frac{\partial(\rho v_x)}{\partial x} + \frac{\partial(\rho v_z)}{\partial z} = -\rho \frac{\partial}{\partial t}\left(\frac{\partial u_x}{\partial x} + \frac{\partial u_z}{\partial z}\right) - n\rho \frac{\partial \theta}{\partial t} \tag{4.20}$$

where: ρ - density of pore fluid [kg/m^3],
v_x, v_z - discharge velocities in x- and z-direction, respectively, [m/s],
u_x, u_z - wave-induced displacements of soil skeleton in x- and z-direction, respectively, [m],
θ - volumetric strain of pore fluid [-],
n - porosity of soil [-],
x, z - horizontal and vertical coordinates of the Cartesian coordinates system, respectively, [m],
t - time [s],

in conjunction with the assumption that the flow of pore fluid is governed by the steady state form of Darcy's law (for hydraulically isotropic conditions):

$$v_x = -\frac{k}{\rho g}\frac{\partial p}{\partial x} \tag{4.21a}$$

$$v_z = -\frac{k}{\rho g}\frac{\partial p}{\partial z} \tag{4.21b}$$

where, additionally:
g - acceleration due to gravity [m/s^2].

The compressibility of pore fluid, β', is given in the following relationship:

$$\frac{\partial \rho}{\partial t} = \rho\beta' \frac{\partial p}{\partial t} \tag{4.22}$$

In principle, the pore fluid consists of two phases, *i.e.*: liquid (*e.g.*, water) and air. According to the discussion in Chapter 3, the compressibility of the water-air mixture, β', can be expressed by Eq. (3.43), depending on soil saturation conditions and the absolute hydrostatic pressure.

Equation (4.19), for the flow of a compressible pore fluid in a compressible porous medium, has a form very similar to the diffusion equation, and it is called the storage equation (Verruijt, 1969; Spierenburg, 1987). For a two-dimensional problem, and treating the porous seabed as hydraulically anisotropic, the storage equation may be given as:

$$\frac{k_x}{k_z}\frac{\partial^2 p}{\partial x^2} + \frac{\partial^2 p}{\partial z^2} = \frac{\gamma n \beta'}{k_z}\frac{\partial p}{\partial t} + \frac{\gamma}{k_z}\frac{\partial (\epsilon_x + \epsilon_z)}{\partial t} \tag{4.23}$$

where, aditionally:

k_x, k_z - coefficients of soil permeability in x- and z-direction, respectively, [m/s].

Assuming the plain strain conditions and hydraulically isotropic soil, the following two equations, describing elastic deformations of the soil skeleton, together with the storage equation, constitute the coupled problem and can be written in the following form of the system of three coupled partial differential equations:

$$G\left(\frac{\partial^2 u_x}{\partial x^2} + \frac{\partial^2 u_x}{\partial z^2}\right) + \frac{G}{1-2\nu}\frac{\partial}{\partial x}\left(\frac{\partial u_x}{\partial x} + \frac{\partial u_z}{\partial z}\right) = \frac{\partial p}{\partial x} \tag{4.24a}$$

$$G\left(\frac{\partial^2 u_z}{\partial x^2} + \frac{\partial^2 u_z}{\partial z^2}\right) + \frac{G}{1-2\nu}\frac{\partial}{\partial z}\left(\frac{\partial u_x}{\partial x} + \frac{\partial u_z}{\partial z}\right) = \frac{\partial p}{\partial z} \tag{4.24b}$$

$$\frac{k}{\gamma}\left(\frac{\partial^2 p}{\partial x^2} + \frac{\partial^2}{\partial z^2}\right) = \beta' n \frac{\partial p}{\partial t} + \frac{\partial}{\partial t}\left(\frac{\partial u_x}{\partial x} + \frac{\partial u_z}{\partial z}\right) \tag{4.24c}$$

where:
- p - wave-induced pore pressure [kPa],
- u_x, u_z - wave-induced displacements of soil skeleton in x- and z-direction, respectively, [m],
- G - shear modulus of soil [kPa],
- ν - Poisson's ratio [-],
- k - coefficient of permeability for isotropic soil [m/s],
- γ - unit weight of pore fluid [kN/m^3],
- β' - compressibility of pore fluid [m^2/kN],
- n - porosity of soil [-].

The above three equations of the governing problem can be found in many publications, *e.g.* Yamamoto *et al.* (1978), Madsen (1978), Nago & Maeno (1984), Okusa (1985[a]). The first Eq. (4.24a) is formed from the equilibrium condition in the x-direction, the second Eq. (4.24b) is formed from the equilibrium condition in the z-direction, and the third Eq. (4.24c) comes from the continuity principle incorporating Darcy's law of fluid flow through a porous medium.

And thus, the governing problem of poro-elastic seabed response to surface water wave loading is mathematically defined and can be solved in terms of the three unknowns, *i.e.*: wave-induced pore pressure, p, and wave-induced displacements of soil skeleton in x- and z-direction, u_x and u_z, respectively.

4.4.2 Constitutive relations

Resulting from the assumption that the seabed can be considered as an isotropic, homogeneous, linear, and elastic medium, stresses and strains are coupled by Hooke's law. According to Terzaghi's principle of effective stress, the deformations in the solid matrix are determined by the difference of the total stress and the pore fluid pressure. This stress difference, called the effective stress, characterizes the contact forces between the individual soil grains. Assuming the soil skeleton to behave as an ideal, isotropic, elastic material, and treating the governing problem under plain strain conditions, one has the following stress-strain relations:

$$\epsilon_x = \frac{\partial u_x}{\partial x} = \frac{-\left(1-\nu^2\right)}{E}\left(\sigma'_x - \frac{\nu}{1-\nu}\sigma'_z\right) \tag{4.25a}$$

$$\epsilon_z = \frac{\partial u_z}{\partial z} = \frac{-\left(1-\nu^2\right)}{E}\left(\sigma'_z - \frac{\nu}{1-\nu}\sigma'_x\right) \tag{4.25b}$$

where: ϵ_x, ϵ_z - volumetric strains in x- and z-direction, respectively, [-],
σ'_x, σ'_z - wave-induced effective normal stresses in x- and z-direction, respectively, [kPa],
u_x, u_z - wave-induced displacements of soil skeleton in x- and z-direction, respectively, [m],
E - Young's modulus of soil [kPa],
ν - Poisson's ratio [-],
x, z - horizontal and vertical coordinates of the Cartesian system, respectively, [m].

From Eqs. (4.25a) and (4.25b), expressions for the wave-induced effective stresses may be obtained in terms of soil displacements:

$$\sigma'_x = -\frac{(1-\nu)E}{(1+\nu)(1-2\nu)}\left(\frac{\partial u_x}{\partial x} + \frac{\nu}{1-\nu}\frac{\partial u_z}{\partial z}\right) \tag{4.26a}$$

$$\sigma'_z = -\frac{(1-\nu)E}{(1+\nu)(1-2\nu)}\left(\frac{\partial u_z}{\partial z} + \frac{\nu}{1-\nu}\frac{\partial u_x}{\partial x}\right) \tag{4.26b}$$

$$\tau' = -\frac{E}{2(1+\nu)}\left(\frac{\partial u_x}{\partial z} + \frac{\partial u_z}{\partial x}\right) \tag{4.26c}$$

where, additionally:
τ' - wave-induced effective shear stress [kPa].

After solving the system of three coupled partial differential equations [Eqs. (4.24a), (4.24b), and (4.24c)] in terms of the three unknowns, *i.e.*: wave-induced pore pressure, p, and wave-induced displacements of soil skeleton in x- and z- direction, u_x and u_z, respectively, the wave-induced effective stresses can be also obtained using the above presented constitutive relationships.

4.4.3 General solution

The following final partial differential equation of the 6^{th} order has to be solved to obtain its general solution (Madsen, 1978):

$$\frac{\partial^6 u_x}{\partial z^6} - a^2\left(2 + \frac{k_x}{k_z} - \frac{\kappa^2}{a^2}\right)\frac{\partial^4 u_x}{\partial z^4} + a^4\left(1 + 2\frac{k_x}{k_z} - 2\frac{\kappa^2}{a^2}\right)\frac{\partial^2 u_x}{\partial z^2} - a^6\left(\frac{k_x}{k_z} - \frac{\kappa^2}{a^2}\right)u_x = 0 \tag{4.27}$$

in which:

$$\kappa^2 = i\frac{\omega\gamma\left[n\beta' + \dfrac{1-2\nu}{2(1-\nu)G}\right]}{k_z} \tag{4.28}$$

where: u_x - horizontal (*i.e.*, in x-direction) wave-induced displacement (complex-valued) of soil skeleton [m],
k_x, k_z - coefficients of soil permeability in x- and z-direction, respect., [m/s],
a - wave number [m^{-1}],
κ - parameter (complex-valued) [m^{-1}],
ω - wave angular frequency [s^{-1}],
γ - unit weight of pore fluid [kN/m^3],
n - porosity of soil [-],
β' - compressibility of pore fluid [m^2/kN],
G - shear modulus of soil [kPa],
ν - Poisson's ratio [-],
i - imaginary unit ($i = \sqrt{-1}$).

The water wave loading on the surface of the seabed changes periodically in time and space. The process of consolidation is dominated by diffusion. Combined with low permeability, which results in small fluid velocities, it is reasonable to assume a harmonic response of the seabed. Therefore, the general solution to the above presented Eq. (4.27) with Eq. (4.28), given by Madsen (1978) in terms of the wave-induced horizontal displacement of soil skeleton, u_x, can be written as:

$$u_x = \left[(A_1 + A_2 z)e^{az} + (A_3 + A_4 z)e^{-az} + A_5 e^{\bar{k}az} + A_6 e^{-\bar{k}az}\right]\exp[i(ax - \omega t)] \tag{4.29}$$

in which:

$$\bar{k} = \sqrt{\frac{k_x}{k_z} - \frac{\kappa^2}{a^2}} \tag{4.30}$$

where, additionally:
$A_1, ..., A_6$ - arbitrary constants (complex-valued), to be determined from appropriate boundary conditions,
$\bar{k}$ - paramater (complex-valued) [-],
x - horizontal coordinate of the Cartesian coordinates system [m],
t - time [s].

4.4.4 Boundary conditions

For a semi-infinite permeable seabed layer only half of the general solution is valid. At infinite depth ($z \to \infty$), all displacements and stresses in the soil matrix together with the pore pressure must vanish. It is assumed that the seabed is homogeneous and occupies the lower part of the (x, z)-plane where $z > 0$ (see Fig. 2.1). The part of the solution with positive expotential powers does not conform to the conditions at infinite depth and, therefore, constants A_1, A_2 and A_5 [see Eq. (4.29)] are set to zero.

On the surface of the seabed ($z = 0$) a water wave loading is present. It is supposed that this load is a travelling two-dimensional harmonic wave, that for convenience will be written in complex form. The amplitude of the wave-induced hydrodynamic bottom pressure, P_0, can be calculated using Airy's linear wave theory [see Eq. (2.7)].

It is also assumed that the main phenomenon is a travelling pressure wave and that the boundary effects near the surface of the seabed can be neglected. As for the wave-induced effective shear stress at the surface of the seabed, it is known that a shear stress is associated with the oscillatory flow above the seabed. The fluid shear exerted at the surface of the seabed is, however, small and may be neglected. The wave-induced pressure field has a length scale which equals the wavelength while the boundary layer effects are rapidly damped because of relatively low soil permeability. Consequently, the wave-induced effective shear stress, τ', is zero at the sea floor. Furthermore, the wave-induced effective vertical normal stress, σ'_z, must vanish at the sea floor because the seabed is loaded by water waves only.

Taking the above into account, the assumption of infinite thickness of the permeable seabed layer implies the need to fulfil the following three boundary conditions at the surface of the seabed ($z = 0$):

$$p = P_0 \exp[i(ax - \omega t)] \tag{4.31a}$$

$$\sigma'_z = 0 \tag{4.31b}$$

$$\tau' = 0 \tag{4.31c}$$

where: p - wave-induced pore pressure [kPa],
σ'_z - wave-induced effective vertical normal stress [kPa],
τ' - wave-induced effective shear stress [kPa].

Field investigations frequently prove the existence of a limited thickness of a permeable and isotropic seabed layer or layers with different properties in the upper part of seabed sediments. The soil vertical profile may often look like a sand layer, possibly with permeable sub-layers, a few metres thick, overlaying an impermeable clay stratum.

At the bottom of the permeable seabed layer ($z = d$), a stiff impermeable base is supposed to exist. From this assumption follows that, at this level, the wave-induced vertical displacement of soil skeleton, u_z, is zero and the pore pressure gradient in z-direction (*i.e.*, normal to the base) is also zero which means that there is no flow normal to the horizontal boundary. The last condition refers to the contact between the permeable layer and the impermeable base. And thus, in the case of perfectly smooth interface, the wave-induced effective shear stress, τ', is zero and horizontal displacements are possible along this boundary. If, on the contrary, the contact is completely rough, a no-slip condition exists along the horizontal boundary $z = d$ and the wave-induced horizontal displacement, u_x, must be zero there. Generally, it can be expected that the

constraint (*i.e.*, no-slip) condition will be a better description of the contact between a permeable soil layer and an impermeable base than a perfectly smooth interface.

Summarizing, the boundary conditions at the bottom of the permeable seabed layer ($z = d$), required for obtaining a particular solution of the governing problem, are as follows:

$$u_z = 0 \tag{4.31d}$$

$$\frac{\partial p}{\partial z} = 0 \tag{4.31e}$$

$$u_x = 0 \quad \text{(for a completely rough base)} \tag{4.31f}$$

$$\tau' = 0 \quad \text{(for a perfectly smooth base)} \tag{4.31g}$$

where, additionally:

u_x, u_z - wave-induced displacements of soil skeleton in x- and z-direction, respectively, [m],

z - vertical coordinate of the Cartesian coordinates system [m].

Basically the same methods, that will be derived here in order to obtain the pore pressure response of a single layer, can be used for the case of a multi-layered seabed; however, the number of mathematical manipulations will increase substantially. If a horizontally layered (*i.e.*, vertically inhomogeneous) seabed is considered the boundary conditions at the interfaces between the sub-layers ($z = d_i$) are that the wave-induced stresses, pore pressure, pore fluid flow, and displacements of the soil skeleton are continuous (Yamamoto, 1981):

$$(\sigma'_z)_i = (\sigma'_z)_{i+1} \tag{4.32a}$$

$$\tau'_i = \tau'_{i+1} \tag{4.32b}$$

$$p_i = p_{i+1} \tag{4.32c}$$

$$k_i \frac{\partial p_i}{\partial z} = k_{i+1} \frac{\partial p_{i+1}}{\partial z} \tag{4.32d}$$

$$(u_x)_i = (u_x)_{i+1} \tag{4.32e}$$

$$(u_z)_i = (u_z)_{i+1} \tag{4.32f}$$

where k is the coefficient of soil permeability, and i ($i = 1, ..., N$) denotes the i-th sub-layer from all N sub-layers, into which the permeable seabed layer is divided.

Substitution of proper boundary conditions into the governing general solution [Eq. 4.29 with Eq. 4.30], and performance of some mathematical manipulations between the fundamental realationships describing the governing problem, lead to a system of six coupled, complex-valued, linear equations that can be solved using, for instance, one of numerical methods.

4.4.5 'Infinite-thickness layer' solution

The analytical solution for the pore pressure response of a homogeneous, poro-elastic, semi-infinite seabed layer was derived by many authors (*e.g.*: Madsen, 1978; Yamamoto *et al.*, 1978; Verruijt, 1982; Okusa, 1985[a]).

If the soil skeleton is incompressible and fully saturated with water, (*i.e.*, $S = 1$), the compressibility of pore fluid, β', is equal to the compressibility of pure water, β_w. The pore pressure response for this case is the same as it was observed from the potential solution [see Eqs. (4.9) and (4.10)] obtained by Putnam (1949), who assumed that the soil is rigid and the pore water is incompressible, and that obtained by Prevost *et al.* (1975), who assumed that the soil is an elastic continuum and no fluid flow takes place in the soil. The pore pressure attenuation for this case is small and independent of the soil permeability. Although the displacements are non-zero, the volumetric strain, ϵ, appears to be zero. The pore pressure satisfies the Laplace equation. In this case, the coupled equations uncouple and it is possible to study the pore fluid pressure separately. The fact that the volumetric strain, ϵ, is zero implies that no consolidation takes place, and that the grain skeleton has a constant volume. As a result, the seabed reacts like an impermeable and elastic material where a good transmission of the pore pressure is associated with the elastic deformation of the soil skeleton.

For partly saturated soil (*i.e.*, $S < 1$), compressibility of the pore fluid may exceed the compressibility of pure water by a considerable amount and, thereby, the relative compressibility of the pore fluid with respect to the compressibility of the soil skeleton increases drastically. For such case, the governing equations are more complicated and can be found in the works of Madsen (1978), Yamamoto *et al.* (1978), and Okusa (1985[a]). For example, Madsen's (1978) 'infinite-thickness layer' solution is cited here:

$$p = P_0 \left[C_1 \exp\left(-\bar{k}az\right) + C_2 C_3 \exp(-az)\right] \exp[i(ax - \omega t)] \tag{4.33}$$

where C_1, C_2, and C_3 are complex-valued constants given by:

$$C_1 = -f_1 \frac{(1-\nu)\left(\bar{k}^2 - 1\right)}{f_2(1-2\nu)} \tag{4.34a}$$

$$C_2 = \frac{(1-2\nu)\bar{k} - (1-\nu)\bar{k}^2 + \nu}{f_2} \tag{4.34b}$$

$$C_3 = \frac{1 - f_1 - 2\nu}{1-2\nu} \tag{4.34c}$$

in which:

$$f_1 = \frac{\left[\omega\gamma n\beta' + i\left(k_x - k_z\right)a^2\right](1-2\nu)}{\omega\gamma\left(n\beta' + \dfrac{1-2\nu}{G}\right) + i\left(k_x - k_z\right)a^2} \tag{4.34d}$$

$$f_2 = (1 - f_1 - 2\nu)\,\bar{k} - (1-\nu)\bar{k}^2 + \nu + f_1 \tag{4.34e}$$

where: p - wave-induced pore pressure (complex-valued) [kPa],
P_0 - amplitude of the wave-induced bottom pore pressure [kPa],
G - shear modulus of soil [kPa],
ν - Poisson's ratio [-],
k_x, k_z - coefficients of soil permeability in x- and z-direction, respect., [m/s],
$\bar{k}$ - parameter (complex-valued), given in Eq. (4.30), [-],
n - porosity of soil [-],
β' - compressibility of pore fluid [m^2/kN],
γ - unit weight of pore fluid [kN/m^3],
a - wave number [m^{-1}],
ω - wave angular frequency [s^{-1}],

t - time [s],
x, z - horizontal and vertical coordinates of the Cartesian coordinates system, respectively, [m],
i - imaginary unit.

4.4.6 'Finite-thickness layer' solution

Using the general solution of the governing problem, together with appropriate boundary conditions adequate to the case of a finite thickness of the permeable seabed layer overlaying a perfectly smooth or rough, stiff and impermeable base, the particular solution for the instantaneous wave-induced pore pressure response in the seabed layer of finite thickness has been derived analytically.

The derived set of six coupled, linear, and complex-valued equations has been obtained. The system of six coupled equations can be solved either in its complex-valued form or in the real-valued form. The later would involve, however, a set of twelve coupled, linear equations involved in the solution procedure. The matrix representation of the system of six coupled, linear, complex-valued equations can be written as:

$$[\mathbf{D}]\{\mathbf{Y}\} = \{\mathbf{B}\} \tag{4.35}$$

where:

$$\mathbf{D} = \begin{bmatrix} D_1^{(1)} & D_2^{(1)} & D_3^{(1)} & D_4^{(1)} & D_5^{(1)} & D_6^{(1)} \\ D_1^{(2)} & D_2^{(2)} & D_3^{(2)} & D_4^{(2)} & D_5^{(2)} & D_6^{(2)} \\ D_1^{(3)} & D_2^{(3)} & D_3^{(3)} & D_4^{(3)} & D_5^{(3)} & D_6^{(3)} \\ D_1^{(4)} & D_2^{(4)} & D_3^{(4)} & D_4^{(4)} & D_5^{(4)} & D_6^{(4)} \\ D_1^{(5)} & D_2^{(5)} & D_3^{(5)} & D_4^{(5)} & D_5^{(5)} & D_6^{(5)} \\ D_1^{(6)} & D_2^{(6)} & D_3^{(6)} & D_4^{(6)} & D_5^{(6)} & D_6^{(6)} \end{bmatrix} \tag{4.36a}$$

$$\mathbf{Y} = \begin{Bmatrix} Y_1 \\ Y_2 \\ Y_3 \\ Y_4 \\ Y_5 \\ Y_6 \end{Bmatrix} \tag{4.36b}$$

$$\mathbf{B} = \begin{Bmatrix} 0 \\ 0 \\ 0 \\ 0 \\ -P_0 \\ 0 \end{Bmatrix} \tag{4.36c}$$

Matrix $\mathbf{D}$ contains constant coefficients accompanied by proper unknowns in equations of the boundary value problem. And thus, $D_j^{(i)}$ represents a set of constant coefficients related to j-th unknown in i-th equation. There are six equations where i-equation ($i = 1, ..., 6$) relates to the boundary condition given in Eq. (4.31a) to Eq. (4.31f), respectively. Matrix $\mathbf{Y}$ represents unknowns Y_j ($j = 1, ..., 6$), and matrix $\mathbf{B}$ is composed of the free terms appearing in each expression for the boundary condition problem.

All the 36 coefficients of matrix **D** can be computed using the following relationships (Magda, 1989[a]):

$$D_1^{(1)} = \exp(-ad) \tag{4.37.1a}$$
$$D_2^{(1)} = -d\exp(-ad) \tag{4.37.1b}$$
$$D_3^{(1)} = \exp(ad) \tag{4.37.1c}$$
$$D_4^{(1)} = -d\exp(ad) \tag{4.37.1d}$$
$$D_5^{(1)} = \exp\left(-\bar{k}ad\right) \tag{4.37.1e}$$
$$D_6^{(1)} = \exp\left(\bar{k}ad\right) \tag{4.37.1f}$$

$$D_1^{(2)} = \left(a^3 - X_2 a + X_3 \frac{1}{a}\right)\exp(-ad) \tag{4.37.2a}$$
$$D_2^{(2)} = \left(3a^2 - a^3 d - X_2 + X_2 ad - X_3 \frac{ad+1}{a^2}\right)\exp(-ad) \tag{4.37.2b}$$
$$D_3^{(2)} = -D_1^{(2)}\exp(2ad) \tag{4.37.2c}$$
$$D_4^{(2)} = \left(3a^2 + a^3 d - X_2 - X_2 ad + X_3 \frac{ad-1}{a^2}\right)\exp(ad) \tag{4.37.2d}$$
$$D_5^{(2)} = \left(\bar{k}^3 a^3 - X_2 \bar{k}a + X_3 \frac{1}{\bar{k}a}\right)\exp\left(-\bar{k}ad\right) \tag{4.37.2e}$$
$$D_6^{(2)} = -D_5^{(2)}\exp\left(2\bar{k}ad\right) \tag{4.37.2f}$$

$$D_1^{(3)} = X_1 a^4 - X_1 X_2 a^2 + X_1 X_3 + X_5 ia \tag{4.37.3a}$$
$$D_2^{(3)} = 4X_1 a^3 - 2X_1 X_2 a \tag{4.37.3b}$$
$$D_3^{(3)} = D_1^{(3)} \tag{4.37.3c}$$
$$D_4^{(3)} = -D_2^{(3)} \tag{4.37.3d}$$
$$D_5^{(3)} = X_1 \bar{k}^4 a^4 - X_1 X_2 \bar{k}^2 a^2 + X_1 X_3 + X_5 ia \tag{4.37.3e}$$
$$D_6^{(3)} = D_5^{(3)} \tag{4.37.3f}$$

$$D_1^{(4)} = a + X_1 ia^4 - X_1 X_2 ia^2 + X_1 X_3 i \tag{4.37.4a}$$
$$D_2^{(4)} = 1 + 3X_1 ia^3 - X_1 X_2 ia - X_1 X_3 i\frac{1}{a} \tag{4.37.4b}$$
$$D_3^{(4)} = -D_1^{(4)} \tag{4.37.4c}$$
$$D_4^{(4)} = D_2^{(4)} \tag{4.37.4d}$$
$$D_5^{(4)} = \bar{k}a + X_1 \bar{k}^3 ia^4 - X_1 X_2 \bar{k}ia^2 + X_1 X_3 \frac{i}{\bar{k}} \tag{4.37.4e}$$
$$D_6^{(4)} = -D_5^{(4)} \tag{4.37.4f}$$

$$D_1^{(5)} = X_7\left(a^4 - X_2 a^2 + X_3\right) + X_4 ia + X_6 \frac{a}{i} \tag{4.37.5a}$$
$$D_2^{(5)} = 2X_7 a\left(2a^2 - X_2\right) + 2X_6 \frac{1}{i} \tag{4.37.5b}$$

$$D_3^{(5)} = D_1^{(5)} \tag{4.37.5c}$$

$$D_4^{(5)} = -D_2^{(5)} \tag{4.37.5d}$$

$$D_5^{(5)} = X_7\left(\bar{k}^4 a^4 - X_2 \bar{k}^2 a^2 + X_3\right) + X_4 i a + X_6 \frac{\bar{k}^2 a}{i} \tag{4.37.5e}$$

$$D_6^{(5)} = D_5^{(5)} \tag{4.37.5f}$$

$$D_1^{(6)} = D_1^{(5)} a \exp(-ad) \tag{4.37.6a}$$

$$D_2^{(6)} = (D' + D'') \exp(-ad) \tag{4.37.6b}$$

$$D_3^{(6)} = -D_1^{(5)} a \exp(ad) \tag{4.37.6c}$$

$$D_4^{(6)} = (D' - D'') \exp(ad) \tag{4.37.6d}$$

$$D_5^{(6)} = D_5^{(5)} \bar{k} a \exp\left(-\bar{k} a d\right) \tag{4.37.6e}$$

$$D_6^{(6)} = -D_5^{(5)} \bar{k} a \exp\left(\bar{k} a d\right) \tag{4.37.6f}$$

in which:

$$D' = X_7(5a^4 - 3X_2 a^2 + X_3) + X_1 X_3 X_6 + X_4 i a + 3X_6 \frac{a}{i} \tag{4.37.7a}$$

$$D'' = -X_7 a d(a^4 - X_2 a^2 + X_3) + X_1 X_3 X_6 - X_4 i a^2 d - X_6 \frac{a^2 d}{i} \tag{4.37.7b}$$

$$X_1 = \frac{2(1-\nu) k_z}{a\omega\gamma\left(n\beta' + \dfrac{1-2\nu}{G}\right) + i\left(k_x - k_z\right) a^3} \tag{4.37.7c}$$

$$X_2 = a^2 + \frac{\left[k_x(1-2\nu) + k_z\right] a^2 - i\omega\gamma n\beta'(1-2\nu)}{2k_z(1-\nu)} \tag{4.37.7d}$$

$$X_3 = a^2\left(a^2 \frac{k_x}{k_z} - \kappa^2\right) \tag{4.37.7e}$$

$$X_4 = -\frac{(1-\nu)E}{(1+\nu)(1-2\nu)} \tag{4.37.7f}$$

$$X_5 = \frac{\nu}{1-\nu} \tag{4.37.7g}$$

$$X_6 = -G \tag{4.37.7h}$$

$$X_7 = X_1\left(X_4 X_5 + X_6\right) \tag{4.37.7i}$$

where: E - Young's modulus of soil [kPa],
G - shear modulus of soil [kPa],
ν - Poisson's ratio [-],
k_x, k_z - coefficients of soil permeability in x- and z-direction, respec., [m/s],
$\bar{k}$ - parameter (complex-valued), given in Eq. (4.30), [-],
κ - parameter (complex-valued), given in Eq. (4.28), [m^{-1}],
n - porosity of soil [-],
β' - compressibility of pore fluid [m^2/kN],
γ - unit weight of pore fluid [kN/m^3],
a - wave number [m^{-1}],
ω - wave angular frequency [s^{-1}],

d - thickness of the permeable seabed layer [m],
i - imaginary unit.

The above presented set of coefficients is derived to solve the pore pressure problem with the assumption of rough and impermeable base under the permeable seabed layer. Principally, the same procedure is applied for a finite layer overlaying a completely smooth base. The only difference is that the boundary condition given in Eq. (4.31f) has to be replaced by Eq. (4.31g) which is foreseen for the smooth base condition. It means that the sub-set of constant coefficients $D_j^{(6)}$ $(j = 1, ..., 6)$ is built up using the constant coefficients appearing in Eq. (4.31g). All elements in the two other matrices (*i.e.*, $\mathbf{Y}$ and $\mathbf{B}$) stay unchanged. Equations (4.37.6a) to (4.37.6f) were derived for the case of perfectly rough base. If a perfectly smooth base is assumed, these equations have to be replaced by the following set of equations, respectively:

$$D_1^{(7)} = X_6 \left(a + X_1 i a^4 - X_1 X_2 i a^2 + X_1 X_3 i\right) \exp(-ad) \tag{4.37.8a}$$

$$D_2^{(7)} = X_6 \left[1 - d + 3X_1 i a^3 - X_1 d i a^4 - X_1 X_2 i a + X_1 X_2 d i a^2 - X_1 X_3 \frac{i(ad+1)}{a}\right] \exp(-ad) \tag{4.37.8b}$$

$$D_3^{(7)} = -D_1^{(7)} \exp(2ad) \tag{4.37.8c}$$

$$D_4^{(7)} = X_6 \left[1 + d + 3X_1 i a^3 + X_1 d i a^4 - X_1 X_2 i a - X_1 X_2 d i a^2 + X_1 X_3 \frac{i(ad-1)}{a}\right] \exp(ad) \tag{4.37.8d}$$

$$D_5^{(7)} = X_6 \left(\bar{k}a + X_1 i \bar{k}^3 a^4 - X_1 X_2 i \bar{k} a^2 + X_1 X_3 \frac{i}{a}\right) \exp\left(-\bar{k}ad\right) \tag{4.37.8e}$$

$$D_6^{(7)} = -D_5^{(7)} \exp\left(2\bar{k}ad\right) \tag{4.37.8f}$$

Because of rather lengthy form of each of 36 coefficients $D_j^{(i)}$ $(i, j = 1, ..., 6)$ accompanied by unknowns Y_j $(j = 1, ..., 6)$, it seems to be wise to use a computer and to program the whole calculation procedure. The solution of the system of six coupled, linear, and complex-valued equations, obtained in terms of coefficients $D_j^{(i)}$ $(i, j = 1, ..., 6)$ constitutes simultaneously the particular solution to the pore pressure (and also to the wave-induced effective stresses and strains) within the permeable seabed layer of finite thickness.

The problem considered is the wave-induced response of a single permeable seabed layer resting on a stiff impermeable base. As it was mentioned before, basically the same solution can be used for the case of multi-layered seabed. However, the number of mathematical operations will increase substantially. Therefore, the use of computer may bring additional benefits and speed up the whole computational procedure reasonably.

After Madsen (1978), the pore pressure can be written as:

$$p = -\left(\sigma_x' + \frac{1}{ia}\frac{\partial \tau'}{\partial z}\right) \tag{4.38}$$

where: σ_x' - wave-induced effective horizontal normal stress (complex-valued) [kPa],
p - wave-induced pore pressure (complex-valued) [kPa],
τ' - wave-induced effective shear stress (complex-valued) [kPa],
a - wave number [m^{-1}],

z - vertical coordinate of the Cartesian coordinates system [m],
i - imaginary unit.

Using the above computed unknowns Y_j $(j = 1, ..., 6)$, one can write:

$$\sigma'_x = X_4 \left(T_1 + X_5 T_2\right) \exp[i(ax - \omega t)] \tag{4.39a}$$

and

$$\begin{aligned}\frac{\partial \tau'}{\partial z} = X_6 \big[&2Y_2 a \exp(-az) + (Y_1 - Y_2 z)\, a^2 \exp(-az) - 2Y_4 a \exp(az) \\ &+ (Y_3 - Y_4 z)\, a^2 \exp(az) + Y_5 \bar{k}^2 a^2 \exp\left(-\bar{k} az\right) \\ &+ Y_6 \bar{k}^2 a^2 \exp\left(\bar{k} az\right) + T_2 ia\big] \exp[i(ax - \omega t)]\end{aligned} \tag{4.39b}$$

in which:

$$\begin{aligned}T_1 = ia \big[&(Y_1 - Y_2 z)\, a^2 \exp(-az) + (Y_3 - Y_4 z)\, a^2 \exp(az) \\ &+ Y_5 \bar{k}^2 a^2 \exp\left(-\bar{k} az\right) + Y_6 \bar{k}^2 a^2 \exp\left(\bar{k} az\right)\big]\end{aligned} \tag{4.39c}$$

$$\begin{aligned}T_2 = X_1 \big\{&4Y_2 a^3 \exp(-az) + (Y_1 - Y_2 z)\, a^4 \exp(-az) \\ &- 4Y_4 a^3 \exp(az) + (Y_3 - Y_4 z)\, a^4 \exp(az) \\ &+ Y_5 \bar{k}^4 a^4 \exp\left(-\bar{k} az\right) + Y_6 \bar{k}^4 a^4 \exp\left(\bar{k} az\right) \\ &- X_2 \big[2Y_2 a \exp(-az) + (Y_1 - Y_2 z)\, a^2 \exp(-az) \\ &\quad - 2Y_4 a \exp(az) + (Y_3 - Y_4 z)\, a^2 \exp(az) \\ &\quad + Y_5 \bar{k}^2 a^2 \exp\left(-\bar{k} az\right) + Y_6 \bar{k}^2 a^2 \exp\left(\bar{k} az\right)\big] \\ &+ X_3 \big[(Y_1 - Y_2 z) \exp(-az) + (Y_3 - Y_4 z) \exp(az) \\ &\quad + Y_5 \exp\left(-\bar{k} az\right) + Y_6 \exp\left(\bar{k} az\right)\big]\big\}\end{aligned} \tag{4.39d}$$

where:
- σ'_x - wave-induced effective horizontal normal stress (complex-valued) [kPa],
- τ' - wave-induced effective shear stress (complex-valued) [kPa],
- $Y_1, ..., Y_6$ - coefficients (complex-valued), being the solution to Eq. (4.35),
- $X_1, ..., X_6$ - coefficients (complex-valued), given in Eqs. (4.37.7c) to (4.37.7h),
- $\bar{k}$ - parameter (complex-valued), given in Eq. (4.30), [-],
- a - wave number [m^{-1}],
- ω - wave angular frequency [s^{-1}],
- x, z - horizontal and vertical coordinate of the Cartesian coordinates system, respectively, [m],
- t - time [s],
- i - imaginary unit.

The wave-induced pore pressure solution to the storage problem of the seabed response due to the propagating surface wave loading is given in the complex-valued form in Eq. (4.38) with Eqs. (4.39a) to (4.39d). As it was formerly explained in Section 2.1.1, a momentary (*i.e.*, for an arbitrary time-point, t) value of the wave-induced pore pressure can be easily found by: (1) extracting only a real part from the complex-valued solution [see Eq. (2.13)], or (2) by using Eq. (2.15) together with the formulas describing the amplitude, P [see Eq. (2.14a)], and the phase lag, δ [see Eq. (2.14b)] (computed with respect to the phase of the hydrodynamic bottom pressure oscillation), of the wave-induced pore pressure cyclic oscillations in seabed sediments.

4.4.7 Results of example calculations

In order to perform illustrative calculations of the wave-induced pore pressure oscillations in the seabed layer of finite thickness, governed by the storage model, the following input data were used:

- thickness of seabed layer $d = 0.5\,\mathrm{m}$
- porosity of soil $n = 0.4$
- coefficient of soil permeability $k = 10^{-4}\,\mathrm{m/s}$
- Poisson's ratio of soil $\nu = 0.3$
- Young's modulus of soil $E = 10^4;\ 10^5\,\mathrm{kPa}$
- compressibility of pure water $\beta = 4.2 \times 10^{-7}\,\mathrm{m^2/kN}$
- degree of saturation $S = 0.95 - 1.0$
- atmospheric pressure $p_{at} = 101.325\,\mathrm{kPa}$
- wave period $T = 6\,\mathrm{s}$
- water depth $h = 4.5\,\mathrm{m}$

Due to the presence of complex numbers in the mathematical formulation of the governing problem, numerical calculations were performed to obtain all the six complex-valued coefficients, Y_j $(j = 1, ..., 6)$, of the analytical 'finite-thickness layer' solution; the LU Decomposition method (Press *et al.*, 1986) was used to solve the system of six coupled linear complex-valued equations.

The following presents the comparison of the wave-induced pore pressure solutions obtained from the potential problem, the diffusion problem, and the storage problem with two different compressibilities of soil skeleton introduced into computations, *i.e.*: $E = 10^5$ kPa for dense or semi-dense sandy sediments, and $E = 10^4$ kPa for loose sandy sediments. The results of the wave-induced pore pressure response in the permeable seabed layer of finite thickness ($d = 0.5\,\mathrm{m}$), overlaying a rough, impermeable, and stiff base, are given in terms of the pore pressure amplitude (Figs. 4.15 and 4.17) and the phase lag (Figs. 4.16 and 4.18) as a function of depth in the seabed and different soil saturation conditions: $S = 0.99$ (Figs. 4.15 and 4.16) and $S = 0.95$ (Figs. 4.17 and 4.18).

Analyzing the influence of different soil saturation conditions (introduction of compressible properties only to the pore fluid reflects the use of the diffusion model to the wave-induced pore pressure response in seabed sediments), by comparing the results obtained for $S = 0.99$ and $S = 0.95$, it was found that the smallest pore pressure damping effects are indicated by the potential solution. Lower values of the degree of saturation ($S < 1$ and $\beta' \neq \beta \cong 0$), possible to be investigated in the diffusion solution, magnifies the pore pressure damping effects that can be recognized by smaller amplitudes (compare Figs. 4.15 and 4.17) and larger phase lags (compare Figs. 4.16 and 4.18) of the wave-induced pore pressure oscillations.

A successive introduction of compressible properties to the second phase (*i.e.*, soil skeleton) of the two-phase seabed system, denoted by: (1) storage problem with $E = 10^5$ kPa, and (2) storage problem with $E = 10^4$ kPa, enlarges – in general – the damping of the pore pressure amplitude (see Figs. 4.15 and 4.17). However, as it is clearly seen in Fig. 4.17, in the upper part ($z \leq 0.2\,\mathrm{m}$) of the seabed layer, the amplitudes of pore pressure oscillations in more compressible sediments ($E = 10^4$ kPa) are greater than the amplitudes computed for less compressible sediments ($E = 10^4$ kPa). The results from the lower part ($z \geq 0.2\,\mathrm{m}$) of the seabed layer show the opposite relation. This change of the relative positions of the two pore pressure amplitude distributions with depth has

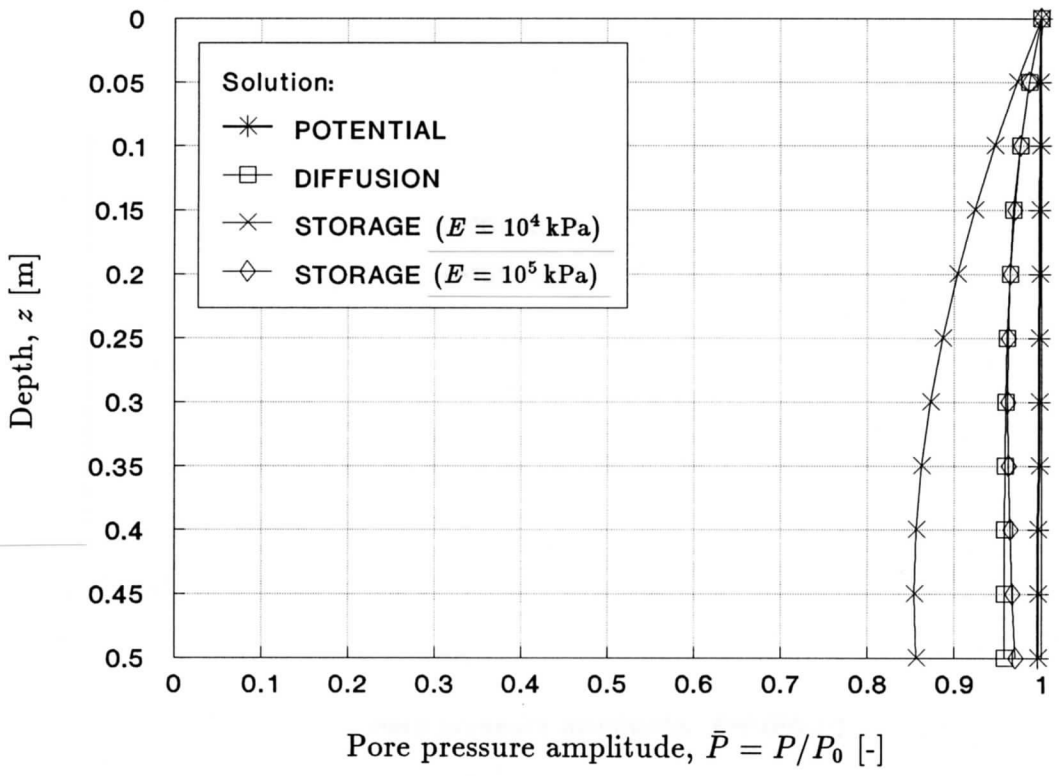

Figure 4.15 Wave-induced pore pressure amplitude distribution with depth ('finite-thickness layer' analytical solution) – comparison between the potential, diffusion ($S = 0.99$), and storage ($S = 0.99$, $E = 10^5$ kPa – dense sandy sediments, and $E = 10^4$ kPa – loose sandy sediments) solutions

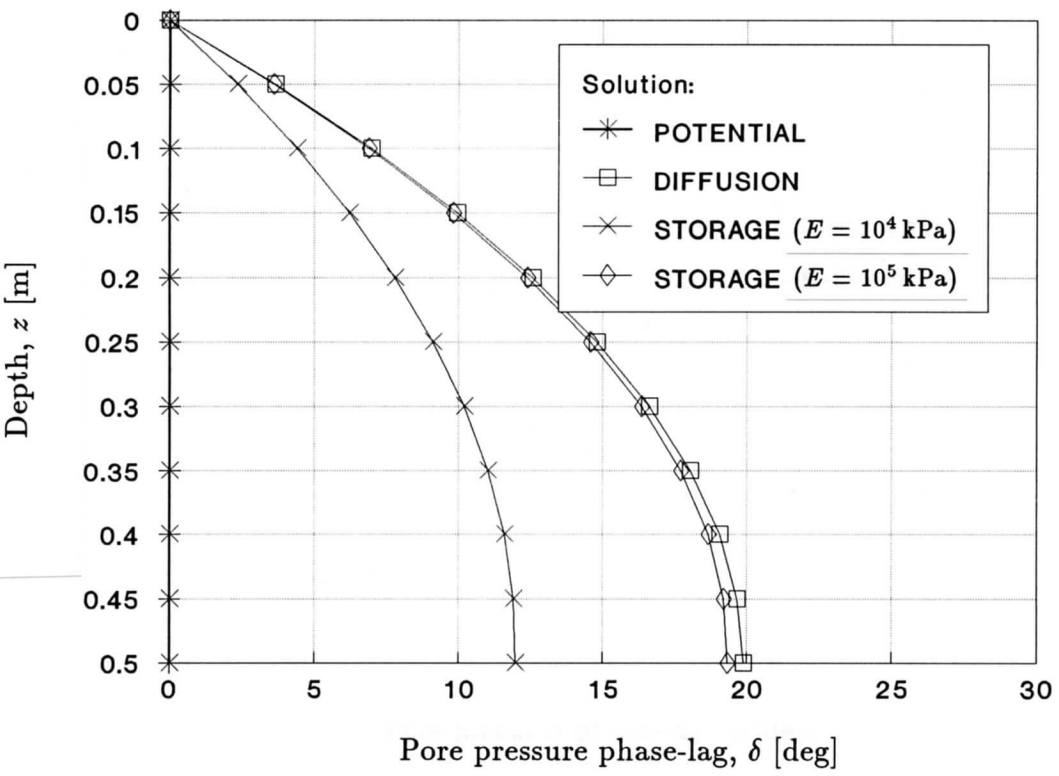

Figure 4.16 Wave-induced pore pressure phase-lag distribution with depth ('finite-thickness layer' analytical solution) – comparison between the potential, diffusion ($S = 0.99$), and storage ($S = 0.99$, $E = 10^5$ kPa – dense sandy sediments, and $E = 10^4$ kPa – loose sandy sediments) solutions

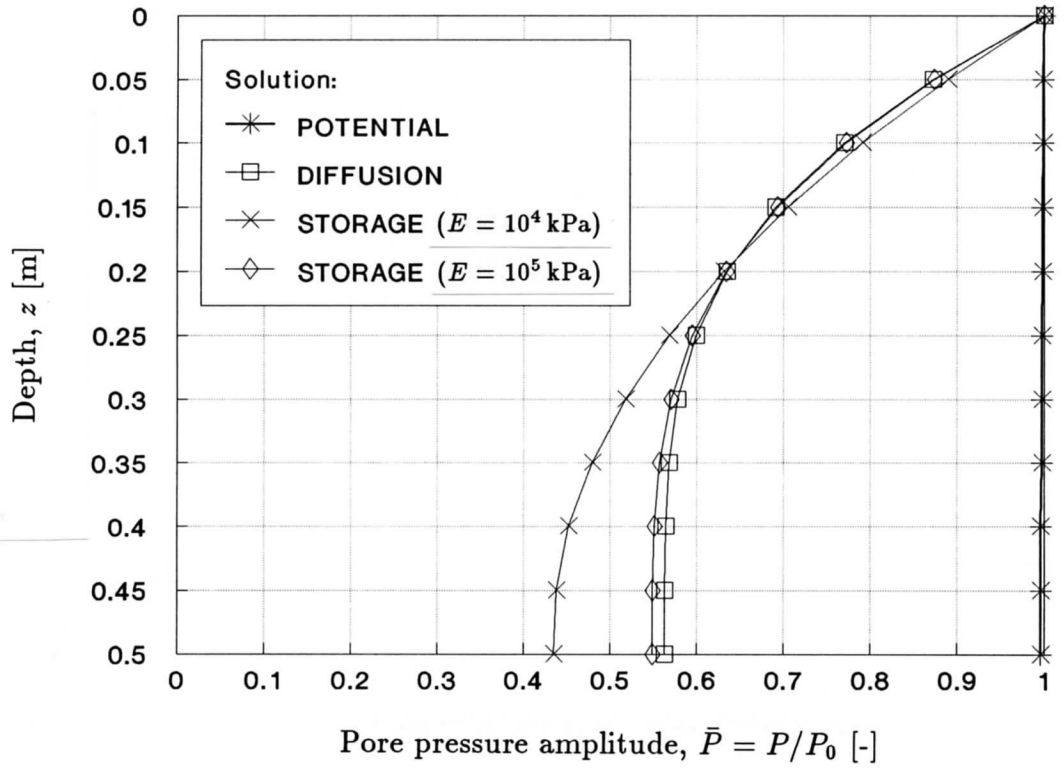

Figure 4.17 Wave-induced pore pressure amplitude distribution with depth ('finite-thickness layer' analytical solution) – comparison between the potential, diffusion ($S = 0.95$), and storage ($S = 0.95$, $E = 10^5$ kPa – dense sandy sediments, and $E = 10^4$ kPa – loose sandy sediments) solutions

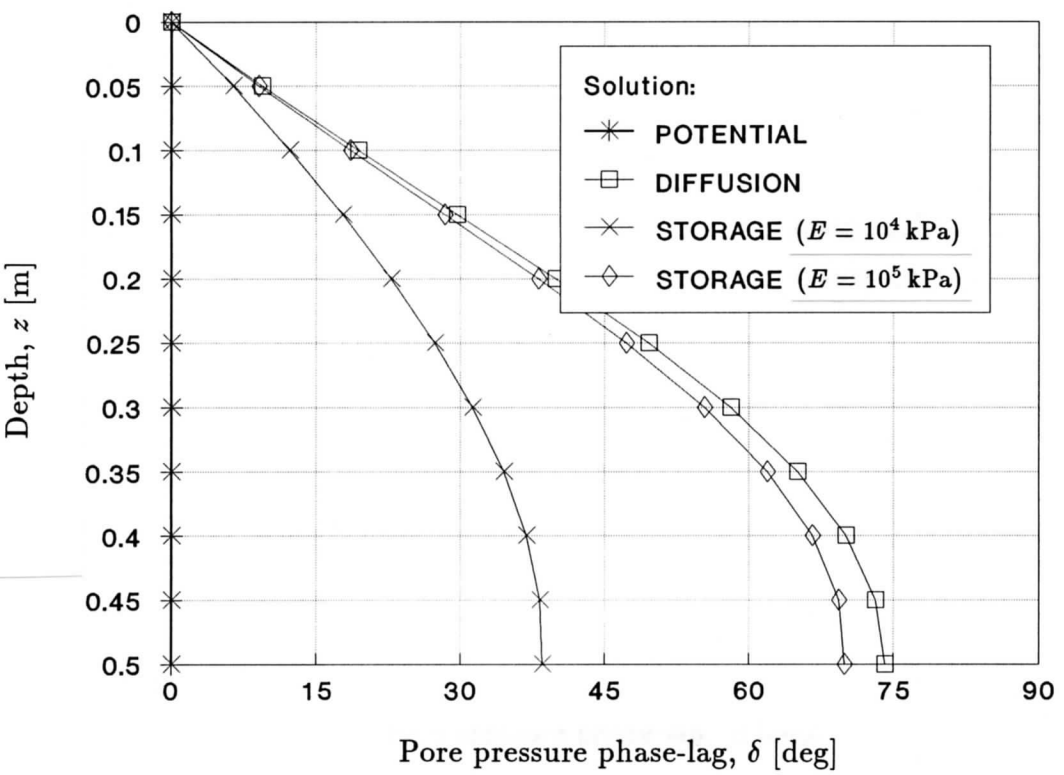

Figure 4.18 Wave-induced pore pressure phase-lag distribution with depth ('finite-thickness layer' analytical solution) – comparison between the potential, diffusion ($S = 0.95$), and storage ($S = 0.95$, $E = 10^5$ kPa – dense sandy sediments, and $E = 10^4$ kPa – loose sandy sediments) solutions

indicated a strong influence of the 'finite-thickness layer' boundary condition on the pore pressure solution according to the storage model. Assuming homogeneous conditions and infinite thickness of the seabed layer, this phenomenon would not be observed. A detailed explanation of this problem will be given in conclusions of Chapter 4.

Taking into account the pore pressure phase-lag, it was found that the potential solution and the diffusion solution constitute the lower limit and the upper limit, respectively, for the linear-elastic storage problem where both components of the two-phase medium are considered to be compressible (see Figs. 4.16 and 4.18).

A proper choice of the type of boundary conditions may by a crucial point in deriving a particular solution to any partial differential equation. Therefore, the boundary conditions at the bottom of the permeable seabed layer [see Eqs. (4.31f) and (4.31g)] were considered. Using the analytically derived 'finite-thickness layer' solution (Magda, 1989[a]), two different boundary conditions were introduced in order to simulate a rough (*i.e.*, constrained movement of the soil skeleton; $u_x = 0$) or smooth (*i.e.*, free linear-elastic movement of the soil skeleton; $\tau' = 0$) surface of a rigid and impermeable base underneath the permeable seabed layer.

The results of the wave-induced pore pressure response in a permeable seabed layer of finite thickness, overlaying either a smooth or rough base, are given in the following four figures where the solid lines denote the rough base condition whereas the dashed lines denote the smooth base condition. The results are presented in terms of the pore pressure amplitude (Figs. 4.19 and 4.21) and the phase lag (Figs. 4.20 and 4.22) as a function of depth in the seabed. Different soil saturation conditions ($S = 0.95 - 1.0$) as well as two different compressibilities of soil skeleton, *i.e.*: $E = 10^5$ kPa for dense or semi-dense sandy sediments (Figs. 4.19 and 4.20), and $E = 10^4$ kPa for loose sandy sediments (Figs. 4.21 and 4.22), were considered in the computational analysis.

In the case of dense sandy sediments (Figs. 4.19 and 4.20), the difference between the rough and smooth base conditions is relatively small. The influence of introduction of the smooth base condition becomes meaningful when loose sandy sediments are considered (Figs. 4.21 and 4.22). In both cases (*i.e.*, loose and dense sediments), the smooth base condition creates the pore pressure damping effects larger (*i.e.*, the pore pressure amplitude decreases while the phase lag increases), compared with the rough base condition. Although the pore pressure gradient is more inconvenient (more dangerous situation for the stability of seabed sediments) when the smooth base is assumed, the rough base condition seems to be more natural.

Regardless compressibility properties of the soil skeleton, soil saturation conditions have always the same pore pressure damping effects, namely: the lower soil saturation is, the smaller amplitude and the larger phase lag of pore pressure oscillations are. As it was already shown in Figs. 4.15 to 4.18, Figs. 4.19 to 4.22 can only certify this statement.

4.5 Storage problem – one-dimensional numerical solution

As an extension to the above presented realistic two-dimensional model, and its analytical solution to the pore pressure response in the permeable seabed layer of finite thickness, due to propagating surface water wave oscillations, a one-dimensional model of the considered problem was adopted after Nago (1981) as a necessary tool for the verification and comparison analysis of results obtained from small-scale laboratory tests

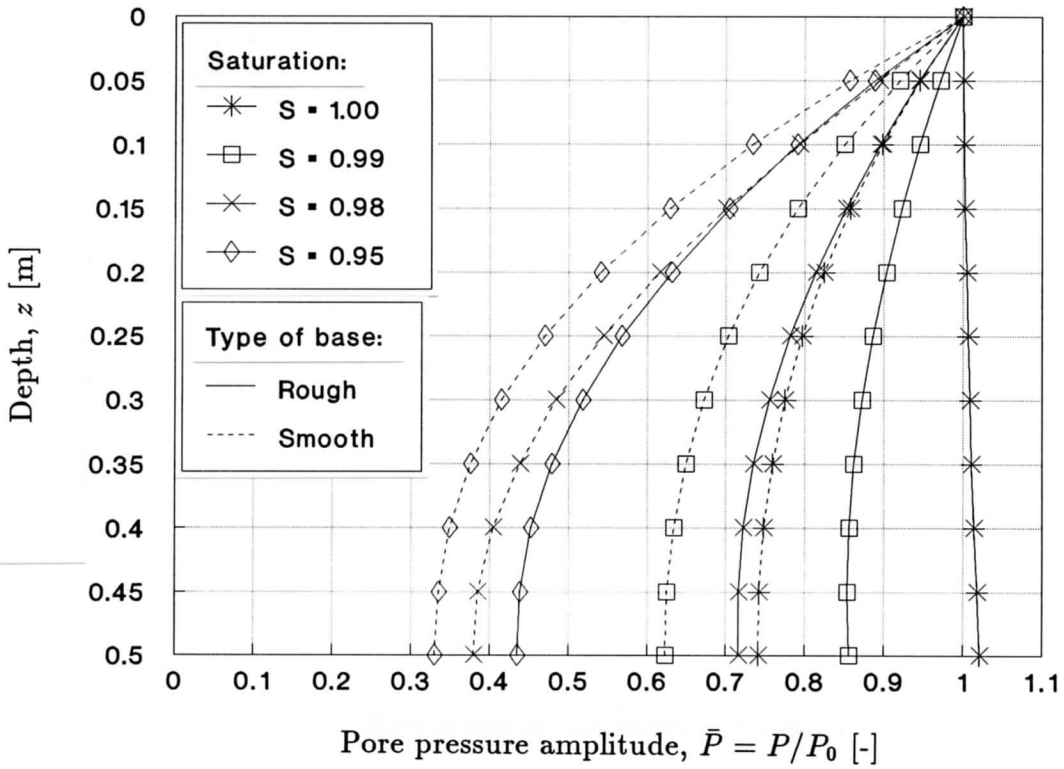

Figure 4.19 Wave-induced pore pressure amplitude distribution with depth, for different soil saturation conditions and types of impermeable base (2-D storage problem – 'finite-thickness layer' analytical solution; $E = 10^5$ kPa – dense sandy sediments)

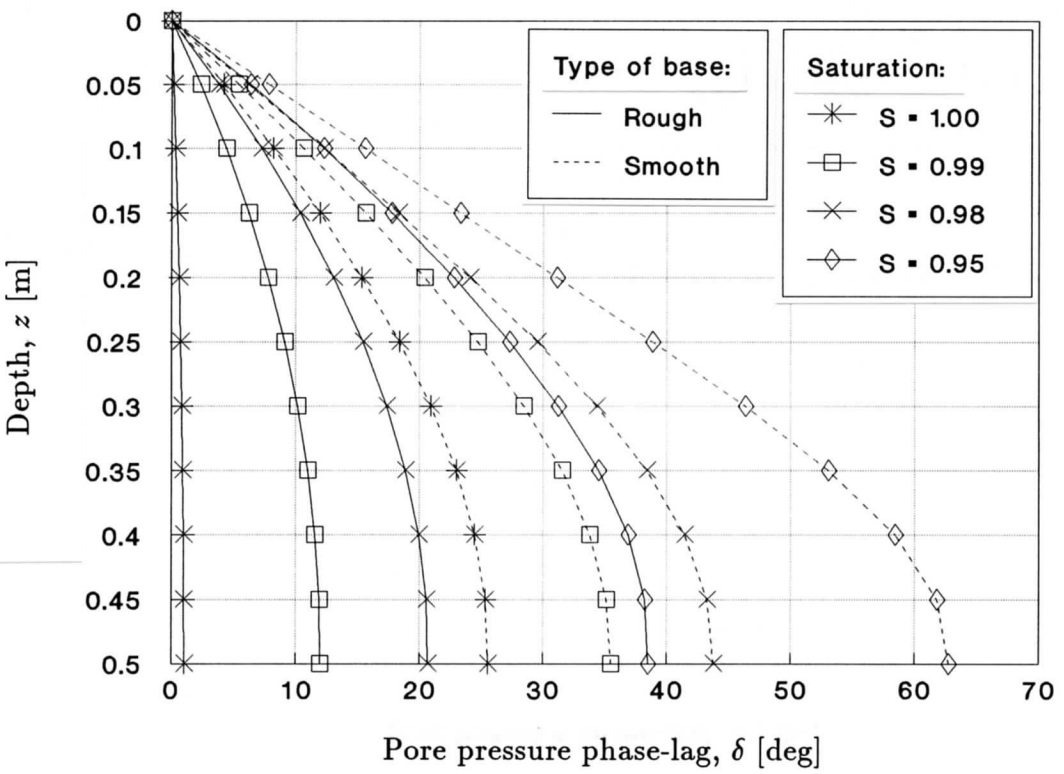

Figure 4.20 Wave-induced pore pressure phase-lag distribution with depth, for different soil saturation conditions and types of impermeable base (2-D storage problem – 'finite-thickness layer' analytical solution; $E = 10^5$ kPa – dense sandy sediments)

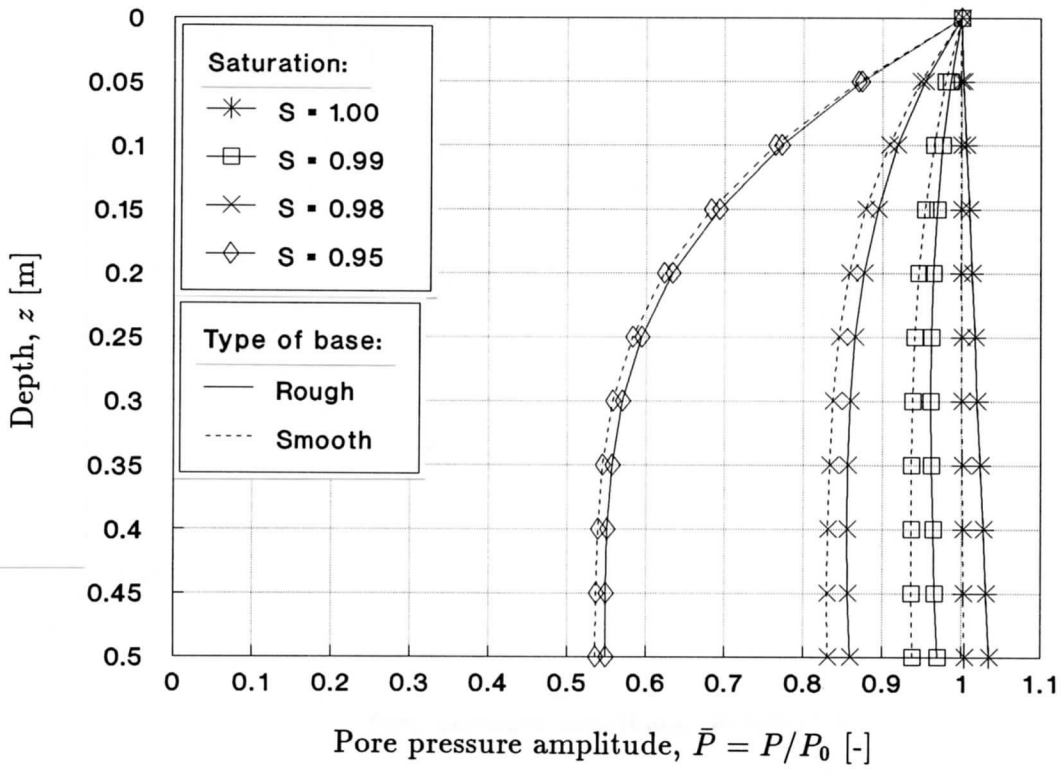

Figure 4.21 Wave-induced pore pressure amplitude distribution with depth, for different soil saturation conditions and types of impermeable base (2-D storage problem – 'finite-thickness layer' analytical solution; $E = 10^4$ kPa – loose sandy sediments)

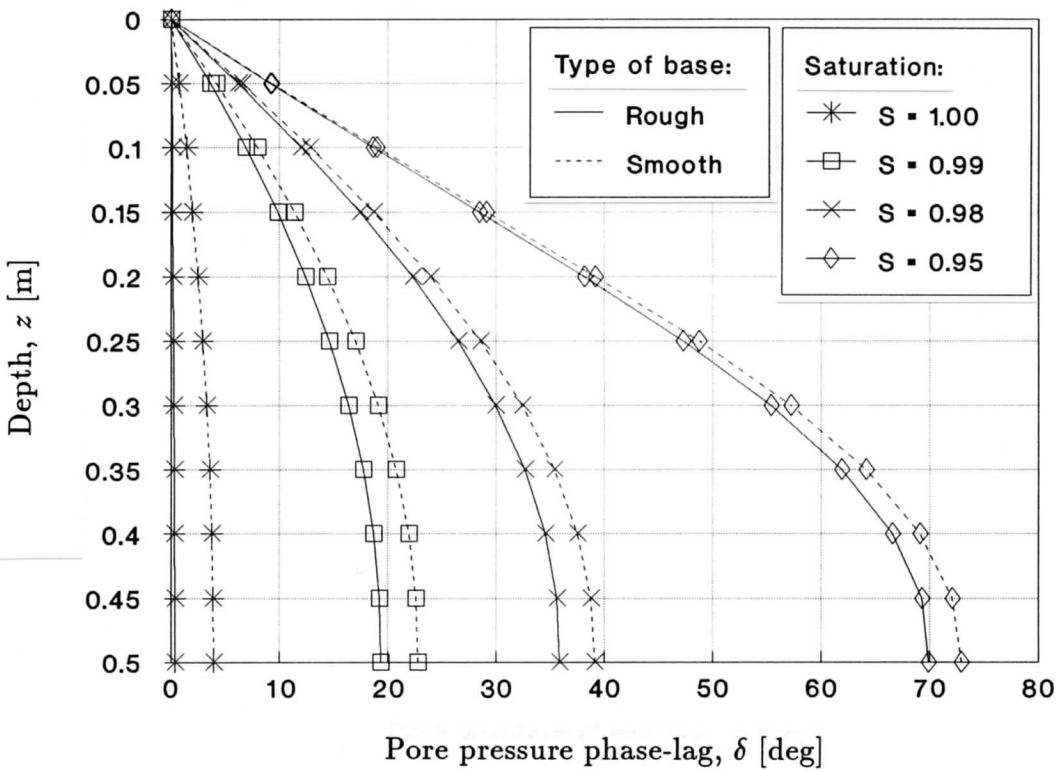

Figure 4.22 Wave-induced pore pressure phase-lag distribution with depth, for different soil saturation conditions and types of impermeable base (2-D storage problem – 'finite-thickness layer' analytical solution; $E = 10^4$ kPa – loose sandy sediments)

performed in a sand column. It has to be emphased that the control of soil saturation conditions, modelled by a wide range of practically possible values of the degree of saturation, is much easier to be performed and more accurate to be measured, in the case of small-scale tests than during large-scale laboratory investigations.

Small-scale tests conducted in a sand column are not very much recommended for the application of a real-shaped progressive surface water wave because models are to small to avoid the combined influence of the vertical side-wall boundary condition and the asymmetry of propagating wave loading with respect to the vertical axis of the sand column model. Nevertheless, these disadvantages can be overcome by introducing as simple type of water loading as possible, that is the water surface vertically oscillating movement instead of the wave-shaped horizontally progressive surface water wave motion above the seabed model. It has to be noticed that the water loading in the form of water surface vertically oscillating movement can be also very relevant for the coastal engineering practice where, for instance, long water waves are considered.

In the following, a description of the theoretical, one-dimensional approach to the governing problem is presented, and illustrated by results of example computations.

4.5.1 Mathematical formulation of the problem

In the theoretical treatment of the governing problem, a vertically one-dimensional sand column is considered, as shown in Fig. 4.23. The sand column is saturated with water and placed on an impermeable and stiff base. The height (thickness) of the sand column is denoted by d, and the oscillating water pressure is assumed to act cyclically on the upper surface of the sand column.

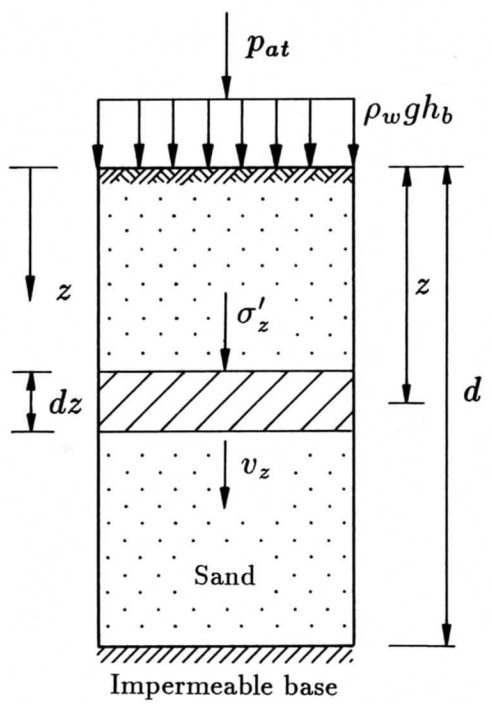

σ'_z - vertical effective stress
v_z - vertical velocity of flow
ρ_w - density of water
g - acceleration due to gravity
h_b - head of bottom pressure oscillations
p_{at} - atmospheric pressure
d - height (thickness) of sand column
z - vertical coordinate (positive downwards; depth in sand column)
dz - depth increment

Figure 4.23 Sand column loaded by water surface vertical oscillations [Nago, 1981]

Motion of the pore fluid and the soil skeleton in the sand column is analysed by the same method as for the ground water problems in the elastic aquifer (*e.g.*, Rouse, 1950). The following assumptions had to be made in order to derive the one-dimensional mathematical model of the governing problem (Nago, 1981):

- the porosity of soil is composed of the part of soil porosity filled with water and the complementary part of soil porosity occupied by air; similarly to the formerly described two-dimensional model, the terms 'pore fluid' and 'pore pressure' will be used in the following, representing the mixture of water and air, and the pressure in this mixture, respectively.
- the soil skeleton and the pore fluid are compressible,
- the density of pore fluid, the porosity of soil and the height (thickness) of sand column are variables,
- the horizontal strain of the soil skeleton is negligible,
- by the law of mass conservation, the net inward flux must equalize the rate at which the pore fluid is accumulating within that volume,
- it is permissible to consider that the volume of solid material in the total volume remains constant since the compressibility of individual sand grains is small compared to the compressibility of pore fluid and the change in the porosity of soil,
- there is no inertia force acting on the soil skeleton; therefore it is permissible to consider that the vertical component of the compressive stress and the pore pressure can be equated to the downward acting force on the plane of contact of the sand,
- the volume of air in the sand column changes in accordance to Boyle's law,
- the velocity of pore fluid in the sand column is represented by Darcy's law.

The fundamental equation for the pore pressure response in the one-dimensional model of the permeable seabed layer, loaded cyclically by an oscillating water surface vertical movement, is given by (Nago, 1981):

$$\left(\beta n_w + \frac{n_a}{P_t} + \alpha_z\right) \frac{\partial h'}{\partial t} + \left(\beta n_w + \frac{n_a}{P_t}\right) \frac{\partial h_b}{\partial t} = \frac{k_z}{\rho g} \frac{\partial^2 h'}{\partial z^2} \tag{4.40}$$

in which:

$$P_t = \rho g h_t + p_{at} = \gamma h_t + p_{at} \tag{4.41}$$

$$h_t = h + z + h' \tag{4.42}$$

where: β - compressibility of pure water [m^2/kN],
n_w - soil porosity part filled with water [-],
n_a - soil porosity part filled with air [-],
P_t - absolute total pressure [kPa],
p_{at} - atmospheric pressure [kPa],
α_z - compressibility of soil skeleton in z-direction ($\alpha_z = 1/E_z$) [m^2/kN],
E_z - Young's modulus of soil in z-direction [kPa],
h' - pore pressure head, induced by cyclic water surface vertical (*i.e.*, in z-direction) oscillations, [m],
h_b - hydrodynamic bottom pressure head (induced by cyclic water surface vertical oscillations, and acting at the upper surface of the sand column) [m],

h_t - total (*i.e.*, hydrostatic and oscillation-induced) pore pressure head, acting at depth z in the sand column, [m],
h - water depth, due to still water level above the upper sand surface, [m],
k_z - coefficient of soil permeability in z-direction [m/s],
ρ - density of pore fluid [Mg/m^3],
g - acceleration due to gravity [m/s^2],
γ - unit weight of pore fluid [kN/m^3],
z - vertical coordinate (depth in the sand column) [m],
t - time [s].

For the case where the water pressure loading, acting on the upper surface of the sand column, changes sinusoidally according to:

$$h_b = H_0 \sin(\omega t) \tag{4.43}$$

where: h_b - hydrodynamic bottom pressure head [m],
H_0 - amplitude of the hydrodynamic bottom pressure head oscillations (approximately equal to the amplitude of water surface vertical oscillations), [m],
ω - angular frequency of water surface vertical oscillations [s^{-1}],
t - time [s],

Eq. (4.40) becomes:

$$\left(\beta n_w + \frac{n_a}{P_t} + \alpha_z\right) \frac{\partial h'}{\partial t} + \omega H_0 \left(\beta n_w + \frac{n_a}{P_t}\right) \cos(\omega t) = \frac{k_z}{\gamma} \frac{\partial^2 h'}{\partial z^2} \tag{4.44}$$

In order to obtain the pore pressure solution in the permeable sand column of finite thickness, Eq. (4.44) must be solved under the following boundary conditions:

$$h' = 0 \qquad \text{at} \qquad z = 0 \tag{4.45}$$

$$\frac{\partial h'}{\partial z} = 0 \qquad \text{at} \qquad z = d \tag{4.46}$$

where, additionally:
d - height (thickness) of the sand column [m].

The loading function [see Eq. (4.43)] is already included in the above final equation of the governing problem. Therefore, the upper boundary condition must be given in the form of Eq. (4.45). If so, it implies that the pore pressure results are obtained with respect to the reference lines (HT-line or HC-line; see Fig. 4.1), denoting the hydrostatic pore pressure profile under the wave trough or wave crest, respectively. The results can be, of course, simply transformed into the results respective to the reference HI-line (see Fig. 4.1), denoting the initial hydrostatic pore pressure distribution with depth in seabed sediments. The reference HI-line is commonly used in presentation techniques of wave-induced pore pressure results.

The form of Eq. (4.44) resembles the very similar basic equation from Madsen's (1978) theory, described in Section 4.4.1 [see Eq. (4.24c)]. It means that the same partial differential equation, called the storage equation, is still valid while investigating the problem of the wave-induced pore pressure cyclic oscillations in seabed sediments with the boundary conditions expected to happen in small-scale laboratory tests simulated in one-dimensional mathematical models.

One can note that Eq. (4.44) can be treated as:

- linear, when the absolute total pressure, P_t, is constant and independent of the oscillation-induced pore pressure, $h'(z,t)$ [see Eqs. (4.41) and (4.42)],
- non-linear, when the absolute total pressure, P_t, depends on $h'(z,t)$.

It has to be emphased that the sum of the water depth, h, and the atmospheric pressure head, p_{at}/γ, is much larger than the sum of the oscillation-induced pore pressure head, h', and the computational depth in the sand column, z. This is true for most cases where both realistic and laboratory-modelled problems in coastal engineering are considered. Concerning this fact, and comparing Eqs. (4.41) and (4.42), it seems permissible to assume the absolute total pressure to be constant and independent of space and time coordinates, *i.e.*:

$$P_t \cong \gamma h + p_{at} \tag{4.47}$$

Although it is possible to solve Eq. (4.44) analytically, this time a numerical solution will be presented in the following.

4.5.2 Numerical solution

The parabolic partial differential equation to be solved can be written in the following general form (Magda, 1990[c]):

$$c_1 \frac{\partial h'}{\partial t} = c_2 \frac{\partial^2 h'}{\partial z^2} + c_3 \tag{4.48}$$

where h' is a function of t and z, and the constant coefficients are equal to:

$$c_1 = \beta n_w + \frac{n_a}{P_t} + \alpha_z \tag{4.49a}$$

$$c_2 = \frac{k_z}{\gamma} \tag{4.49b}$$

$$c_3 = -\omega H_0 \left(\beta n_w + \frac{n_a}{P_t} \right) \cos(\omega t) \tag{4.49c}$$

where: β - compressibility of pure water [m^2/kN],
n_w - part of soil porosity filled with water [-],
n_a - part of soil porosity filled with air [-],
P_t - absolute total pressure [kPa],
h' - pore pressure head, induced by cyclic water surface vertical oscillations, [m],
H_0 - amplitude of the hydrodynamic bottom pressure head oscillations [m],
α_z - compressibility of soil skeleton in z-direction [m^2/kN],
ω - angular frequency of water surface vertical oscillations [s^{-1}],
k_z - coefficient of soil permeability in z-direction [m/s],
γ - unit weight of pore fluid [kN/m^3],
z - vertical coordinate (depth in the sand column) [m],
t - time [s].

Equation (4.48), together with Eqs. (4.49a) to (4.49c), has to be solved satisfying simultaneously the boundary conditions given in Eqs. (4.45) and (4.46). By treating Eq. (4.48) numerically, the derivatives are replaced by adequate differential quotients which are refered to nodes of the mesh which is used to cover the governing integration area (z,t). Such a rectangular mesh is created by two families of lines which have identical reciprocal distances, and which are parallel to z- and t-axis (Fig. 4.24).

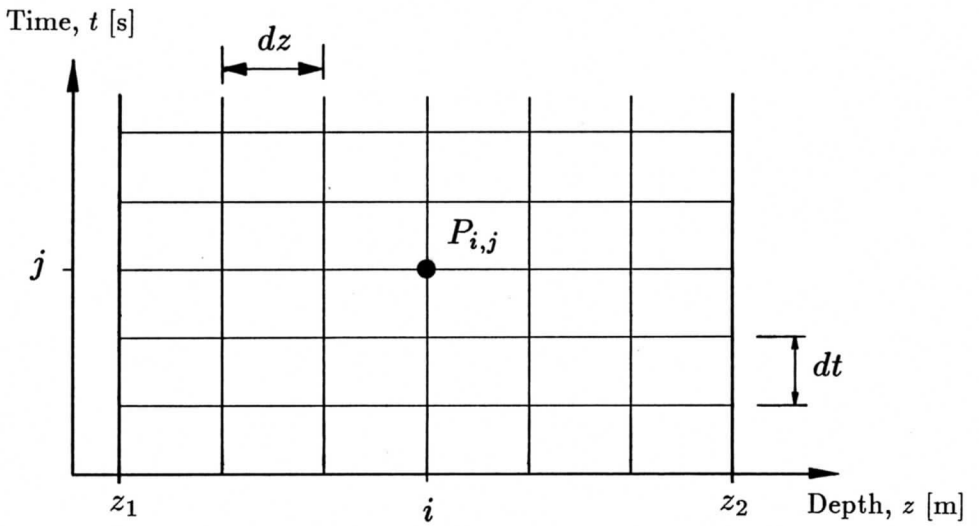

Figure 4.24 Rectangular mesh used in Finite Difference Methods [Jankowski, 1983]

A typical integration area for the parabolic partial differential equation is shown in Fig. 4.25. In principle, it is an infinite area but the results of integration can be interesting for finite values of t. The edge of the area is limited by semi-lines, denoted by L_b (boundary condition semi-line) and L_i (initial condition semi-line). Initial conditions exist on the segment ($z_1 \leq z \leq z_2$ for $t = 0$) of semi-line L_i, and the boundary conditions are assumed on semi-lines $L_b^{(1)}$ ($z = z_1$), and $L_b^{(2)}$ ($z = z_2$).

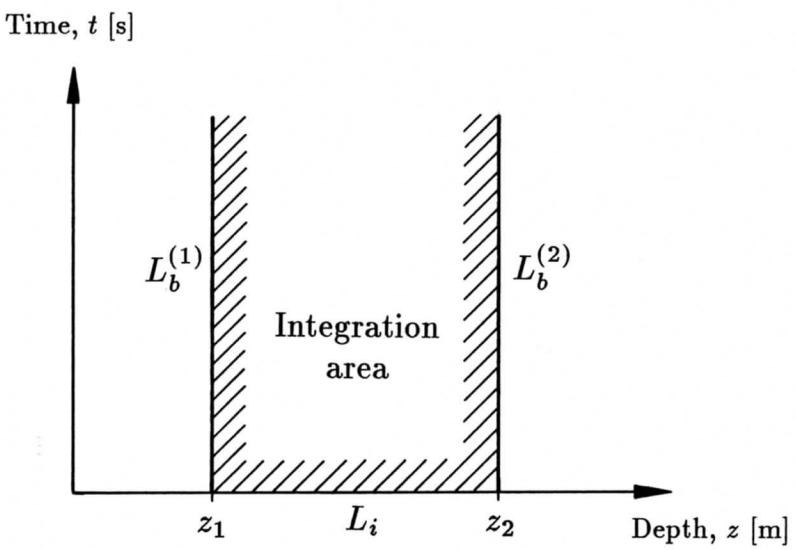

Figure 4.25 Typical area of integration for parabolic partial differential equations [Jankowski, 1983]

Assuming the rectangular mesh with dimensions $(dt) \times (dz)$ (see Fig. 4.24), and denoting:

$$z_i = z_0 + i(dz) \qquad \text{for} \qquad i = 0, 1, 2, ..., N \tag{4.50a}$$

$$t_j = t_0 + j(dt) \qquad \text{for} \qquad j = 0, 1, 2, ... \tag{4.50b}$$

$$dz = \frac{z_2 - z_1}{N} \tag{4.50c}$$

$$h'_{i,j} = h'\left[z_0 + i(dz),\, t_0 + j(dt)\right] \tag{4.50d}$$

where: z_i - spatial coordinate (in z-direction) of nodal point $P_{i,j}$ [m],
dz - spatial-step (in z-direction) [m],
t_j - time coordinate of nodal point $P_{i,j}$ [s],
dt - time-step [s],
$h'_{i,j}$ - pore pressure head at point $P_{i,j}$, induced by water surface vertical oscillations, [m],
z_0, t_0 - spatial and time coordinates of the system origin (normally, $z_0 = t_0 = 0$ is assumed), respectively, [m], [s],
N - number of sub-intervals in main depth-domain $< z_1, z_2 >$.

When treating a parabolic partial differential equation, a mixed type of boundary conditions (*i.e.* boundary conditions of the third order) is involved in most cases:

- initial-value condition ($j = 0$, $t = t_0 = 0$; $z_1 \leq z \leq z_2$)

$$h'(z,t) = h'(z) = 0 \tag{4.51a}$$

- boundary-value condition of the third order

$$h'_{0,j} = h'_0[j(dt)] \qquad \text{for} \qquad z = z_1 = 0 \tag{4.51b}$$

$$h'_{N,j} = h'_{N-1,j} \qquad \text{for} \qquad z = z_2 = d \tag{4.51c}$$

$$h'_{N,j+1} = h'_{N-1,j+1} \qquad \text{for} \qquad z = z_2 = d \tag{4.51d}$$

The six-point difference scheme (see Fig. 4.26) was adapted into the solution procedure for solving Eq. (4.48) together with the initial condition defined in Eq. (4.51a) and the boundary conditions given in Eqs. (4.51b) and (4.51c). This method implies the approximation of the first derivative with respect to depth variable, z, as a linear combination of differential quotients approximating second derivatives with respect to time variable, t, in two adjacent lines of the rectangular mesh. And thus [Jankowski, 1983]:

$$\frac{h'_{i,j+1} - h'_{i,j}}{dt} = \frac{1}{(dz)^2}\left[\sigma_d\left(h'_{i+1,j+1} - 2h'_{i,j+1} + h'_{i-1,j+1}\right) + (1-\sigma_d)\left(h'_{i+1,j} - 2h'_{i,j} + h'_{i-1,j}\right)\right] \tag{4.52}$$

It is easy to notice that the solution of the so-formulated problem can be found in a similar way like in the case of reverse differences; a system of $(N-1)$ coupled linear equations for the following lines of the mesh can be solved, or the method of the back substitution can be applied.

And thus, for the governing problem defined in Eq. (4.48), Eq. (4.52) becomes:

$$c_1\frac{h'_{i,j+1} - h'_{i,j}}{dt} = c_2\frac{1}{(dz)^2}\left[\sigma_d\left(h'_{i+1,j+1} - 2h'_{i,j+1} + h'_{i-1,j+1}\right) + (1-\sigma_d)\left(h'_{i+1,j} - 2h'_{i,j} + h'_{i-1,j}\right)\right] + c_3 \tag{4.53}$$

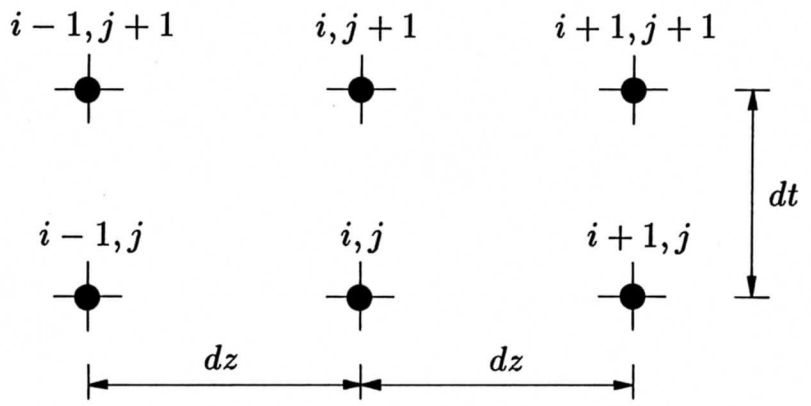

Figure 4.26 Six-point scheme for Crank-Nicolson method [Jankowski, 1983]

The Crank-Nicolson method was used in the following numerical computations. This implies that $\sigma_d = 0.5$ was assumed. Introducing additionally a new parameter:

$$\vartheta = \frac{c_2}{c_1}\frac{dt}{(dz)^2} \tag{4.54}$$

and performing some simple mathematical operations, one has for $1 < i < N-1$:

$$-\vartheta h'_{i-1,j+1} + 2(1+\vartheta)h'_{i,j+1} - \vartheta h'_{i+1,j+1} = \vartheta h'_{i-1,j} + 2(1-\vartheta)h'_{i,j} + \vartheta h'_{i+1,j} + 2\frac{c_3}{c_1}dt \tag{4.55}$$

The Crank-Nicolson method is stable and convergent for all values of ϑ.
For $i = 1$, Eq. (4.55) becomes:

$$2(1+\vartheta)h'_{1,j+1} - \vartheta h'_{2,j+1} = \vartheta h'_{2,j} + 2(1-\vartheta)h'_{1,j} + \vartheta\left(h'_{0,j} + h'_{0,j+1}\right) + 2\frac{c_3}{c_1}dt \tag{4.56}$$

Remembering that the upper boundary condition (of the first order) is defined in Eq. (4.51b), Eq. (4.56) leads to:

$$2(1+\vartheta)h'_{1,j+1} - \vartheta h'_{2,j+1} = \vartheta h'_{2,j} + 2(1-\vartheta)h'_{1,j} + \vartheta\left[h'_0(j) + h'_0(j+1)\right] + 2\frac{c_3}{c_1}dt \tag{4.57}$$

Using the value of the upper boundary condition assumed for the governing problem [see Eq. (4.45)], Eq. (4.57) becomes:

$$2(1+\vartheta)h'_{1,j+1} - \vartheta h'_{2,j+1} = \vartheta h'_{2,j} + 2(1-\vartheta)h'_{1,j} + 2\frac{c_3}{c_1}dt \tag{4.58}$$

For $i = N-1$, Eq. (4.55) becomes:

$$-\vartheta h'_{N-2,j+1} + 2(1+\vartheta)h'_{N-1,j+1} - \vartheta h'_{N,j+1} = \vartheta h'_{N-2,j} + 2(1-\vartheta)h'_{N-1,j} + \vartheta h'_{N,j} + 2\frac{c_3}{c_1}dt \tag{4.59}$$

Assuming the lower boundary condition as a boundary condition of the second order [Eqs. (4.51c) and (4.51d)], Eq. (4.59) leads to:

$$-\vartheta h'_{N-2,j+1} + (2+\vartheta)h'_{N-1,j+1} = \vartheta h'_{N-2,j} + (2-\vartheta)h'_{N-1,j} + 2\frac{c_3}{c_1}dt \tag{4.60}$$

For all other values of i, Eq. (4.55) together with Eq. (4.54) has to be used.

Using the matrix notation, the system of $(N-1)$ coupled linear equations, incorporating the above assumed boundary conditions, can be written as (Magda, 1990[c]):

$$[\mathbf{M}]\{\mathbf{H}\} = \{\mathbf{K}\} \tag{4.61}$$

in which:

$$\mathbf{M} = \begin{bmatrix} 2(1+\vartheta) & -\vartheta & 0 & \dots & \dots & \dots & 0 \\ -\vartheta & 2(1+\vartheta) & -\vartheta & 0 & \dots & \dots & 0 \\ 0 & -\vartheta & 2(1+\vartheta) & -\vartheta & 0 & \dots & 0 \\ \vdots & \ddots & \ddots & \ddots & \ddots & \ddots & \vdots \\ 0 & \dots & 0 & -\vartheta & 2(1+\vartheta) & -\vartheta & 0 \\ 0 & \dots & \dots & 0 & -\vartheta & 2(1+\vartheta) & -\vartheta \\ 0 & \dots & \dots & \dots & 0 & -\vartheta & 2+\vartheta \end{bmatrix} \tag{4.62a}$$

$$\mathbf{H} = \begin{Bmatrix} h'_{1,j+1} \\ h'_{2,j+1} \\ h'_{3,j+1} \\ \vdots \\ h'_{N-3,j+1} \\ h'_{N-2,j+1} \\ h'_{N-1,j+1} \end{Bmatrix} \tag{4.62b}$$

$$\mathbf{K} = \begin{Bmatrix} 2(1-\vartheta)h'_{1,j} + \vartheta h'_{2,j} + 2\frac{c_3}{c_1}dt \\ \vartheta h'_{1,j} + 2(1-\vartheta)h'_{2,j} + \vartheta h'_{3,j} + 2\frac{c_3}{c_1}dt \\ \vartheta h'_{2,j} + 2(1-\vartheta)h'_{3,j} + \vartheta h'_{4,j} + 2\frac{c_3}{c_1}dt \\ \vdots \\ \vartheta h'_{N-4,j} + 2(1-\vartheta)h'_{N-3,j} + \vartheta h'_{N-2,j} + 2\frac{c_3}{c_1}dt \\ \vartheta h'_{N-3,j} + 2(1-\vartheta)h'_{N-2,j} + \vartheta h'_{N-1,j} + 2\frac{c_3}{c_1}dt \\ \vartheta h'_{N-2,j} + (2-\vartheta)h'_{N-1,j} + 2\frac{c_3}{c_1}dt \end{Bmatrix} \tag{4.62c}$$

where: **M** - matrix of constant coefficients,
H - matrix of unknowns,
K - matrix of free terms (forces).

For a repeatable and harmonic (*e.g.*, sinusoidal) water loading induced on the top of the sand column it is necessary to incorporate a computational continuity condition as illustrated in Fig. 4.27. If this condition is to be fulfilled it must be assumed that all the pore pressure values computed in all nodes for the last time-point of the period of

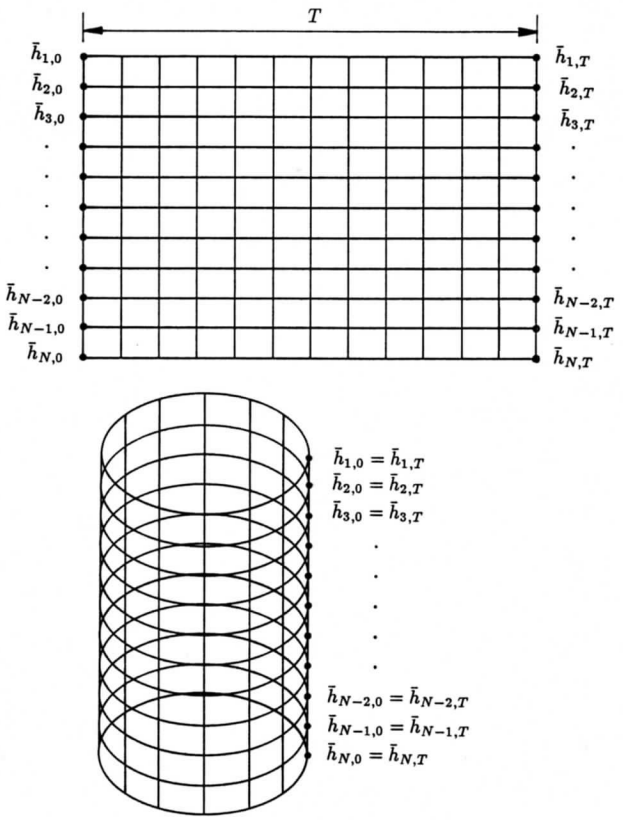

Figure 4.27 Rectangular mesh used in numerical computations with a repeatable and harmonic water loading induced on the top of one-dimensional sand column numerical model

harmonic water loading become automatically initial values of the pore pressure for the begining of the next period of water loading.

Simultaneously, the pore pressure values computed for the last time-step within one period of water loading oscillations can be used in evaluation of the end-test in the numerical procedure. If all the differences (*i.e.*, in all nodes of one-dimensional domain) between pore pressures computed for the last time-points of the two adjacent periods of water loading oscillations are less than a certain required computational accuracy, the end-test is fulfilled and the whole computational procedure can be terminated. If required, all pore pressure values computed within one period of water loading oscillations, and not only for the last time-point, can be used for the end-test comparison.

4.5.3 Results of example calculations

Numerical computations, based on the above described solution procedure for the parabolic partial differential equation [Eq. (4.48) with Eqs. (4.49a) to (4.49c)], were used to examine the one-dimensional storage model of the pore pressure response in the permeable seabed layer due to oscillating water surfce vertical movements (Magda, 1990[c]). The numerical computations were based on the following input data:

- height of sand column $d = 0.8\,\mathrm{m}$
- porosity of water part of soil $n_w = 0.4$
- porosity of air part of soil $n_a = 0.0 - 0.020$
- coefficient of soil permeability $k_z = 1.5 \times 10^{-4}\,\mathrm{m/s}$

- Poisson's ratio of soil $\nu = 0.3$
- compressibility of soil $\alpha_z = 10^{-5}; 10^{-7}\,\mathrm{m^2/kN}$
- compressibility of pure water $\beta = 4.2 \times 10^{-7}\,\mathrm{m^2/kN}$
- atmospheric pressure $p_{at} = 101.325\,\mathrm{kPa}$
- wave period $T = 1\,\mathrm{s}$
- water depth $h = 1.0\,\mathrm{m}$

Similar to the formerly described two-dimensional storage model, the pore pressure in the one-dimensional storage model is presented, for simplicity and convenience of illustration, using the following relative and dimensionless parameters:

$$\bar{h} = \frac{h'}{H_0} \tag{4.62a}$$

$$\bar{H} = \frac{H'}{H_0} \tag{4.62b}$$

where: $\bar{h}$ - relative pore pressure head, induced within the sand column by water surface vertical oscillations, [-],

$\bar{H}$ - relative amplitude of the pore pressure head, induced within the sand column by water surface vertical oscillations, [-],

h' - pore pressure head, induced within the sand column by water surface vertical oscillations, [m],

H' - amplitude of the pore pressure head, induced within the sand column by water surface vertical oscillations, [m],

H_0 - amplitude of the hydrodynamic bottom pressure head, induced at the sand column surface by water surface vertical oscillations, [m].

Figure 4.28 shows the distribution of the relative pore pressure head, $\bar{h}$, with depth z in the sand column. Eight lines correspond to eight different phases of the oscillating water loading on the top of the sand column. Only one half of the full period of oscillations is considered [*i.e.*, up to $t_{max} = (8/16)T$ with a time step of $dt = (1/16)T$, where T is the period of water loading oscillations]. Because of a regular character of water loading, the results from the second half of the period can be easily obtained as a mirror image of the results from the first half.

Figures 4.29 and 4.30 show the distributions of the amplitude of the relative pore pressure head, $\bar{H}$, and the phase lag, δ, in the pore pressure oscillations with depth z in the sand column. The soil sediment is assumed to be near-incompressible ($\alpha_z = 10^{-7}\,\mathrm{m^2/kN}$). Different soil saturation conditions are introduced, namely: fully saturated soil conditions ($n_a = 0$), and five cases of partly saturated soil conditions ($n_a = 0.004$ to 0.020, with a step of 0.004). It has to be noted, for example, that according to Eq. (3.8), the values of soil porosity part occupied by air, $n_a = 0.004$ and $n_a = 0.020$, correspond with the degree of saturation $S = 0.99$ and $S = 0.95$, respectively, if the soil porosity is assumed to be $n = 0.4$. The results indicate dramatic differences in the calculated amplitudes and phase lags of the pore pressure head oscillations, which can only be a good confirmation of a very large sensitivity of the magnitude of pore pressure oscillations on soil saturation conditions.

Up to a depth of about 0.6 m (*i.e.*, 75 % of the height of the sand column), a linear increase of the phase lag can be observed. Going deeper, the increase of the phase lag developes further but it has a non-linear character due to the impermeable condition assumed at the rigid base of the permeable seabed layer. Through the whole

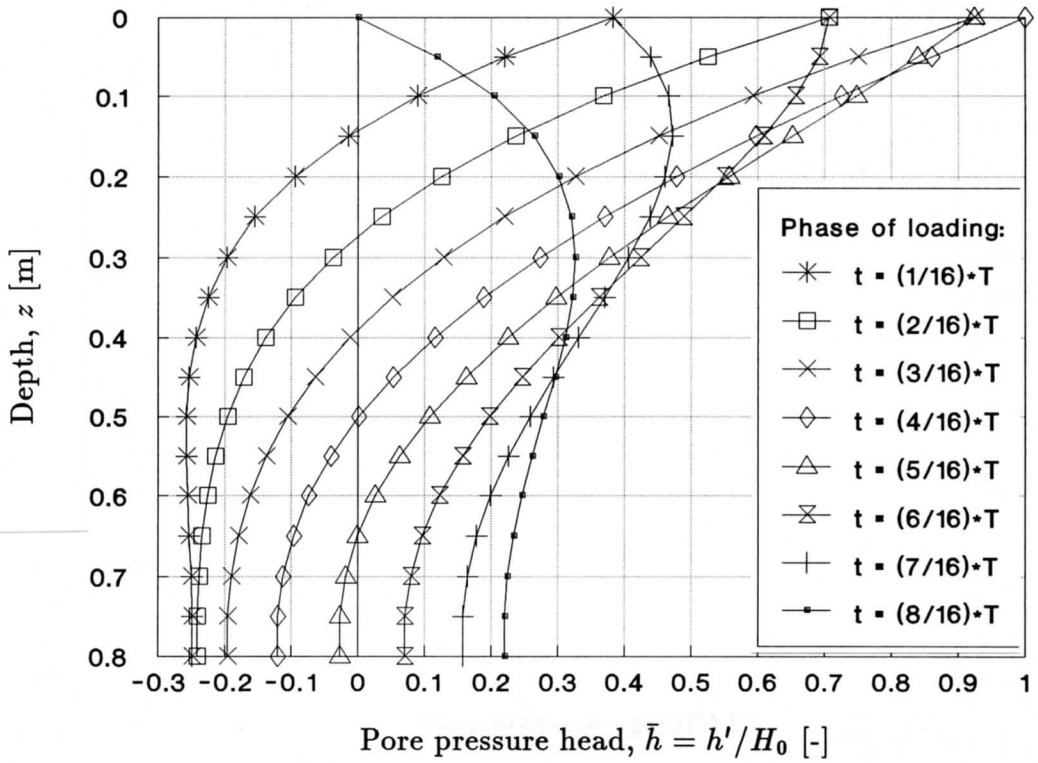

Figure 4.28 Pore pressure head distribution with depth, at different phases of water surface loading cycle, for near-incompressible soil ($\alpha_z = 10^{-7}\,\mathrm{m^2/kN}$) and partly saturated soil conditions ($n_a = 0$); 1-D storage model

height ($d = 0.8\,\mathrm{m}$) of the sand column assumed for computations, practically there is no phase lag observed in the case of fully saturated soil conditions ($n_a = 0$) whereas partly saturated sediments create the phase lag which can be even larger than one half of the period of water surface oscillations, reaching approximately 270° for $n_a = 0.020$ ($S = 0.95$) at the impermeable base.

Analogous to Figs. 4.29 and 4.30 are Figs. 4.31 and 4.32, respectively. However, this time, the soil sediment is assumed to be compressible ($\alpha_z = 10^{-5}\,\mathrm{m^2/kN}$). The imposition of compressibility properties to the second phase (*i.e.*, soil skeleton) of the two-phase seabed medium enables an easier transmission of the wave-induced pore pressure through the soil. This is clearly certified by the pore pressure results where smaller pore pressure damping effects are identified by higher values of the pore pressure amplitude (Fig. 4.31) and lower values of the pore pressure phase-lag (Fig. 4.32), compared to the previous case of the near-incompressible soil skeleton.

The appearance of smaller values of the pore pressure phase-lag in the more compressible soil skeleton has enabled an obervation of an additional element which is a maximum of the pore pressure phase-lag distribution with depth. In the upper part of the sand column, the phase lag increases gradually until its maximum is reached at a certain depth ($z \cong 0.15\,\mathrm{m}$). Going deeper, the phase lag decreases and disappears practically at a depth equal to approximately one half of the height of the sand column.

The illustrative computations have shown that the potential model and the diffusion model create the upper and lower limits, respectively, of the pore pressure amplitude, and the lower and upper limits, respectively, of the pore pressure phase-lag, obtained for the storage model of the oscillation-induced pore pressure response in seabed sediments.

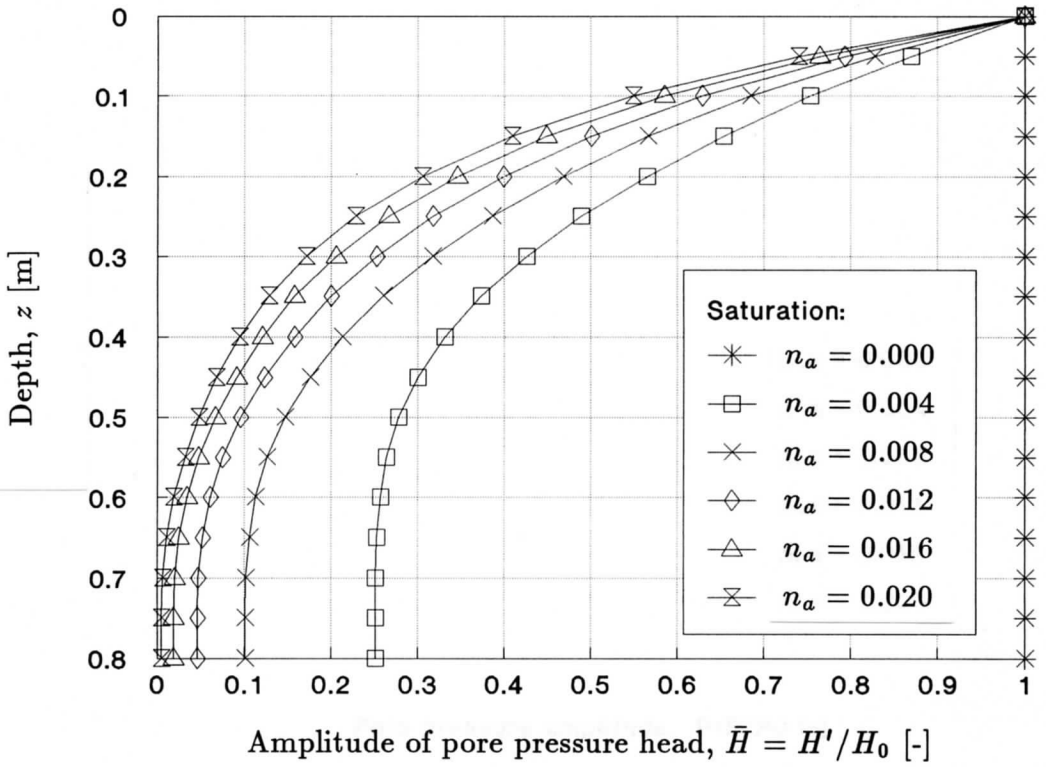

Figure 4.29 Distribution of the amplitude of pore pressure head with depth, for different soil saturation conditions and near-incompressible soil (1-D storage model; $\alpha_z = 10^{-7}\,\mathrm{m^2/kN}$)

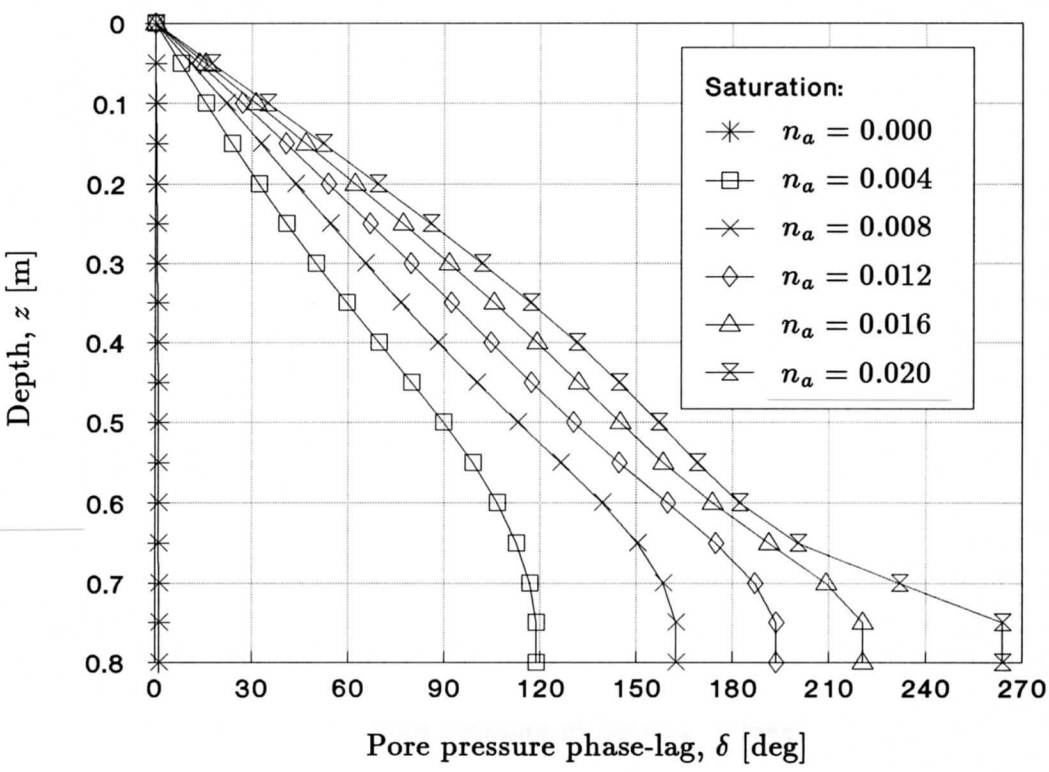

Figure 4.30 Distribution of the pore pressure phase-lag with depth, for different soil saturation conditions and near-incompressible soil (1-D storage model; $\alpha_z = 10^{-7}\,\mathrm{m^2/kN}$)

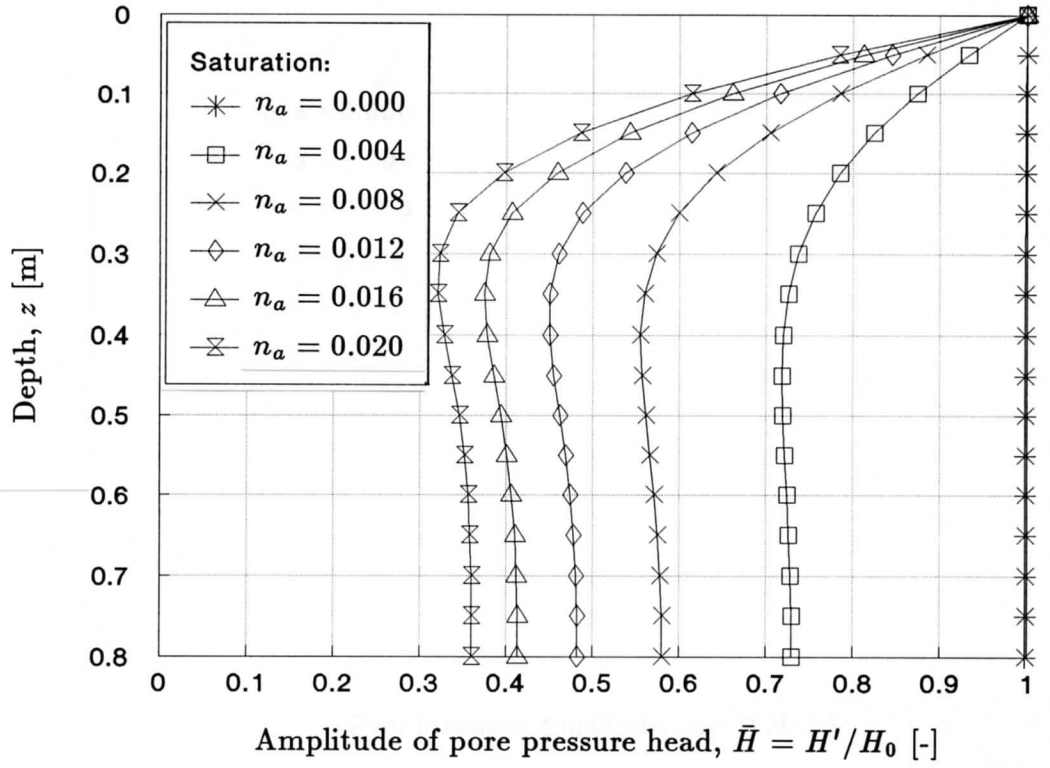

Figure 4.31 Distribution of the amplitude of pore pressure head with depth, for different soil saturation conditions and compressible soil (1-D storage model; $\alpha_z = 10^{-5}\,\mathrm{m^2/kN}$)

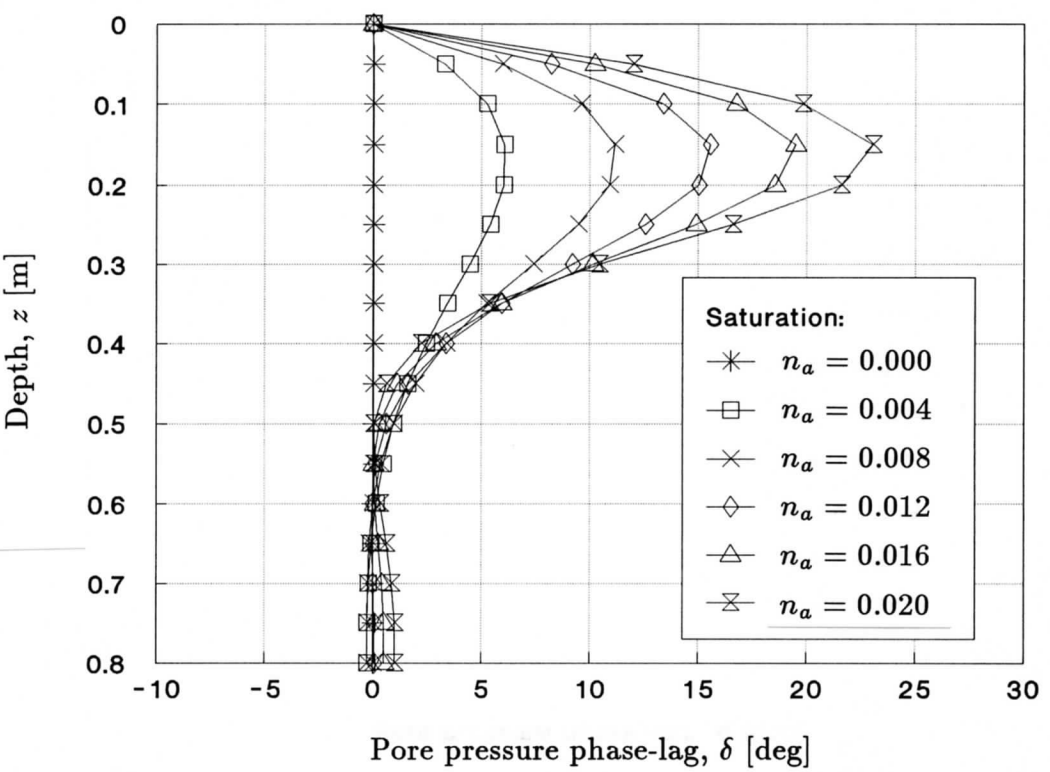

Figure 4.32 Distribution of the pore pressure phase-lag with depth, for different soil saturation conditions and compressible soil (1-D storage model; $\alpha_z = 10^{-5}\,\mathrm{m^2/kN}$)

4.6 Conclusions

The problem of pore pressure oscillations in seabed sediments loaded by progressive surface water waves (in two-dimensional storage model) and water surface vertical oscillations (in one-dimensional storage model) has been solved analytically and numerically, respectively, for the 'finite-thickness layer' boundary condition.

Any analytical solution of the dynamic phenomenon in a multi-phase medium is a complex task and it implies a large number of mathematical operations which normally have to be supported at the end by numerical procedures (Massel, 1985). This was also the case in the present work while deriving the two-dimensional pore pressure solution, especially elaborated for further analyses of pore pressure data recorded from large-scale laboratory models. The governing problem requires the solution of 6 (or 12) coupled linear complex-valued (or real-valued) equations where $6 \times 6 = 36$ (or $12 \times 12 = 144$) constant coefficients, given in rather lengthy forms, have to be considered.

The derived analytical and numerical solutions are based on the storage equation for the pore fluid flow through permeable media (Verruijt, 1969; Madsen, 1978). This gives an opportunity to take very important soil skeleton and pore fluid compressibilities into account. The results of the pore fluid pressure response in sandy seabed sediments are presented in terms of the pore pressure amplitude and the pore pressure phase-lag with respect to the phase of inducing hydrodynamic bottom pressure oscillations.

The input data for the presented solutions contain all meaningful parameters (*e.g.*: the degree of saturation, Young's modulus or compressibility of soil, the coefficient of permeability, and the wave period) influencing a course of the pore pressure fluctuations in seabed sediments. It has to be stressed that the satisfactory solution could not be successfully obtained when the governing problem would be described by the Laplace equation (*i.e.*, potential problem, in which only the geometry of the problem can be reflected). An application of the more advanced diffusion equation creates a better possibility of obtaining a more realistic pore pressure picture, because a natural compressibility of the pore fluid is taken into account. A further complication of the wave-induced pore pressure problem, by introducing the storage model, in which the soil skeleton compressibility can be additionally considered, has indicated the additional influences on the wave-induced pore pressure oscillations in seabed sediments.

The results of example calculations obtained from both the one- and the two-dimensional storage models present, among others, a high sensitivity of the pore pressure solution on the pore fluid compressibility (indirectly on the degree of saturation) and soil permeability. Different values of Young's modulus (or soil compressibility) assumed with respect to different states of soil densification (*i.e.*, dense or loose) can also influence the pore pressure solution significantly.

The pore pressure damping effects (recognized by changes in the amplitude and the phase lag distributions with depth in the permeable seabed layer), influenced by compressibility properties of the two-phase seabed medium and soil saturation conditions, are – in general – qualitatively the same regardless the model considered (*i.e.*, one- or two-dimensional storage model). The existing differences in shapes of the amplitude and phase-lag distribution curves result obviously from different periods and types of water loading applied in the calculation examples for the mentioned two models. The 1-D storage model enables only a vertical (*i.e.*, unidirectional) flow of the pore fluid, induced by cyclic and vertical water surface oscillations, whereas the 2-D storage model gives a possibility of a multidirectional filtration of the pore fluid, induced by progressive and harmonic surface water waves.

The relative compressibility of the two-phase seabed medium has undoubtedly a very meaningful bearing on the wave-induced pore pressure response in seabed sediments. However, it has to be strongly emphased that the influence of the compressibility of the singular phase (*i.e.*, pore fluid or soil skeleton) is qualitatively different. The imposition of compressibility properties to the pore fluid (*i.e.*, the medium flowing through the soil skeleton) enlarges simply the pore pressure damping effects, where the pore pressure amplitude becomes smaller, and the pore pressure phase-lag increases simultaneously. The additional introduction of compressibility properties to the soil skeleton does not contribulte to the further increase of the pore pressure damping effects. If the medium, in which the pore fluid is flowing through, is treated to be compressible, this enables an easier transmission (*i.e.*, smaller damping effects) of the wave-induced pore pressure through the soil, which can be recognized by higher values of the pore pressure amplitude and, simultaneously, lower values of the pore pressure phase-lag, compared to the case where only the pore fluid is assumed to be compressible. The compressible soil skeleton bahaves as a sponge and takes an additional part in the propagation process of the pore pressure through seabed sediments.

The potential model and the diffusion model create the upper and lower limits, respectively, of the pore pressure amplitude, and the lower and upper limits, respectively, of the pore pressure phase-lag, obtained for the storage model of the oscillation-induced pore pressure response in seabed sediments. This observation stays in accordance with the above given explanation concerning the influence of the compressibility of the singular phases distinguished in the two-phase seabed medium.

The studies of the two-dimensional storage model, where the case of more compressible sediments was considered, have indicated that the pore pressure amplitude can – under certain conditions – experience a further decrease, instead of the anticipated increase of its value. In this case, the diffusion solution cannot be treated as the lower limit of the storage solution any more, and becomes the upper limit thereof. This discrepancy seems to be caused only by the imposition of the 'finite-thickness layer' boundary condition, and a very special value of the relative thickness, d/L, of the permeable seabed layer. For certain fixed values of parameters, characterizing the pore fluid and soil skeleton physical properties, and for a certain computational depth in the seabed, an optimum value of the relative thickness, $(d/L)_{opt}$, exists. If the relative thickness is greater than its optimum value, the pore pressure amplitude behaves as for the 'infinite-thickness layer' storage solution, increasing its value with respect to the diffusion solution. If, on the other hand, the relative thickness of the seabed layer is smaller than its optimum value (this was certainly the case in the presented computational example; see Fig. 4.17), the pore pressure amplitude undergoes a further decrease, compared to the case of near-incompressible soil skeleton, and therefore the diffusion solution becomes the upper limit of the storage solution. This problem needs certainly further studies.

The values of the finite thickness of the permeable seabed layer ($d = 0.5\,\mathrm{m}$ in the 2-D model, and $d = 0.8\,\mathrm{m}$ in the 1-D model), used in the example computations, were adjusted with respect to laboratory modelling foreseen as a verification of the 'finite-thickness layer' solution to the storage model of the two-phase seabed medium.

All the calculations performed have an illustrative character only, and the next Chapter 5 will bring a wide comparison of theoretically computed values with results obtained from large- and small-scale laboratory modelling.

Chapter 5

Experimental verification of the 'finite-thickness layer' solution

This Chapter presents results from experimental investigations, the main goal of which was to verify the 'finite-thickness layer' solution to the wave-induced pore pressure distribution with depth, analytically derived (2-D model) and numerically obtained (1-D model) in Chapter 4. The following brings a description of laboratory modelling procedures, explains test instrumentation, and presents a verification of experimental results using theoretically computed values of pore pressure oscillations in sandy sediments. Large-scale laboratory modelling, thought as a tool for qualitative evaluation of the governing problem, were followed by small-scale tests where individual influences of some leading and decesive parameters of the two-phase (*i.e.*, soil skeleton and pore fluid) system were possible to be checked precisely with a relatively high accuracy.

5.1 Large-scale model tests

As a verification of the analytical 'finite-thickness layer' solution, derived in Chapter 4, series of laboratory tests were conducted in the large wave flume 'Grosser Wellenkanal' (GWK), at the University of Hannover, Germany (Magda, 1990[a]). Huge dimensions (*i.e.*, 5 m wide, 7 m deep, and 324 m long) of the flume (Fig. 5.1) create a very unique laboratory facilitity, in which modelling in a near-natural scale becomes feasible.

5.1.1 Test facilities and instrumentation

5.1.1.1 Sand

The sand, called the 'Norderney Sand' and used in the laboratory experiments in the large wave flume, was taken from its natural source which is the western coast of Norderney Island (Germany). It is a quartz type of sand and the specific gravity of the solid

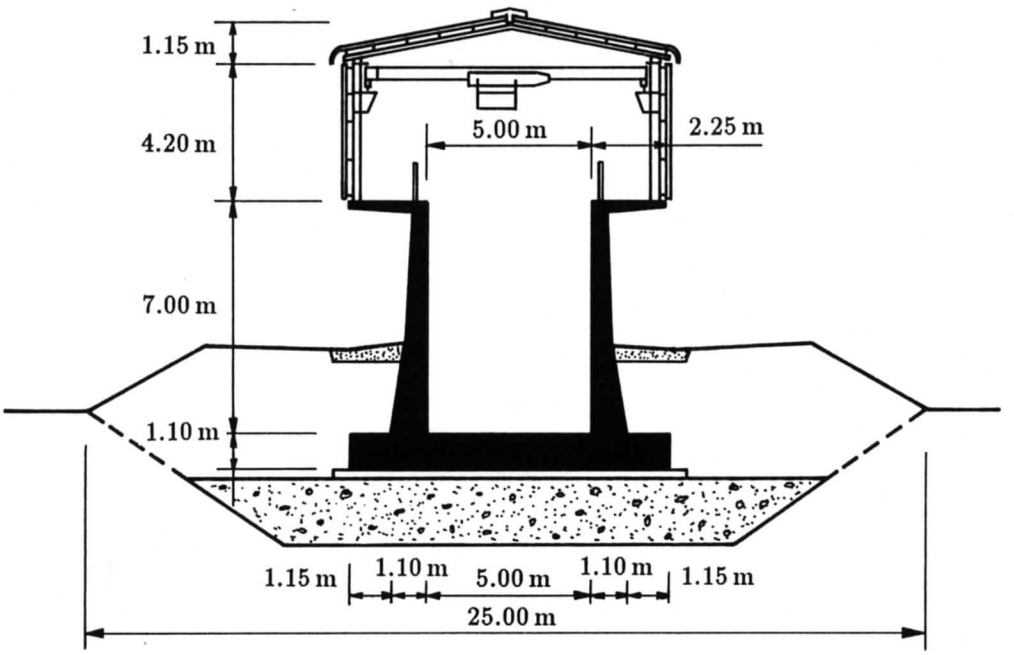

Figure 5.1 Cross-section of the large wave flume (GWK)

soil particles is equal $\varrho_s = 2.65$. The particle size distribution of the sand is presented on a semi-logarythmic plot (Fig. 5.2). Estimated as medium, the 'Norderney Sand' has the following characteristic parameters:

- specified particle size $d_{50} = 0.23\,\text{mm}$
- coefficient of uniformity $C_U = 1.61$
- coefficient of curvature $C_C = 1.03$
- minimum porosity $n_{min} = 0.321$
- maximum porosity $n_{max} = 0.427$
- coefficient of permeability $k = 1.3 \times 10^{-4}\,\text{m/s}$

5.1.1.2 Data acquisition system

The data acquisition system consists mainly of a set of pore pressure transducers, signal processing unit, and data recording system (Fig. 5.3).

The pore pressure transducers are connected to the signal processing unit by means of water-tight cables. An electrical signal coming out from transducers is, first of all, amplified. The second function of the signal processing unit is to convert analog input signals (from transducers) to digital output signals which are, in the next step, recorded by PC-AT computer using a BASIC control program. The data recording system is also equipped with three terminals, namely: monitor, plotter, and multi-pen recorder, in order to visualize pore pressure signals immediately during their recording.

Pore pressure sensor KS 2150 (Fig. 5.4), made by 'Philips', is designed to convert an input pressure of the span ranging from 0 to 150 kPa, into an output electrical signal of value up to $50\,\text{mV} \pm 2\,\%$.

The transducer must be supplied with 10 V d.c. (*i.e.*, different current possible), and is predestinated to work properly in different fluid media, like: gases and liquids.

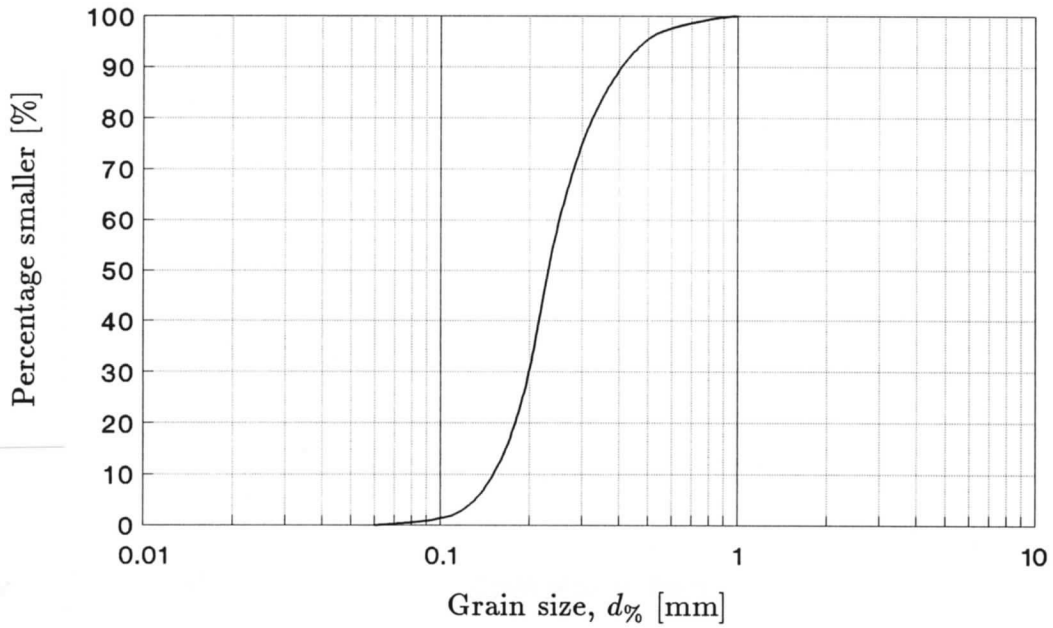

Figure 5.2 Sand particle size distribution curve

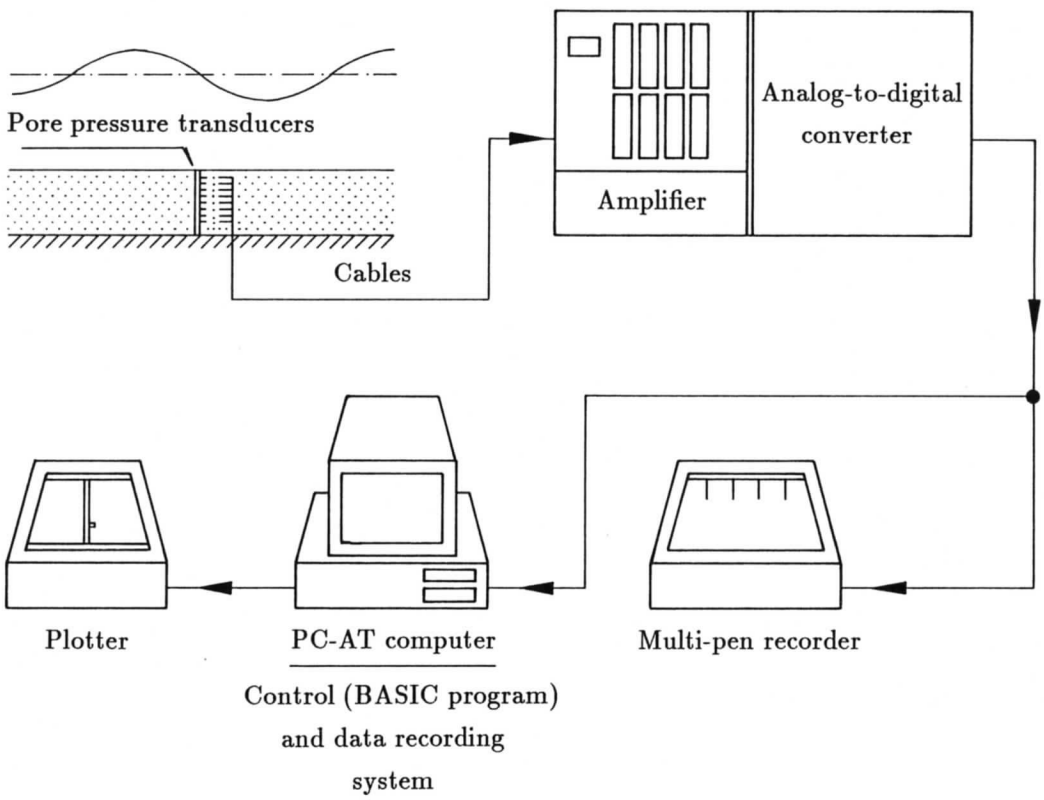

Figure 5.3 Scheme of data acquisition system

Pressure sensor KS 2150 is equipped with a miniature silicon-semiconductor element of high sensitivity and minimum displacement volume. The semiconductor, in the form of a silicon membrane, is placed behind a separating and protecting diaphragm made of high-quality alloy steel, and homed in a small stainless steel cavity filled with a silicon oil.

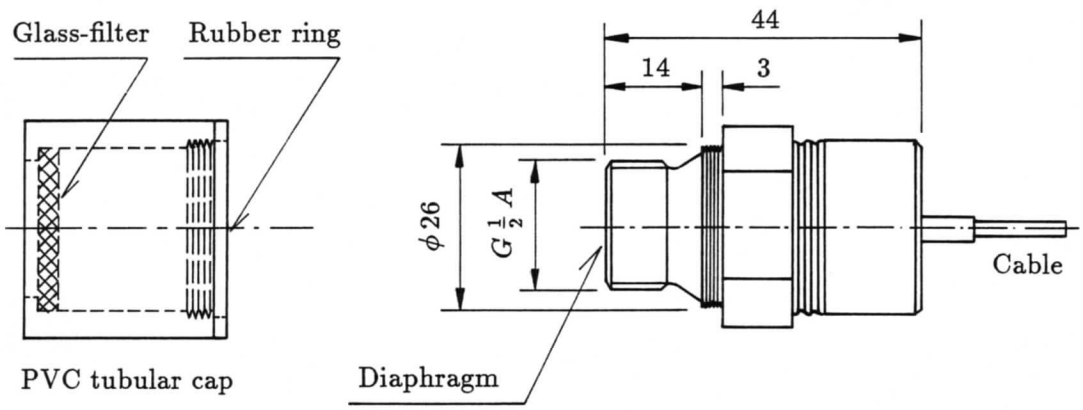

Figure 5.4 Cross-section of pore pressure transducer and glass-filter cap

The characteristic of the sensor's work is linear where the linearity error is less than 0.5 % of the span. Allowable environmental conditions are described by the ambient temperature limits which are −30 and +80 °C. Thanks to a high free vibration (natural) frequency of the membrane, the setting time is very short (*i.e.*, less than 1.5 ms).

All the above technical specifications suit the testing conditions in the large wave flume (GWK) very well. The only problem which had to be solved was how to separate simultaneous actions of pore pressure and soil pressure on the sensor's steel diaphragm. The problem has been solved by adding a specially constructed filter on the top of the transducer (see Fig. 5.4).

The glass-filter, built into a PVC tubular cap, serves as an isolation of an active area of the transducer from the soil matrix, giving possibility to flow the pore fluid through and to measure its actual pressure.

The sandy bed layer, 0.5 m thick, was equipped all together with 10 pore pressure transducers. A sketch of the test facilities is shown in Fig. 5.5. The pore pressure transducers were installed both in the centre (5 transducers) and on the side-wall (5 transducers) of the same cross-section of the wave flume, about 200 m from the wave generating machine to assure that the waves rolling over the sandy are already well-formed. The main purpose of division of the pore pressure transducers into two groups was to study the effect of the side-wall boundary influence on the pore pressure cyclic oscillations induced in sandy sediments. Each transducer was fixed to a flexible PVC rod (in the centre profile) or to the wall of the wave flume (in the side-wall profile) to preserve its unchanged position during the whole testing period.

Before the final installation, the PVC cap containing the glass-filter was screwed tightly to each from 10 pore pressure transcucers. This operation was done underwater in a special container to assure that the free space in the PVC cap, between the glass-filter and the transducer active area, is filled totally with water. This was very meaningful for the final success of the measuring campaign; any intrusion of even small amount of air into the hollow space of the transducer might have been caused unwanted damping effects for measured pore pressure oscillations, destroying thereby a real picture of the soil-water interaction.

It was also necessary to have at least one wave gauge, in the cross-section where all transducers were installed, in order to provide a continueous correlation between wave characteristics (*i.e.*, actual water elevation) and the wave-induced pore pressure measured in two profiles in sandy sediments.

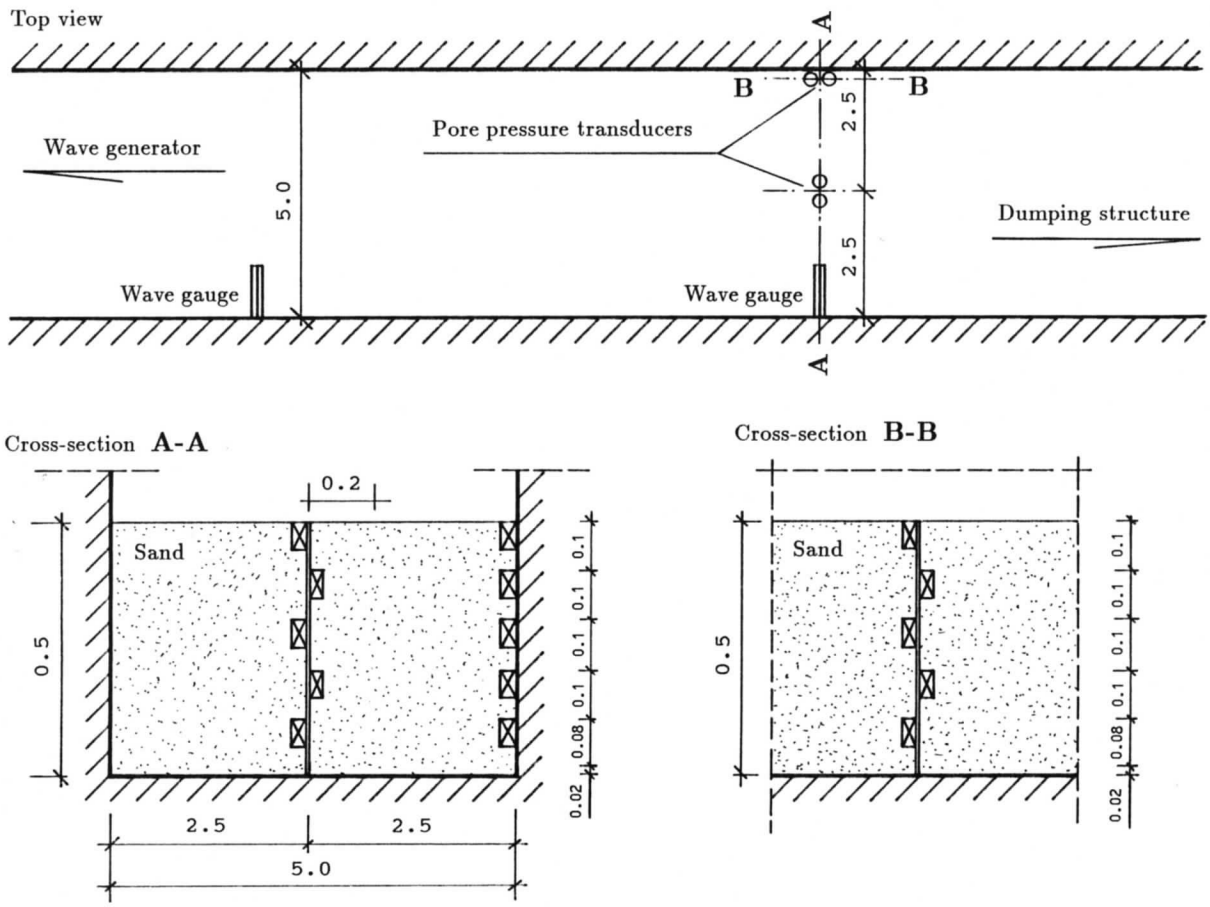

Figure 5.5 Layout of test instrumentation in the large wave flume (GWK)

The wave flume was filled with sand, creating a seabed layer of thickness $d = 0.5\,\text{m}$. After the transducers had been installed, saturation of the sand layer was performed. A slow water inflow into the wave flume was associated with vibrating of the sand layer (using 5 vibrating needles, each 0.5 m long). This procedure helped to achieve both soil saturation conditions and density as high and homogeneous as possible. The filling of the wave flume with water was continued up to $h = 4.5\,\text{m}$ water depth above the sand surface.

5.1.2 Test procedure

To get a better and clear insight into the question of pore pressure cyclic oscillations induced in sandy seabed sediments, all test series were performed with regular waves only, where different wave conditions were modelled by the wave height and the wave period. And thus, the applied wave height was between $H = 0.25$ and $1.0\,\text{m}$, and the applied wave period was between $T = 3$ and $10\,\text{s}$. Taking the above values into account, together with a water depth of $h = 4.5\,\text{m}$ kept constant in all tests, it is possible to define a type of the wave generated in the wave flume. Figure 5.6 presents the range

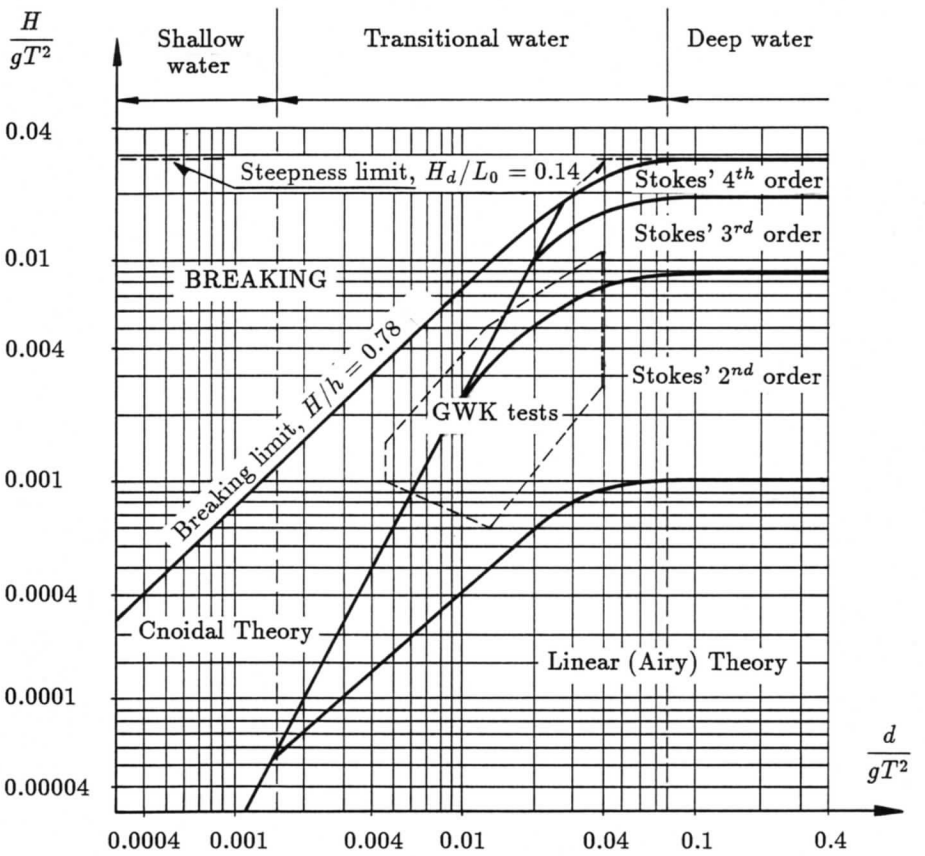

Figure 5.6 Regions of validity for various wave theories, [Shore Protection Manual, 1984]

(middle area marked by a dashed polygon) of waves applied during test performances in the wave flume, comparing with well-known regions of validity for various wave theories.

Because of a relatively small water depth (transitional water) and high wave hights, most of the waves generated in the wave flume can be theoretically described by Stokes' 2nd order wave theory, being sometimes very close to Stokes' 3nd order wave theory or even the cnoidal wave theory.

The wave parameters (*i.e.*, wave period, T, and wave height, H), applied in the pore pressure experiments in the large wave flume, were grouped into two sets, as listed below:

- Set I (constant wave height: $H = 1.0\,\mathrm{m}$)
  wave period: $T = 3,\ 5,\ 6,\ 8,\ 10\,\mathrm{s}$
- Set II (constant wave period: $T = 6\,\mathrm{s}$)
  wave height: $H = 0.25,\ 0.5,\ 0.75,\ 1.0\,\mathrm{m}$

The duration of execution of each test was long enough to obtain stable wave conditions over the testing section in the wave flume; only a few first waves were always sufficient to have the following waves already well-formed.

All pore pressure data recorded by the data acquisition system were sampled with a sampling frequency of $f_s = 25\,\mathrm{Hz}$ (*i.e.*, with a time-interval of $dt_s = 0.04\,\mathrm{s}$).

5.1.3 Results of measurements and comparison with the 'finite-thickness layer' solution

5.1.3.1 Hydrodynamic bottom pressure

The hydrodynamic part of the wave-induced pressure at the sea floor can be given by the following equation derived from Stokes' 2^{nd} order wave theory [Shore Protection Manual, 1984]:

$$p_b = \gamma_w \frac{H}{2} \frac{1}{\cosh(ah)} \cos(ax - \omega t) + \frac{3}{8}\gamma_w \frac{\pi H^2}{L} \frac{\tanh(ah)}{\sinh^2(ah)} \left[\frac{1}{\sinh^2(ah)} - \frac{1}{3}\right] \cos[2(ax - \omega t)] \tag{5.1}$$

where: p_b - bottom pressure [kPa],
γ_w - unit weight of water [kN/m^3],
H - wave height [m],
a - wave number ($a = 2\pi/L$) [m^{-1}],
L - wavelength [m],
h - water depth [m],
ω - wave angular frequency ($\omega = 2\pi/T$) [s^{-1}],
T - wave period [s],
t - time [s],
x - horizontal coordinate of the Cartesian coordinates system [m].

The first term of the above equation is linear with respect to the wave height, and therefore reflects the bottom pressure equation described by Airy's linear theory for waves of small amplitude. The second term in Eq. (5.1), resulting from the Stokes's 2^{nd} order wave theory, is responsible for the non-linear influence of the wave height on the hydrodynamic bottom pressure.

The measured values of the bottom pressure are compared with values computed theoretically using Eq. (5.1). Taking, for example, a constant wave period of $T = 6$ s, and different wave heights ranging from $H = 0.25$ to 1.0 m, Figure 5.7 illustrates the hydrodynamic bottom pressure under the wave crest and the wave trough. Both the linear (Airy's wave theory) and the non-linear (Stokes' 2^{nd} order wave theory) theoretical solutions are indicated.

Generally, Fig. 5.7 shows larger values of the bottom pressure measured under the wave crest than under the wave trough. This only confirms a non-linear character of waves generated in the large wave flume; the height of the wave crest is always higher than the depth of the wave trough when non-linear (*i.e.*, of higher order) wave theories are applied.

For the intermediate water depth condition (*i.e.*, $H = 0.25$ m and $h = 4.5$ m, $H/h \cong 0.056$), the both wave theories considered in the comparison analysis give very similar values of the hydrodynamic bottom pressure, which are simultaneously almost the same as the measured values. The both theories overestimate the values measured under the wave crest and the wave trough; the highest difference between the theoretical and experimental values was observed for the highest applied wave hight, $H = 1.0$ m

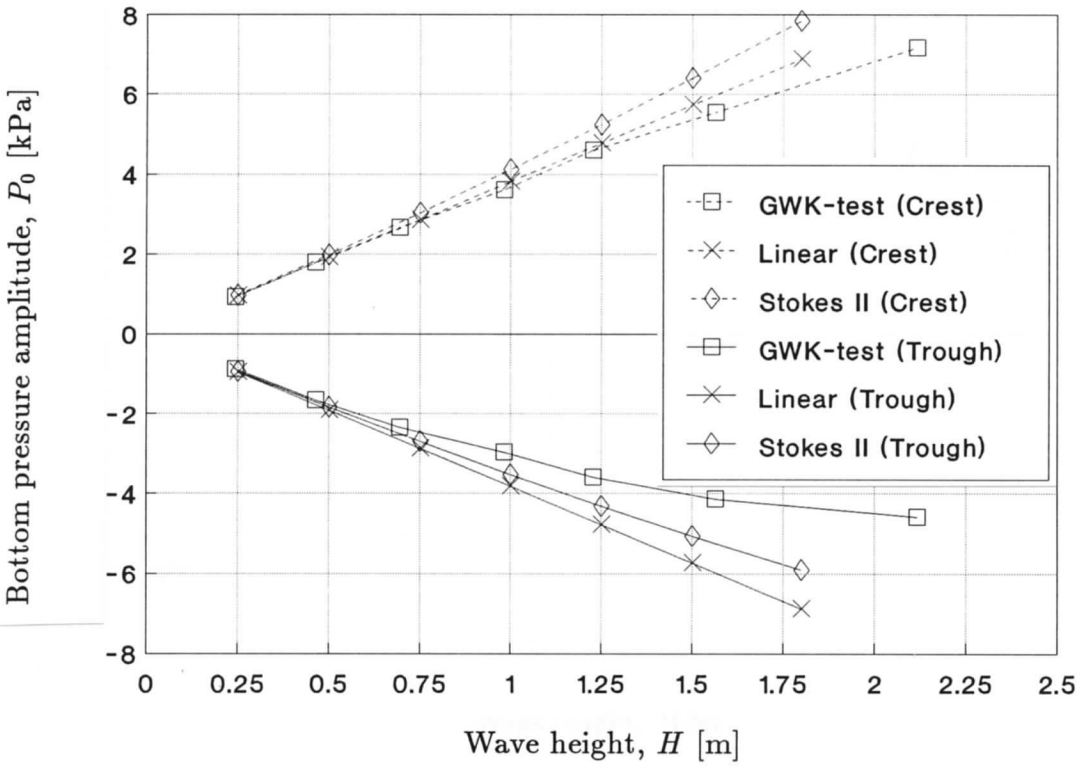

Figure 5.7 Comparison of measured and calculated values of the bottom pressure under wave crest and wave trough (for constant wave period, $T = 6\,\mathrm{s}$)

($H/h \cong 0.22$), and is about 3 % (crest) and 27 % (trough) of the measured value (for the linear wave theory), and 12 % (crest) and 16 % (trough) of the measured value (for Stokes' 2$^{\mathrm{nd}}$ order wave theory).

The linear wave theory gives a better approximation of the measure values of the hydrodynamic bottom pressure in the case of wave crest, whereas Stokes' 2$^{\mathrm{nd}}$ order wave theory seems to be more appropriate as far as the wave trough is concerned.

5.1.3.2 Pore pressure distribution with depth

An example of the recorded signals from a short time interval, adequate to one period of oscillations, is shown in Fig. 5.8. This multi-plot compares qualitatively transient values of the pore pressure, recorded by the transducers situated in the centre profile of the large wave flume, with respect to the water wave profile recorded simultaneously in the same cross-section of the wave flume.

Two main phenomena, expected from the theoretical solution, can be easily recognized, namely: the attenuation of pore pressure with depth, and the increase of pore pressure phase lag with depth.

The data recorded from the tests performed for the constant wave height $H = 1.0\,\mathrm{m}$ ($T = 3$ to $10\,\mathrm{s}$) and for the constant wave period $T = 6\,\mathrm{s}$ ($H = 0.25$ to $1.0\,\mathrm{m}$) was chosen to illustrate the above mentioned effects. Applying the Fast Fourier Transform (FFT) method into the data analysis procedure (Ramirez, 1985), it was possible to compute precisely the characteristic parameters (*i.e.*, amplitude and phase lag) of the recorded oscillations of pore pressure in sandy sediments. An example of a graphical presentation

of the signals, recorded in Test No. GWK-23 ($H = 1.0\,\text{m}$, $T = 6\,\text{s}$, $h = 4.5\,\text{m}$), and their FFT-analysis, is shown in Fig. 5.8.

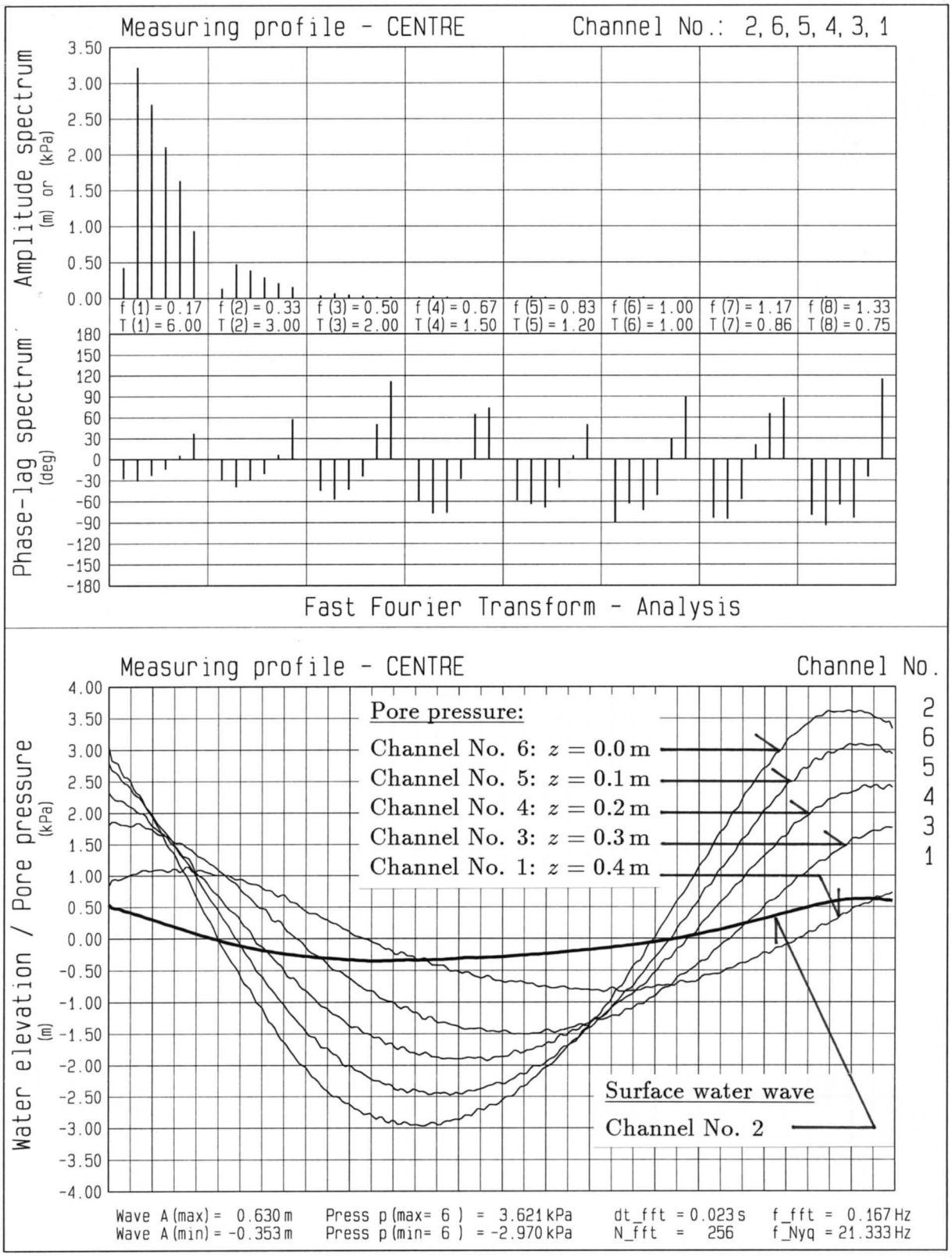

Figure 5.8 Example of graphical presentation of GWK-data analysis (FFT-analysis and plot of recorded signals; Test No. GWK-23, $H = 1.0\,\text{m}$, $T = 6\,\text{s}$, $h = 4.5\,\text{m}$)

In the lower part of Fig. 5.8, a plot of the windowed and sampled wave-like signals (one channel for the surface water wave elevation, and five channels for pore pressure oscillations at five different depths in the central vertical profile of the wave flume) is presented. The signals are windowed by virtue of deciding to plot the waveform over a finite time interval. The time span of the integer number of cycles is usually determined in order to reduce discontinuities at the window edges, and thus reduce leakage to a tolerable level; in the present case, the window has a length of exactly one period ($T = 6\,\mathrm{s}$) of surface water wave oscillations applied in the experiment. The signals are sampled by virtue of the decision to find and show its actual values at only a certain number, N_s, of discrete points. The measurements were conducted with a sampling frequency $f_s = 25\,\mathrm{Hz}$ (*i.e.*, with a sampling time-interval $dt_s = 0.04\,\mathrm{s}$). It means that the windowed data consist of $N_s = T \times f_s = 150$ samples for each of six channels.

A spectral analysis of the data recorded was based on the Fast Fourier Transform (FFT). Most of FFT algorithms are for operating on N_F samples, where N_F is equal to 2 raised to an integer power (*i.e.*, 2, 4, 8, 16,...). The $N_F = 2^j$ (j is an integer) algorithms, also known as power-of-two algorithms, are more straightforward and relatively faster to execute than the more general algorithms. A power-of-two algorithm can only transform records of 2, 4, 8, 16,..., 2^j samples. So a 150-point FFT cannot be done with a power-of-two-algorithm. Therefore, for the purpose of the FFT-analysis applied in the present work, it was decided to take such a number of samples, N_F, which is the next to the number of input samples, N_d. And thus, $N_F = 256$ was assumed, implying new values of the sampling frequency, $f_F = N_F/T = 42.667\,\mathrm{Hz}$, and the sampling time-interval, $dt_F = 1/f_F = 0.023\,\mathrm{s}$, required by the power-of-two algorithm.

Usually, the computed new sample locations will not match the locations where the waveform samples were actually taken. So the next step was to use the actual sample values and locations to interpolate what the sample values should be for the new sample locations. In such a situation, a linear interpolation is the simplest way to overcome this problem, but other methods of interpolation may prove more accurate. In the present analysis, a trygonometric interpolation [Discrete Fourier Transform (DFT)] was used.

The lower plot of Fig. 5.8, where the interpolated samples are shown in $N_F = 256$ discrete points, connected by line segments, indicates clearly the pore pressure damping effects (*i.e.*, decreasing amplitudes and increasing phase lags with depth). The surface water wave record has a cnoidal shape, characterized by higher crests ($A^{(c)} = 0.630\,\mathrm{m}$) and smaller troughs ($A^{(t)} = -0.353\,\mathrm{m}$), which makes the wave shape asymmetrical with respect to the still water level. The cnoidal character of surface water wave propagating oscillations, due to a small value of the relative water depth, has its direct influence on also asymmetrical values of the hydrodynamic bottom pressure and pore pressure oscillations in the seabed. For example, the hydrodynamic bottom pressure, recorded in Channel No. 2, shows a higher crest value ($P_0^{(c)} = 3.621\,\mathrm{kPa}$) with respect to a trough value ($P_0^{(t)} = -2.970\,\mathrm{kPa}$).

The upper part of Fig. 5.8 illustrates the results of a spectral analysis of the six signals recorded during the run of Test No. GWK-23, in terms of the amplitude spectrum and the phase-lag spectrum. The diagram is divided into eight vertical sectors, denoting eight waveform components (so-called harmonic components), contributing to the initial waveform (see the lower part of Fig. 4.8) taken for the spectral analysis. The next harmonic components, have frequencies which are multiples of the frequency interval, given by $df_F = 1/(N_F\, dt_F) = 0.167\,\mathrm{Hz}$. Knowing the frequency of a certain harmonic component, the period of oscillations, T_F, can be easily computed. And thus, the first harmonic has a period of $T_F^{(1)} = 6\,\mathrm{s}$ which is exactly equal to the period of the initial

waveform. The next harmonics are characterized by higher frequencies (*i.e.*, smaller periods) of oscillations. The highest frequency that can be defined at a given sampling rate is called the Nyquist frequency. For equally spaced samples (dt_F = const), the Nyquist frequency is $f_N = 1/(2\,dt_F)$, and was found to be equal to $f_N = 21.333$ Hz in the considered example.

In each of the eight vertical sectors, 'bar' diagrams show the spectral results obtained for each of the six signals taken for the FFT-analysis. The first bar indicates the results obtained for the surface water wave oscillations (Channel No. 2), and the resting five bars indicate the results for the pore pressure oscillations, recorded by respective Channels No. 6, 5, 4, 3, and 1. In the case of a purely sinusoidal waveform, only the first harmonic would be relevant, and the others would have negligible values due to a digital noise and can be considered to be zero compared to the major value. However, as it was mentioned before, the waveforms of the signals recorded differ slightly from the sinusoidal shape, which is visibly indicated by the presence of non-zero results obtained for the higher-order harmonics. The spectral diagrams have also indicated very clearly the pore pressure damping effects existing in the seabed layer.

Based on the results of the FFT-analyses performed for other test runs, Figs. 5.9 and 5.10 show the pore pressure amplitude and the phase lag distributions with depth, respectively, under the condition of a constant wave height, $H = 1.0$ m, and different wave periods ranging from $T = 3$ s to $T = 10$ s. As it was the case in the theoretical considerations in Chapter 4, the pore pressure amplitude, P, is represented by the relative (and dimensionless) pore pressure amplitude parameter, $\bar{P}$ [see Eq. (2.16b)], calculated with respect to the hydrodynamic bottom pressure amplitude, P_0. The pore pressure phase-lag distribution with depths in seabed sediments is computed with respect to the phase of surface water wave oscillations.

The influence of different wave periods on the pore pressure damping in the seabed is clearly seen, and this relationship has a constant tendency, namely: the longer wave period is (*i.e.*, longer wavelength), the smaller damping rate is. This is certified by larger amplitudes (Fig. 5.9) and smaller phase lags (Fig. 5.10), when the wave period increases. The pore pressure amplitude at the lower part of the sand layer ($z = 0.4$ m) is, for example of a wave period of $T = 3$ s, as much as 5 times smaller than for a wave period of $T = 10$ s. Simultaneously, a wave period of $T = 10$ s induces the phase lag which is about 70 % of that occured for a wave period of $T = 3$ s.

An analogous situation, but this time for a constant wave period of $T = 6$ s and different wave heights ranging from $H = 0.25$ to $H = 1.0$ m, is illustrated in Figs. 5.11 (pore pressure amplitude) and Fig. 5.12 (pore pressure phase-lag). The use of the formerly introduced relative pore pressure amplitude, $\bar{P}$, is now particularly helpful for comparison purposes. It allows a simultaneous comparison of shapes of pore pressure amplitude distribution curves belonging to the same family of tests conducted for a constant wave period and different wave heights. This way of presentation makes the pore pressure amplitude distribution with depth independent of the hydrodynamic bottom pressure amplitude, P_0, linearly proportional to the wave height. Therefore, all the curves shown in Fig. 5.11 should be theoretically the same. And this is the case in the discussed example. The results shown in Fig. 4.12 have indicated that the pore pressure phase-lag is independent of the height of water wave loading oscillations.

Soil saturation conditions play a very important role in the process of wave-induced pore pressure oscillations within sandy seabed sediments. The theoretical analysis performed in Chapter 4 demonstrated a great sensitivity of the pore pressure solution on soil saturation conditions represented by the degree of saturation. During the measuring campaigne in the large wave flume it was also possibile to take some sand samples

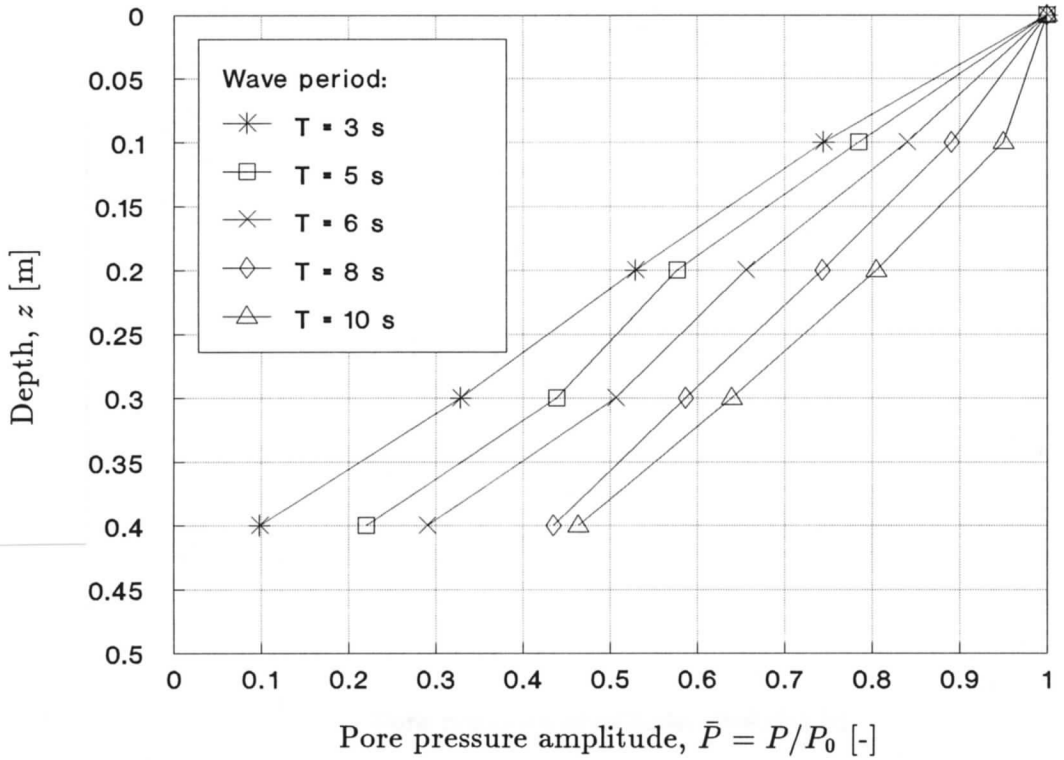

Figure 5.9 Pore pressure amplitude distribution with depth (tests with constant wave height, $H = 1.0\,\mathrm{m}$)

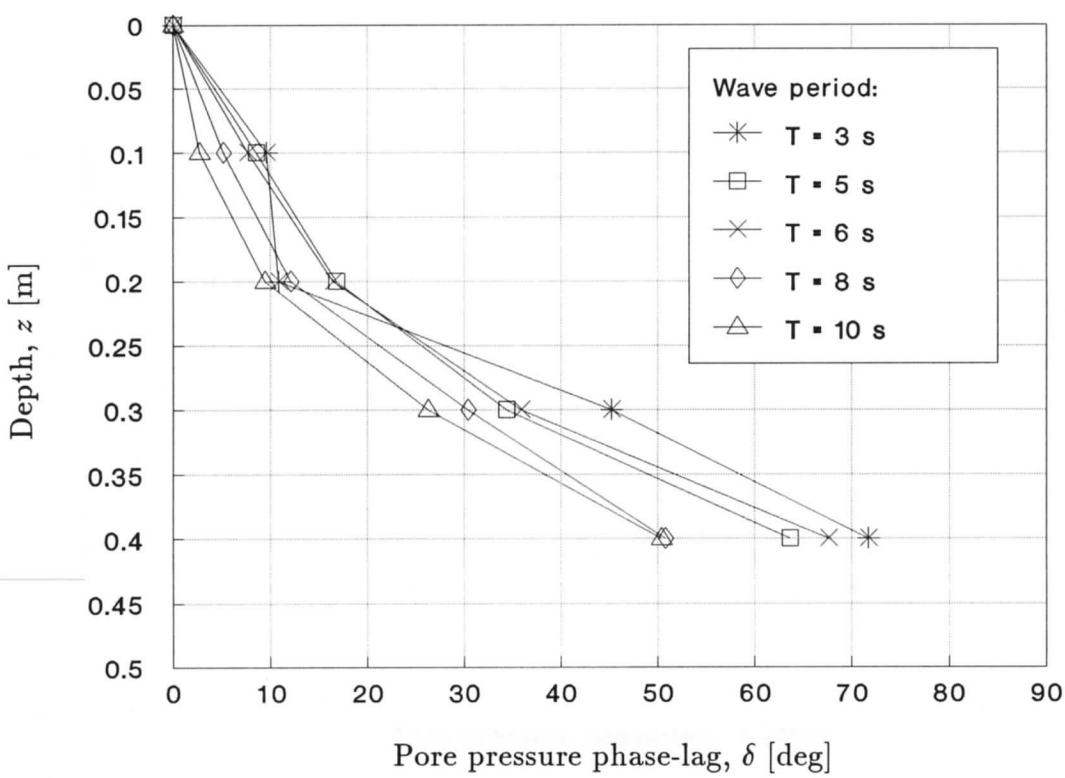

Figure 5.10 Pore pressure phase-lag distribution with depth (tests with constant wave height, $H = 1.0\,\mathrm{m}$)

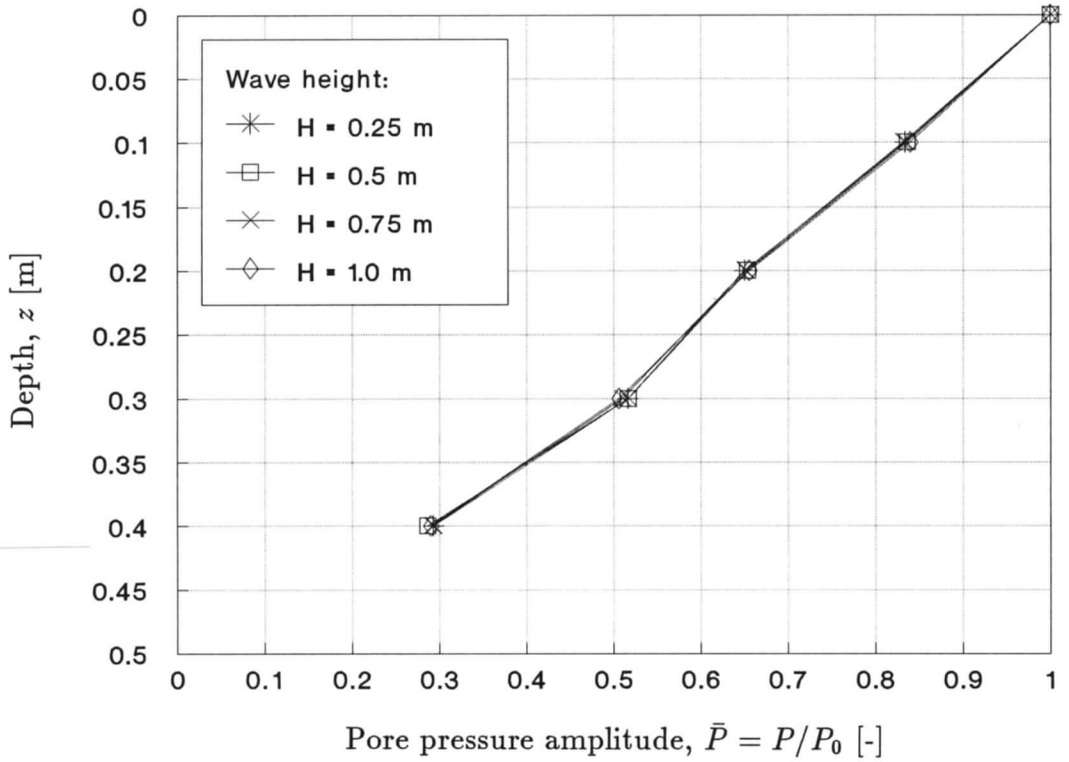

Figure 5.11 Pore pressure amplitude distribution with depth (GWK-tests with constant wave period, $T = 6\,\mathrm{s}$)

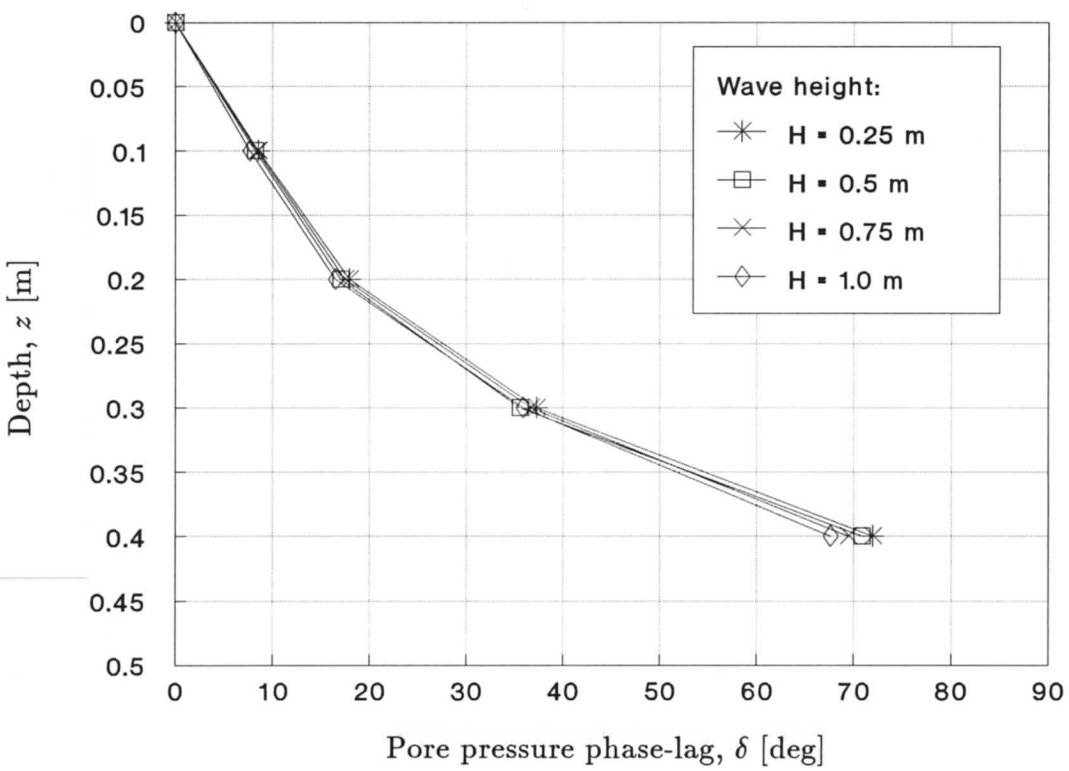

Figure 5.12 Pore pressure phase-lag distribution with depth (GWK-tests with constant wave period, $T = 6\,\mathrm{s}$)

from the upper part of the sand bed layer in order to define existing, real soil saturation conditions. The mean value of the degree of saturation, obtained from 25 samples, was found to be $\bar{S} = 0.98$.

Because of the existence of a certain measuring error (a real value of S cannot be higher than 1), the obtained mean value of the degree of saturation cannot be treated as representative and, therefore, should not be used in calculations of the pore pressure response. However, as it was shown in Chapter 3, there exists another powerful method to evaluate a mean value of the degree of saturation properly and more precisely. Thanks to the statistical analysis performed in Chapter 3 for the case of the 'Norderney Sand' (*i.e.*, assuming the variabilities from the seabed sampling on Norderney Island to be the same as in the sand sampling performed in the large wave flume) it was possible to determine soil saturation conditions typical for the tests performed in the large wave flume. It has to be noted that 3 from 25 sand samples had calculated values of the degree of saturation exceeded 1. It means that 12 % of all the values will be plotted above so-called ZAVL (Zero-Air-Void-Line). By entering Fig. 3.16, an approximate value of the real degree of saturation was found to be $\bar{S} \cong 0.95$. Using this value, some comparisons were made between the results obtained from the analytically derived two-dimensional 'finite-thickness layer' solution, and those recorded during the pore pressure measurements in the large wave flume.

A comparison of the measuremed values with the theoretical 'finite-thickness layer' solution, derived in Chapter 4, is presented in Figs. 5.13 and 5.14. As an example, the surface wave loading, specified by a wave period of $T = 6\,\mathrm{s}$ and a wave height of $H = 1.0\,\mathrm{m}$, was chosen. Other soil parameter input data used in the calculations are as follows:

- thickness od seabed layer $d = 0.5\,\mathrm{m}$
- porosity of soil $n = 0.4$
- coefficient of soil permeability $k = 1.3 \times 10^{-4}\,\mathrm{m/s}$
- Poisson's ratio of soil $\nu = 0.3$
- Young's modulus of soil $E = 10^4;\ 10^5\,\mathrm{kPa}$
- compressibility of pure water $\beta = 4.2 \times 10^{-7}\,\mathrm{m^2/kN}$
- degree of saturation $S = 0.95$
- atmospheric pressure $p_{at} = 101.325\,\mathrm{kPa}$
- water depth $h = 4.5\,\mathrm{m}$

Figures 5.13 and 5.14 illustrate the comparison of the pore pressure amplitude, $\bar{P}$, and the pore pressure phase-lag, δ, distributions with depth, z, respectively. Two thiner lines indicate the theoretical solutions, based on the 2-D storage model, obtained for two different values of Young's modulus of soil, *i.e.*: $E = 10^4\,\mathrm{kPa}$ and $E = 10^5\,\mathrm{kPa}$, simulating thereby different density states of the sand model.

It is very characteristic that in the upper part (up to approximately $z = 0.2\,\mathrm{m}$) of the sand bed model, a better agreement between the measured and the theoretical values is reached for the lower compressibility of the soil (*i.e.*, $E = 10^4\,\mathrm{kPa}$). This is very evident, especially when the pore pressure phase-lag is examined. Such behaviour of the pore pressure response can be explained by the existence of looser sediments in the upper part of the layer, due to stronger movements of water particles in the vicinity of the upper surface of the seabed model loaded by surface water waves.

In the deeper parts of the sandy layer, the discrepancy between the experimental and theoretical solutions increases with depth. Here, the theoretical solution obtained for more dense sediments (*i.e.*, $E = 10^5\,\mathrm{kPa}$) seems to fit the experimental values better than in the case of loose sandy sediments, although the agreement can be estimated

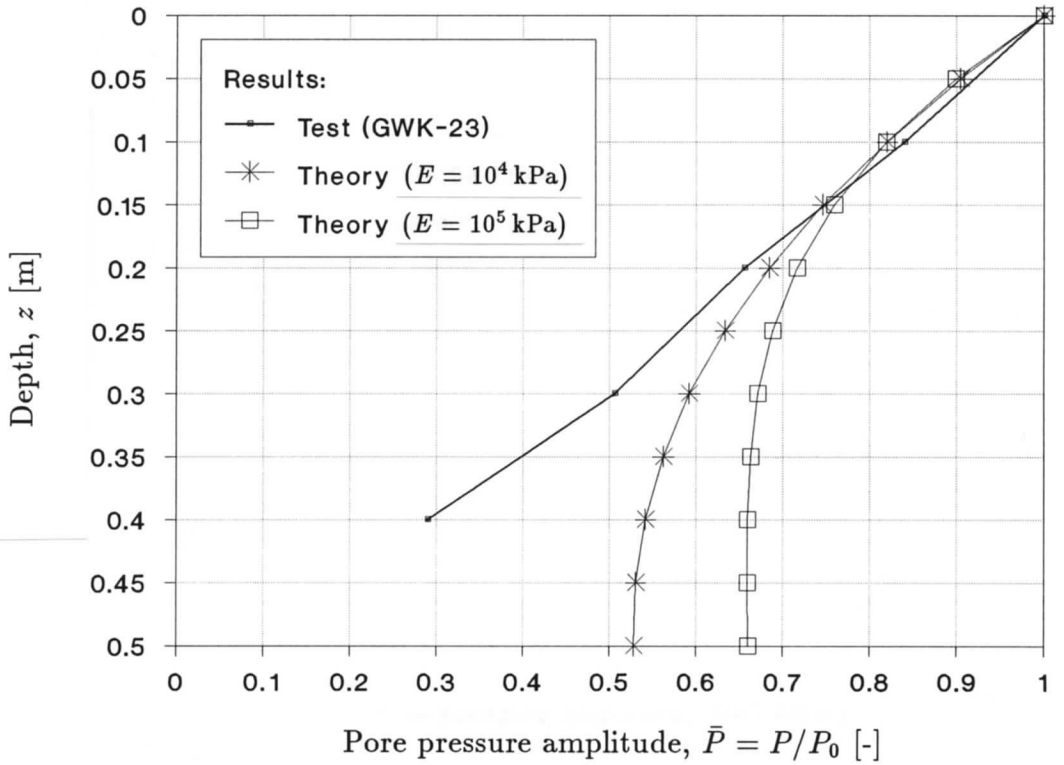

Figure 5.13 Comparison of measured (Test No. GWK-23; $H = 1.0\,\mathrm{m}$, $T = 6\,\mathrm{s}$) and calculated ($S = 0.95$) pore pressure amplitude distributions with depth

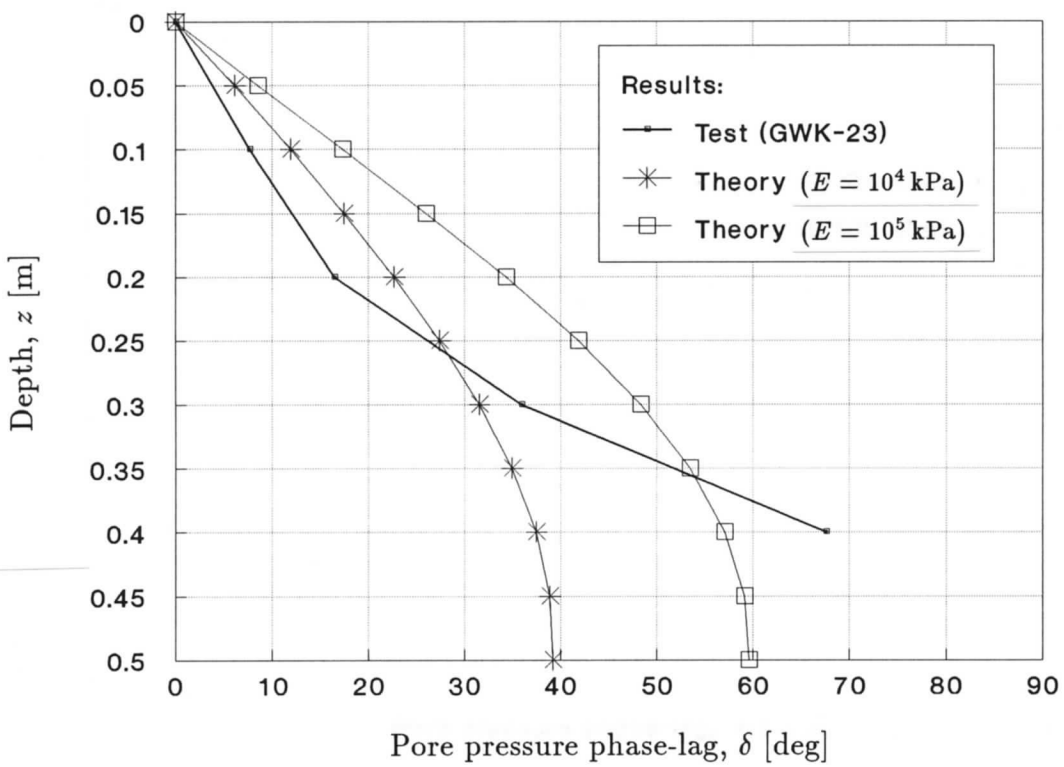

Figure 5.14 Comparison of measured (Test No. GWK-23; $H = 1.0\,\mathrm{m}$, $T = 6\,\mathrm{s}$) and calculated ($S = 0.95$) pore pressure phase-lag distributions with depth

as rather poor. The very probable reason of the obtained picture can be the fact that the soil, in the vicinity of the impermeable and stiff base of the large wave flume, is not so well-saturated as it was the case in the upper region of the sand layer. Unfortunately, inhomogeneous saturation conditions were probably reached during the saturation process where large parts of the sand model were saturated from the sand surface downwards. Even a long-term additional work of the vibrators did not bring too much help in achieving, at least, homogeneous soil saturation. However, the correctness of this explanation could be checked only when performing some additional computations based on: (1) theoretical pore pressure solution, derived for inhomogeneous soil, or (2) numerical analysis, where introduction of inhomogeneous soil paramerers is a normal procedure. In both cases, values of the degree of saturation representative for deeper parts of the sand layer have to be known. And this was unfortunately not possible to obtain in the present work.

The pore pressure measurements were, in fact, performed in two vertical profiles of the same cross-section of the large wave flume. One of them was located in the middle point and the second one in the wall-side of the cross-section. The pore pressure values measured in the wall-side profile have shown almost the same pore pressure distributions with depth as those of recorded in the central profile, indicating thereby no visible influence of the side-wall boundary condition on the course of the investigated phenomenon. This observation was a good confirmation for the two-dimensional theoretical treatment of the governing problem as a verification of the pore pressure measurements conducted in the large wave flume.

5.2 Small-scale model tests

Large-scale laboratory tests serve mainly as a qualitative investigation of a governing phenomenon. Practically, it is almost impossible to define important soil parameters with an accuracy required for mathematical and numerical modelling of the governing problem. Because homogenity of a tested seabed material can be hardly reached, soil parameters used to describe the state of the soil medium are in most cases represented by mean values computed from a wide range of values that can be found through a random sampling in different regions of the soil used for the seabed modelling. Moreover, an application of desired variations of certain soil parameters in large-scale modelling brings usually costs of laboratory investigations on a relatively very high level.

Therefore, laboratory modelling performed in a large scale, which is very convenient and favourable with respect to natural-like environmental conditions, needs usually supplementary small-scale laboratory experiments where the application of a wider range of governing paramerers and the control of them presents, in general, no difficulties and is not so much time- and cost-demanding.

Taking the above into account, the need of further investigations in order to verify the theoretical solutions is obvious. Below, a setup of small-scale laboratory experiments is presented and followed by a discussion of the results obtained from the tests (Magda, 1990[d]).

5.2.1 Test facilities and instrumentation

For the small-scale experiment, a vertical cylinder shown in Fig. 5.15 was used. The cylinder is made of transparent plexiglass and has the inside diameter $D_c = 0.2\,\text{m}$ and the height $H_c = 0.9\,\text{m}$.

A set of 16 pore-pressure transducers was mounted into the cylinder wall in its vertical profile. The type of transducers is exactly the same (*i.e.*, KS 2150 from 'Philips') like in the large-scale experiments, described in Section 5.1.1.2. The only difference consists in the design of the PVC tubular cap installed on the top of each pore pressure transducer. This time, because of the very important functional reason, the glass-filter element (used in the large-scale experiments) is replaced by a steel connector with 0.15 m long needle on the top (Fig. 5.16).

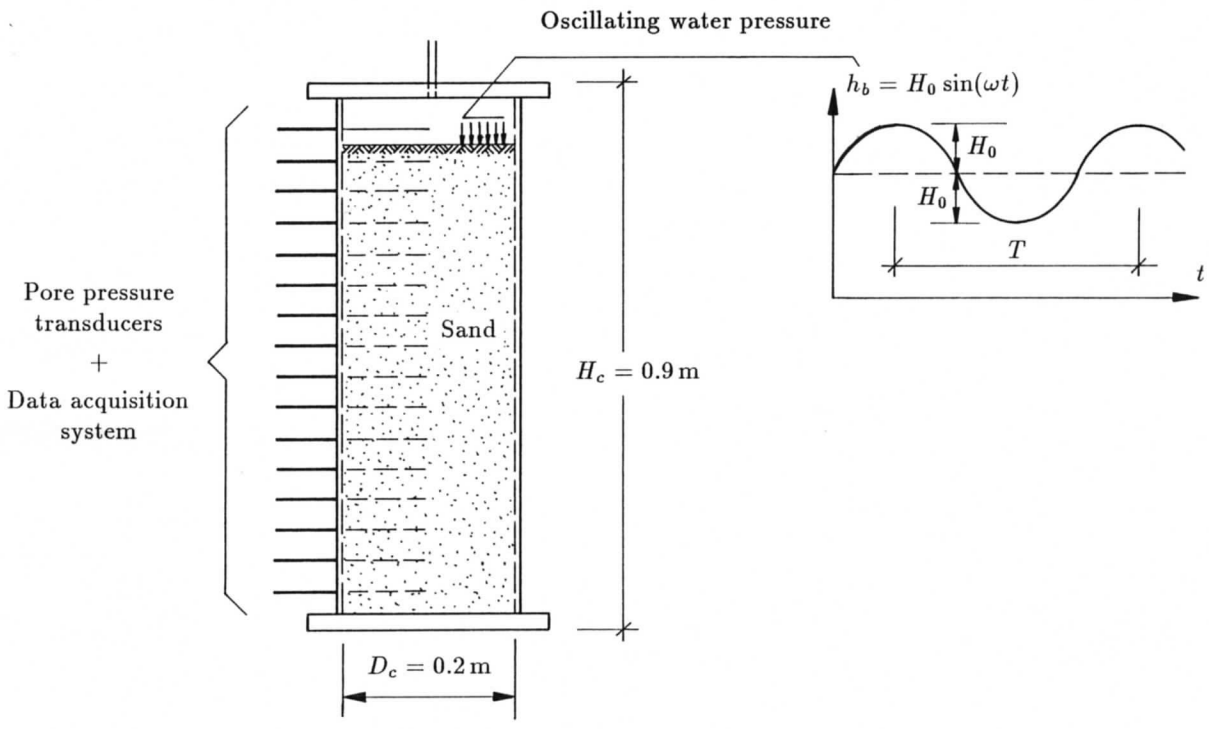

Figure 5.15 Sand-column test facilities

The needle was long enough to reach a centre point of the cylinder inside. By inserting the needle into the inside of the cylinder through a small opening furnished with a rubber tight membrane, it was possible to transmit the oscillating pore pressure through the needle to an active area of the transducer and to measure it precisely, keeping the transducer all the time outside the cylinder. An eventual installation of the transducers inside the cylinder could influence the pore pressure patern within the sand column and destroy a real picture of the soil-water interaction.

A data acquisition system (Fig. 5.17) does not differ significantly from that one used in the previously described large-scale laboratory tests. A periodically oscillating water pressure loading acts through the top of the cylinder onto the sand column surface. These pressure variations are hydraulically induced in a separate container by changing its inside volume induced by an oscillating movement of a piston. The piston is combined with an electromagnetic lifting device. The movement of the electomagnetic piston system is computer controlled, using the back coupling (feedback) principle.

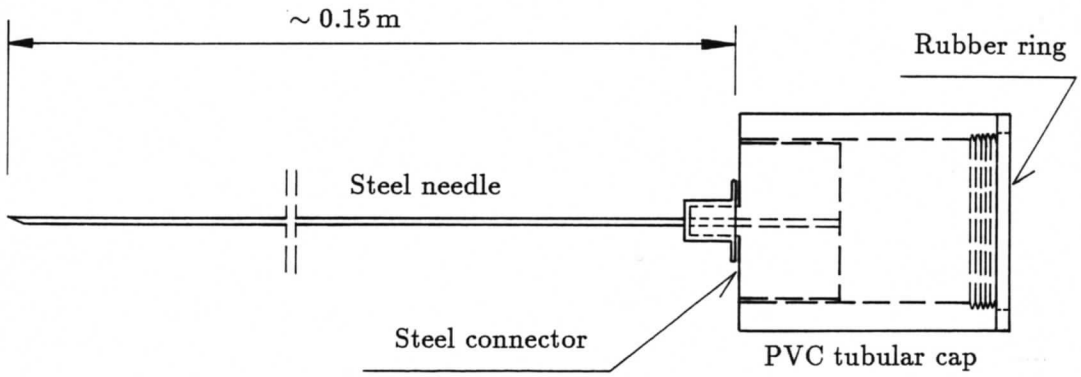

Figure 5.16 Cross-section of transducer cap with needle

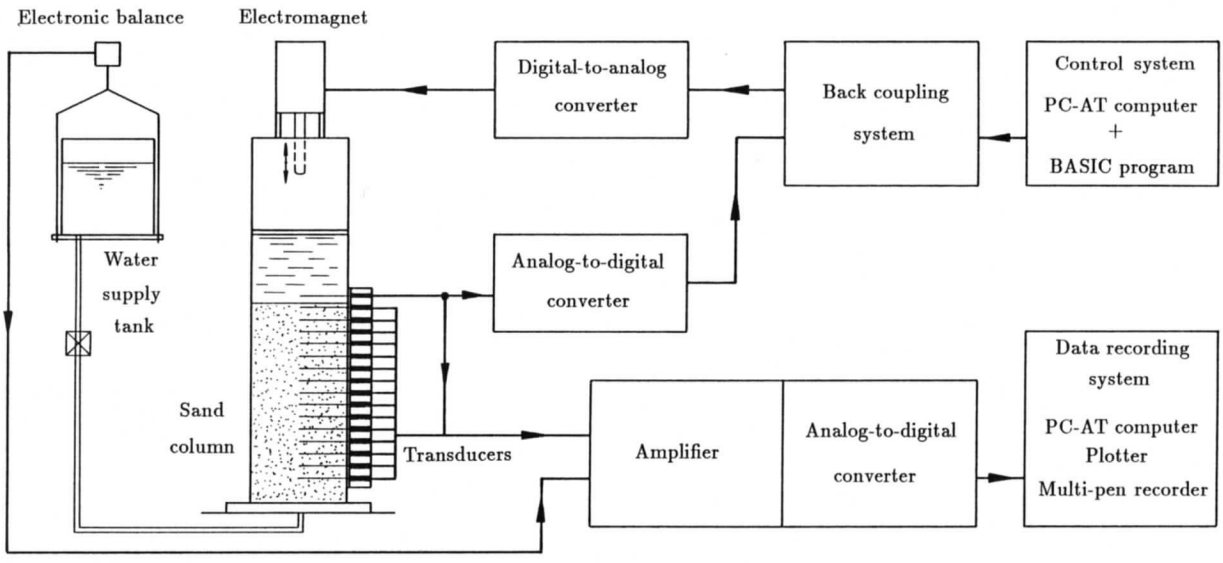

Figure 5.17 Data acquisition system for small-scale sand-column experiments

An installation of one more device was necessary for a proper test execution: this was, namely, an electronic ballance for precise measuring of the water amount (from a water supply tank) used for saturation of the sand column.

5.2.2 Sand specimen preparation

Laboratory tests, where the soil is one of the main considered medium, need special techniques of soil preparation. A type of chosen technique depends on a character of soil, soil parameters to be modelled, and a scale of tests to be performed. In most cases, a homogeneous (uniform) state of the soil is required. Performing representative series of tests, it is also necessary to assure repeatable soil conditions for all tests. Because of this fact, a reconstitution of soil specimens is estimated to be the best way in achieving test results which are going to be representative for a certain group of tests. In the case of cohesive (clayey) soils, a preparation procedure seems to be easier compared with procedures used for sandy specimens. Uniform and repeatable clayey specimens can be

obtained simply by trimming it from a natural consolidated material. However, having a cohesionless material like sand, it is impossible to follow this idea and each specimen has to be prepared individually from the sandy material in its loose state.

A scale of tests influences strongly the way of sand model preparation. Investigations performed in a small-scale (*e.g.*, triaxial tests or tests in a small container) make it possible to produce necessary densities already during sand placing into the model (Jørgensen & Steensen-Bach, 1988) (Fig. 5.18a). A huge mass of sand, used in some large-scale laboratory experiments [for instance, in a large big wave-flume (Fig. 5.18b)], can be deposited without such a great attention. However, in such case, the whole procedure would usually require additional activities in the form of compaction or even fluidization in order to assure sand uniformity and desired density (Lindenberg *et al.*, 1982).

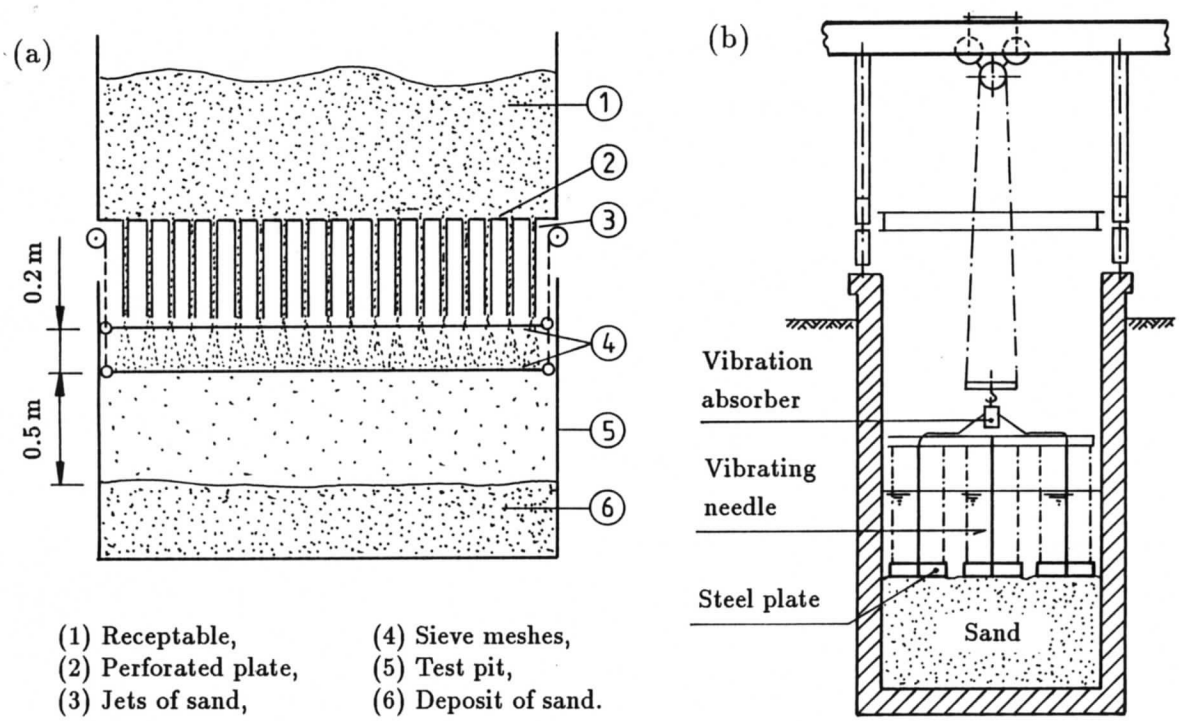

Figure 5.18 Techniques providing uniformity and certain density of sand model; (a) [Jørgensen *et al.*, 1988], (b) [Lindenberg *et al.*, 1982]

It is desired to produce homogeneous (uniform) sand samples during their artificial preparation (reconstitution) before each test run. Repeatability of an initial soil sample state can assure that results of measurements from a certain test series belong to one and the same group and can be used in averaging of results. On another hand, uniformity of sand sample is very helpful for data interpretation and comparison with theoretical approaches which are usually possible to be derived only under the assumption that the main physical parameters involved are constant and representative for the entire soil specimen.

Small-scale laboratory tests, performed in a sand column, on the pore pressure response to oscillating water loading require very careful sand specimen preparation with respect to: (1) uniformity, (2) density, and (3) saturation conditions. The way of fulfilling all of these requirements is described in the following.

5.2.2.1 Sand pouring

Uniformity of a sand sample requires not only a well-graded soil but also the sand sample preparation has to be able to create the same density within the entire sand sample. This condition can be fulfilled when applying a proper technique. A need to form an uniform sand specimen induces necessity of continuous control of sand grain package factor during the whole process of the sand model preparation. Reconstitution by pouring is the most promising technique for obtaining uniform sand samples under laboratory conditions. Sand specimens prepared by pouring, which can take place in water or in air, tend to be uniform (Vaid and Negussey, 1988).

The pouring height (*i.e.*, the height, from which the sand is dropped during pouring in air) is the main factor for obtaining samples of controlled densities. Sand pouring technique in water cannot be useful to produce different densities of sand sample but can be treated as a good tool for preparing a sand sample of a very uniform and relatively loose state regardless of the drop height.

The density of the sand specimen is controlled by the kinetic energy of sand particles at the instant of impact at deposition. It means that the impact velocity influences directly the sand specimen density. The sand grain velocity, starting from zero, can grow up to a certain limit which is called the terminal velocity. As a consequence, for the same test conditions, a certain optimum drop height exists, at which the terminal velocity is reached. Further increasing drop height will not enlarge the kinetic energy.

Apart applying a certain variation in the drop height, there is a second possibility to influence the relative density of the sand sample, namely, by controlling the sand mass flow during sand pouring.

Taking the above into account, a preliminary test programme was established in order to get a better insight into the process of modelling of sand specimen density. The influence of both different pouring heights and mass flows was investigated.

The 'Norderney Sand', taken to be investigated, has been already described in Section 5.1.1.1. Using plexiglass cylinders of different heights, it was possible to apply 10 different drop heights, from 0.2 m up to 2.0 m with a step of 0.2 m. The uniform sand particle distribution in the cross-section area of the sand sample was assured by using special PVC-sieves which also controlled the sand mass flow and kept it constant during the whole time of sand pouring. Two PVC-sieve plates of different paterns of openings layout were used. In the first sieve, 69 openings were formed, each 4 mm in diameter; in the second one, each of 69 openings had a diameter of 2.5 mm.

The results of the density tests are illustrated in Fig. 5.19. The largest difference in porosity achieved for a constant height of sand pouring and changing sand mass flow rate equals to about 0.02 with almost no respect to the method of the sand mass flow rate control. Taking into account the method of the sand mass-flow rate control, it is clear that the change in the sample porosity can be much more larger when the drop height of sand pouring varies. And thus, changing the drop height from 0.20 m to 0.80 m, the porosity decreases from 0.429 (sieve 69/4 mm) and 0.420 (sieve 69/2.5 mm) to 0.352 and 0.343, respectively. It means that the maximum difference in the porosity, obtained during the density tests, was equal to 0.077. Transforming this result into another soil parameter, it was found that the maximum relative density was about $D_r = 80\,\%$.

Finally, in order to reproduce a relatively dense state of the sand specimen, the sand pouring height of $H_p = 0.8\,\mathrm{m}$ was chosen. As shown in the theoretical consideration (see Section 4.6.3), the solution for the pore pressure is not so much dependent on the compressibility of the soil skeleton in the case of dense and very dense states of the soil. Nevertheless, the assumption of high densities enables to make another assumption

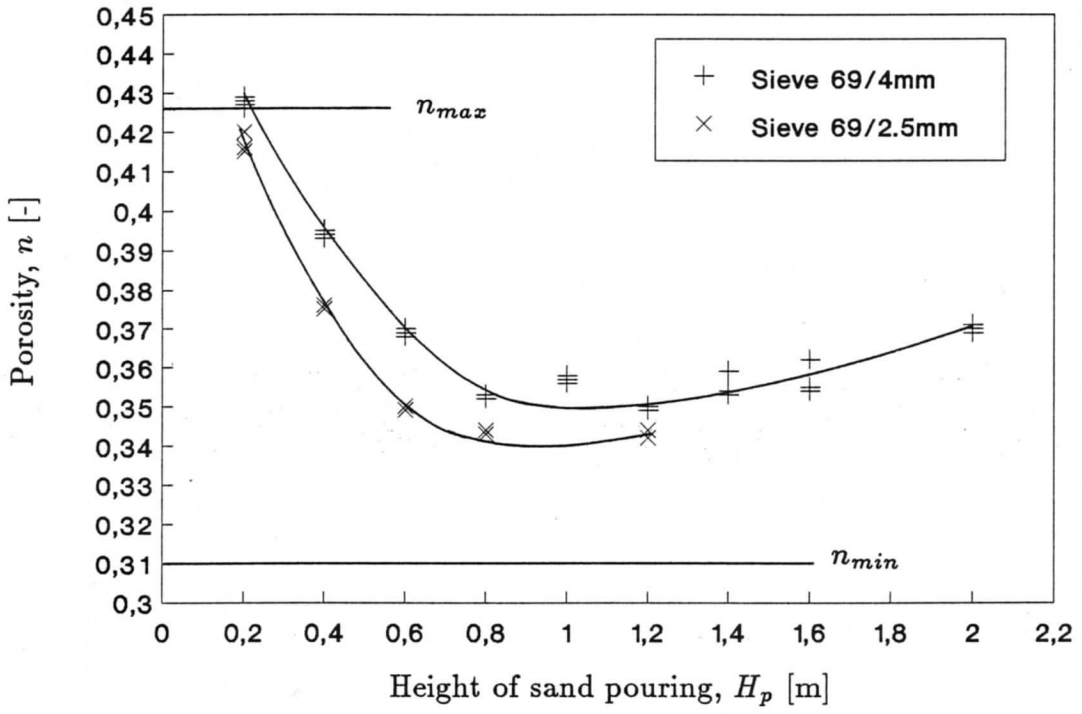

Figure 5.19 Influence of the drop height on sand specimen porosity

concerning a relatively low and constant value of the soil skeleton compressibility for all types of sand.

Four different types of sand were used to form the soil specimen. The characteristic parameters of each sand are put together in Tab. 5.1.

Table 5.1
Soil parameters of different types of sand used in small-scale experiments

Soil parameter		Type of sand		
		'Norderney'	G30T	S40
d_{50}	[mm]	0.23	0.42	0.70
C_U	[-]	1.61	2.00	1.67
C_C	[-]	1.03	1.10	1.07
n_{min}	[-]	0.32	0.32	0.32
n_{max}	[-]	0.43	0.42	0.41
k	[m/s]	1.3×10^{-4}	3.2×10^{-4}	6.2×10^{-4}

The parameters included in Tab. 5.1 have the following meaning:

d_{50} – specified particle size [mm],
C_U – coefficient of uniformity [-],
C_C – coefficient of curvature [-],
n_{min} – minimum porosity [-],

n_{max} – maximum porosity [-],
k – coefficient of permeability [m/s].

The permeability coefficient was measured under the dense state conditions of the soil.

5.2.2.2 Saturation

Jacobsen & Magda (1988) and Magda (1989$^{(b)}$) made some observations of the effectiveness of certain saturation techniques used in small-scale laboratory tests pertained to the problem of the sea bottom erosion potential influenced by the pore pressure vertical gradient and the sea current action. Three main methods of soil saturation were tested in order to obtain the degree of saturation as high as possible, and the effects of their application were discussed.

Searching for the most effective method of saturation, the following three techniques can be distinguish, namely:

- vacuum saturation,
- gravitational saturation,
- capillary saturation.

The common feature of all of these types of saturation was the same direction, in which the saturation took place. Saturation of the sand model was carried out always from the model bottom upwards. This condition enabled an easier monitoring of the rate, at which saturation occured to be fairly uniform in the whole horizontal cross-section of the sand specimen. Pore water pulled down gravitationally and randomly would form large spatial areas (air traps). In the case of smaller volumes, the air traps would remain entrapped in sand pores, decreasing thereby the degree of saturation significantly, whereas – in the case of larger volumes – the air traps would damage the carefully prepared structure of the soil specimen because they would tend to be released out from the soil model.

The principle of operation of the vacuum saturation system requires a continuous vacuum condition in the whole volume of the soil model (a vacuum-pump is connected to the top of the model) when supplying water from the bottom of the sand model.

Omitting the element of the vacuum suction force, the first system can be easily converted into the gravitational saturation system. The rate of saturation process can be controlled by applying a proper water pressure gradient. Magda (1989$^{(b)}$) showed that both very slow and very fast rate of saturation resulted in lower values of the degree of saturation compared with the results from saturation performed at a medium rate. Moreover, the fast rate of saturation enables easily trapping of air bubbles in the soil pores which was indicated by air bubbles self-releasing from the inside of saturated soil onto the sandy model surface.

The third technique, *i.e.* capillary saturation, is based on the principle of the capillary force suction. Applying this method, however, relatively low values of the degree of saturation were obtained. This was not very surprising since the capillary saturation method is only slightly different from the gravitational saturation at a slow rate. The trapping effect for air bubbles in the soil skeleton pores may be explained as follows. The capillary forces help to moisten surfaces of soil grains just above the bottom of the capillary water meniscus. Then, a certain moment can occur when the surfaces of all soil grains grouped around a single pore are already moistened but still

there is a meniscus in the soil pore. In this way a trap for the air above the pore water meniscus is formed.

The gravitational saturation at slow rate gave results comparable with the gravitational saturation at fast rate. However, the obtained values were worse than in the case of the gravitational saturation at medium rate where the highest value of the degree of saturation was about $S = 0.95$. It means that the optimum rate of saturation exists. The worst results ($S = 0.85$) came from the capillary saturation [Magda ($1989^{(b)}$)].

Modelling of different soil saturation conditions was concentrated on preparation of three qualitatively different saturation conditions of the sand model, namely: fully saturated ($S = 1$), and partly saturated ($S < 1$) with relatively high and low values of the degree of saturation. Near-fully saturated soil conditions were possible to create using sand pouring in water together with additional manual stiring and vibrating. Such procedure resulted in extremely high value of the degree of saturation ($S \cong 1.0$). Using sand pouring in air (drop height of $H_t = 0.8$ m was applied) followed by the gravitational saturation from the model bottom upwards, saturation conditions were obtained in the range of $S = 0.96 - 0.99$. Additionally, very poor saturation conditions were artificially forced by means of dewatering of already saturated sand model (ground water level was lowered) and saturating it again. Considering the effects of water flow through a wet soil (see Section 3.1.2), relatively small values of the degree of saturation were expected. In fact, the measured degree of saturation was equal to $S = 0.83$, which was enough to distinguish a clear difference in soil saturation conditions from the above mentioned first two representative states. It has to be stressed that the obtained low values of the degree of saturation were still in the range of application of the assumed relationship [see Eq. (3.39)] between the degree of saturation and the compressibility of pore fluid.

5.2.3 Test procedure

Before each test the sand was dried and weighted. During the sand pouring process, a very dense state of the soil specimen was achieved in all tests (*i.e.*, relative density $D_r \cong 0.8$, or porosity $n \cong n_{min}$). Water used for saturation was boiled beforehand. Deaerating frees off to a large extent the water from air particles, normally contained in it. Saturation of the model was carried out from the bottom upwards. This ensured easier monitoring of the rate at which saturation occured to be fairly uniform in the whole horizontal cross-section of the model. In the case of an opposite direction of saturation, this would be practically impossible; pore water pulled down gravitionally and randomly would form air spaces which, in the case of smaller volumes, would remain trapped in the soil skeleton, lowering significantly the degree of saturation. Larger volumes of air could additionally damage carefully prepared soil body because they would tend to go out from the saturated model.

The free gravitational saturation was used to saturate the model. A constant medium rate of upward saturation was controlled by a positive water pressure gradient, which value was kept constant and equal to 0.2 m of water height. The intention was to obtain the degree of saturation as high as possible. Magda ($1989^{(b)}$) showed that both very slow (*e.g.*, free capillary saturation) and very fast saturation result in lower values of the degree of saturation when comparing it with saturation conducted at a medium rate.

Knowing the amount of water, used for the sand-column model saturation, and the density of soil skeleton, it was possible to compute the degree of saturation. The

relative small height of the sand-column model ($H_c = 0.8\,\mathrm{m}$), together with a careful and very precise performance of preparation and saturation of the sand model, allowed to believe to obtain homogeneous soil saturation conditions, which was not the case in the large-scale laboratory experiments described in Section 5.1.

Two different periods of water pressure oscillation were applied, namely: $T = 1$ and $2\,\mathrm{s}$. The head of hydrostatic water pressure above the sand surface was kept constant $h = 1.2\,\mathrm{m}$, and the amplitude of the bottom water pressure head oscillations was equaled to $H_0 = 0.4\,\mathrm{m}$.

5.2.4 Results of measurements and comparison with the 'finite-thickness-layer' solution

The results of measurements, performed in the sand column model (Magda, 1990[d]), are presented in a graphical form in Figs. 5.20 to 5.29. Besides of the presentation of the data measured, each figure contains the results of numerical computations according to the one-dimensional pore pressure storage solution described in Section 4.6. As input data for calculations, the values of the coefficient of soil permeability for the three different types of sand (Tab. 5.1), tested in the small-scale laboratory experiments, were taken. Other geometric and physical parameters, required by the computational procedure, were assumed to have the following values:

- height of sand column $d = 0.5\,\mathrm{m}$ $(d = H_c)$
- porosity of soil filled with water $n_w = 0.35$
- Poisson's ratio of soil $\nu = 0.3$
- compressibility of soil $\alpha_z = 10^{-5}\,\mathrm{m^2/kN}$
- compressibility of pure water $\beta = 4.2 \times 10^{-7}\,\mathrm{m^2/kN}$
- atmospheric pressure $p_{at} = 101.325\,\mathrm{kPa}$
- wave period $T = 1;\,2\,\mathrm{s}$
- water depth $h = 1.2\,\mathrm{m}$
- amplitude of bottom pressure $H_0 = 0.4\,\mathrm{m}$

Similar to the analysis of the data recorded in the large-scale modelling of the governing problem, the pore pressure signals measured in the sand column tests were analysed using the Fast Fourier Transform (FFT). The main results of the analysis are given in terms of the relative amplitude, $\bar{H}$, and the phase lag, δ, of pore pressure head oscillations in the sand column.

The first group of results is related to the tests performed on the 'Norderney Sand'. Figures 5.20 and 5.21 present results for the pore pressure amplitude and the phase lag, respectively, from the test where the degree of saturation was measured to be $S = 0.989$, which is – according to Eq. (3.8) – adequate to the soil porosity part occupied by air $n_a = 0.00385$. Next two respective illustrations, Figs. 5.22 and 5.23, show a situation where the same type of sand had worse saturation conditions, *i.e.* $S = 0.969$ $(n_a = 0.01085)$, compared with the former test. A two-percent-difference in the degree of saturation creates very well-distinguished differences in the pore pressure response in sandy sediments. These differences are in a good accordance with the values predicted by the 1-D numerical solution to the storage model of the pore pressure response in sandy sediments.

Next four illustrations, Figs. 5.24 to 5.27, present the results of tests performed on the sand S40, and they are used to present mainly the following two effects in the pore

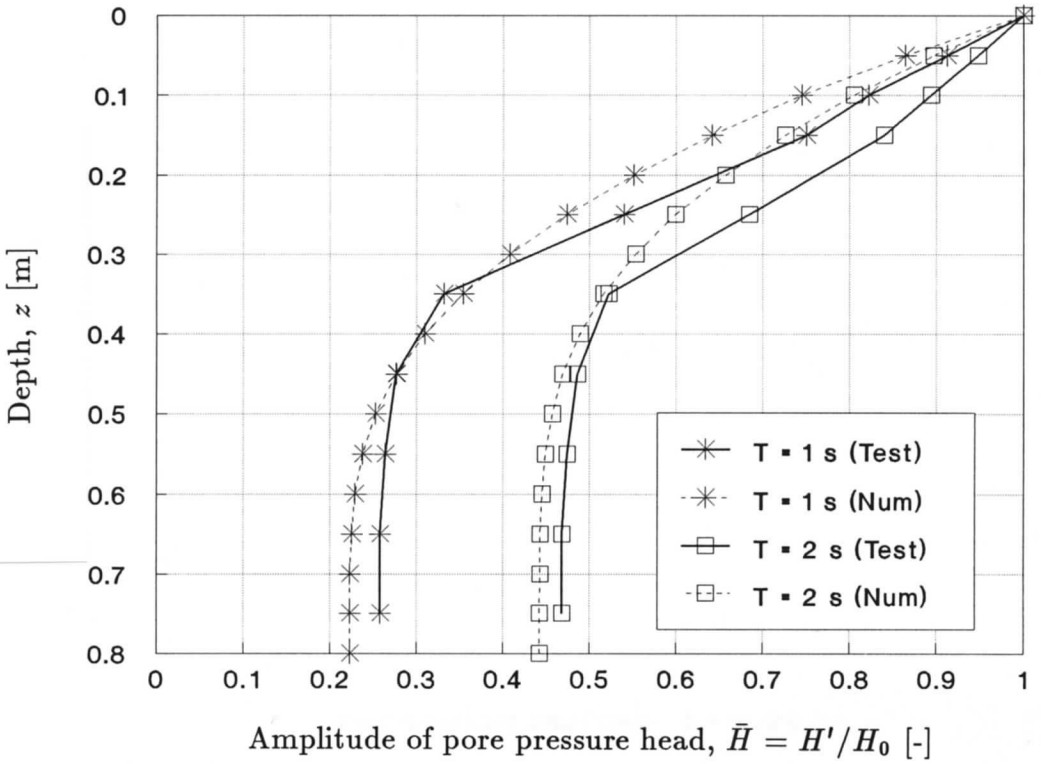

Figure 5.20 Distribution of the amplitude of pore pressure head with depth in the sand column; measurement (Test) versus numerical solution (Num) to 1-D storage problem [Sand: 'Norderney', saturation $S = 0.989$]

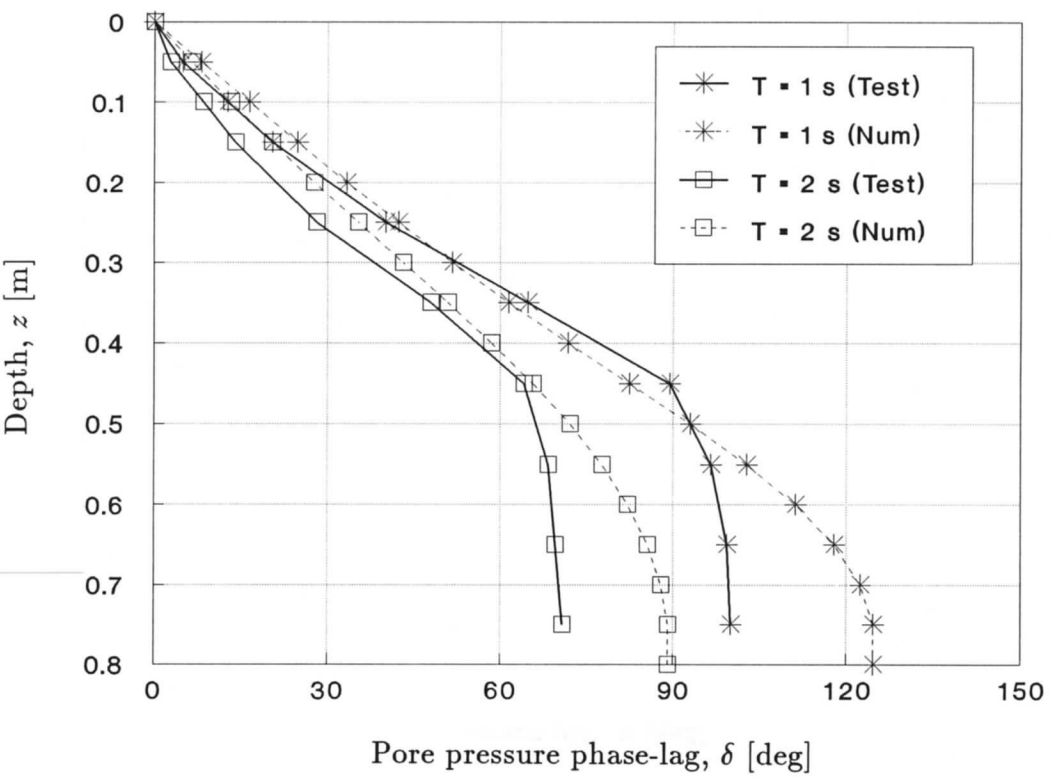

Figure 5.21 Distribution of the pore pressure phase-lag with depth in the sand column; measurement (Test) versus numerical solution (Num) to 1-D storage problem [Sand: 'Norderney', saturation $S = 0.989$]

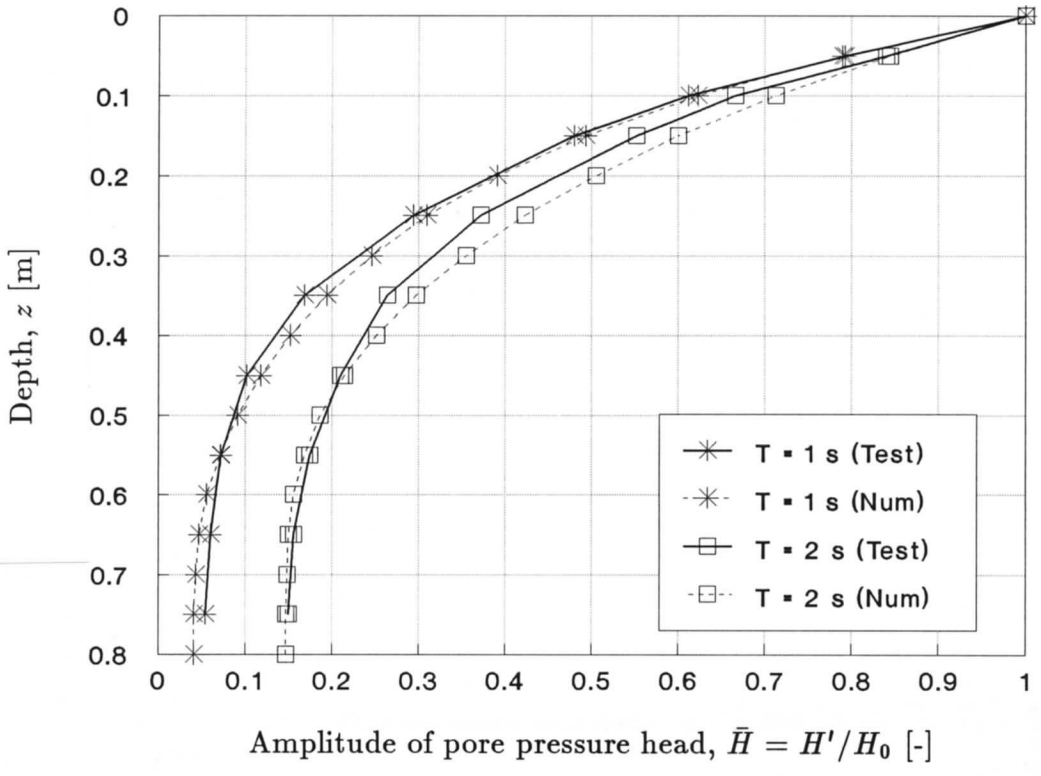

Figure 5.22 Distribution of the amplitude of pore pressure head with depth in the sand column; measurement (Test) versus numerical solution (Num) to 1-D storage problem [Sand 'Norderney', $S = 0.969$]

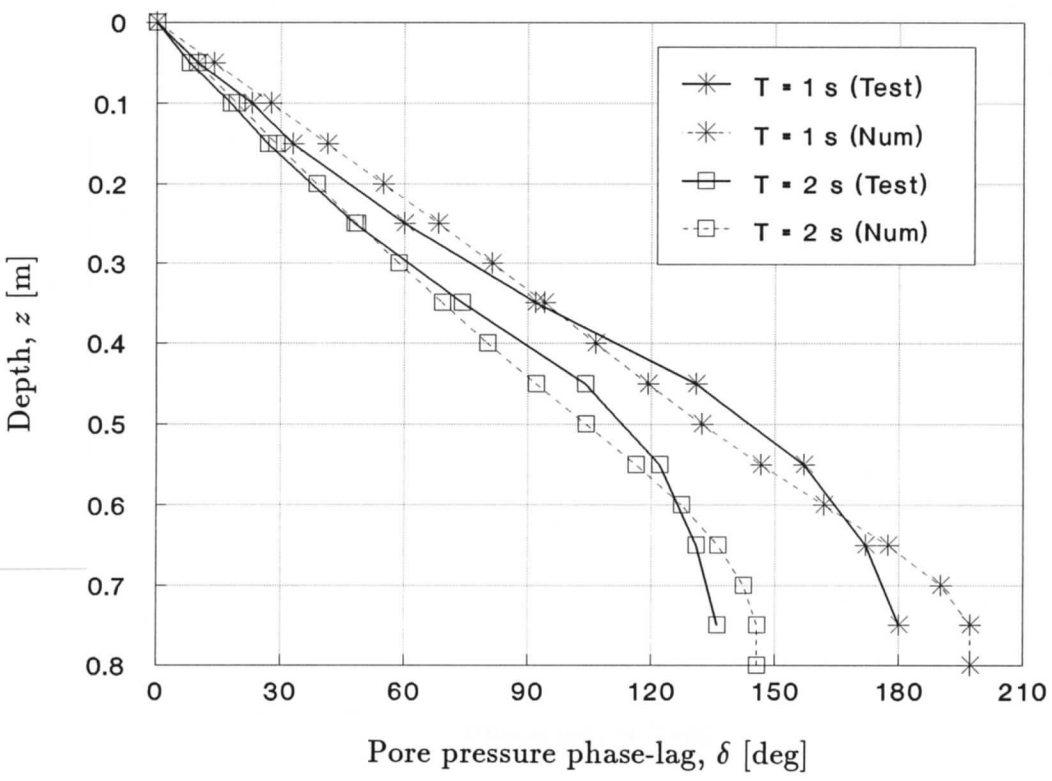

Figure 5.23 Distribution of the pore pressure phase-lag with depth in the sand column; measurement (Test) versus numerical solution (Num) to 1-D storage problem [Sand 'Norderney', $S = 0.969$]

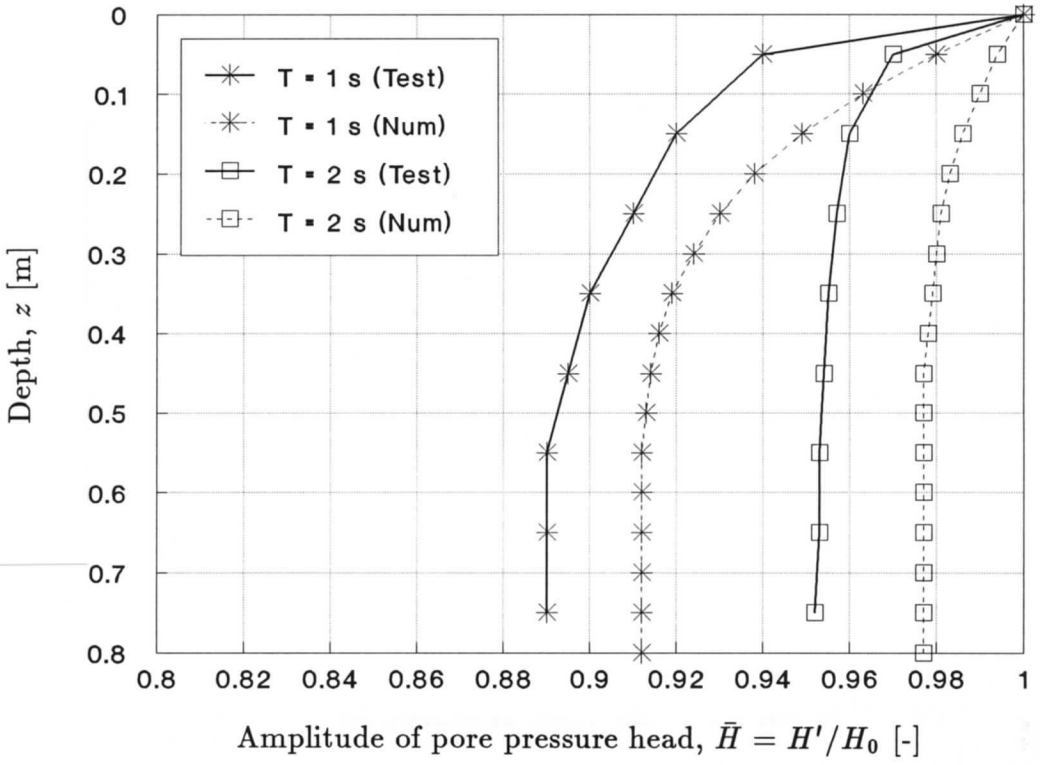

Figure 5.24 Distribution of the amplitude of pore pressure head with depth in the sand column; measurement (Test) versus numerical solution (Num) to 1-D storage problem [Sand S40, $S = 0.994$]

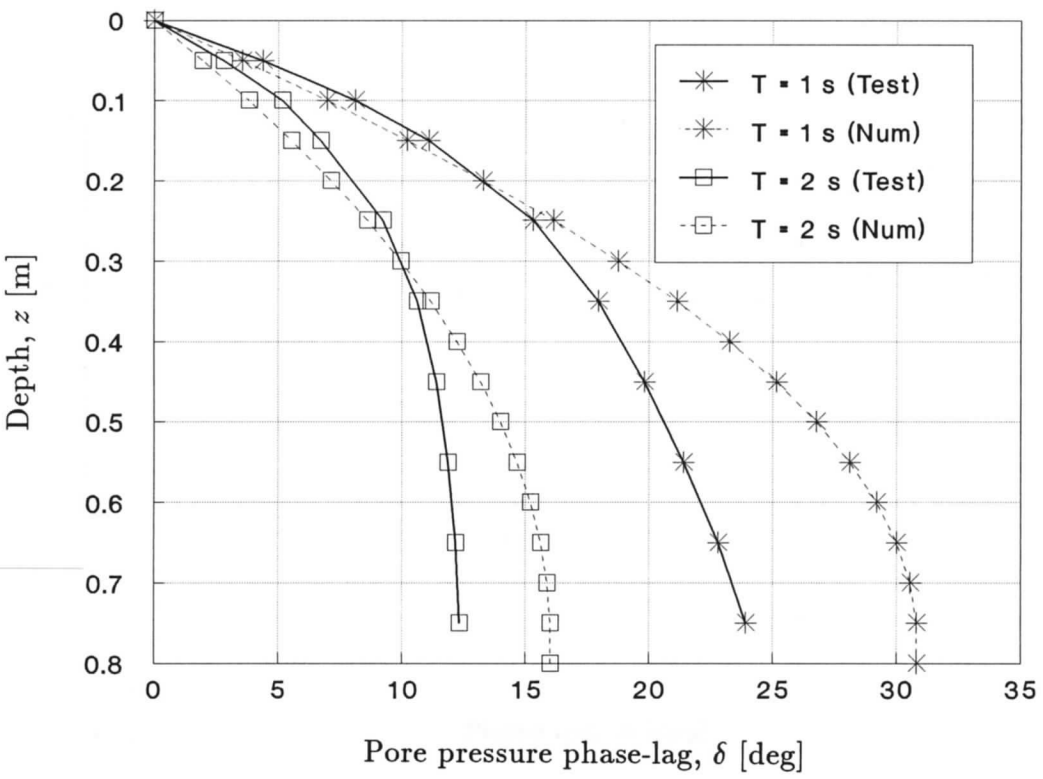

Figure 5.25 Distribution of the pore pressure phase-lag with depth in the sand column; measurement (Test) versus numerical solution (Num) to 1-D storage problem [Sand S40, $S = 0.994$]

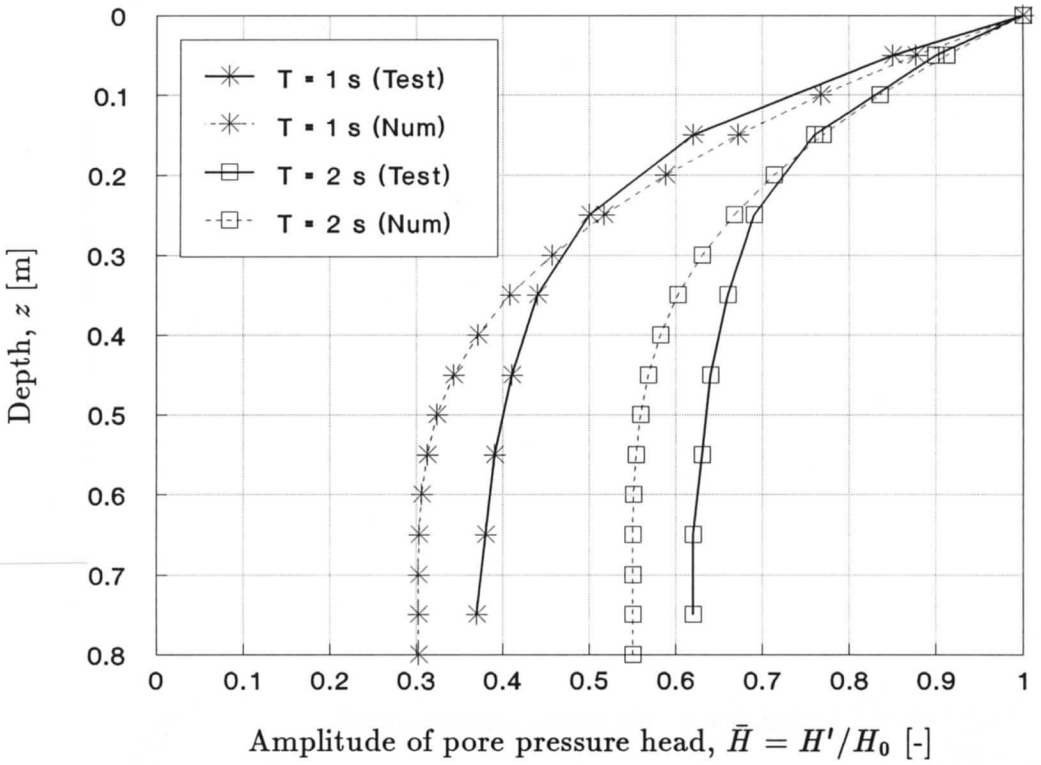

Figure 5.26 Distribution of the amplitude of pore pressure head with depth in the sand column; measurement (Test) versus numerical solution (Num) to 1-D storage problem [Sand S40, $S = 0.960$]

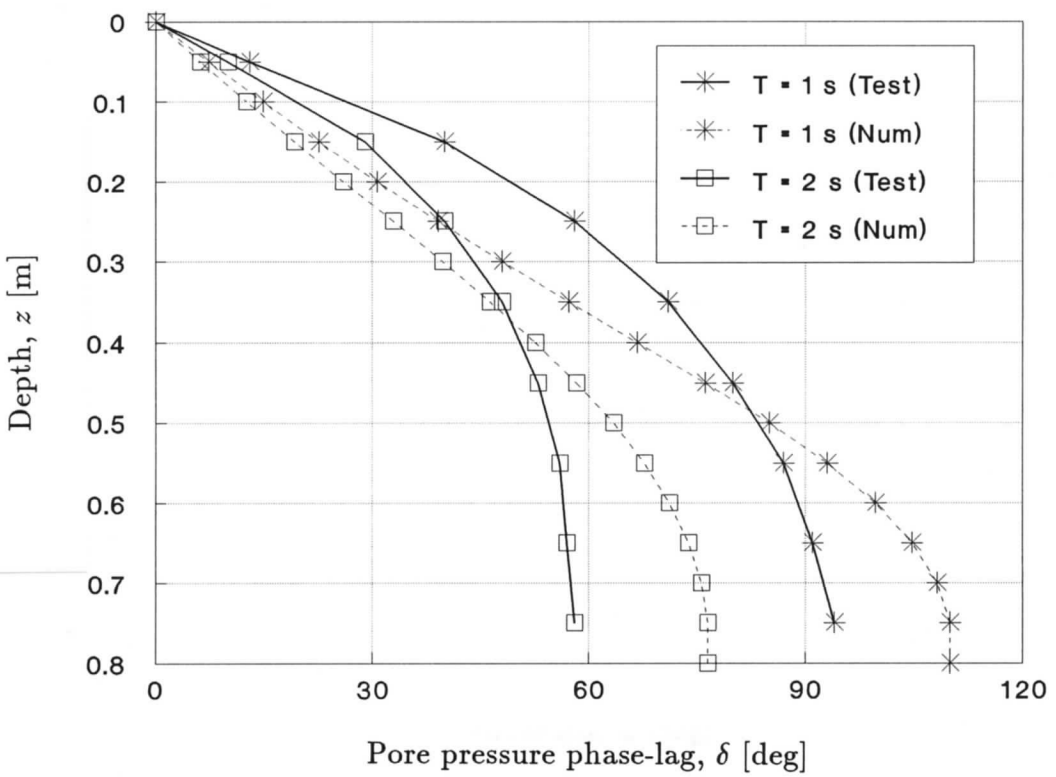

Figure 5.27 Distribution of the pore pressure phase-lag with depth in the sand column; measurement (Test) versus numerical solution (Num) to 1-D storage problem [Sand S40, $S = 0.960$]

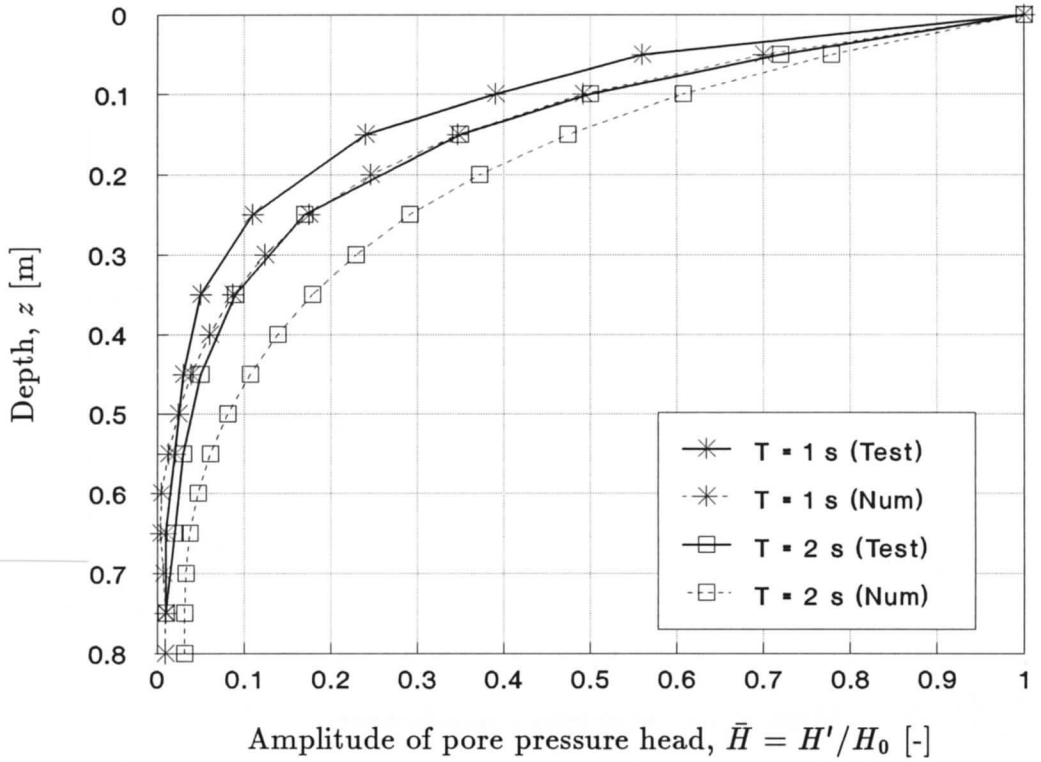

Figure 5.28 Distribution of the amplitude of pore pressure head with depth in the sand column; measurement (Test) versus numerical solution (Num) to 1-D storage problem [Sand G30T, $S = 0.830$]

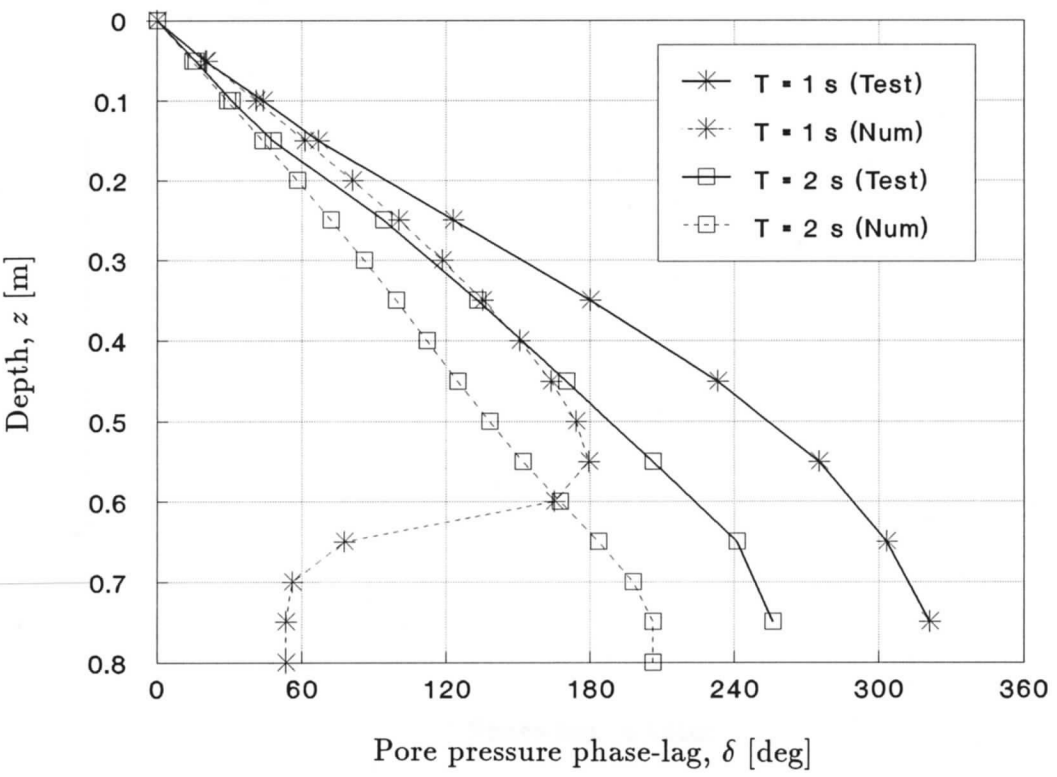

Figure 5.29 Distribution of the pore pressure phase-lag with depth in the sand column; measurement (Test) versus numerical solution (Num) to 1-D storage problem [Sand G30T, $S = 0.830$]

pressure distribution, namely: the difference between partly saturated and near-fully saturated soil, and the difference influenced by changes in soil permeability. Figures 5.24 and 5.25 identify results for near-fully saturated soil, $S = 0.994$ ($n_a = 0.00210$). This very high value of the degree of saturation (*i.e.*, $S = 0.994$) was possible to be obtained through applying a very careful sand pouring in water with a simultaneously executed manual vibration of the sand model. Figures 5.26 and 5.27 pertain to partly saturated soil, $S = 0.960$ ($n_a = 0.01400$). A good agreement between the 1-D numerical storage solution and the experimental measurements has been obtained here, too. Secondly, a comparison of Figs. 5.24 to 5.27 with Figs. 5.20 to 5.23, respectively, confirms the anticipated behaviour in the pore pressure damping effects, although – under almost the same soil saturation conditions – the difference in soil permeability of the two soil specimens was quite meaningful and had a factor of 5. The smaller permeability the soil has, the higher pore pressure damping effects in the soil are observed.

Finally, a special situation was arranged where soil saturation conditions were very poor, *i.e.* $S = 0.830$ ($n_a = 0.05950$). Performing tests on the sand G30T, this low value of the degree of saturation was achieved by dewatering already saturated specimen followed by a repeated saturation procedur. The both numerical and experimental results, presented in Figs. 4.28 and 4.29, show a similar tendency to that observed in the former test, however, they are not so much coherent to each other as it was in the tests higher values of the degree of saturation. Probably, a real value of the compressibility of such a system does not stay in accordance with that one predicted theoretically. It has to be remembered that, for partly saturated soils, the compressibility relationship used in the theoretical/numerical considerations is limited by the degree of saturation equal to $S \cong 0.85$ (Verruijt, 1969).

Higher periods (*e.g.*, $T = 2$ s versus $T = 1$ s) of water surface vertical oscillations, or hydrodynamic bottom pressure oscillations, cause higher rates of pore pressure damping effects which is clearly seen in smaller values of the pore pressure amplitude accompanied by larger values of the pore pressure phase-lag.

No influence of application of different values of the amplitude of water surface vertical oscillations (hydrodynamic bottom pressure head oscillations) on the pore pressure distribution with depth in the sand column was observed. As far as the amplitude of pore pressure head oscillations is concerned, there is a linear dependency between the magnitude of the inducing water pressure, acting on the top surface of the sand column, and the magnitude of pore pressure head oscillations in the soil. Presenting this relationship in the relative and dimensionless form, $\bar{H}$ [see Eq. (4.62b)], with respect to the amplitude of the hydrodynamic bottom pressure head, H_b, this linear dependency disappears and all the distribution curves obtained for different values of the amplitude of the hydrodynamic bottom pressure head – keeping all other pore fluid and soil skeleton parameters the same – are described only by one and the same curve.

5.3 Conclusions

The large-scale tests performed in the large wave flume, and the small-scale laboratory experiments conducted in the sand column, have indicated the following:

- the pore pressure damping effects in sandy seabed sediments:
  - the pore pressure amplitude attenuation with depth,
  - the increase of the pore pressure phase-lag with depth,

- the dependency of the pore pressure damping effects in sandy seabed sediments on:
  - soil saturation conditions (defined by the degree of saturation),
  - compressibility of soil skeleton (defined by Young's modulus),
  - soil filtration conditions (defined by the coefficient of filtration),
  - frequency (or period) of water loading oscillations, induced either by surface water waves propagating over the seabed, or by water surface vertical cyclic fluctuations,
- a good agreement between the experimental and theoretical (Airy's linear wave theory) results of the hydrodynamic bottom pressure induced at the seabed floor,
- a good agreement between the results obtained from the measurements and the analytical (2-D model) and numerical (1-D model) 'finite-thickness layer' storage solutions for the pore pressure oscillations in sandy seabed sediments,
- no influence of the wave-flume sidewall, as a natural boundary condition, on the pore pressure oscillations, compared to the pore pressure values recorded in the central-positioned measuring profile.

The large-scale modelling of the pore pressure response in sandy seabed sediments have shown that the calculated values overestimate the measured pore pressure damping effects, showing smaller amplitudes and larger phase lags in the upper region of the seabed models, whereas the oposite relation was found in the lower part of the seabed model. This fact has been also found in the sand column test, when the same type of sand (*i.e.*, 'Norderney Sand') was used. The observed phenomenon can be probably explained by the existance of inhomogeneous conditions of the seabed model, with respect mainly to:

- compressibility of the soil skeleton,
- compressibility of the pore fluid,
- coefficient of filtration.

Lower densities in the upper part of the seabed sediment, compared with deeper regions, were caused mainly due to water particle motions induced by surface water wave propagating oscillations (large-scale modelling) or water surface vertical oscillations (small-scale sand column test). A lower density, which means a looser state of the soil, implies certainly higher values of compressibility of the soil skeleton. Therefore, the soil skeleton, reacting like a sponge, contributes to easier transmission of pore pressure oscillations in seabed sediments. On the other hand, logically, lower parts of the seabed layer were characterized by higher densities, having thereby more restrictive influences on the pore pressure damping effects. This conclusion is based on the observation, indicating smaller values of the measured pore pressure damping effects in the upper part than in the lower part, compared to the analytical storage solution.

Because of a very difficult procedure of preparation and saturation of the seabed model in the large wave flume, a certain doubt exists concerning the homogenity of soil saturation, too. It was very probable that the lower parts of the sand layer had poor saturation conditions compared with the upper regions. This was certified by even stronger rate of the pore pressure damping in the vicinity of impermeable base of the wave flume than closer to the seabed floor.

The pore pressure storage solution, derived analytically in Section 4.4, is capable to treat the soil skeleton and the pore fluid as media, which are, among others, homogeneous from the compressibility point of view. This is a small disadventageous feature of the analytical solution when applying it to the problems where the relative compressibility of the two-phase seabed medium is certainly a function of depth in the seabed.

This problem can be easily overcome by adapting the derived analytical solution into a multi-layered system, introducing additional interface boundary conditions. However, a number of mathematical operations will increase substantially with respect to the solution derived and analysed in the present work.

The comparison analysis, performed for the sand column modelling, has indicated a good agreement between the numerically computed and experimentally measured values of both the pore pressure amplitude and the pore pressure phase-lag. The use of relatively more precise measurements of the degree of saturation has proved the correctness of the theoretical/numerical formulation of the governing problem, as long as soil saturation conditions stay in accordance with Verruijt's (1969) range of application of the formula describing the pore fluid compressibility. Not only soil saturation conditions precisely defined, but also high densities carefully modelled during the sand column test preparation have helped to achieve possibly uniform saturation/copressibility conditions in the total height of the sand column model. This was a very crucial point for having more satisfactory comparison between the experimental and numerical pore pressure results, compared with the large-scale modelling.

Chapter 6

Wave-induced uplift force on a submarine buried pipeline – example application of the pore pressure storage model

Submarine pipelines buried in seabed sediments are engineering means of transport for crude oil and natural gas from offshore oil fields onto a land. Generally, problems associated with a design of submarine pipelines buried in seabed sediments depend strongly on soil-water/wave conditions. A wave climate plays a very important role and can influence the interaction between a submarine buried pipeline and the surrounding soil significantly. In practice, pipelines located in water depths up to 60 m are buried, whilst the cover must have a thickness ranging from 0.5 to 1.0 m, depending upon the water depth and the covering material (Dursthoff & Mazurkiewicz, 1985).

Among all considered environmental loads usually taken into account in the design procedure, the most critical problem in determining the stability of a pipeline buried in permeable soils under surface water wave loading is the prediction of the wave-induced pore pressure response of the soil in the vicinity of a submarine pipeline. The main object of Chapter 6 is to present a study of the distribution patern of the wave-induced pore pressure acting on a submarine pipeline, and to calculate the seepage force, the hydrodynamic uplift force particularly, affecting the pipeline under the assumption of the storage seabed model (*i.e.*, compressible pore fluid and soil skeleton), for the case of an arbitrary thickness of a permeable seabed layer.

Wind waves are accompanied by the movement of water particles within the whole mass of water. In spite of the permanently existing hydrostatic pressure, a value of which depends only on the water depth, this phenomenon generates additionally an oscillating water pressure on the seabed floor. This pressure, because of its character and the place of existence, is called the wave-induced bottom pressure or the hydrodynamic bottom pressure.

A character of the bottom pressure depends on the type of waves assumed for the analysis. If the waves are regular, the wave-induced bottom pressure fluctuations follow the cyclic surface water wave oscillations, having a frequency equal to the wave frequency. If the waves considered in the analysis are irregular then the bottom pressure

changes will be characterized by the stochastic process. Usually, when a certain problem is going to be solved analytically, a regular (sinusoidal in most cases) type of surface water waves is chosen for the convenience of required mathematical operations. If random (*i.e.*, irregular) surface water waves are considered, the use of the Fast Fourier Transform (FFT) makes it also possible to adapt a solution to a particular problem derived for sinusoidal water waves loading. It is also the case in the present analysis where the wave-induced uplift force acting on a submarine pipeline buried in seabed sediments is studied under the assumption of sinusoidal surface water waves propagating over the permeable seabed.

The hydrodynamic bottom pressure, p_b, and its amplitude, P_0, can be computed directly from Eq. (2.6) and Eq. (2.7), respectively, for the subsurface pressure under a progressive wave, derived from Airy's linear theory for waves of small amplitudes. The comparison with values obtained from the laboratory measurements (see Section 5.1) has shown that this theory is capable to predict the bottom pressure reasonably good.

Considering a porous permeable seabed (*e.g.*, consisted of sandy sediments), the bottom pressure fluctuations will have direct and continuous influence on changes in pore pressure within the seabed medium (Fig. 6.1). An overpressure (with respect to the initial hydrostatic pressure distribution defined by the still water level) generated in the soil due to a passage of a wave crest, creates seepage forces acting downwards. Contrary to that, an underpressure induced by a passage of a wave trough is responsible for seepage forces directed upwards.

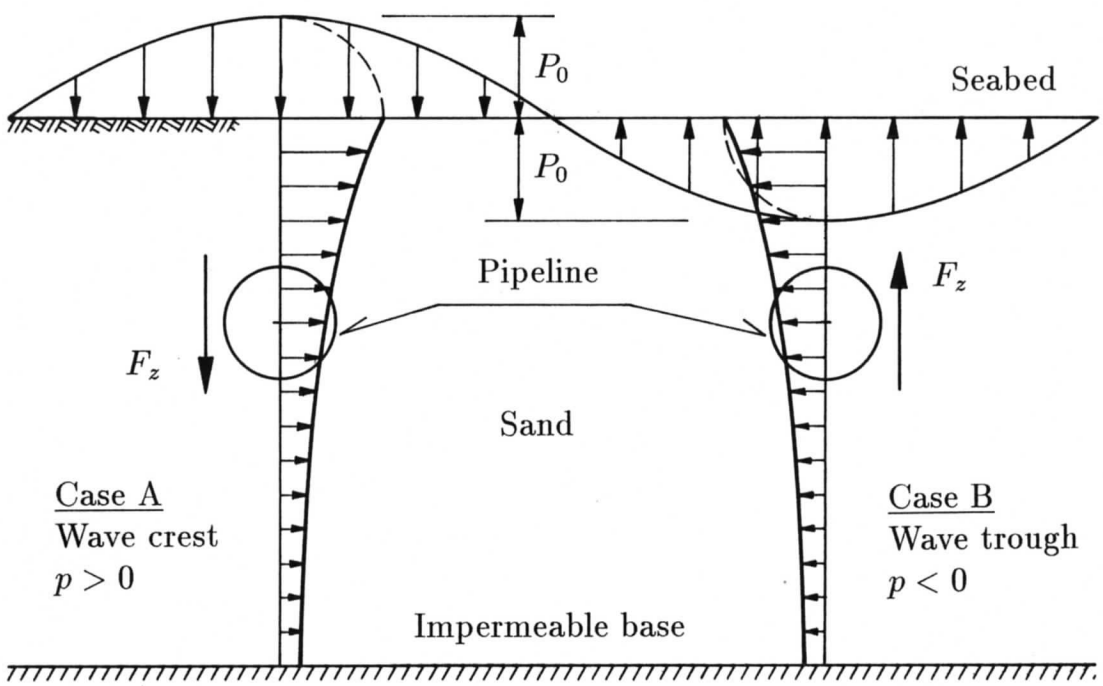

Figure 6.1 Wave-induced pore pressure distributions under two characteristic phases (*i.e.*, wave crest and wave trough) of surface water wave oscillations, and vertical forces acting on a submarine pipeline buried in sandy seabed sediments

6.1 Hydrodynamic uplift force

Should one assume an existence of a submarine pipeline buried in a seabed, this pipeline will be exposed to the seepage forces induced in seabed sediments due to a passage of surface water waves. The resultant force, being the effect of all seepage forces acting on a submarine pipeline, has a magnitude and a direction alternating cyclically with the same frequency as the frequency of surface water wave oscillations. In each moment of wave oscillations it is possible to compute a vertical component of the resultant hydrodynamic force, and to distinguish two special cases thereof, namely: a vertical force acting downwards, trying to suck the pipeline out of the seabed, and a vertical force acting upwards, pressing the pipeline down (see Fig. 6.1).

The second case can only be dangerous in a situation when oscillations of the instantaneous wave-induced pore pressure cause a pore pressure gradient to be critical, leading thereby to the seabed instability. In such a case, the seabed is loosing its bearing capacity due to a liquefaction phenomenon. Usually, the bearing capacity of the soil supporting the pipeline is sufficient with no respect to the depth of burial, and cannot be a reason of a dangerous pipeline instability. As far as the first case of loading is concerned, the resultant force acting on a pipeline is called the wave-induced uplift force or hydrodynamic uplift force. Only uplift forces, comparing to the confining (resisting) forces, play a very important role and have to be taken into consideration in the vertical stability analysis. When the hydrodynamic uplift force exceeds the pipeline effective (*i.e.*, with respect to the buoyancy of water) gravity force, the stability condition is not satisfied. This can lead to large displacements of the pipeline onto the seabed floor, even to the pipelne floatation up to the sea level, and sometimes breakout which normally results in a serious failure of the pipeline and severe environmental catastrophe.

The hydrodynamic uplift force on a unit length of the pipeline, F_z, can be obtained by integrating the wave-induced pore pressure along the pipeline circumference:

$$F_z = \int_0^{2\pi} p\, r_p \cos\psi \, d\psi \tag{6.1}$$

where: F_z - hydrodynamic uplift force (defined to be negative upwards) [kN/m],
p - wave-induced pore pressure [kPa],
r_p - outside radius of the pipeline [m],
ψ - angular coordinate of the polar coordinates system (with the origin placed in the centre of the pipeline cross-section) [rad].

Only in the very special case where the wave-induced pore pressure distribution around the pipeline is symmetrical with respect to z-axis, Eq. (6.1) can be simplified:

$$F_z = 2 \int_0^{\pi} p\, r_p \cos\psi \, d\psi \tag{6.2}$$

If the pore pressure function, p, is given in the complex form (which happens very often when an advanced pore pressure theory is considered), the real part of the hydrodynamic uplift force solution is of a physical meaning and has to be considered. It means that Eq. (6.1) can be rewritten as:

$$F_z = \Re\left\{\int_0^{2\pi} p\, r_p \cos\psi\, d\psi\right\} = \int_0^{2\pi} \Re\{p\}\, r_p \cos\psi\, d\psi \tag{6.3}$$

where, additionally:

p - wave-induced pore pressure (complex-valued) [kPa],
$\Re\{\ \}$ - denotes a real part of $\{\ \}$.

For further analysis and comparison purposes it is convenient to introduce the relative wave-induced pore pressure, $\bar{p}$ (see Eq. 2.16a), and also the relative hydrodynamic uplift force, $\bar{F}_z$, because it will make the uplift force independent of the wave height (*i.e.*, the shape of the distribution of the relative wave-induced pore pressure with depth in the seabed is not influenced by the wave height). Therefore, by dividing both sides of Eq. (6.3) by the amplitude of hydrodynamic bottom pressure, P_0, the hydrodynamic uplift force can be presented in its relative form:

$$\bar{F}_z = \frac{F_z}{P_0} = \int_0^{2\pi} \bar{p}\, r_p \cos\psi\, d\psi \tag{6.4}$$

where, additionally:

$\bar{F}_z$ - relative hydrodynamic uplift force [kN/m/kPa],
$\bar{p}$ - relative wave-induced pore pressure [-].

Of course, the solution to the hydrodynamic uplift force [Eq. (6.4)] can be found using one of numerical integration methods. In many cases, however, a performance of simple algebraic summation of the component forces acting along the pipeline circumference can be very helpful. These can be of a particular interest, especially when the wave-induced pore pressure function is decribed by an expression which is mathematically complicated, as it is the case in the diffusion model or the storage model of the seabed two-phase medium (see Sections 5.2 and 5.3). The summation algorithm is very simple and can be illustrated in Fig. 6.2.

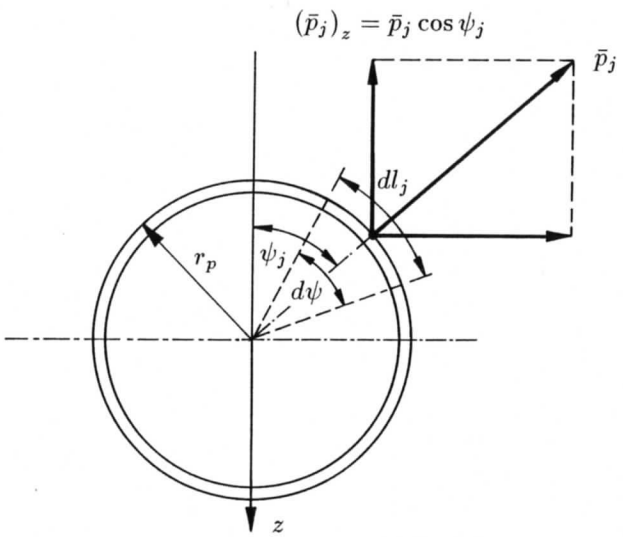

Figure 6.2 Discretization of pipeline circumference, used in computations of the hydrodynamic uplift force by means of a simple algebraic summation of vertical components of seepage forces

Adequately to Eq. (6.4), the summation formula for the hydrodynamic uplift force is as follows:

$$\bar{F}_z = \sum_{j=1}^{n_s} \bar{p}_j \, dl_j \cos\psi_j = \sum_{j=1}^{n_s} \bar{p}_j \, r_p \, d\psi_j \cos\psi_j \qquad (0 < \psi_j \leq 2\pi) \tag{6.5}$$

where: $\bar{F}_z$ - relative hydrodynamic uplift force [kN/m/kPa],
n_s - number of sectors distinguished by discretizing the pipeline circumference [-],
$\bar{p}_j$ - relative wave-induced pore pressure, acting on j-th sector arc of the pipeline circumference, and assumed to be constant on the entire j-th sector arc [-],
dl_j - length of j-th sector arc [m],
ψ_j - angular coordinate of the bisector of j-th sector [rad],
$d\psi_j$ - angular width of j-th sector [rad],
r_p - outside radius of the pipeline [m].

6.2 Review of existing computational algorithms

When a submarine pipeline is buried in a porous seabed, the problem of solving the wave-induced pore pressure oscillations becomes very complicated. In order to simplify this problem some researches assumed that the porous medium is incompressible and the wave-induced pore pressure oscillations are governed by the potential model. Under this assumption Lai *et al.* (1974), Liu & O'Donnell (1979), Lennon (1983, 1985) and Spierenburg (1985, 1986, 1987) investigated this problem using a numerical analysis. Liu & O'Donnell (1979) considered two different types of waves acting on the seabed, namely, monochromatic and solitary, and introduced the integral equation method to solve the resulting integral equation. In a numerical solution procedure developed by Lennon (1983, 1985), the pressure distribution on the pipeline was calculated using also the boundary integral equation method (BIEM). MacPherson (1978) and McDougal *et al.* (1988) presented analytical solutions for the case of infinite depth of the seabed, whereas Monkmeyer *et al.* (1983), using the method of image pipes, found a similar solution, the advantage of which is that it can also be applicable for the case of finite depth of the permeable seabed layer. The common feature of all the studies mentioned above is that the effect of compressibility of both the pore fluid and the porous medium was neglected. Using Biot's equation and continuity equation for the pore fluid flow in a permeable medium, Kokkinowrachos (1985) considered the effect of the pore fluid and porous medium compressibility and calculated the pore pressure around a semi-embedded pipeline by means of the microelement approach. However, his solution concerns a very special geometrical position of the pipeline and therefore has not any strong practical meaning. The vertical stability of a submarine pipeline buried or half-buried in the seabed under wave action was studied by Magda (1987), Foda (1985) and Spierenburg (1985, 1986, 1987).

In the following, a short review of some of computational methods for the calculation of the wave-induced pore pressure around the pipeline is introduced. Finally, a comparison between simplified methods and the more general method developed in the

present work will be shown together with a discussion about the importance of existence of the soil-water mixture parameters in the solution for the uplift force acting on a submarine pipeline buried in seabed sediments.

6.2.1 A simplified method with no pipeline in the seabed

One of the first approximations of the uplift force acting on a submarine buried pipeline consists in a separate treatment of the wave-induced pore pressure oscillations phenomena and the existence of the pipeline in seabed sediments. In other words, it is assumed that the pipeline has not any disturbing influence on the wave-induced pore pressure oscillations in the soil. However, under real natural conditions, an impermeable and relatively stiff body of the pipeline acts like a barrier and changes the pattern of the pore pressure field around. The pore pressure difference, in the situations with and without a pipeline inserted into the seabed, can be reffered to as the perturbation pressure. For the first estimation of the hydrodynamic uplift force, the perturbation pressure is simply assumed to be zero.

An example of such analysis is shown in Fig. 6.3. In order to carry out this type of calculation, the knowledge of two elements is required, namely: a geometry of the system and an analytical description of the wave-induced pore pressure distribution with depth in the permeable seabed layer.

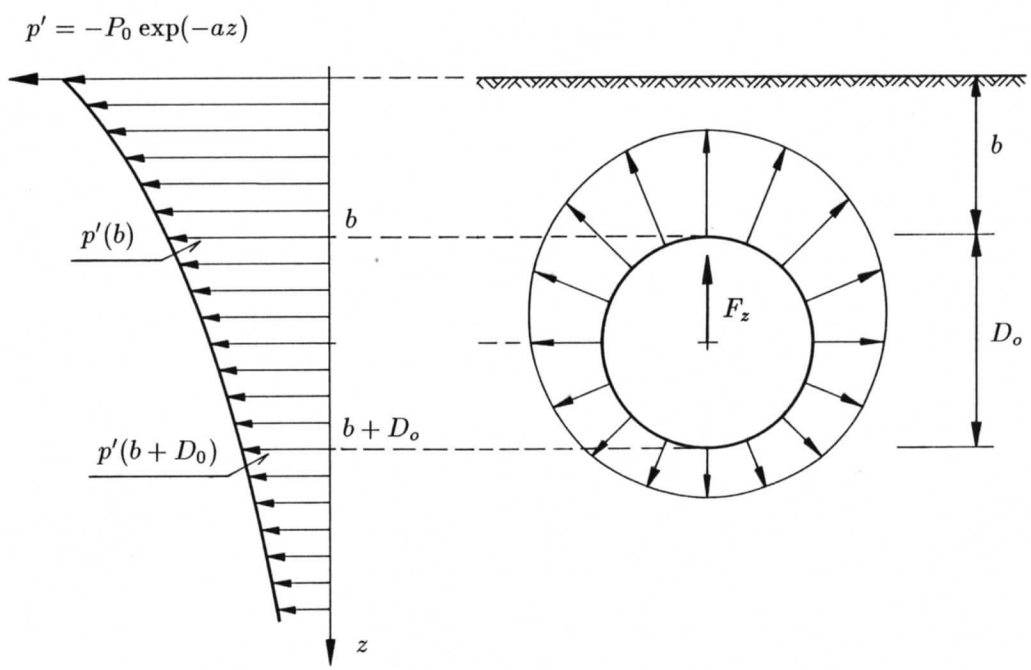

Figure 6.3 Wave-induced pore pressure distribution with depth (potential solution), acting on a submarine buried pipeline located just under the wave trough [*i.e.*, $(ax - \omega t) = \pi$]

Biot's consolidation theory, for most applications, appears to represent the small amplitude dynamic response of soil quite adequately for a variety of wave-soil interaction phenomena. However, it has been suggested for sands and very dense silts that the

full Biot's equations are not required to determine the dynamic pressure and that the potential pressure model is adequate for these materials (Madsen, 1978; Sleath, 1970). For these permeable and relatively stiff materials, the soil deformations are small and do not seem to influence the pore pressure significantly. Therefore, many researchers decoupled the pore pressure from the displacements of the soil skeleton. For this reason, and mostly due to the complex geometry of the problem, all studies related to submarine buried pipelines were based on the potential pressure model, derived under the condition of incompressibility of both the pore fluid and the soil skeleton. The potential pore pressure solution, initially given by Putnam (1949) and Ried & Kajiura (1957), was already presented in Section 4.2 [Eqs. (4.7) and (4.8) – in the complex-form notation, and Eqs. (4.9) and (4.10) – in the real-form notation]. Taking the potential solution to the wave-induced pore pressure oscillations in the seabed layer of infinite thickness [see Eq. (4.9)], Eq. (6.4) leads to:

$$\bar{F}_z = \int_0^{2\pi} \exp(-az)\cos(ax - \omega t)\, r_p \cos\psi \, d\psi \tag{6.6}$$

where: $\bar{F}_z$ - relative hydrodynamic uplift force [kN/m/kPa],
a - wave number ($a = 2\pi/L$) [m^{-1}],
L - wavelength [m],
ω - wave angular frequency ($\omega = 2\pi/T$) [s^{-1}],
T - wave period [s],
x, z - horizontal and vertical coordinates of the Cartesian coordinates system, respectively, [m],
t - time [s],
r_p - outside radius of the pipeline [m],
ψ - angular coordinate of the polar coordinates system [rad].

It is obvious that the horizontal and vertical coordinates of the Cartesian coordinates system are related to the angular coordinate of the polar coordinates system. Assuming that the vertical axes of the both coordinates systems are coaxial (see Fig. 6.3), these corelations can be expressed in the following functions:

$$z = b + r_p(1 - \cos\psi) \tag{6.7a}$$

$$x = r_p \sin\psi \tag{6.7b}$$

where, additionally:
b - depth of burial of the pipeline (measured from the seabed floor to the top of the pipeline) [m].

Assuming the most inconvenient situation for the potential solution, in which the pipeline is located directly under the wave trough; this happens when the phase of wave-induced pore pressure oscillations is equal to its optimum value [*i.e.*, $(ax - \omega t) = \Theta_{opt} = \pi$; see Fig. 6.3], the relative hydrodynamic uplift force reaches its maximum value (a negative sign of this value is only due to the definition of the hydrodynamic uplift force), and can be defined in the following expression:

$$\left(\bar{F}_z\right)_{max,\Theta} = -\int_0^{2\pi} \exp\left\{-a\left[b + r_p(1 - \cos\psi)\right]\right\} \cos\left(a r_p \sin\psi\right)\, r_p \cos\psi \, d\psi \tag{6.8}$$

where, additionally:

$(\bar{F}_z)_{max,\Theta}$ - maximum relative hydrodynamic uplift force, obtained for the optimum phase of water wave loading oscillations, for which the pore pressure gradient (acting on a pipeline) is maximal [kN/m/kPa].

The solution to the integral given in Eq. (6.8) is surprisingly simple:

$$(\bar{F}_z)_{max,\Theta} = -\pi a r_p^2 \exp\left[-a\,(b + r_p)\right] \tag{6.9}$$

As an example, used for the comparison purposes in the hydrodynamic uplift force analysis, the following values of the required parameters were used as input data:

- depth of burial of the pipeline $b = 0.5\,\mathrm{m}$
- outside diameter of the pipeline $D_o = 1.0\,\mathrm{m}$
- wavelength $L = 10.0\,\mathrm{m}$

Using these input data, Eq. (6.9) gives the following value of the relative hydrodynamic relative uplift force, which does not take the pipeline perturbation effect into account:

$$(\bar{F}_z)_{max,\Theta} = \left(\bar{F}_z^{(a)}\right)_{max,\Theta} = -0.263\,\mathrm{kN/m/kPa}$$

where: $\left(\bar{F}_z^{(a)}\right)_{max,\Theta}$ - relative simplified hydrodynamic uplift force (based on the undisturbed pore pressure field), maximum with respect to the phase of water wave loading oscillations [kN/m/kPa].

6.2.2 Pipeline-perturbation methods

Assuming that a submarine pipeline is an impermeable (not porous) submerged body, and is buried parallel to wave fronts (*i.e.*, wave crests), the governing problem can be expressed in the form of Eqs. (4.6a) and (4.6b), together with Eq. (4.6c) or Eq. (4.6d), and additionally by the pipeline impermeable surface condition in the form:

$$\frac{\partial p}{\partial r} = 0 \qquad \text{for} \qquad r = r_p \tag{6.10}$$

where: p - wave-induced pore pressure [kPa],
r - linear coordinate (normal to the pipeline surface) of the polar coordinates system [m],
r_p - outside radius of the pipeline [m].

The solution of the problem can be found by means of superposition of two separate solutions: one is the wave-induced pore pressure solution with the absence of the pipeline structure in the seabed, and the second one is a kind of pore pressure correction of the wave-induced pore pressure solution, such that the gradient of the pore pressure at the pipeline surface is zero. And thus:

$$p = p^{(p)} = p^{(a)} + p^{(c)} \tag{6.11}$$

where: $p^{(p)}$ - perturbated (disturbed) wave-induced pore pressure, due to the pipeline presence in the seabed [kPa],
$p^{(a)}$ - undisturbed wave-induced pore pressure, due to the pipeline absence in the seabed [kPa],
$p^{(c)}$ - wave-induced pore pressure correction, due to the pipeline presence in the seabed [kPa].

By simple adding $p^{(a)}$ and $p^{(c)}$, the perturbated wave-induced pore pressure variations around the submarine pipeline buried in seabed sediments can be easily obtained. Two typical pressure fields are shown in Fig. 6.4. The first picture illustrates the contours of the undisturbed wave-induced pore pressure distribution in the soil, where there is no pipeline buried in seabed sediments; the second picture shows the perturbated wave-induced pore pressure field in the closest vicinity of the pipeline, where the pipeline is located directly under the wave trough. As one would expect, the isobars (*i.e.*, the lines of constant pore pressure) are perpendicular to the pipeline impermeable surface. There is a net pore pressure gradient at the pipeline, and clearly this will result in a force acting on the pipeline. The influence of the pipeline on the pore pressure field is a fairly local effect. Pore pressures induced by higher frequency waves are more highly attenuated with depth. Therefore, absolute values of the pore pressure are less for short waves than for long waves, but the pore pressure gradient may be larger.

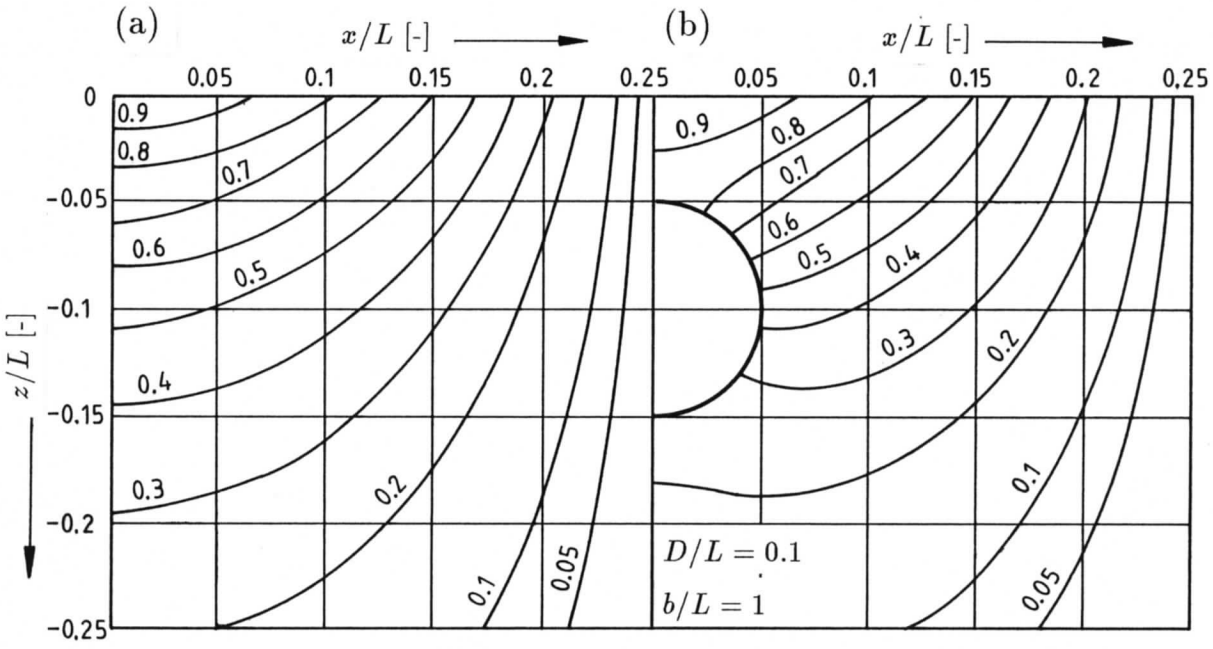

Figure 6.4 Wave-induced pore pressure $\bar{p} = p'/P_0$ induced by: (a) wave trough above seabed without pipeline, (b) wave trough above pipeline buried in seabed, [McPherson, 1978]

The boundary value problem, defined by Eqs. (4.6a) and (4.6b), together with Eq. (4.6c) or Eq. (4.6d), and Eq. (6.10), is difficult to be analysed in rectangular coordinates. However, this difficulty may be overcome by transforming to a space in which the variables become separable. Therefore, McPherson (1978) suggested the use of bipolar

coordinates, whereas McDougal *et al.* (1988) proposed a transformation that maps the problem in one imaginary plane into an annulus centered at the origin in another imaginary plane. Contrary to the solution presented by McPherson (1978), McDougal *et al.* (1988) treated the pore pressure totally, *i.e.* without distinguishing and superpositioning of the two pore pressure components obtained for the case of pipeline absence and presence in seabed sediments.

McPherson (1978) stated that in extereme conditions, beneath the wave trough the seepage force will act vertically upwards and its magnitude per unit length may be as large as 30 % of the buoyant force due to the weight of water displaced.

Results of calculations, based on the above mentioned two different conformal mapping methods and the so-called image-pipe method, have shown, of course, identical values of the wave-induced pore pressure around a submarine buried pipeline, and therefore the same values of the hydrodynamic uplift force are obtained.

Adequately to Eq. (6.11), the relative hydrodynamic uplift force, taking into account the presence of pipeline structure in the seabed, can be also presented as a sum of two separate solutions, *i.e.*:

$$\bar{F}_z = \bar{F}_z^{(p)} = \bar{F}_z^{(a)} + \bar{F}_z^{(c)} \tag{6.12}$$

where: $\bar{F}_z^{(p)}$ - relative perturbated hydrodynamic uplift force [kN/m/kPa],
$\bar{F}_z^{(a)}$ - relative simplified hydrodynamic uplift force [kN/m/kPa],
$\bar{F}_z^{(c)}$ - correction of the relative hydrodynamic uplift force [kN/m/kPa].

Using the perturbation pore pressure solutions derived by McPherson (1978) and McDougal *et al.* (1988), the maximum hydrodynamic uplift force, computed for the same geometry [assuming the wave trough located directly above the pipeline, denoted by $(ax - \omega t) = \Theta_{opt} = \pi$, which is the most unfavourable case for the potential solution] as in the formerly considered example with the pipeline absence in seabed sediments, is equal:

$$\left(\bar{F}_z^{(a)}\right)_{max,\Theta} = -0.263\,\text{kN/m/kPa}$$

$$\left(\bar{F}_z^{(c)}\right)_{max,\Theta} = -0.230\,\text{kN/m/kPa}$$

$$\left(\bar{F}_z^{(p)}\right)_{max,\Theta} = \left(F_z^{(a)}\right)_{max,\Theta} + \left(F_z^{(c)}\right)_{max,\Theta} = -0.493\,\text{kN/m/kPa}$$

Comparing the values obtained for the undisturbed and disturbed (perturbated, due to the presence of the pipeline structure in the seabed) wave-induced pore pressure field in seabed sediments, it is obvious that – using one of the more sophisticated perturbation methods – the maximum hydrodynamic uplift force, $\left(\bar{F}_z^{(p)}\right)_{max,\Theta}$, computed for the realistic boundary conditions formed by the impermeable pipeline structure, is as much as twice larger than the maximum hydrodynamic uplift force, $\left(F_z^{(a)}\right)_{max,\Theta}$, computed for the undisturbed case with the pipeline absence in the seabed.

The results of the wave-induced pore pressure (undisturbed and perturbated) distribution around the pipeline circumference, respective to the above presented computational example, are illustrated in Fig. 6.5. The inclusion of the perturbation pore pressure into the global solution leads to the increase of the (under)pressure in the upper part of the pipeline circumference, and to the decrease of the (under)pressure in the lower part, increasing thereby the hydrodynamic uplift force.

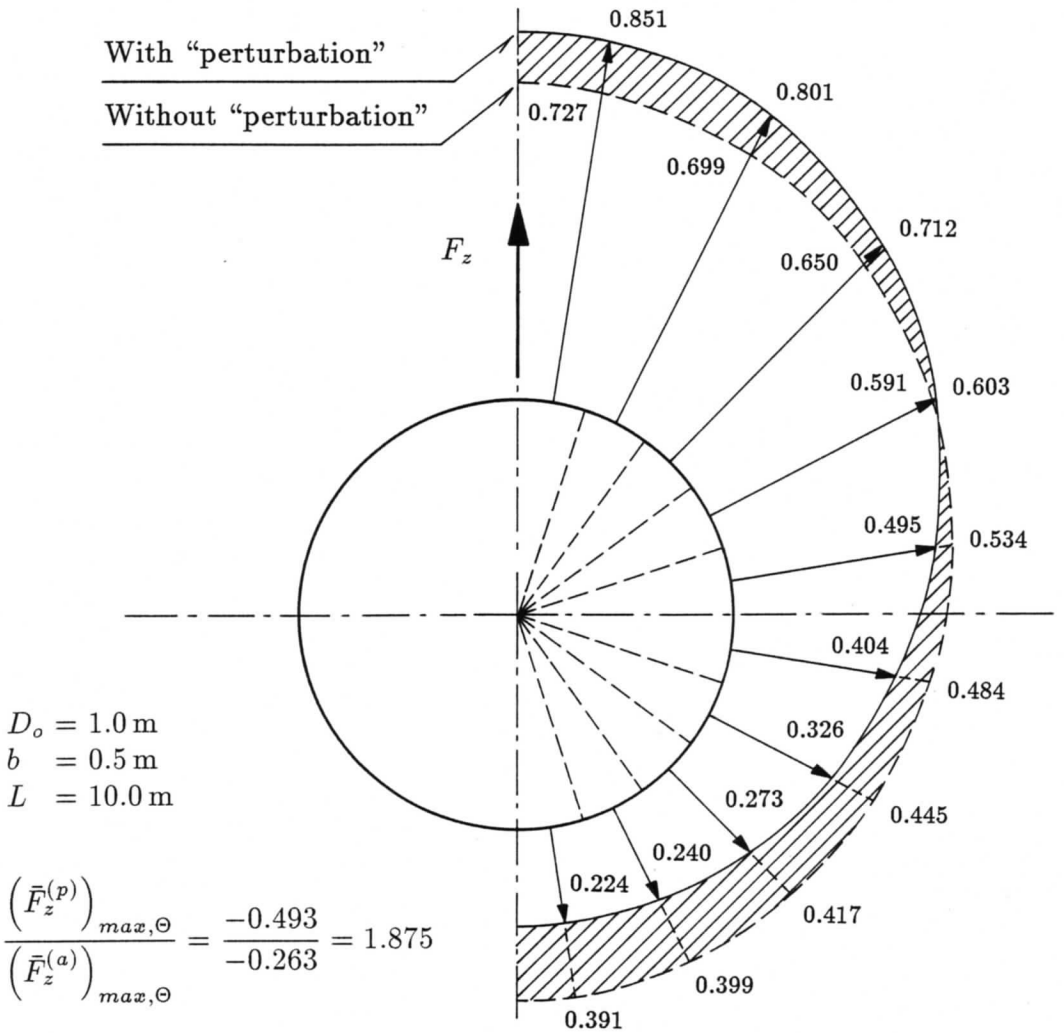

Figure 6.5 Wave-induced pore pressure distribution (undisturbed, $p^{(a)}$, and perturbated, $p^{(p)}$) around a submarine pipeline buried in seabed sediments

In order to study the influence of geometrical parameters involved in the problem of hydrodynamic uplift force, based on the potential model of the seabed, some additional computations were performed, using the pore pressure perturbation methods. The main input data was, as before: $L = 10\,\mathrm{m}$, and $D_o = 1.0\,\mathrm{m}$. Three different cases of the relative depth of burial, $b/L = 0.025, 0.05, 0.1$, for the relative thickness of seabed layer $d/D_o = 2 - 10$, were examined. The results of example computations are presented in Fig. 6.6, illustrating the maximum relative hydrodynamic uplift force, $\left(\bar{F}_z^{(p)}\right)_{max,\Theta}$, and in Fig. 6.7, where the influence of the perturbation pore pressure on the hydrodynamic uplift force was investigated by introducing the following uplift force ratio:

$$r_F = \frac{\left(\bar{F}_z^{(c)}\right)_{max,\Theta}}{\left(\bar{F}_z^{(a)}\right)_{max,\Theta}} \tag{6.13}$$

where, additionally:

r_F - hydrodynamic uplift force ratio [-].

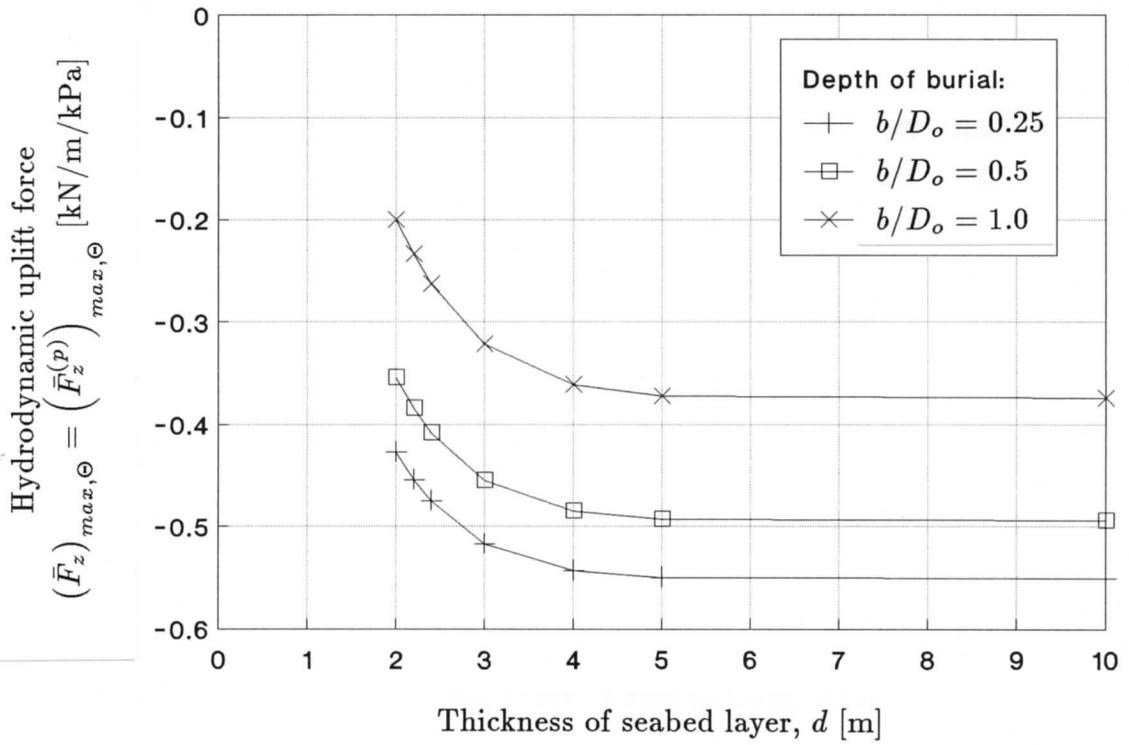

Figure 6.6 Influence of seabed layer thickness and depth of burial on the hydrodynamic uplift force (potential model)

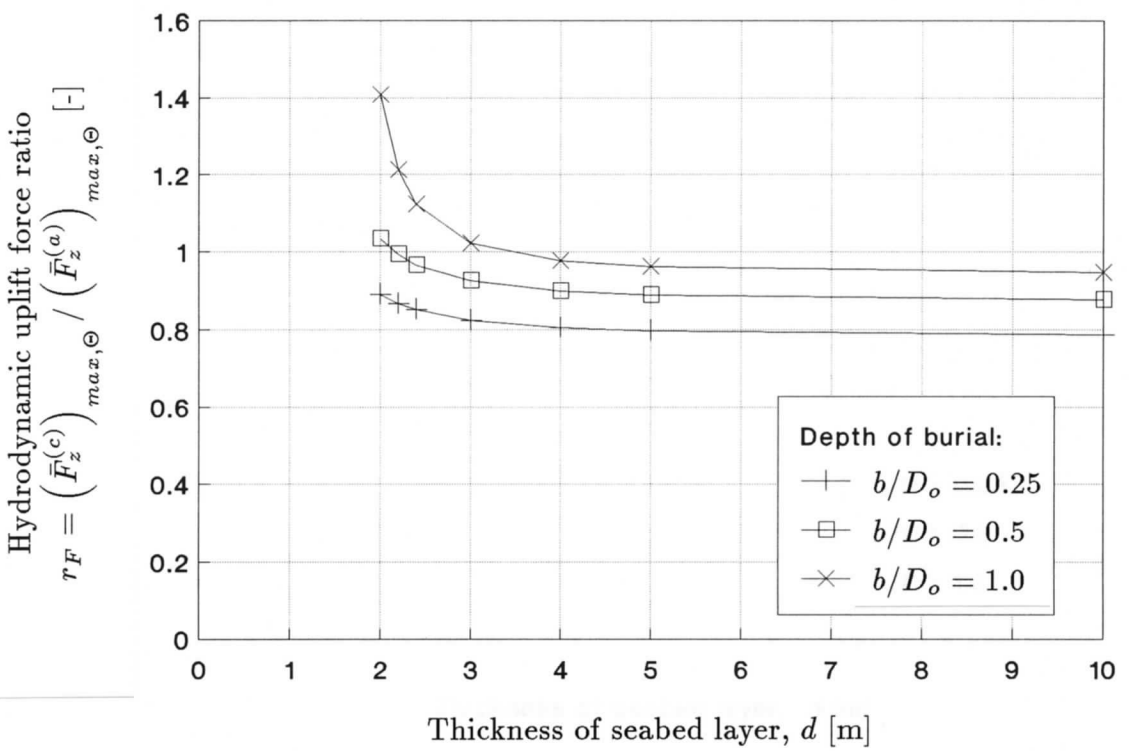

Figure 6.7 Influence of seabed layer thickness and depth of burial on the hydrodynamic uplift force ratio (potential model)

It is interesting to note that for the thickness of the permeable seabed layer greater than approximately $d = 5D_o$ there is almost no meaningful influence of the seabed thickness on the hydrodynamic uplift force. Only for the case where $d < 5D_o$, and especially for a possiblly small seabed thickness ($d = 2D_o$ in the example), which can be of great importance from the laboratory modelling point of view, the hydrodynamic uplift force becomes smaller and ranges from about 53 % (for $b/L = 0.1$) to 77 % (for $b/L = 0.025$) of the value typical for the relatively large seabed thickness ($d = 10D_o$ in the example).

Generally, smaller depths of burial, or longer waves, enlarge a value of the hydrodynamic uplift force. This constant tendency (*i.e.*, the smaller burial depth, the greater hydrodynamic uplift force) seems to be quite logical and is directly related to the pore pressure gradient which tends to its maximum when approaching the seabed surface. The hydrodynamic uplift force, computed for the relative depth of burial $b/L = 0.1$, is 2.14 (for $d/D_o = 2$) and 1.47 (for $d/D_o = 10$) times larger than the hydrodynamic uplift force computed for the deeper depth of burial ($b/L = 0.025$).

Figure 6.7 indicates the influence of the perturbarion pore pressure on the hydrodynamic uplift force, by comparing two single components of the solution, represented in the hydrodynamic uplift force ratio [see Eq. (6.13)]. The most important finding is that the uplift force ratio is in the range of $r_F \cong 0.8 - 1.0$, or even higher ($r_F \cong 1.4$) for the relatively smaller thickness of the seabed layer ($d/L = 2$). As it was shown in Fig. 6.6, the influence of smaller thicknesses ($d/L = 2-3$) is larger than for the deep-soil condition. It means that the contribution of the corrected hydrodynamic uplift force, $F_z^{(c)}$, due to the perturbation pore pressure effects only, can be of the same magnitude as the hydrodynamic uplift force, $F_z^{(a)}$, approximated due to the assumption of the pipeline absence and the undisturbed pore pressure field in seabed sediments.

6.2.3 Conclusions

McDougal *et al.* (1988) compared theoretical results with small-scale laboratory measurements. The theory was also compared with observations from a set of large-scale experiments. The pore pressure measurements revealed several anticipated trends. And thus, the amplitude of the dynamic pore pressure is largest on the top of the cylinder and smallest on the bottom and the shorter waves are more highly attenuated with depth.

McDougal *et al.* (1988) concluded that the theory generally underpredicts the measured pore pressures for longer waves and overpredicts for shorter waves. The theory is for an infinitely deep soil, but in the experiments the soil layer had a limited thickness and waves were described as shallow-to-intermediate water waves, with respect to the wave length. Infinitely deep soil cause greater dynamic pressure attenuation than finite depth soils. Consequently, the theory for infinitely deep soils should fall below the experimental observations. The deep-soil assumption was compared with numerical model results for the laboratory experiment conditions. The small-scale tests were in a good agreement, while the large-scale comparisons were fair. This, however, may have been the result of a finite thickness of the soil layer.

In the theory presented by Monkmeyer *et al.* (1983), where the problem of proper geometrical bounary conditions approaches reality of laboratory tests, there is still a certain deviation between theoretically computed values of pore pressure and values

obtained during experiments. Giving the reasons why the experimental values overestimate theoretical ones, Monkmeyer *et al.* (1983), pointed out some possible explanations of this phenomenon, which were neglected in the theory, namely:

- sand ripples in the sand causing irregularity of the upper boundary,
- the possibility that a small surface layer of sand was liquefied,
- possible anisotropy in the sand bed, which was assumed to be isotropic,
- elastic effects in the sand skeleton.

The test preparation procedure seems to play an important role. Only McDougal *et al.* (1988) reported fluidization as a method of sand bed layer preaparation in order to achieve possibly isotropic soil conditions.

All the mentioned theories are based on the potential model of the two-phase seabed medium, where the number of parameters is limited only to a few. These parameters are responsible for the geometry of the problem only, and they are rather easy to be defined with a relatively high occuracy. Therefore, one of the main conclusions can be that not only a real geometry has to be mapped in a theoretical treatment of the problem considered, but also proper values of the parameters describing elastic properties of soil skeleton and pore fluid have to be taken into account. It means that soil saturation conditions, having a direct influence on the pore fluid compressibility, form a very important factor and must be incorporated into a proper pore pressure theory used for the prediction of the hydrodynamic uplift force acting on a submarine pipeline buried seabed sediments.

The reported differences, up to 10 % [Monkmeyer *et al.* (1983)], and up to 8 % [McDougal *et al.* (1988)], between theoretically predicted values and experimental results of the wave-induced pore pressures on the pipeline surface, can have two main sources, namely:

- the theories are simplified and do not contain all important soil-water mixture parameters and possible boundary conditions,
- the theories reflect natural soil-water-pipeline behaviour in a proper way, but values of parameters used in calculation are not proved to be exactly the same like these 'in-situ' which accompanied laboratory investigations.

The importance of the 'perturbation' pore pressure on the hydrodynamic uplift force was shown in the above presented simple comparison (see Fig. 6.5). A value of the hydrodynamic uplift force, computed taking the 'perturbation' pore pressure into account, is approximately of the same order as the hydrodynamic uplift force calculated neglecting the disturbing effects of a pipeline on the pore pressure field in the seabed. Therefore, it seems to be obvious that any calculation procedure should follow the perturbation method.

A new developed or modified method of computation of the hydrodynamic uplift force should be based on:

- pore pressure theory, where soil and soil-water mixture parameters are considered and a finite thickness of the sand bed layer is taken into account,
- analytical solution (*e.g.*, using Monkmeyer's 'image pipe' theory) or numerical solution (*e.g.*, finite element method), which is able to take into account both the upper (seabed floor level) and the lower (impermeable and stiff base under the permeable seabed layer) boundary conditions, and also the boundary condition induced by the presence of the impermeable and stiff pipeline structure in seabed sediments.

Implementation of certain soil and pore fluid parameters (*e.g.*: compressibility, permeability, and saturation) does not lead to the potential problem formulation (defined by the Laplace equation), which is independent of these parameters, but to much more advanced and realistic diffusion problem or even storage problem (see Sections 4.2 and 4.3), where the governing equations are mathematically more complicated than the Laplace equation.

An analytical solution of the above mentioned boundary problem, with the diffusion equation or storage equation as a main governing partial differential equation, seems to be very difficult and has not been derived yet. Of course, one of the numerical methods can be applied. However, there is another simple way of calculation of the hydrodynamic uplift force. And thus, the following paradigm is proposed to be applied:

- solution of the diffusion (or storage) equation, under the assumption that there is no pipeline structure inserted in the seabed,
- finding the phase of wave-induced pore pressure oscillations, in which the pore pressure gradient is the most critical (*i.e.*, becomes maximal),
- computation of the pore pressure distribution around a pipeline, assuming the imaginary presence of the pipeline in the seabed,
- computation of the hydrodynamic uplift force, based on the undisturbed pore pressure field (*i.e.*, using the simplified method; see Section 6.2.1),
- taking into account the perturbation pore pressure effects, by introducing a factor of 2 to the already computed simplified hydrodynamic uplift force, *i.e.*:

$$\left(\bar{F}_z^{(p)}\right)_{max,\Theta} \cong 2\left(\bar{F}_z^{(a)}\right)_{max,\Theta} \tag{6.14}$$

where: $\left(\bar{F}_z^{(p)}\right)_{max,\Theta}$ - relative perturbated hydrodynamic uplift force, maximum from the phase of wave-induced pore pressure oscillations point of view [kN/m/kPa],

$\left(\bar{F}_z^{(a)}\right)_{max,\Theta}$ - relative simplified hydrodynamic uplift force, maximum from the phase of wave-induced pore pressure oscillations point of view [kN/m/kPa].

6.3 Results of calculations based on the storage model

Some simple calculations performed in Section 6.2 have shown the importance of the contribution of perturbation pore pressure which has always to be taken into account where a calculation of the hydrodynamic uplift force is concerned. The computational example has proved that neglecting the disturbing function of the impermeable pipeline structure on the pore pressure field around can cause a serious design fault (*i.e.*, hydrodynamic uplift force calculated excluding the perturbation pore pressure is, more or less, about a half of that which is expected to be when the perturbation effects are incorporated into a computational procedure).

The above mentioned calculation example was performed under the assumption of the potential theory (the Laplace equation) used to describe the pore pressure response

in a porous seabed sediment under a wave action. The 'finite-thickness layer' solution for the case of compressible soil skeleton and pore fluid, derived analytically (see Section 4.4) and obtained numerically (see Section 4.5), gives an additional opportunity of much more detailed and advanced analyses of the hydrodynamic uplift force acting on a submarine pipeline buried in the seabed. Implementation of some important soil and pore fluid parameters into the theoretical description creates more realistic picture of the pore pressure behaviour in the porous seabed sediment.

Input data used in the analysis of the hydrodynamic uplift force, based on the storage model of the wave-induced pore pressure response in the two-phase seabed medium, are listed below:

- outside diameter of pipeline $D_o = 1.0\,\mathrm{m}$
- thickness of seabed layer $d = 2 - 100\,\mathrm{m}$
- depth of burial $b = 0.5\,\mathrm{m}$
- water depth $h = 10\,\mathrm{m}$
- wave period $T = 8\,\mathrm{s}$
- Young's modulus of soil $E = 10^4;\ 10^7\,\mathrm{kPa}$
- Poisson's ratio $\nu = 0.3$
- porosity $n = 0.4$
- coefficient of soil permeability $k = 10^{-4}\,\mathrm{m/s}$
- degree of saturation $S = 0.95 - 1.0$
- compressibility of pure water $\beta = 4.2 \times 10^{-7}\,\mathrm{m^2/kN}$
- atmospheric pressure $p_{at} = 101.325\,\mathrm{kPa}$

Normally, a maximum possible value of the hydrodynamic uplift force is required when performing the analysis of the pipeline vertical stability. Assuming the seabed response to be governed by the potential model, this was an easy task because the maximum value was simply achieved when the wave trough was located directly above the longitudinal axis of the pipeline. However, considering the diffusion model or the storage model of the seabed response to progressive surface water waves, this very special location of the pipeline with respect to the surface water wave is not synonymous with obtaining a maximum value of the hydrodynamic uplift force. The phase lag of pore pressure oscillations in the seabed is responsible for a certain phase lag in the hydrodynamic uplift force oscillations with respect to the phase of surface water wave oscillations. It means that the detection of a maximum value of the hydrodynamic uplift force requires a wide analysis from the whole period of oscillations.

In order to simplify the following analysis, the results presented below were obtained for only one time- and space-point of surface water wave oscillations [*i.e.*, $(ax - \omega t) = \Theta_{opt} = \pi$ was assumed, which denotes a pipeline position just under the wave trough]. However, due to the phase-lag phenomenon in the diffusion and storage models of the pore pressure response in seabed sediments, this special case may not always be adequate to the most unfavourable case of the pore pressure gradient in the vicinity of submarine pipeline buried in seabed sediments, and therefore a maximum value of the hydrodynamic uplift force may not be precisely defined. Although taking the above into account, a geometric case denoted by the term $(ax - \omega t) = \Theta_{opt} = \pi$ will be treated in the following as the most relevant for the present example analysis, and the relative hydrodynamic uplift force will be, for this case, called the maximum relative hydrodynamic uplift force, $(\bar{F}_z)_{max,\Theta}$.

The results of the hydrodynamic uplift force analysis, based on the storage model of the pore pressure response in the two-phase seabed medium, are presented in Fig. 6.8, showing the wave-induced pore pressure distributions with depth (up to $z = 1.5\,\mathrm{m}$),

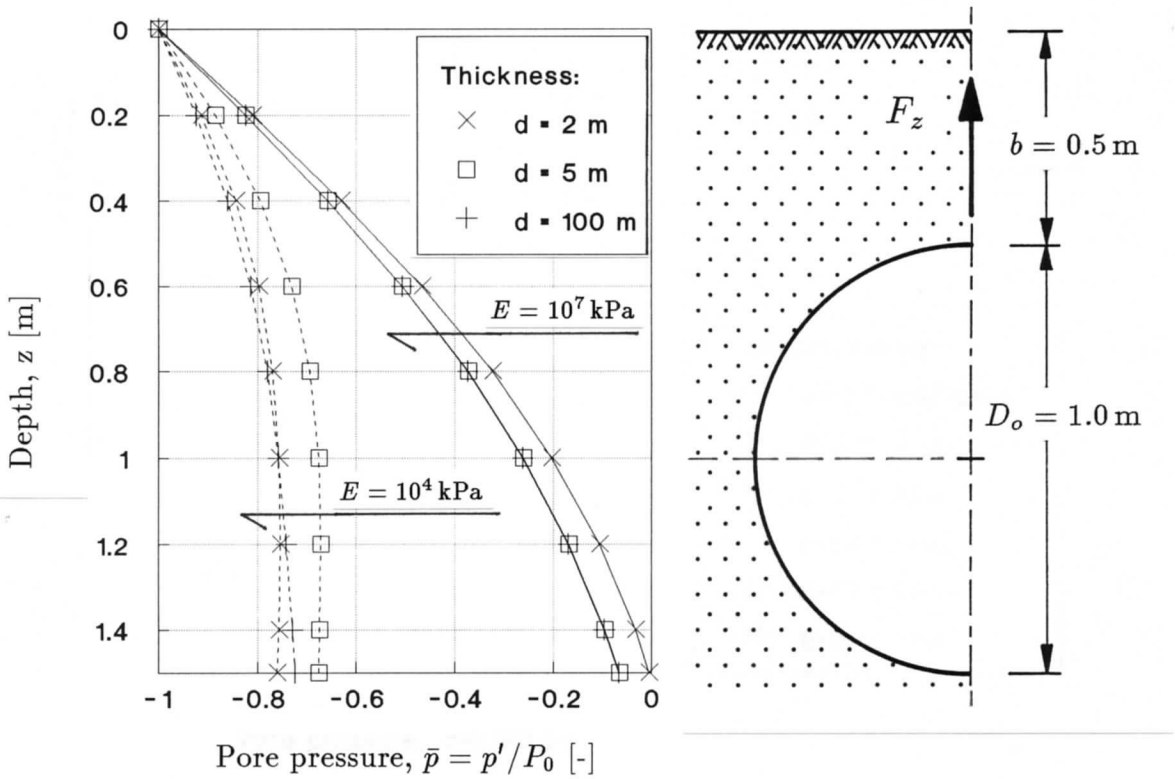

Figure 6.8 Definition sketch for the hydrodynamic uplift force analysis (pore pressure gradient influenced by soil skeleton compressibility and seabed layer thickness; degree of saturation $S = 0.99$)

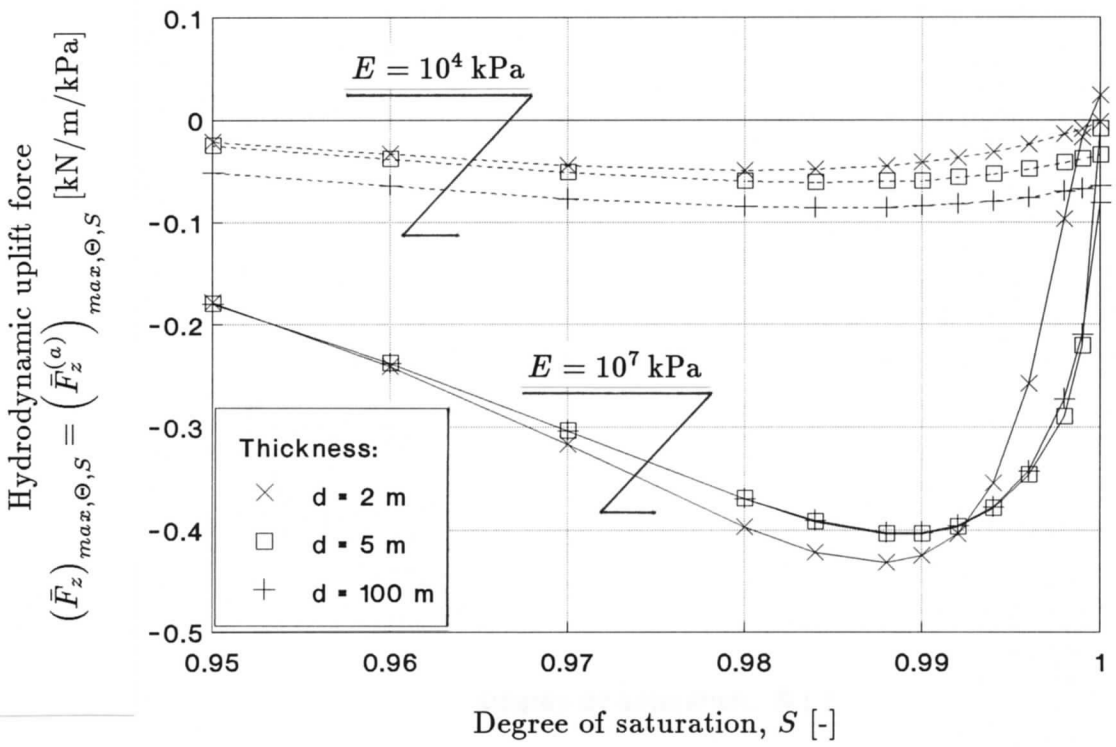

Figure 6.9 Hydrodynamic uplift force versus different soil saturation conditions and compressibility (represented by Young's modulus, E) of soil skeleton

obtained – as an example – for $S = 0.99$. Figure 6.9 illustrates the maximum relative hydrodynamic uplift force influenced by different values of the degree of saturation ($S = 0.95 - 1.0$). Simultaneously, two different values of Young's modulus of soil skeleton are introduced, in order to represent either a dense state ($E = 10^7$ kPa) or a loose state ($E = 10^4$ kPa) of seabed sediments. It has to be emphased that the maximum hydrodynamic uplift force was computed using the undisturbed pore pressure distributions (see Fig. 6.8), which were obtained for the pipeline absence in the seabed; it means that $\left(\bar{F}_z\right)_{max,\Theta} = \left(\bar{F}_z^{(a)}\right)_{max,\Theta}$.

Assuming a constant value of the degree of saturation (*e.g.*, $S = 0.99$), Fig. 6.8 indicates higher values of the pore pressure gradients, in the whole vertical profile ($0 < z < 1.5$ m) considered in the example, for the dense sandy seabed sediments than for the loose ones. A simple and direct consequence of this fact is reflected in the results of the hydrodynamic uplift force, shown in Fig. 6.9. Additionally, the variation of soil saturation conditions has indicated much more stronger influence on the pore pressure response in dense seabed sediments than in loose ones. Especially in the case of dense sandy seabed sediments, it can be easily recognized that the degree of saturation very close to fully saturated soil conditions brings the hydrodynamic uplift force to its maximum value. This value of the degree of saturation is called the optimum degree of saturation, S_{opt}, *i.e.*,

$$S = S_{opt} \quad \Longrightarrow \quad \bar{F}_z = \left(\bar{F}_z\right)_{max,S} \tag{6.15}$$

where: S - degree of saturation [-],
S_{opt} - optimum degree of saturation [-],
$\bar{F}_z$ - relative hydrodynamic uplift force [kN/m/kPa],
$\left(\bar{F}_z\right)_{max,S}$ - relative hydrodynamic uplift force, maximum with respect to soil saturation conditions [kN/m/kPa].

Remembering that the wave-induced pore pressure gradient can be strongly influenced by both the phase of pore pressure oscillations and soil saturation conditions, one can imagine a situation where these two effects are overlapped leading thereby to the most critical case, in which the hydrodynamic uplift force becomes absolutely maximal. This is the most relevant case for the analysis of vertical stability of a submarine pipeline buried in seabed sediments. And thus,

$$(ax - \omega t) = \Theta_{opt} \quad \text{and} \quad S = S_{opt} \quad \Longrightarrow \quad \bar{F}_z = \left(\bar{F}_z\right)_{max,\Theta,S} \tag{6.16}$$

where, additionally:
$(ax - \omega t)$ - phase of water wave loading oscillations [rad],
Θ_{opt} - optimum phase of water wave loading oscillations [rad],
$\left(\bar{F}_z\right)_{max,\delta,S}$ - relative hydrodynamic uplift force, maximum with respect to the phase of water wave loading oscillations and soil saturation conditions [kN/m/kPa].

Taking the above into account, the most important results indicated in Fig. 6.9 are as follows:

- dense sandy seabed sediments

$$\left(\bar{F}_z^{(a)}\right)_{max,\Theta,S} = -0.432\,\mathrm{kN/m/kPa} \qquad \text{(for: } d = 2\,\mathrm{m} \text{ and } S = S_{opt} = 0.988\text{)}$$

$$\left(\bar{F}_z^{(a)}\right)_{max,\Theta,S} = -0.403\,\mathrm{kN/m/kPa} \qquad \text{(for: } d = 100\,\mathrm{m} \text{ and } S = S_{opt} = 0.988\text{)}$$

- lose sandy seabed sediments

$$\left(\bar{F}_z^{(a)}\right)_{max,\Theta,S} = -0.049\,\mathrm{kN/m/kPa} \qquad \text{(for: } d = 2\,\mathrm{m} \text{ and } S = S_{opt} = 0.982\text{)}$$

$$\left(\bar{F}_z^{(a)}\right)_{max,\Theta,S} = -0.086\,\mathrm{kN/m/kPa} \qquad \text{(for: } d = 100\,\mathrm{m} \text{ and } S = S_{opt} = 0.986\text{)}$$

Using the above presented computational example, it has to be stressed that the hydrodynamic uplift force analysis is very sensitive on the variation of the degree of saturation and, therefore, must be carefully performed in order to define properly a maximum value of the hydrodynamic uplift force. It was shown that, by changing the degree of saturation with a step of $\Delta S = 0.01$ (*i.e.*, 1 %), the most important and relevant situation, denoted by the optimum degree of saturation, S_{opt}, can be easily omitted. Therefore, it is required to apply much more smaller increments of the degree of saturation when performing a parameter study to obtain a full picture of possible variations in the hydrodynamic uplift force.

Applying now the last conclusion from Section 6.2.3 and using Eq. (6.14), one can compute an approximated value of the perturbated hydrodynamic uplift force (pore pressure perturbation effects included), related to the optimum phase lag of wave-induced pore pressure oscillations, Θ_{opt}, and the optimum degree of saturation, S_{opt}, making the hydrodynamic uplift force absolutely maximal. And thus, for $d = 100\,\mathrm{m}$ and the other geometric and physical parameters assumed for this example analysis:

$$\left(\bar{F}_z^{(p)}\right)_{max,\Theta,S} \cong 2\left(\bar{F}_z^{(a)}\right)_{max,\Theta,S} = 2(-0.403) = -0.806\,\mathrm{kN/m/kPa}$$

The obtained maximum values of the relative hydrodynamic uplift force are higher than those obtained for fully saturated ($S = 1$) [*i.e.*, near-incompressible ($\beta' = \beta \cong 0$)] soils, where the pore pressure response can be described by the potential solution. The results presented in Figs. 6.8 and 6.9 were obtained for a certain set of geometric parameters: $L = 70.9\,\mathrm{m}$; $D_o = 1.0\,\mathrm{m}$; $b = 0.5\,\mathrm{m}$ (*i.e.*, $b/D_o = 0.5$); and $d/D_o = 2$, 5, 100. If one compute the potential solution to the hydrodynamic uplift force, assuming the same geometric parameters, it appears that the hydrodynamic uplift force would be from 72 (!) ($d/D_o = 2$), through 17.6 ($d/D_o = 5$), to 6.3 ($d/D_o = 100$) times smaller than the respective values obtained for the storage solution.

On the other hand, a rather minor influence of the 'finite-thickness layer' boundary condition on the pore pressure gradient (see Fig. 6.8) and the hydrodynamic uplift force (see Fig. 6.9) is observed. Comparing the two density states of seabed sediments, more compressible soil ($E = 10^4\,\mathrm{kPa}$) seems to be a little bit more sensitive on the introduction of this boundary conditions. Although the relative differences between the absolutely maximum values of the hydrodynamic uplift force, obtained for the loose seabed sediments of thicknesses $d = 100$ and $d = 2\,\mathrm{m}$, reaches approximately 43 %, the loose sediments cause the hydrodynamic uplift force which is from 4.7 ($d = 100\,\mathrm{m}$) to 8.8 ($d = 2\,\mathrm{m}$) times smaller than those computed for the case of dense sediments.

Using the advanced pore pressure theory (*e.g.*: Madsen, 1978; Yamamoto *et al.*, 1978; Okusa, 1985), it becomes possible to calculate a realistic value of the hydrodynamic uplift force acting on a submarine pipeline buried in seabed sediments. The above presented analysis has shown evidently that the maximum hydrodynamic uplift force, based on the diffusion or storage model, appears to be greater than this one calculated from the potential model. This general finding stays in accordance with some observations from laboratory tests reported in the literature. Additionally, the application of the 'finite-thickness layer' pore pressure storage solution (Magda, 1989$^{(a)}$, 1990$^{(a)}$, 1990$^{(c)}$) have proved that the uplift force solution is not so much sensitive on the 'finite-thickness layer' boundary condition, compared to the half-space solution.

Chapter 7

Conclusions

The main purpose of the present work was to prove the following thesis:

> *The wave-induced pore pressure theory of Madsen (1978), after the introduction of the author's particular 'finite-thickness layer' solution, gives a realistic picture of the soil-water/wave system interaction under natural environmental conditions, and can be used, with a satisfactory accuracy, for quantitative evaluations of the wave-induced pore pressure field in the seabed.*

A proof of the above statement was tried to be achieved gradually by means of both theoretical considerations and experimental modelling of the problem concerned. Single steps of the work have been described in six chapters.

After the formulation of the problem in Chapter 1, a wide review of the existing theories for the wave-induced pore pressure oscillations in sandy seabed sediments was performed (Chapter 2) in order to compare theoretical assumptions and applications, and to select only one pore pressure theory which is to be the most suitable for mapping real soil-water physical parameters into a computation procedure. Finally, a theory proposed by Madsen (1978) was chosen. This theory, among others having the same physical background, appears to have a clear mathematical structure convenient for its further possible treatment. An idea of such choice was also supported by many publicated reports where comparisons between a certain theory and experiments bring many doubts about applications of simple solutions based mainly on the potential theory (*e.g.*, Putnam, 1949).

Chapter 3 relates to the pore fluid compressibility as a one of the most important parameters incorporated into the theoretical description for the wave-induced pore pressure behaviour in sandy soils. As far as the compressibility is concerned, the theory reflects a real three-phase system (soil skeleton, pore water, and pore air) into an equivalent two-phase system where the water part and the air part are treated as one mixture. Therefore, it was necessary to deal with a problem of the soil saturation (*i.e.*, amount of air trapped in water) and its influence on the compressibility of the two-phase pore fluid. Another reason for paying so much attention to the pore fluid compressibility is a very high sensitivity of the wave-induced pore pressure field in seabed sediments on

this parameter, which is a direct function of soil saturation conditions. Many different formulas and reported values of the pore fluid compressibility were put together and compared to each other. It was shown that most of the existing equations, defining the pore fluid compressibility, are too complicated, from the practical point of view, because some of their parameters are extremely difficult to be measured. As a result of the analysis, it was suggested to use the expression proposed by Verruijt (1969).

In order to get a better knowledge about realistic values of saturation conditions existing in seabed sediments under natural environmental conditions, the expedition to Norderney Island (German coastline of the North Sea) was organized. Series of *in-situ* samplings, laboratory measurements and statistical analysis showed the existance of partly saturated soil conditions (*i.e.*, the mean value of the degree of saturation was found to be $\bar{S} = 0.975$), proving thereby a necessity of taking this fact into theoretical considerations.

Usefulness of the wave-induced pore pressure theory was planned to be checked by means of an experimental verification. However, in order to perform such a comparison, the theory had to be first of all adapted to the boundary conditions typical for large-scale laboratory investigations. This was done and is described in Chapter 4. A two-dimensional solution for the pore pressure has been analytically derived from the partial differential equation of the sixth order, under the assumption of limited thickness of the permeable seabed layer. Using some illustrative examples, the meaning of the 'finite thickness layer' storage solution and its dependency on some fundamental parameters of soil skeleton and pore fluid are well-documented. For the need of small-scale laboratory tests, a similar one-dimensional 'finite thickness layer' storage solution has been formulated but, this time, a numerical method (*i.e.*, Crank-Nicolson method) was used in the solution procedure.

Chapter 5 contains a detailed description of the experimental verification of the both analytical and numerical wave-induced pore pressure solutions, described in Chapter 4. Large-scale investigations, performed in the large wave flume, have confirmed qualitatively all the tendencies and effects predicted by the 2-D analytical 'finite-thickness layer' storage solution. Thanks to a very unique laboratory facility like the large wave flume (GWK) in Hannover, Germany, it was possible to observe and analyse a character of the wave-induced pore pressure oscillations under quasi-natural water and surface wave conditions.

As an extension of the experimental part of the work, the execution of small-scale laboratory tests has enabled to check quantitatively the influence of single parameters of the two-phase (*i.e.*, soil skeleton and pore fluid) seabed medium on the pore pressure distribution within sandy seabed sediments. A wide range of values of the degree of saturation and soil permeability, applied during the testing procedure, gave a good opportunity for a deep verification of the 1-D numerical 'finite-thickness layer' solution.

It can be concluded that the proposed 'finite-thickness layer' solutions for the wave-induced pore pressure oscillations in seabed sediments have been successfuly verified in the both large- and small-scale experiments. The results, presented in terms of the pore pressure amplitude and phase lag, and obtained for many different values of the pore fluid and soil skeleton parameters, are in good accordance with the values measured in the laboratory tests.

In the last part of the present work (Chapter 6), some practical implications of the wave-induced pore pressure phenomena are discussed. The 2-D 'finite-thickness layer' storage solution is used in the soil-water-structure anylysis where an existence of a submarine pipeline buried in seabed sediments is assumed. Calculated values of the wave-induced (*i.e.*, hydrodynamic) uplift force acting on a pipeline certify that

the derived solution for the pore pressure can be a powerful tool in solving some of important enginereing problems. When the upper part of seabed sediments, where the pore pressure gradient is expected to reach its maximum, is concerned, it is very important to define properly the pore pressure field within the soil. This can be of a great meaning not only when a certain onshore or offshore structure is concerned, but also when basic problems of stability and liquefaction of seabed sediments are studied.

Taking the above final conclusions into accout, the thesis submitted for the present work is believed to be proved.

As original components of the present thesis, the author would like to point out:

- mathematical derivation and formulation of the particular solution of the wave-induced pore pressure theory, proposed by Madsen (1978), under the boundary condition of finite thickness of the permeable seabed layer,
- conduction of *in-situ* measurements in order to detect natural conditions of seabed saturation in the coastline region,
- performance of laboratory tests, both in large- and small-scales, on a cyclic oscillation of the wave-induced pore pressure in the soil,
- preparation of numerical codes for a personal computer in order to handle complex computations of the wave-induced pore pressure oscillations in the seabed layer of finite thickness, for the case of 1-D and 2-D problems,
- application of the derived 2-D 'finite-thickness layer' storage solution into the analysis of the hydrodynamic uplift force acting on a submarine pipeline buried in seabed sediments.

Principal symbols

a	Wave number	$[m^{-1}]$
a_1, a_2	Coefficients	[-]
A	Cross-sectional area	$[m^2]$
$A^{(c)}$	Crest-amplitude of cnoidal wave	[m]
$A^{(t)}$	Trough-amplitude of cnoidal wave	[m]
$Arg(\mu)$	Argument of complex-valued parameter μ	[rad]
$A_1, ..., A_6$	Coefficients (complex-valued)	
b	Depth of burial of submarine pipeline	[m]
B	Skempton's pore pressure parameter	[-]
B_{aw}	Pore pressure parameter	[-]
c_d	Coefficient of diffusion	$[m^2/s]$
$c_1, ..., c_3$	Coefficients	[-]
$C_1, ..., C_3$	Coefficients (complex-valued)	
d	Thickness of permeable seabed layer; height of sand column	[m]
df_F	Frequency interval in FFT-analysis	[Hz]
$\frac{dl_j}{dN_t}$	Length of j-th sector arc	[m]
	Normalized number of tests with soil saturation $S_1 < S \leq S_2$	[-]
dt	Time-step	[s]
dt_F	Time-step of data sampling in FFT-analysis	[s]
dt_s	Time-step of data sampling	[s]
dz	Depth-step	[m]
$d\psi_j$	Angular width of j-th sector	[rad]
$d_{10}, d_{50}, d_{\%}$	Characteristic grain sizes	[mm]
D_c	Diameter of sand column	[m]
D_o	Outside diameter of submarine pipeline	[m]
D_r	Relative density of soil	[-]
$D_{1,...,6}^{(1,...,7)}$	Coefficients (complex-valued)	
D', D''	Coefficients (complex-valued)	
e	Void ratio of soil	[-]
E	Young's modulus of elasticity for isotropic soil	[kPa]
E_z	Young's modulus of elasticity of soil in z-direction	[kPa]
f_F	Sampling frequency in FFT-analysis	[Hz]

$f_n(v)$	Normal probability density function of random variable $\mathbf{v}$	[-]
$f_n(v')$	Normal probability density function of standarized random variable $\mathbf{v'}$	[-]
$f_n(S')$	Normal probability density function of standarized random degree of saturation $\mathbf{S'}$	[-]
f_N	Nyquist frequency	[Hz]
f_s	Sampling frequency	[Hz]
f_1, f_2	Coefficients (complex-valued)	
F_z	Hydrodynamic uplift force acting on submarine pipeline	[kN/m]
$\bar{F}_z$	Relative hydrodynamic uplift force acting on submarine pipeline	[kN/m/kPa]
$(\bar{F}_z)_{max}$	Maximum relative hydrodynamic uplift force acting on submarine pipeline	[kN/m/kPa]
$(\bar{F}_z)_{max,S}$	Maximum relative hydrodynamic uplift force (with respect to soil saturation)	[kN/m/kPa]
$(\bar{F}_z)_{max,\Theta}$	Maximum relative hydrodynamic uplift force (with respect to water wave oscillations)	[kN/m/kPa]
$(\bar{F}_z)_{max,\Theta,S}$	Maximum relative hydrodynamic uplift force (with respect to water wave oscillations and soil saturation)	[kN/m/kPa]
$\bar{F}_z^{(a)}$	Relative simplified hydrodynamic uplift force	[kN/m/kPa]
$\bar{F}_z^{(c)}$	Correction of the relative hydrodynamic uplift force	[kN/m/kPa]
$\bar{F}_z^{(p)}$	Relative perturbated hydrodynamic uplift force	[kN/m/kPa]
g	Acceleration due to gravity	[m/s^2]
G	Shear modulus for isotropic soil	[kPa]
h	Water depth	[m]
h_b	Hydrodynamic bottom pressure head	[m]
h_{sl}	Coefficient of volumetric solubility of air in water	[-]
h_t	Total pore pressure head	[m]
h'	Pore pressure head	[m]
$h'_{i,j}$	Pore pressure head at point $P_{i,j}$	[m]
$\bar{h}$	Relative pore pressure head	[-]
H	Wave height	[m]
HC	Line, denoting hydrostatic pore pressure distribution under wave crest	
HI	Line, denoting initial hydrostatic pore pressure distribution	
HT	Line, denoting hydrostatic pore pressure distribution under wave trough	
H_c	Height of sand column	[m]
H_d	Deep-water wave height	[m]
H_{sl}	Henry's coefficient of air solubility in water	[-]
H_0	Amplitude of the hydrodynamic bottom pressure head	[m]
H'	Amplitude of the pore pressure head	[m]
$\bar{H}$	Relative amplitude of the pore pressure head	[-]
i	Imaginary unit	
i_h	Hydraulic gradient	[-]
j	An integer	
k	Coefficient of permeability for isotropic soil	[m/s]
$k_a^{(r)}$	Coefficient of relative permeability of soil to air	[m/s]

$k_w^{(r)}$	Coefficient of relative permeability of soil to water	[m/s]
k_x, k_z	Coefficients of soil permeability in x- and z-direction, respectively	[m/s]
$k_{0.85}$	Coefficient of soil permeability at a void ratio of $e = 0.85$	[m/s]
k_η	Absolute coefficient of permeability	[m^2]
$\bar{k}$	Parameter (complex-valued)	[-]
K_w	Bulk modulus of elasticity of pure water	[kPa]
K'	Bulk modulus of elasticity of pore fluid	[kPa]
L	Wavelength	[m]
L_b	Semi-line, denoting boundary conditions	
L_i	Semi-line, denoting initial conditions	
L_0	Deep-water wavelength	[m]
m_s	Mass of solids in soil (mass of soil skeleton)	[kg]
m_w	Mass of water in soil pores	[kg]
m_{ws}	Mass of wet soil sample	[kg]
n	Porosity of soil	[-]
n_a	Soil porosity part filled with air	[-]
n_{max}	Maximum soil porosity	[-]
n_{min}	Minimum soil porosity	[-]
n_s	Number of sectors discretized in pipeline circumference	[-]
n_w	Soil porosity part filled with water	[-]
N	Number of depth-intervals in sand column	
N_F	Number of data samples required by FFT-analysis	
N_s	Number of data samples	
N_t	Number of tests on soil saturation	
$N_t^{(S_2-S_1)}$	Number of tests with soil saturation $S_1 < S \leq S_2$	
p	Wave-induced pore pressure (complex-valued)	[kPa]
p_a	Pore air pressure	[kPa]
p_{at}	Atmospheric pressure	[kPa]
p_b	Hydrodynamic bottom pressure	[kPa]
p_h	Hydrostatic pressure	[kPa]
p_t	Total pore pressure	[kPa]
p_{wv}	Water-vapour pressure	[kPa]
$p^{(a)}$	Undisturbed wave-induced pore pressure	[kPa]
$p^{(c)}$	Correction of the wave-induced pore pressure	[kPa]
$p^{(p)}$	Perturbated wave-induced pore pressure	[kPa]
p'	Wave-induced pore pressure	[kPa]
$\bar{p}$	Relative wave-induced pore pressure	[-]
$\bar{p}_j$	Relative wave-induced pore pressure, acting on j-th sector arc of pipeline circumference	[-]
$\|p\|$	Modulus of complex-valued wave-induced pore pressure	[kPa]
P	Amplitude of the wave-induced pore pressure	[kPa]
P_a	Absolute air pressure	[kPa]
P_f	Absolute fluid pressure	[kPa]
P_g	Absolute gas pressure	[kPa]
P_h	Absolute hydrostatic pressure	[kPa]
P_i	Absolute pore pressure at initial state	[kPa]
$P_{i,j}$	Nodal point	
$P_n(v)$	Normal probability distribution function of random variable **v**	[-]

P_r	Absolute reference pressure in water-air mixture	[kPa]
P_S	Point, denoting degree of saturation on probability curve	
$P_S^{(l)}, P_S^{(u)}$	Points, denoting lower and upper critical degree of saturation, respectively	
P_t	Absolute total pressure	[kPa]
P_w	Absolute water pressure	[kPa]
P_0	Amplitude of the hydrodynamic bottom pressure	[kPa]
$P_0^{(c)}$	Crest-amplitude of the hydrodynamic bottom pressure	[kPa]
$P_0^{(t)}$	Trough-amplitude of the hydrodynamic bottom pressure	[kPa]
$P_1^{(i-f)}$	Absolute difference in the relative pore pressure amplitude at base	[-]
$P_2^{(i-f)}$	Relative difference in the relative pore pressure amplitude at base	[-]
$\bar{P}$	Relative amplitude of the wave-induced pore pressure	[-]
$\bar{P}^{(i)}$	Relative pore pressure amplitude ('infinite-thickness layer' solution)	[-]
$\bar{P}^{(f)}$	Relative pore pressure amplitude ('finite-thickness layer' solution)	[-]
q	Volumetric discharge of water	[m^3/s]
r	Linear coordinate of the polar coordinates system	[m]
r_b	Free air-bubble radius	[m]
r_{bi}	Initial free air-bubble radius	[m]
r_F	Hydrodynamic uplift force ratio	[-]
r_p	Outside radius of submarine pipeline	[m]
R	Universal molar gas constant [$R = 8.314\,\mathrm{kJ/(kmol \cdot K)}$]	
S	Degree of saturation	[-]
$S_c^{(l)}, S_c^{(u)}$	Upper and lower critical degrees of saturation, respectively	[-]
S_{cr}	Critical degree of saturation	[-]
S_i	Degree of saturation at initial state	[-]
S_{opt}	Optimum degree of saturation	[-]
S_1, S_2	Degrees of saturation	[-]
$\bar{S}$	Mean degree of saturation	[-]
$\bar{S}^{(a)}$	Mean degree of saturation, computed analytically	[-]
S'	Standarized value of degree of saturation	[-]
t	Time	[s]
t_j	Time coordinate of nodal point $P_{i,j}$	[s]
t_0	Time coordinate of the system origin	[s]
T	Wave period	[s]
T_F	Period of waveform component in FFT-analysis	[s]
T_a	Absolute temperature	[K]
T_1, T_2	Coefficients (complex-valued)	
u_x, u_z	Soil displacements in x- and z-direction, respectively	[m]
v	Value of random variable **v**	
v_a	Specific volume of air	[m^3/kmol]
v_b	Relative volume of bonded air bubbles	[-]
v_f	Specific volume of fluid (gas)	[m^3/kmol]
v_f	Specific volume of fluid (liquid)	[m^3/kg]
v_g	Specific volume of gas	[m^3/kmol]
v_q	Discharge velocity	[m/s]

v_x, v_z	Discharge velocities in x- and z-direction, respectively	[m/s]
$\bar{v}$	Mean value of random variable $\mathbf{v}$	
v'	Standarized value of random variable $\mathbf{v}'$	[-]
V_a	Volume of free air in water-air mixture	[m^3]
V_{ab}	Volume of free air bubbles in water-air mixture	[m^3]
V_{ad}	Volume of air dissolved in water	[m^3]
V_g	Volume of gas	[kmol]
V_s	Volume of solids in soil	[m^3]
V_t	Total volume of soil (soil sample)	[m^3]
V_{ti}	Initial total volume of soil	[m^3]
V_v	Volume of voids in soil skeleton	[m^3]
V_{var}	Coefficient of variation	[-]
$V_{var}(S)$	Coefficient of variation of the degree of saturation	[-]
$V_{var}^{(a)}(S)$	Coefficient of variation of the degree of saturation, computed analytically	[-]
$V_{var}^{(avg)}$	Average value of coefficient of variation	[-]
$V_{var}^{(high)}$	High value of coefficient of variation	[-]
$V_{var}^{(low)}$	Low value of coefficient of variation	[-]
V_w	Volume of water in soil pores (in water-air mixture)	[m^3]
w	Water content	[-]
W_g	Amount of gas	[m^3]
x	Horizontal coordinate of the Cartesian coordinates system	[m]
$X_1, ..., X_7$	Coefficients (complex-valued)	
$Y_1, ..., Y_6$	Coefficients (complex-valued)	
z	Vertical coordinate of the Cartesian coordinates system	[m]
z	Depth in permeable seabed layer	[m]
z_i	Depth coordinate of nodal point $P_{i,j}$	[m]
z_0	Depth coordinate of the system origin	[m]
α	Compressibility of soil skeleton	[m^2/kN]
α_z	Compressibility of soil skeleton in z-direction	[m^2/kN]
β_a	Compressibility of air	[m^2/kN]
β_f	Isotermal compressibility of fluid	[m^2/kN]
β_w	Compressibility of water	[m^2/kN]
β'	Compressibility of pore fluid	[m^2/kN]
γ	Unit weight of pore fluid	[kN/m^3]
γ_{sat}	Unit weight of saturated soil	[kN/m^3]
γ_w	Unit weight of water	[kN/m^3]
γ'	Buoyant unit weight of soil	[kN/m^3]
δ	Phase lag of wave-induced pore pressure oscillations	[rad] [deg]
Δ	Increment or laplacian	
ϵ	Volumetric strain of soil skeleton	[-]
$\epsilon_x, \epsilon_y, \epsilon_z$	Normal volumetric strains in x-, y- and z-direction, respectively	[-]
η_v	Dynamic viscosity of water	[kPa · s]
η_w	Surface water wave elevation	[m]
ϑ	Parameter	[-]
θ	Volumetric strain of pore fluid	[-]

Θ_{opt}	Optimum phase of water wave loading oscillations	[rad]
κ	Parameter (complex-valued)	[m^{-1}]
λ	Parameter	[-]
μ	Parameter (complex-valued)	[m^{-1}]
$\|\mu\|$	Modulus of complex-valued parameter μ	[m^{-1}]
ν	Poisson's ratio for isotropic soil	[-]
ξ	Variable of integration	
ρ	Density of pore fluid	[Mg/m^3] [kg/m^3]
ρ_g	Density of gas	[$kmol/m^3$]
ρ_w	Density of water	[kg/m^3]
ϱ_s	Specific gravity of soil particles	[-]
$\bar{\varrho}_s$	Mean of specific gravity of soil particles	[-]
σ	Total normal stress	[kPa]
σ_m	Standard deviation of wet sample mass	[kg]
σ_t	Water-air surface tension of free air bubbles	[kN/m]
σ_v	Standard deviation of random variable $\mathbf{v}$	
σ_w	Standard deviation of water content	[-]
σ_z	Total vertical stress	[kPa]
σ_S	Standard deviation of degree of saturation	[-]
$\sigma_S^{(a)}$	Standard deviation of degree of saturation, computed analytically	[-]
σ'	Effective normal stress	[kPa]
σ'_x, σ'_z	Effective normal stresses in x- and z-direction, respectively	[kPa]
$\sigma_1, \sigma_2, \sigma_3$	Total principal stresses in x-, y- and z-direction, respect.	[kPa]
σ_ϱ	Standard deviation of specific gravity of solid particles	[-]
τ'	effective shear stress	[kPa]
ϕ	Arbitrary function (dependent on x, z, t)	[m] [kPa]
$\tilde{\phi}$	Arbitrary function (dependent on z only)	[m] [kPa]
ψ	Angular coordinate of the polar coordinates system	[rad]
ψ_j	Angular coordinate of the bisector of j-th sector	[rad]
ω	Angular frequency of water wave oscillations or water surface vertical oscillations	[s^{-1}]
∇	Hamilton's operator	
$\Im\{\ \}$	denotes an imaginary part of $\{\ \}$	
$\Re\{\ \}$	denotes a real part of $\{\ \}$	
$\mathbf{v}$	random variable	
$\mathbf{v}'$	standarized random variable	
$\mathbf{B}, \mathbf{K}$	Matrix of free terms	
$\mathbf{D}, \mathbf{M}$	Matrix of coefficients	
$\mathbf{H}, \mathbf{Y}$	Matrix of unknowns	

References

BARENDS, F.B.J. (1980). The compressibility of an air-water mixture in a porous medium. *IGM Mededelingen*, Delft Soil Mechanics Laboratory, The Netherlands, pp. 49-66.

BENDAT, J.S., PIERSOL, A.G. (1971). *Random Data: Analysis and Measurement Procedures*. John Wiley & Sons, Inc.

BENNETT, R.H., FARIS, J.R. (1979). Ambient and dynamic pore pressures in fine-grained submarine sediments: Mississippi Delta. *Applied Ocean Research*, Vol. 1, No. 3, pp. 115-123.

BIOT, M.A. (1941). General theory of three-dimensional consolidation. *Journal of Applied Physics*, Vol. 12, pp. 155-164.

BISHOP, A.W., ELDIN, A.F.G. (1950). Undrained triaxial tests on saturated sands and their significance in the general theory of shear strength. *Géotechnique*, Vol. 2, pp. 13-32.

BISHOP, A.W. (1960). The measurement of pore pressure in the triaxial test. *Proc. of the Conference on Pore Pressure and Suction in Soils, London*, pp. 38-46.

CHARI, T.R., DAWE, C.R., BARBOUR, S.A. (1987). Model studies of wave-seabed interactions. *Journal of Offshore Mechanics and Arctic Engineering*, Vol. 109, pp. 67-74.

CHENG, A.H-D., LIU, P.L-F. (1986). Seepage force on a pipeline buried in a poroelastic seabed under wave loadings. *Applied Ocean Research*, Vol. 8, No. 1, pp. 22-32.

CRAIG, R.F. (1983). *Soil Mechanics*. Van Nostrand Reinhold (UK) Co. Ltd.

CROSS, R.H., HUNTSMAN, S.R., TREADWELL, D.D., BAKER, V.A. (1979). Attenuation of wave-induced pore pressures in sand. *Proc. of the Speciality Conference Civil Engineering in the Oceans IV, San Francisco, California*, pp. 745-757.

DEMARS, K.R., VANOVER, E.A. (1985). Measurements of wave-induced pressures and stresses in a seabed. *Marine Geotechnology*, Vol. 6, No. 1, pp. 29-59.

DORSEY, N.E. (1940). Properties of ordinary water-substances. *Am. Chem. Soc., Monogr. Ser.*, Reinhold Publishing Corporation, New York.

DUNLAP, W.A., BRYANT, W.R., BENNETT, R.H., RICHARDS, A.F. (1978). Pore pressure measurements in unconsolidated sediments. *Proc. of the Offshore Technology Conference*, Vol. 2, pp. 1049-1058.

DUNNICLIFF, J. (1988). *Geotechnical Instrumentation for Monitoring Field Performance.* John Wiley & Sons, Inc.

DURSTHOFF, W., MAZURKIEWICZ, B. (1985). Problems related to submarine pipelines. *Mitteilungen des Franzius-Instituts für Wasserbau und Küsteningenieurwesen der Universität Hannover, Heft 61*, pp. 176-238.

EAU 1985. Recommendations of the Committee for Waterfront Structures. Ernst & Sohn, Berlin, 1986.

ESRIG, M.I., KIRBY, R.C. (1977). Implications of gas content for predicting the stability of submarine slopes. *Marine Geotechnology*, Vol. 2, pp. 81-100.

FINN, W.D.L., SIDDHARTHAN, R., MARTIN, G.R. (1983). Response of seaflor to ocean waves. *Journal of Geotechnical Engineering, ASCE*, Vol. 109, No. 4, Paper No. 17880, pp. 556-572.

FODA, M.A. (1985). Pipeline breakout from sea floor under wave action. *Applied Ocean Research*, Vol. 7, No. 2, pp. 79-84.

FREDLUND, D.G. (1976). Density and compressibility characteristics of air-water mixtures. *Canadian Geotechnical Journal*, Vol. 13, pp. 386-396.

GATMIRI, B. (1990). A simplified finite element analysis of wave-induced effective stresses and pore pressures in permeable sea beds. *Géotechnique*, Vol. 40, No. 1, pp. 15-30.

GHABOUSSI, J., WILSON, E.L. (1973). Flow of compressible fluid in porous elastic solids. *International Journal of Numerical Methods in Engineering*, Vol. 5, pp. 419-442.

HARR, M.E. (1966). *Foundatios of Soil Mechanics.* McGraw-Hill, New York.

HUNT, J.N. (1959). On the damping of gravity waves propagated over a permeable surface. *Journal of Geophysical Research*, Vol. 64, No. 4, pp. 437-442.

JACOBSEN, H.M., MAGDA, W. (1988). Erosion and pore pressure gradients. *X Nordiske Geoteknikermote (X Nordic Geotechnical Meeting), Oslo*, pp. 49-53.

JANKOWSKI, A. (1983). *Algorytmy metod numerycznych. Skrypt do przedmiotu Programowanie i Metody Numeryczne.* Wydawnictwo Politechniki Gdańskiej, Gdańsk.

JØRGENSEN, M.J., STEENSEN-BACH, J.O., STEENFELT, J.S. (1988). Lateral resistance and displacement patterns for cyclically loaded pipelines in sand inferred from model testting. *Proc. of the International Symposium on Modelling Soil-Water-Structure Interactions (SOWAS), Delft*, pp. 33-42. A.A. Balkema, Rotterdam.

KÉZDI, A. (1974). *Handbook of Soil Mechanics. Vol I: Soil Physics.* Elsevier Scientific Publishing Company.

KOKKINOWRACHOS, K. (1985). Hydrodynamic analysis of large offshore structures on porous elastic seabed. *Proc. of the 4th International Offshore Mechanics and Arctic Engineering Symposium (OMAE)*, Vol. 1.

KONING, H.L. (1963). Some observations on the modulus of compressibility of water. *Proc. of the Conference on Settlement and Compressibility of Soils, Wiesbaden*, pp. 33-36.

KRAFT, L.M., HELFRICH, S.C., SUHAYDA, J.N., MARIN, J.E. (1985). Soil response to ocean waves. *Marine Geotechnology*, Vol. 6, No. 2, pp. 173-203.

LAI, N.W., DOMINGUEZ, R.F., DUNLAP, W.A. (1974). Numerical solutions for determining wave-induced pressure distributions around buried pipelines. *Texas A & M University, Sea Grant Pub. No. TAMU-SG-75-205.*

LENNON, G.P. (1983). Wave-induced forces on buried pipelines. *Proc. of Coastal Structures '83, Arlington*, pp. 505-518.

LENNON, G.P. (1985). Wave-induced forces on buried pipelines. *Journal of Waterway, Port, Coastal and Ocean Engineering, ASCE*, Vol. 111, No. 3, pp. 511-524.

LINDENBERG, L., SWART, J.H., KENTER, C.J., DEN BOER, K. (1982). Wave induced pressures underneath a caisson; a comparison between theory and large scale tests. *Proc. of the 3rd International Conference on the Behaviour of Offshore Structures (BOSS'82), Cambridge, Massachusetts, U.S.A.*.

LIU, P.L-F. (1973). Damping of water waves over porous bed. *Journal of Hydraulics Division, ASCE*, Vol. 99, No. HY12, Paper No. 10218, pp. 2263-2271.

LIU, P.L.F., O'DONNEL, T.P. (1979). Wave-induced forces on buried pipelines in permeable seabed. *Journal of Waterway, Port, Coastal and Ocean Division, ASCE*, Vol. 104, No. WW4.

MACPHERSON, H. (1978). Wave forces on pipeline buried in permeable seabed. *Journal of Waterway, Port, Coastal and Ocean Division, ASCE*, Vol. 104, No. WW4, pp. 407-419.

MADSEN, O.S. (1978). Wave-induced pore pressures and effective stresses in a porous bed. *Géotechnique*, Vol. 28, No. 4, pp. 377-393.

MAGDA, W. (1987). *Stateczność rurociągu zagłębionego w dnie morskim i poddanego oddziaływaniu falowania.* Studia i Materiały, Zeszyt nr 2, Katedra Budownictwa Morskiego, Politechnika Gdańska, Gdańsk.

MAGDA, W. (1989$^{(a)}$). *Wave-induced pore water pressure generation in a sand bed.* Internal Report No. 1, Sonderforschungsbereich-205 "Küsteningenieurwesen," TP A13, University of Hannover, Hannover, Germany.

MAGDA, W. (1989$^{(b)}$). Influence of saturation method on saturation degree of soil model in laboratory investigations. *Proc. of the 3rd Polish-Yugoslav Symposium "Research on Hydraulic Engineering," Gdańsk*, pp. 207-215.

MAGDA, W. (1990$^{(a)}$). Pore water pressure generation in a highly saturated sea bed for shallow water conditions. *Proc. of the 1st International Symposium LITTORAL 1990, EUROCOAST Association, Marseille*, pp. 110-114.

MAGDA, W. (1990$^{(b)}$). *On the pore water compressibility and its dependence on the degree of saturation.* Internal Report No. 3, Sonderforschungsbereich-205 "Küsteningenieurwesen," TP A13, University of Hannover, Hannover, Germany.

MAGDA, W. (1990$^{(c)}$). *On one-dimensional model of pore pressure generation in a highly saturated sandbed due to cyclic loading acting on a sand surface; Part I, theoretical description and numerical approach.* Internal Report No. 4, Sonderforschungsbereich-205 "Küsteningenieurwesen," TP A13, University of Hannover, Hannover, Germany.

MAGDA, W. (1990$^{(d)}$). *On one-dimensional model of pore pressure generation in a highly saturated sandbed due to cyclic loading acting on a sand surface; Part II, laboratory tests and comparison with theoretical approach.* Internal Report No. 5, Sonderforschungsbereich-205 "Küsteningenieurwesen," TP A13, University of Hannover, Hannover, Germany.

MAGDA, W., DAVIDOV, N. (1990). *On determining of the degree of saturation from in-situ measurements of the seabed performed on Norderney Island.* Internal Report No. 2, Sonderforschungsbereich-205 "Küsteningenieurwesen," TP A13, University of Hannover, Hannover, Germany.

MASSEL, S.R. (1976). Gravity waves propagated over permeable bottom. *Journal of Waterways, Harbors and Coastal Engineering Division, ASCE*, Vol. 102, No. WW2, Paper No. 12107, pp. 111-121.

MASSEL, S.R. (1985). Zastosowanie teorii gruntowej warstwy granicznej w hydromechanice i inżynierii morskiej. *Archiwum Hydrotechniki*, Vol. 32, No. 2, pp. 157-194.

MASSEL, S.R., KACZMAREK, L. (1988). Pore pressure induced by wind waves in sand bed. *Proc. of the 3rd Polish-German Seminar on Hydraulics Phenomena in Offshore, Coastal & Inland Waters, Hannover, Fed. Rep. of Germany.*

MAZURKIEWICZ, B. (1985). *Mechanika gruntów dna morskiego.* Studia z Zakresu Inżynierii, Nr 23, Polska Akademia Nauk, Komitet Inżynierii Lądowej i Wodnej, Państwowe Wydawnictwo Naukowe, Warszawa – Łódź.

MCDOUGAL, W.G., SOLLITT, C.K. (1984). Geotextile stabilization of seabeds; I: theory; II: large scale experiments. *Engineering Structures*, Vol. 6, pp. 211-216, 217-222.

MCDOUGAL, W.G., DAVIDSON, S.H., MONKMEYER, P.L., SOLLITT, C.K. (1988). Wave-induced forces on buried pipelines. *Journal of Waterway, Port, Coastal, and Ocean Engineering, ASCE*, Vol. 114, No. 2, pp. 220-236.

MEI, C.C., FODA, M.A. (1981). Wave-induced responses in a fluid-filled poro-elastic solid with a free surface – a boundary layer theory. *Geophysical Journal of the Royal Astronomical Society*, No. 66, pp. 597-631.

MONKMEYER, P.L., MANTOVANI, P., VINCENT, H. (1983). Wave-induced seepage effects on a buried pipeline. *Proc. of the Coastal Structures '83 Conference*, pp. 519-531.

MOSHAGEN, H., TØRUM, A. (1975). Wave-induced pressures in permeable seabeds. *Journal of Waterways, Harbors and Coastal Engineering Division, ASCE*, Vol. 101, No. WW1, Paper No. 11099, pp. 49-57.

MURRAY, J.D. (1965). Viscous damping of gravity waves over a permeable bed. *Journal of Geophysical Research*, Vol. 70, No. 10, pp. 2325-2331.

MUTHUKRISHNAIAH, K. (1989). Experimental studies on wave-current-seabed interaction. *Proc. of the 3rd National Conference on Dock & Harbour Engineering, Surathkal, India*, pp. 189-198.

NAGESWARAN, S. (1983). *Effect of Gas Bubbles on the Seabed Behaviour.* Ph.D. dissertation, Oxford University.

NAGO, H. (1981). Liquefaction of highly saturated sand layer under oscillating water pressure. *Memoirs of the School of Engineering, Okayama University, Tsushima, Okayama, Japan*, Vol. 16, No. 1, pp. 93-104.

NAGO, H., MAENO, S. (1984). Pore water pressure in sand bed under oscillating water pressure. *Memoirs of the School of Engineering, Okayama University, Tsushima, Okayama, Japan*, Vol. 19, No. 1, pp. 13-31.

NAGO, H., MAENO, S. (1986). Dynamic behavior of sand bed under oscillating water pressure. *Memoirs of the School of Engineering, Okayama University, Tsushima, Okayama, Japan*, Vol. 20, No. 2, pp. 35-45.

NAGO, H., MAENO, S. (1987). Pore pressure and effective stress in a highly saturated sand bed under water pressure variation on its surface. *Natural Disaster Science*, Vol. 9, No. 1, pp. 23-35.

NAKAMURA, H., ONISHI, R., MINAMIDE, H. (1973). On the seepage in the seabed due to waves. *Proc. of the 20th Coastal Engineering Conference.*

OKUSA, S. (1985[a]). Wave-induced stresses in unsaturated submarine sediments. *Géotechnique*, Vol. 35, No. 4, pp. 517-532.

OKUSA, S. (1985[b]). Measurements of wave-induced pore pressure in submarine sediments under various marine conditions. *Marine Geotechnology*, Vol. 6, No. 2, pp. 119-144.

PHILLIPS, B.A., GHAZZALY, O.I., KALAJIAN, E.H. (1979). Stability of pipeline in sand under wave pressure. *Proc. of the Speciality Conference Civil Engineering in the Ocean IV, San Francisco*, pp. 122-136.

PRESS, W.H., FLANNERY, B.P., TEUKOLSKY, S.A., VETTERLING, W. (1986). *Numerical Recipes. The Art of Scientific Computing.* Cambridge University Press.

PREVOST, J.H., EIDE, O., ANDERSON, K.H. (1975). Wave induced pressures in permeable seabeds. Discussion. *Journal of Waterways, Harbours and Coastal Engineering Division, ASCE*, Vol. 101, No. WW4, pp. 464-465.

PUTNAM, J.A. (1949). Loss of wave energy due to percolation in a permeable sea bottom. *Transactions American Geophysical Union*, Vol. 30, No. 3, pp. 349-356.

RAMIREZ, R.W. (1985). *The FFT: Fundamentals and Concepts.* Prentice-Hall, Inc., Englewood Cliffs, New York.

RIED, R.O., KAJIURA, K. (1957). On the damping of the gravity waves over a permeable sea bed. *Transactions American Geophysical Union*, Vol. 38, No. 5.

ROUSE, H. (1950). *Engineering Hydraulics.* John Willey & Sons, New York.

SCHMERTMANN, J.H. (1989). Density tests above zero air voids line. *Journal of Geotechnical Engineering, ASCE*, Vol. 115, No. 7, pp. 1003-1018.

SCHUURMAN, E. (1966). The compressibility of an air/water mixture and a theoretical relation between the air and water pressure. *Géotechnique*, Vol. 16, No. 4, pp. 269-281.

Shore Protection Manual. U.S. Army Corps of Engineers, Coastal Engineering Research Center, Vol. I, Washington, 1984.

SKEMPTON, A.W. (1954). The pore pressure coefficients A and B. *Géotechnique*, Vol. 4, No. 4, pp. 143-147.

SKEMPTON, A.W., BISHOP, A.W. (1954). *Soils.* In *Building Materials*, Ch. 10. North Holland Pub. Co, Amsterdam.

SKORKO, M. (1978). *Fizyka.* Państwowe Wydawnictwo Naukowe, Warszawa.

SLEATH, J.F.A. (1970). Wave induced pressures in beds of sand. *Journal of Hydraulics Division, ASCE*, Vol. 96, No. HY2, Paper No. 7057, pp. 367-378.

SPIERENBURG, S.E.J. (1985). Geotechnical aspects of submarine pipelines. *Proc. of the Behaviour of Offshore Structures Conference (BOSS'85), Delft, The Netherlands*, pp. 797-805.

SPIERENBURG, S.E.J. (1986). Wave-induced pore pressures around submarine pipeline. *Coastal Engineering*, No. 10, pp. 33-48.

SPIERENBURG, S.E.J. (1987). *Seabed Response to Water Waves.* Ph.D. dissertation, Delft University.

TERZAGHI, K. (1943). *Theoretical Soil Mechanics.* John Wiley & Sons, New York.

THOMAS, S.D. (1991). Measurements and modelling of wave induced pore pressures in the seabed. *Proc. of the 5th Young Geotechnical Engineers Conference, Grenoble, France.*

TSUI, Y., HELFRICH, S.C. (1983). Wave-induced pore pressures in submerged sand layer. *Journal of Geotechnical Engineering, ASCE*, Vol. 109, No. 4, Paper No. 17883, pp. 603-618.

VAID, Y.P., NEGUSSEY, D. (1988). Preparation of reconstituted sand specimens. In *Advanced Triaxial Testing of Soil and Rock*, ASTM STP 977, R.T. Donaghe, R.C. Chaney, and M.L. Silver (eds), American Society for Testing and Materials, Philadelphia, pp. 405-417.

VERRUIJT, A. (1969). *Elastic Storage of Aquifers.* In *Flow Through Porous Media*, Ch. 8, de Wiest (ed.). Accademic Press, London.

VERRUIJT, A. (1980). Long and short waves on a consolidating half-plane. *International Symposium on Soils under Cyclic and Transient Loading, Swansea*, pp. 695-696.

WHEELER, S.J., SILS, G.C., THOMAS, S.D., GARDNER, T.N. (1991). Behaviour of offshore soils containing gas bubbles. *Géotechnique*, Vol. 41, No. 2, pp. 227-241.

YAMAMOTO, T. (1977). Wave-induced instability in seabeds. *Proc. of the 5th Symposium Coastal Sediments '77, Charleston*, pp. 898-913.

YAMAMOTO, T. (1978). Sea bed instability from waves. *Proc. of the 10th Offshore Technology Conference, Houston*, Paper No. OTC 3262.

YAMAMOTO, T. (1981). Wave-induced pore pressures and effective stresses in inhomogeneous seabed foundations. *Ocean Engineering*, Vol. 8, pp 1-16.

YAMAMOTO, T. (1983). On the response of a Coloumb-damped poro-elastic bed to water waves. *Marine Geotechnology*, Vol. 5, No. 2, pp. 93-130.

YAMAMOTO, T., KONING, H.L., SELLMEIJER, H., HIJUM, E. (1978). On the response of a poro-elastic bed to water waves. *Journal of Fluid Mechanics*, Vol. 87, Part 1, pp. 193-206.